Investigation Into The Molecular Mechanisms Underlying Idiopathic Intracranial Hypertension

Thesis

Investigation into the Molecular Mechanisms Underlying Idiopathic Intracranial Hypertension

Zerin Alimajstorovic, B.Sc, M.Res

A thesis submitted to the School of Life, Health and Chemical Sciences
Degree of Doctor of Philosophy
The Open University

Supervised by:

Prof. Ignacio Romero
School of Life, Health and Chemical Sciences
The Open University
United Kingdom

Dr. A. Jane Loughlin
School of Life, Health and Chemical Sciences
The Open University
United Kingdom

Prof. Basil Sharrack
Department of Neurology
Sheffield University
United Kingdom

Dr. Jane E. Preston
Institute of Pharmaceutical Science
King's College London
United Kingdom

November 2016

Acknowledgments

I would like to express my special appreciation and thanks to my supervisors Prof. Ignacio Romero and Dr. Jane Loughlin both of whom have been tremendous mentors for me. I would like to thank you for encouraging my research and for allowing me to grow as a scientist. Your advice on both research as well as on my career have been invaluable. I would also like to my third supervisor from King's College London, Dr. Jane Preston whose guidance and experimental expertise were invaluable for me throughout the project. You gave me the initial confidence needed to make this project a success and I will always be extremely grateful. I would also like to thank Prof. Basil Sharrack for his added support and who without this project would not have been possible.

This work would not have been completed without the research assistance and support from Julia Barkans, Prof. David Male, Dr. Cheryl Hawkes, Brett Keith, Dr. Suzanne Simmons, Karen Evans, Agata Stramek, Dee Shaw and Alexander Beazleigh, all of whom I owe a sincere debt of gratitude for their added input, kind nature and professionalism throughout my degree. And, a special thanks to Dr. Igor Kraev for his help in guiding me through the electron microscopy technique.

My whole research experience was improved thanks to the amazing colleagues and friends I met over the years in both Milton Keynes and London including: Mohammad Daas, Conor McQuaid, David Roig-Carles, Shereen Nizari, Radka Gromnicova, Joyce Wang, Edu Frias, Ester Pascal-Baixuali, Laura Contu, Camilla Cerutti, Dongsheng Wu, Juzaili Azizi, Ana Georgian, Gayathri Sekhar and Svetlana Drndarski. You are all amazing scientists, who I know are destined for great careers. And to all of the friends outside of my research group that I have had the pleasure of meeting and enjoying every moment with, you will always be in my thoughts and I wish you all every success in the future.

A special mention to my family who have supported me in every way; for your strength and advice, which will never be forgotten and to which I have a lot to be thankful for.

I would like to thank The Open University, King's College London and Sheffield Hallam University – NHS trust for providing me with the facilities, expertise and funding my research project.

Abstract

Idiopathic intracranial hypertension (IIH) is a neurological disorder characterised by raised cerebrospinal fluid (CSF) pressure in the absence of any intracranial pathology. IIH mainly affects obese women between the ages of 15 and 45. Two possible mechanisms that could explain the increased CSF pressure in IIH are excessive CSF production by the choroid plexus epithelium or impaired CSF drainage back into the venous blood but the molecular mechanisms controlling these in IIH remain to be determined.

In vivo ventriculo-cisternal perfusion and variable rate infusion techniques assessed changes in rates of CSF secretion/resistance to CSF drainage in male and female Wistar rats fed either a normal control or high-fat (HF) diet, following treatment with inflammatory mediators already found to be elevated in the CSF of IIH patients: chemokine (C-C motif) ligand 2 (CCL2), interleukin (IL)-17 (IL-17), IL-6, IL-1β, tumour necrosis factor-α (TNF-α), as well as adipocyte-derived hormone leptin and the glucocorticoid hydrocortisone (HC).

Female Wistar rats raised on a HF diet were shown to have the highest CSF secretion and lowest CSF drainage rates under untreated conditions. Increased CSF secretion was observed in rats of all genders and diets following TNF-α or HC treatment, however the greatest increase by TNF-α and HC over basal levels was observed in female rats raised on a HF diet. In addition, female rats on a HF diet, treated with CCL2 or IL-17, displayed an increase in resistance to CSF drainage when compared to untreated controls (indicating lower levels of CSF drainage).

Therapies targeting HC, TNF-α, CCL2 and/or IL-17, whether separately or in combination, may be beneficial to modulate rates of CSF secretion and/or resistance to CSF drainage pathways, both factors likely contributing to the raised intracranial pressure observed in obese female IIH patients.

Study supported by: Prof. Ignacio A. Romero, Dr. A. Jane Loughlin, Prof. Basil Sharrack, Dr. Jane E. Preston.

Publication List

Poster presentation at scientific conferences:

All posters and presentations titled: Investigation into the Molecular Mechanisms Underlying Idiopathic Intracranial Hypertension. Z Alimajstorovic., IA Romero., AJ Loughlin., B Sharrack., JE Preston.

- 67th American Academy of Neurology 2015', Washington D.C, USA (Apr 2015).
- 17th International Symposium on Signal Transduction at the Blood-Brain and Blood- Retina Barriers, Dublin, Ireland (Sep 2014).
- 'Early Career Blood Brain Barrier Symposium at Medimmune, Cambridge, UK (Nov 2013).

Oral presentation at scientific conferences:

- Invited speaker at Royal Hallamshire Hospital, Sheffield, UK (Oct 2015).
- 'Early Career Blood Brain Barrier Symposium' at University of Southampton (Nov 2015)
- 'Early Career Blood Brain Barrier Symposium' at University College London, London, UK (Nov 2014).
- 'Biomedical Research Network Symposium' at The Open University, Milton Keynes, UK (Apr '13, '14 & '15).
- '3 Minute Thesis' (3MT) presentation at The Open University, Milton Keynes, UK (May 2015).

- **Abstract Publication:**
  - Alimajstorovic, Z. (2015). Investigation into the Molecular Mechanisms Underlying Idiopathic Intracranial Hypertension. *Neurology*. 84(14), Supplement P2.099. **http://www.neurology.org/content/84/14_Supplement/P2.099.long**

Table of Contents

List of figures

List of tables

List of equations

List of figures, tables and equations in appendix

Abbreviations

11β-HSD	11β-hydroxysteroid dehydrogenase
aCSF	Artificial cerebrospinal fluid
ACTH	Adrenocorticotropic hormone
AE2	Chloride-bicarbonate exchanger
AFE	Atwater Fuel Energy
ANP	Atrial natriuretic peptide
AQP	Aquaporin
AR	Androgen receptor
ATII	Alveolar epithelial type II cells
ATP	Adenosine triphosphate
BBB	Blood brain barrier
BCSFB	Blood-cerebrospinal fluid-barrier
BMI	Body mass index
BSA	Bovine serum albumin
cAMP	Cyclic adenosine monophosphate
CBX	Carbenoxolone
CCL2	Chemokine (CC-motif) ligand 2
CCM2	Cerebral cavernous malformation 2
CCR2	Chemokine (CC-motif) ligand 2 receptor
cGMP	Cyclic guanosine monophosphate
C_{in}	concentration in
CNS	Central nervous system
C_{out}	Concentration out
COX	Cyclooxygenase
CP	choroid plexus

CSF	Cerebrospinal fluid
CT	Computerised tomography
DDSA	Dodecenyl succinic anhydride
DIC	Days in culture
DMP-30	2,4,6-tris diemthylaminomethyl phenol
ECF	Extracellular fluids
EM	Electron microscopy
ENaC	Epithelial sodium channels
EpiCGS	Epithelial cell growth supplement
ERK	Extracellular signal-regulated kinases
FBS	Foetal bovine serum
FDR	False discovery rate
FITC	Fluorescein isothiocyanate
GC	Guanylyl cyclase
GMC	Glomerular mesangial cells
GO	Gene ontology
GR-α	Glucocorticoid receptor-α
HBSS	Hank's balanced salt solution
HC	Hydrocortisone (Cortisol)
hCPEPiC	Human choroid plexus epithelial cells
HDL	High-density lipoprotein
HeLa	Human cervix carcinoma cells
hER	Human oestrogen receptor
HF	High-fat
HPA	Hypothalamo-pituitary-adrenal axis
HT-29	human colorectal adenocarcinoma cells
i.p.	Intraperitoneal/peripheral

ICP	Intracranial pressure
IFN	Interferons
IFT	Intraflagellar transport
IIH	Idiopathic intracranial hypertension
IL	Interleukin
IL-17R	Interleukin-17 receptor
IL-1R	Interleukin-1 receptor
IL-6R	Interleukin-6 receptor
IMCD3	Intermedullary collecting duct cells
ISF	Interstitial fluid
JAK	Janus kinase pathways
LDL/VLDL	Low-density lipoprotein/very-low density lipoprotein
LP shunt	Lumbar SAS to the peritoneal cavity shunt
MAPK	Mitogen-activated protein kinase
MRI	Magnetic resonance imaging
MTHFR	Methylenetetrahydrofolate reductase
Na^+-K^+-ATPase	Sodium-potassium adenosine triphosphatase pump
NADP(H)	Nicotinamide adenine dinucleotide phosphate
NCDN	Neurochondrin
NF-κB	Nuclear factor-kappa-light-chain-enhancer of activated B cells
NHE1	Sodium-hydrogen antiporter 1
NKCC1	Na^+-K^+-$2Cl^-$ cotransporter
NO	Nitric oxide
NPD	Normal pellet diet
NPE	Non-pigmented epithelial cells
Ob	Obese gene
P/S	Penicillin/streptomycin solution

PB	Phosphate buffer
PBMC	Peripheral blood mononuclear cells
PBS	Phosphate buffered saline
PCOS	Polycystic ovarian syndrome
PFA	*para*-formaldehyde
PGE2	Prostaglandin E2
PKA	Protein kinase A
PKC	Protein kinase C
PKG	Protein kinase G
PLA2	Phospholipase A2
PMVEC	Pulmonary microvascular endothelial cells
RM	Rodent maintenance diet
RM1	Rat and mouse no. 1 maintenance diet
RT-qPCR	Real-time quantitative PCR
SAS	Subarachnoid space
SDS	Special diet services
SGK1	Serum and glucocorticoid-regulated kinase-1
SPAG16	Sperm associated antigen 16
SSA2	Sjögren's syndrome antigen 2
STATS	Signal transducers and activators of transcription
TACE	TNF-α converting enzyme
TBI	Traumatic brain injury
TF	Tissue factor gene
TNF-R1	Tumour necrosis factor receptor-1
TNFR1BP-Fc	Tumour necrosis factor receptor-1 blocking peptide-Fc fusion protein
TNF-α	Tumour necrosis factor-α
TROVE2	Telomerase and Ro and Vault protein 2

TTF-1	Thyroid transcription factor-1
TTR	Transthyretin
VP shunt	Ventricle to the peritoneal cavity shunt
VST	Variance stabilization transformation
ZO-1	Zonula Occludens-1

1 General introduction

Idiopathic intracranial hypertension (IIH) is a neurological disorder characterized by raised cerebrospinal fluid (CSF) pressure in the absence of any intracranial pathology or secondary causes of IIH (Dhungana et al. 2009). The first description of the condition was outlined by Heinrich Quincke (1893), a German physician, calling it "serous meningitis" (Rowe & Sarkies 1998). When identifying the cause of a disease, clinical observations and a pathological link first need to be recognised. Various causative factors have been postulated as to the incidence of IIH, however, with little strong evidence. There may not be a single cause of the disease but many aetiological factors. Identifying biomarkers within the CSF, as indicators of increased CSF pressure has been used to present an insight into the pathogenesis of IIH. Two mechanisms that could explain the increased CSF pressure in IIH are excessive CSF production or impaired absorption of CSF (Pearce 2009) (Bateman 2008). However, the most accurate pathological theory of IIH is likely to be multifactorial (Raoof et al. 2011).

1.1 Central nervous system fluid dynamics

In order to understand the pathogenesis of IIH, the dynamics of the central nervous system (CNS) fluid movement will first be reviewed. The blood brain barrier (BBB) (see Section 1.2) is one of three barrier sites between the brain and the blood (Figures 1.1, 1.2, 1.3 and 1.4); the other two comprising of the blood-CSF-barrier (BCSFB) (see Section 1.3) and the arachnoid epithelium (see Section 1.5) (Abbott

2004). All of which are essential for the normal function of the central nervous system.

The BBB is a highly selective permeability barrier that allows the passage of water and lipid soluble molecules, which are essential for neural function, from the blood and into the brain. Overcoming the BBB is essential for the delivery of therapeutic agents into the brain.

The interstitial fluid (ISF) and the CSF constitute the two major extracellular fluids (ECF) in the brain (Redzic et al. 2005). The brain capillary endothelium of the BBB is the main interface between blood and ISF and regulates the production of ISF, which is secreted into the brain parenchyma or perivascular space (Figure 1.1).

The CSF is produced by the choroid plexus epithelium which lies as the main barrier between the blood and ventricular CSF, therefore constituting the BCSFB. The BCSFB allows the flow of CSF along the ventricular system and into the subarachnoid space (SAS). In addition, even though there is a bidirectional movement of ISF and CSF between the two compartments through the ependyma; there is a net movement of ISF from the brain parenchyma into the CSF (Figure 1.1). The BBB and the BCSFB regulate molecular exchange at the interfaces between the blood and the neural tissue (Abbott et al. 2010). The third barrier is the arachnoid membrane, which is the main site of CSF drainage back into the venous blood

(Figure 1.2). This occurs through a hydrostatic pressure gradient pushing the CSF through the openings of the arachnoid granulations and villi.

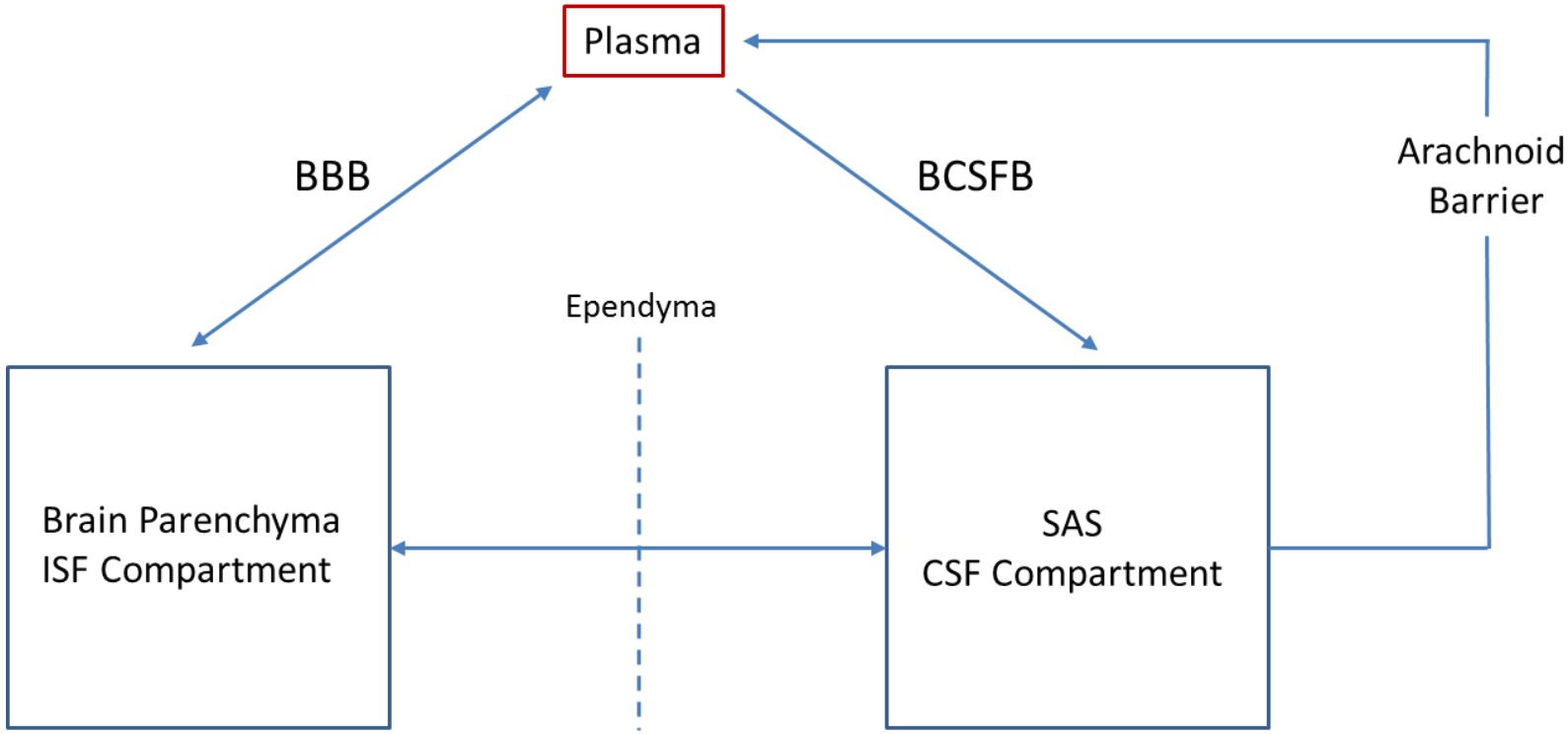

Figure 1.1: Diagram of the CSF and ISF movement between the brain barriers.
Fluid movement is shown by the blue arrows between the BBB (brain capillary endothelium); BCSFB (choroid plexus epithelium) into the brain compartments and drainage through the arachnoid barrier back into the blood (based on information by Abbott et al. 2010).

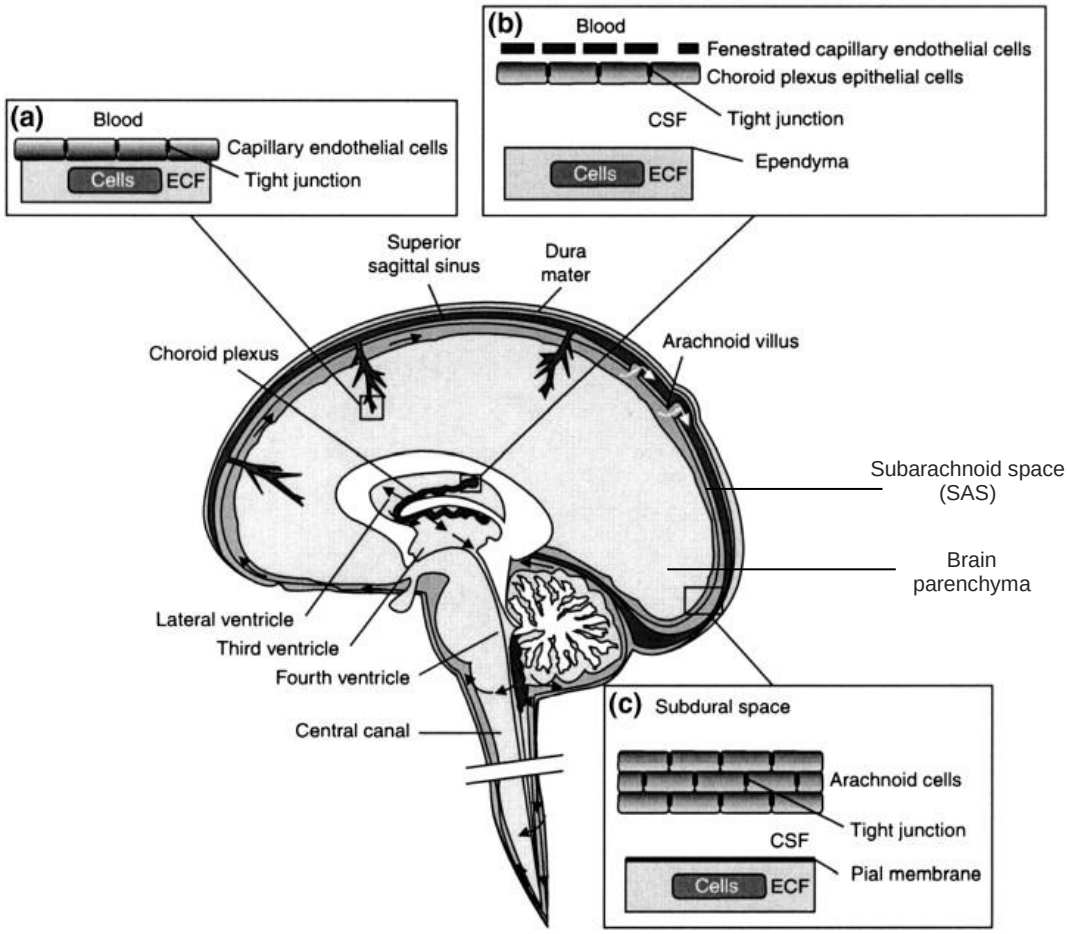

Figure 1.2: Three main barrier sites between the brain and the blood.
(a) The BBB consists of the cerebral capillary endothelial cells joined by tight junctions. (b) The BCSFB is located at the choroid plexuses consisting of epithelial cells joined by apical tight junctions in the lateral, third and fourth ventricles of the brain. (c) The arachnoid barrier lies next to the dura which separates the arachnoid membrane from the superior sagittal sinus. The arachnoid epithelium is joined by tight junctions between cells of the inner layer. ECF refers to extracellular fluid and interstitial fluid (Kandel et al. 2000).

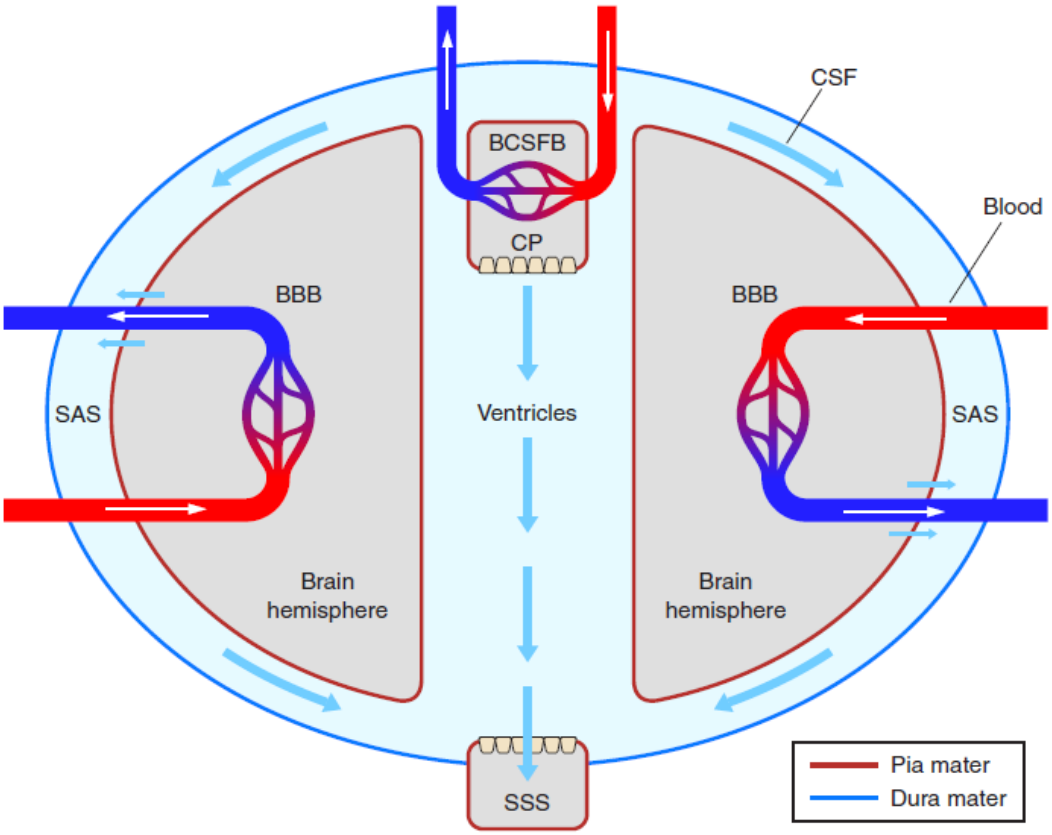

Figure 1.3: The fluid compartments in the brain.
The choroid plexus (CP) or blood CSF barrier (BCSFB) secretes cerebrospinal fluid (CSF, blue arrows) which flows through the ventricle system into the subarachnoid space (SAS). The SAS is located between the dura and the pia mater. CSF returns to the venous blood and into the superior sagittal sinus (SSS). The blood-brain barrier (BBB) limits the blood supply to the brain. The brain interstitial fluid makes up the final portion of CSF and drains to the SAS though the perivascular spaces (small blue arrows) (Damkier et al. 2013).

1.2 Interstitial fluid and the blood-brain barrier

Fluid that surrounds the tissue cells of all multicellular organisms is known as the ISF. Within the brain, ISF is produced by the brain capillary endothelium which forms the BBB. Characteristics of the BBB endothelial cells which differ from endothelial cells in the rest of the body include the absence of fenestrations and a greater number of tight junctions. The roles of these tight junctions include limiting the paracellular pathway (between cells) and this the flux of hydrophilic molecules across the BBB (Abbott et al. 2010) (Ballabh et al. 2004).

As well as the endothelial cells, the BBB is formed of the capillary basement membrane, astrocytes, microglia, neurons, and pericytes; the structure better described as a neurovascular unit (Figure 1.4) (Ballabh et al. 2004) (Brinker et al. 2014). Pericytes are important for the structural integrity of the vessel and formation of endothelial tight junctions (Allt & Lawrenson 2001) (Balabanov & Dore-Duffy 1998). The astrocytes form a barrier surrounding the cerebral capillaries. Water-transporting pores, or aquaporins, located on the astrocytic end feet play a role in maintaining brain water homeostasis (Rash et al. 1998).

In adult humans, the BBB surface area ranges from 12 to 18m^2 and is the largest of the three barrier sites between the brain and the blood for exchange. Each endothelial cell is at most approximately 25 μm from a neurone allowing for short solute and drug diffusion distances, making the BBB the favoured route for delivery of drugs to the brain (Abbott et al. 2010). Movement of solutes across the BBB is

either passive, driven by a concentration gradient from plasma to brain, or facilitated by passive or active transporters in the endothelial cell membranes (Abbott et al. 2010).

The role of the BBB in ISF production involves ISF flow being driven by the ionic gradient set up by the abluminal Na^+-K^+-ATPase transporter (Abbott 2004). Water passes through the endothelial cell membrane, driven by a hydrostatic pressure gradient, before entering the perivascular space from where it flows along neuronal tracts and blood vessels. However, bulk ISF flow is not permitted due to the narrow spaces between cells within the neuropil (a network of nerve fibres) as described in Figure 1.5 (Abbott 2004).

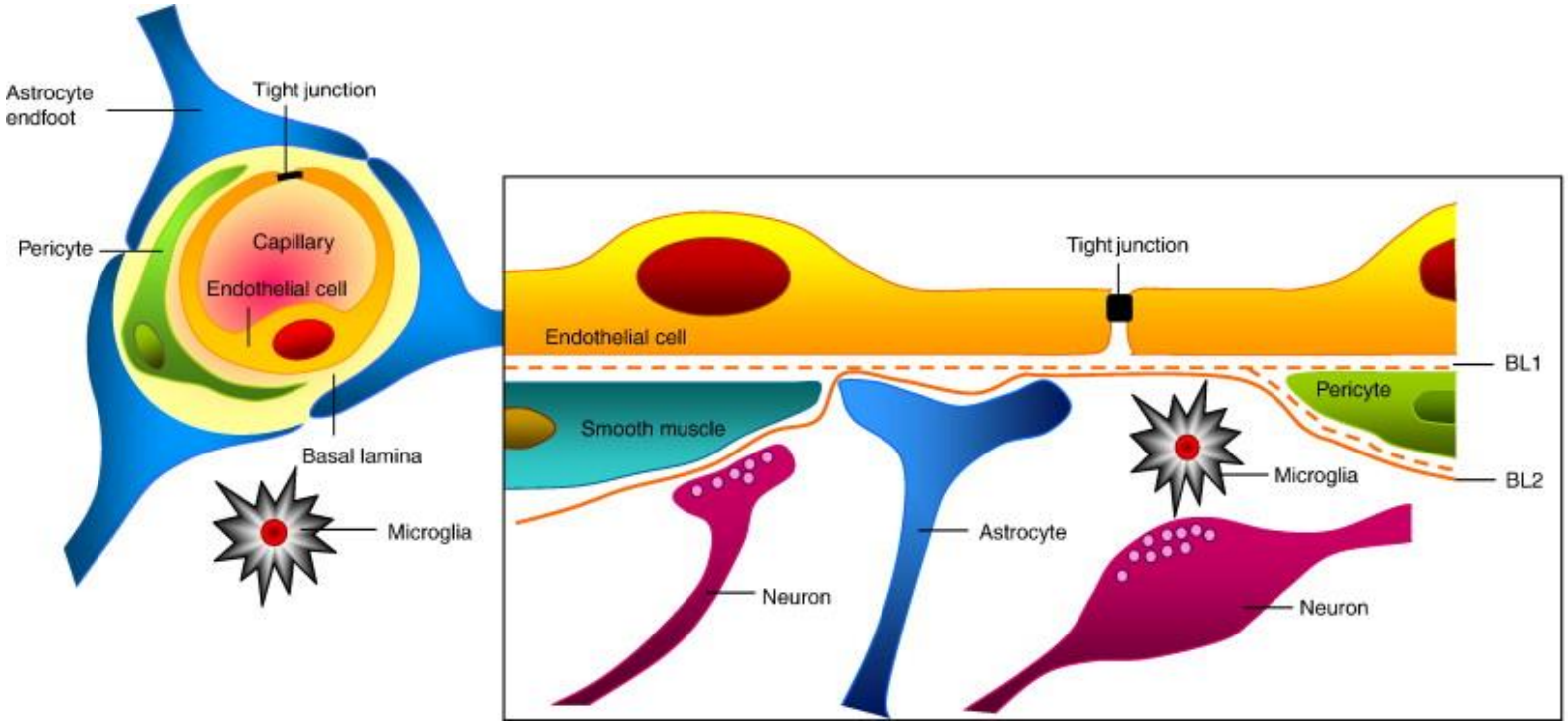

Figure 1.4: The BBB cellular architecture.

Tight junctions are formed between the endothelial cells and are surrounded by pericytes. The endothelial cells and the pericytes form the basement membrane and perivascular extracellular matrix (basal lamina 1, BL1). The extracellular matrix binds the brain parenchyma (BL2). Astrocytes surround the capillaries. Cerebral blood is regulated by axonal projections from neurons onto smooth muscle cells. Normal immune responses are regulated by microglia (Abbott et al. 2010).

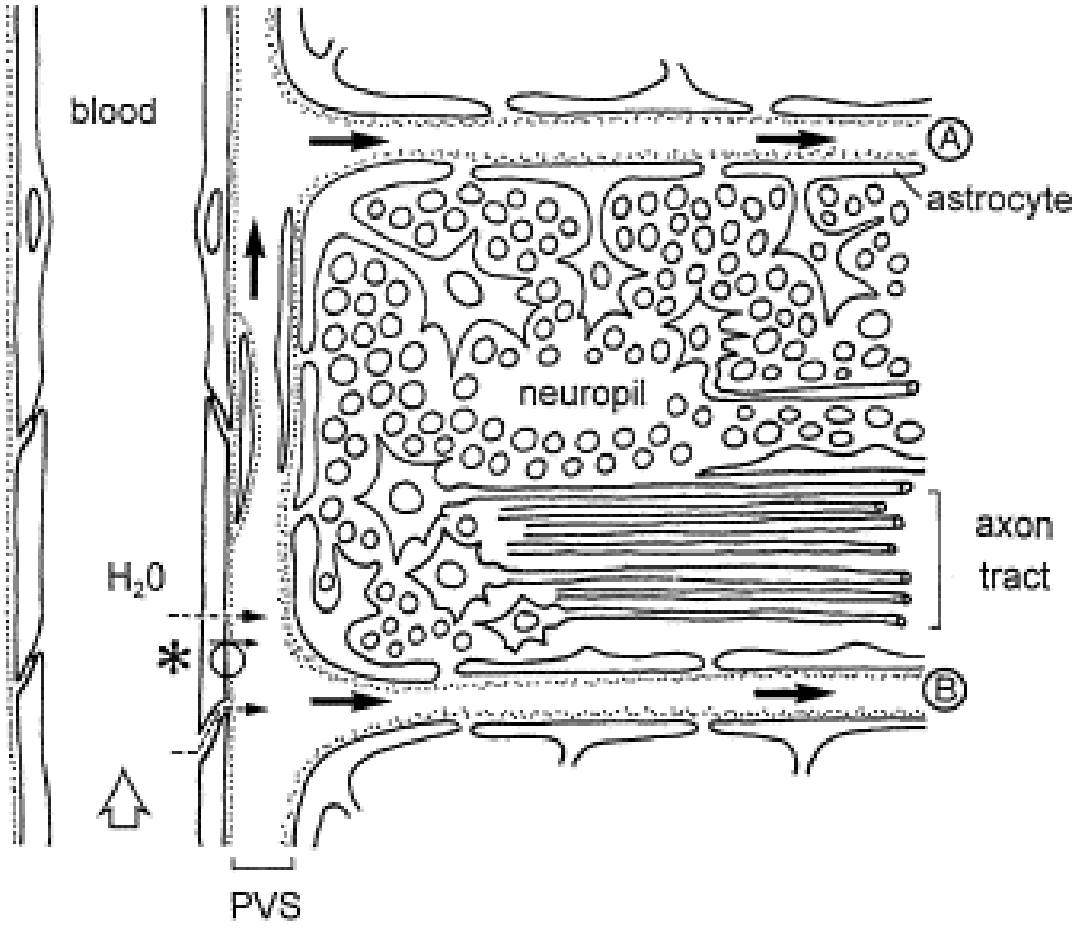

Figure 1.5: Routes of ISF generation and flow.
ISF is formed by brain capillary endothelium, generated by the abluminal Na^+-K^+-ATPase ionic gradient (circle + arrow). ISF enters through the tight junctions of the endothelial cells (dashed arrows) and moves into perivascular spaces with the aid of a hydrostatic pressure gradient, joining between blocks of neuropil (A), and areas next to axon tracts (B) (Abbott 2004).

The choroid plexus has a greater secretory capacity than the BBB ($ml \cdot min^{-1} \cdot g\ tissue^{-1}$ surface area) which explains the large amount of CSF secretion by the BCSFB (Damkier et al. 2013), detailed further in Section 1.3.

1.3 Cerebrospinal fluid production

CSF is a clear fluid that surrounds the brain and spinal cord and is produced by the epithelial cells of the choroid plexus. The choroid plexuses are anatomical structures in the third, fourth and lateral ventricles within the brain (Figure 1.6) formed of blood vessels lined by the choroidal epithelium. The capillary endothelium in the choroid plexus is fenestrated and surrounded by these epithelial cells, joined by tight junctions, all of which constitute the BCSFB and control CSF composition (Figures 1.7 and 1.8) (Valls-Solé 2004).

Each choroid plexus consists of branches protruding into the CSF. Each protrusion consists of several villous processes. The epithelium lies on the basal lamina (stemming from the adjacent ependyma lining the ventricle walls), which defines the inner stromal core consisting of connective collagen tissue, fibroblasts, macrophages, dendritic cells and smooth muscle cells. Microvilli, cilia, and tight junctions are found on the apical surface of the epithelium, and large fenestrated capillaries are found within each villus of the choroid plexus (Figures 1.7, 1.8 and 1.9) (Strazielle & Ghersi-Egea 2000).

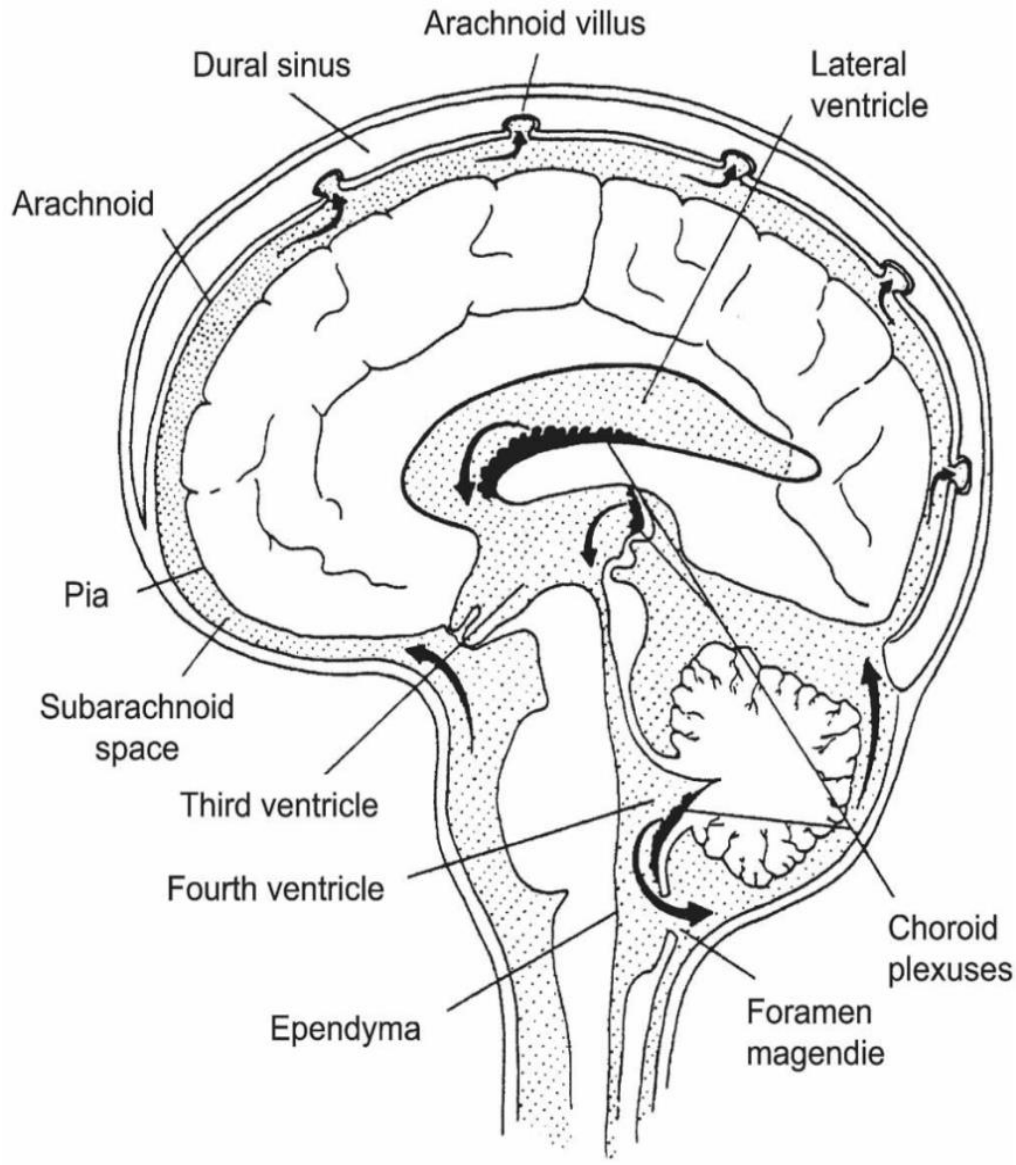

Figure 1.6 The locations of the choroid plexuses and the circulation of CSF in the human brain.
The stippled area indicates the distribution of CSF and the arrows indicate the direction of flow (Brown et al. 2004).

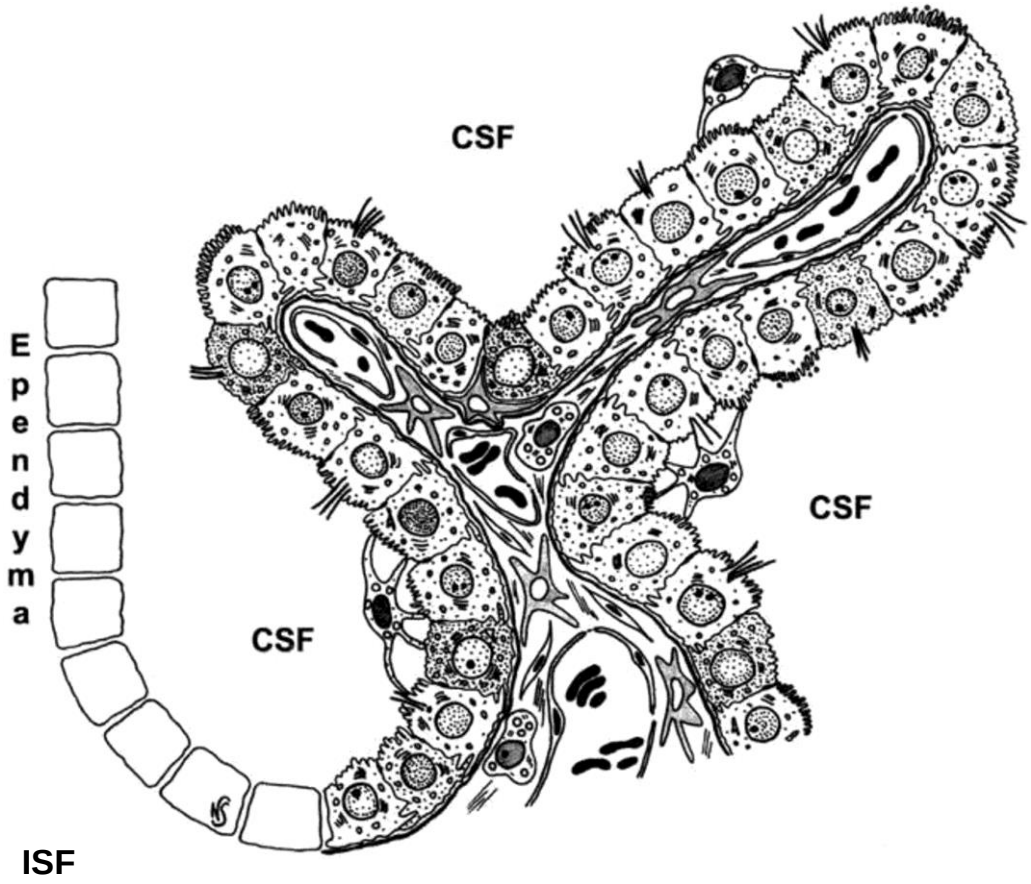

Figure 1.7: Schematic cross-section showing the main features of the choroidal tissue.

Fenestrated capillaries with thin endothelial walls are located within each villus and are covered by a single layer of epithelial cells, held together by apical tight junctions. Each villi projects into the CSF and contains several microvilli and cilia located on the apical surface. The cuboidal epithelium is situated on the basal lamina which covers an inner stromal core of connective and highly vascularized tissue, which stems from the adjacent ependyma lining the ventricle walls (Strazielle & Ghersi-Egea 2000).

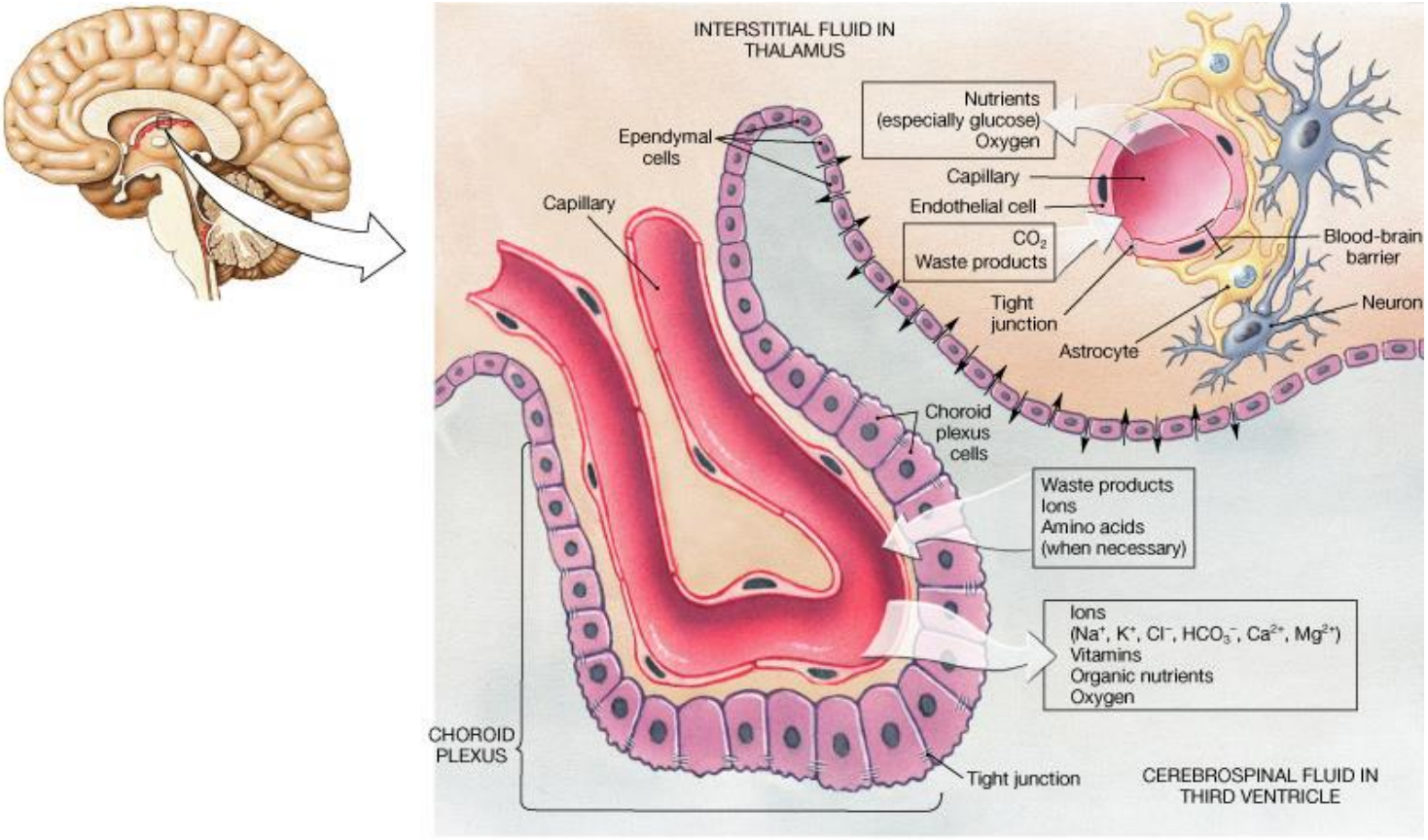

Figure 1.8: Schematic representation of the location of the choroid plexus (BCSFB) and BBB.
Capillaries are covered by a single layer of epithelial cells, held together by tight junctions which permit the movement of ions and water across the epithelium and into the CSF compartment (Brown et al. 2004) .

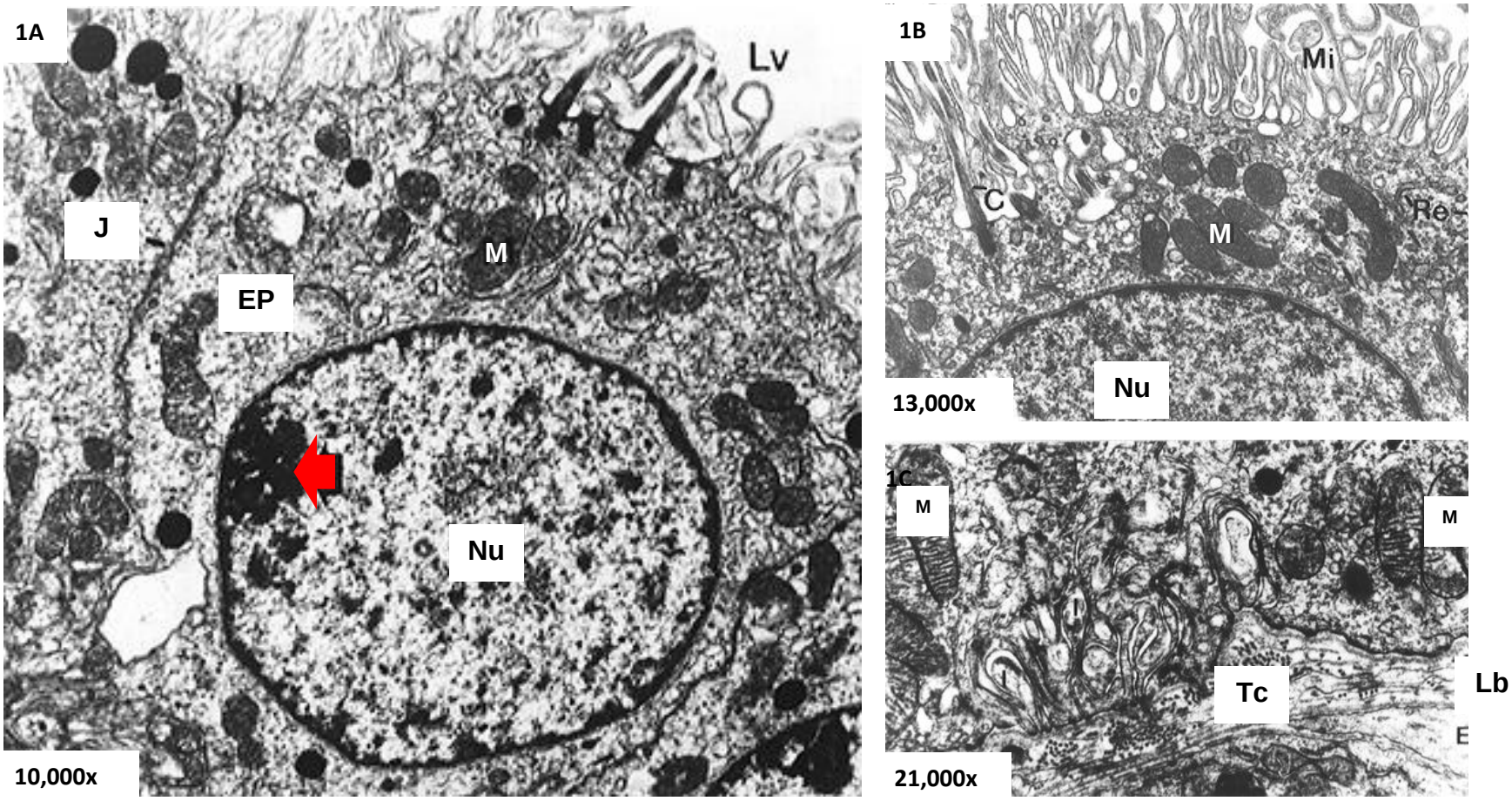

Figure 1.9: Electron micrographs of the rat lateral ventricles choroid plexuses.
Fig. 1A: Cuboidal epithelial cell (Ep) of the choroid villus illustrating the tight junction (J), ventricular lumen (Lv), mitochondria (M), nucleus (Nu) and nucleolus (arrow). Fig. 2A: Apical membrane of the choroid epithelial cell showing the cilium (C); golgi complex (G); microvilli (Mi); mitochondria (M); nucleus (Nu) and rough endoplasmic reticulum (Re). Fig. 1C: Basal portion of the choroid epithelium. Basolateral interdigitations (I) are located between the choroid epithelial cells. Endothelium (End), basal lamina (Lb), mitochondria (M) and connective tissue (Tc) (Tirapelli et al. 1998).

The CSF, secreted from the choroid plexus epithelial cells, travels through the lateral and third ventricles before exiting through the fourth ventricle and into the SAS or spinal cord, where it is absorbed via the arachnoid villi into the dural venous sinuses (Figure 1.6) (Valls-Solé 2004).

The total volume of CSF within adult humans is ±140 ml and the rate of secretion by each choroid plexus is 0.2 ml/min (Speake et al. 2001). The pressure required for the circulation of CSF is maintained by a hydrostatic pressure gradient between the choroid plexus (where CSF is produced) and the arachnoid villi (where CSF is drained) (Valls-Solé 2004). The choroid plexus epithelial cells are indispensable for directed transport processes from blood into the CSF, for the removal of substances out of the brain, and for CSF production (Haselbach et al. 2001).

1.4 Molecular mechanisms of fluid secretion

In terms of the location of ion transporters and channels on epithelial cells; the mechanism of CSF secretion in the choroid plexus shares similarities with, but is slightly different to fluid secretion by other epithelia such as the renal proximal tubule, the gall bladder or submucosal glands. Therefore, it is important to understand how fluid is secreted in the other epithelia first (Figure 1.10). Fluid secretion by epithelial cells depends on the transport of ions, facilitated by transport proteins that are found in the apical (lumen) and basolateral (blood) membranes of the cells, and which create an osmotic gradient that drives the movement of water (Hladky & Barrand 2016).

The net movement of Na^+ and Cl^-, in the apical direction, creates the osmotic gradient, which is strong enough to drive water secretion across the epithelium through aquaporin (AQP) water channels located in the basolateral (water secreted into the cell) and apical membranes (water secreted out of the cell) (Brown et al. 2004).

When comparing the choroid plexus epithelium to most other epithelia, for example, the basolateral membranes contain the Na^+-K^+-ATPase pump which drives Na^+ efflux and K^+ influx using energy from the hydrolysis of adenosine triphosphate (ATP) (Damkier et al. 2013). The influx of Cl^- occurs through the Na^+-K^+-$2Cl^-$ (also known as NKCC1) cotransporter which is also located on the basolateral membrane. This activity is helped by Na^+-H^+ (NHE1) and Cl^--HCO_3^- (AE2)

exchangers which are also localised on the basolateral membrane (Damkier et al. 2013) (Brown et al. 2004).

Influx of Cl^- takes place against the electrochemical gradient by secondary active transport driven by the Na^+ gradient. Cl^- then exits the cell through Cl^- channels in the apical membrane (Damkier et al. 2013). The cell forces Na^+ out by the basolateral Na^+-K^+-ATPase in other epithelia, and Na^+ possibly translocates to the apical side via the tight junctions driven by the apical-negative voltage created by the transepithelial Cl^- transport (Damkier et al. 2013).

The K^+ channels in other epithelia, such as the submucosal glands, is located on the basolateral membrane, which allow K^+ influx through Na^+-K^+-ATPase pump and Na^+-K^+-$2Cl^-$ cotransporter (Hertz et al. 2013). Cell swelling as a consequence of the K^+ accumulation is prevented by the loss of K^+ from the cell via a K^+ channel located on the basolateral membrane (Speake et al. 2001).

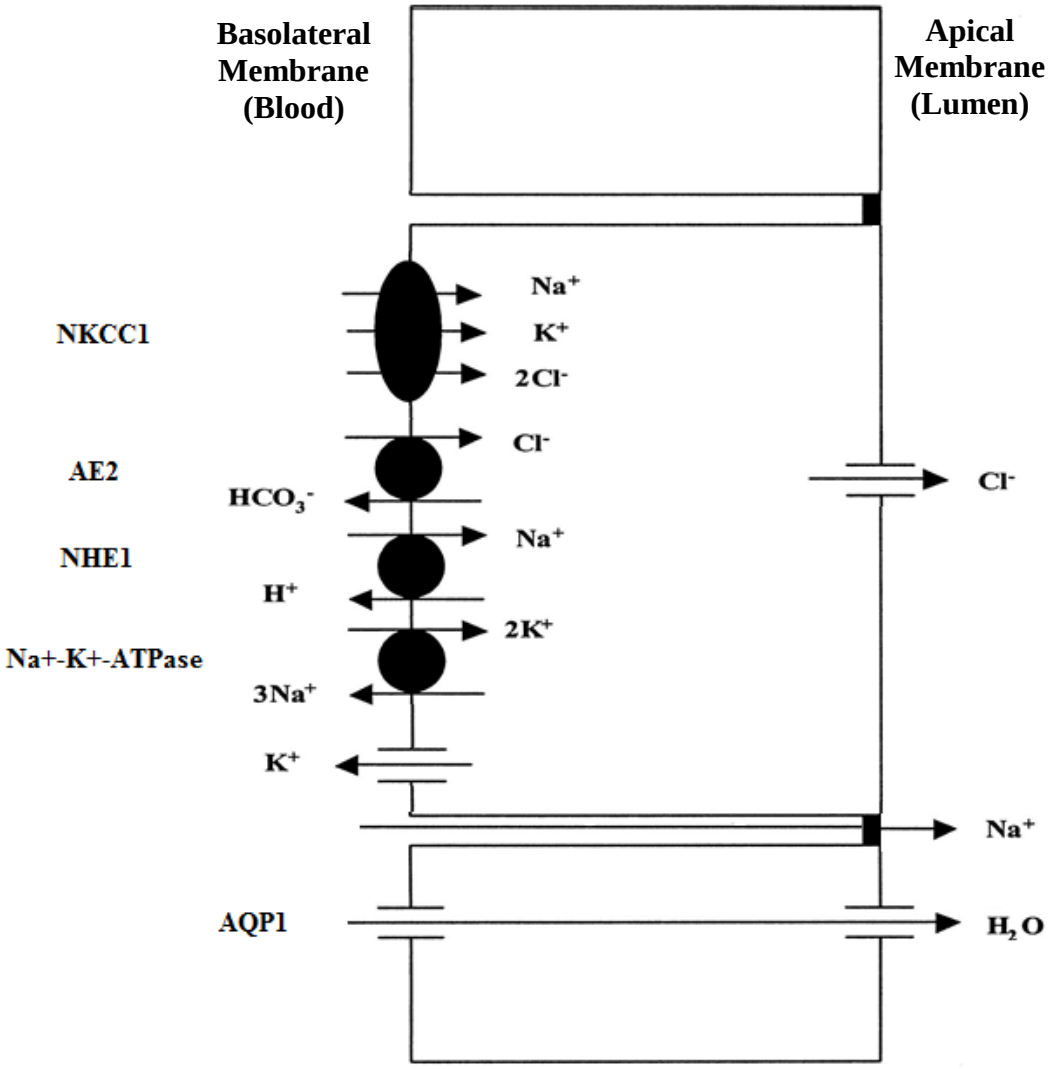

Figure 1.10: The model of epithelial fluid secretion.
The net transport of Na^+, Cl^-, and water, from basolateral (blood) to apical (lumen) membranes, with K^+ movement in the opposite direction and with schematic locations of ion transporters in other epithelia such as the renal proximal tubule, gall bladder and submucosal glands (based on diagram by Speake et al., 2001 and Hladky & Barrand 2016).

1.4.1 Ion movement and CSF secretion in the choroid plexus

As mentioned previously, CSF secretion takes place within the choroid plexus, with the choroid plexus epithelial cells transporting fluid from the basolateral (blood) to the apical (CSF) compartments (Figure 1.11).

In choroid plexus epithelia, the Na^+-K^+-ATPase, NKCC1 transporters, K^+ (KCC4, Kv1.1 and 1.3, Kir7.1), HCO_3^- (NBCe2) and Cl^- (CIC-2) channels are all expressed on the apical membrane (Figure 1.11), as opposed to other epithelia as shown in Figure 1.10. The basolateral transporters such as AE2 and NHE1, occupy the same membrane domain as in other epithelia. The molecular mechanisms of fluid transport in choroid plexus epithelia are further described from Section 1.4.2.

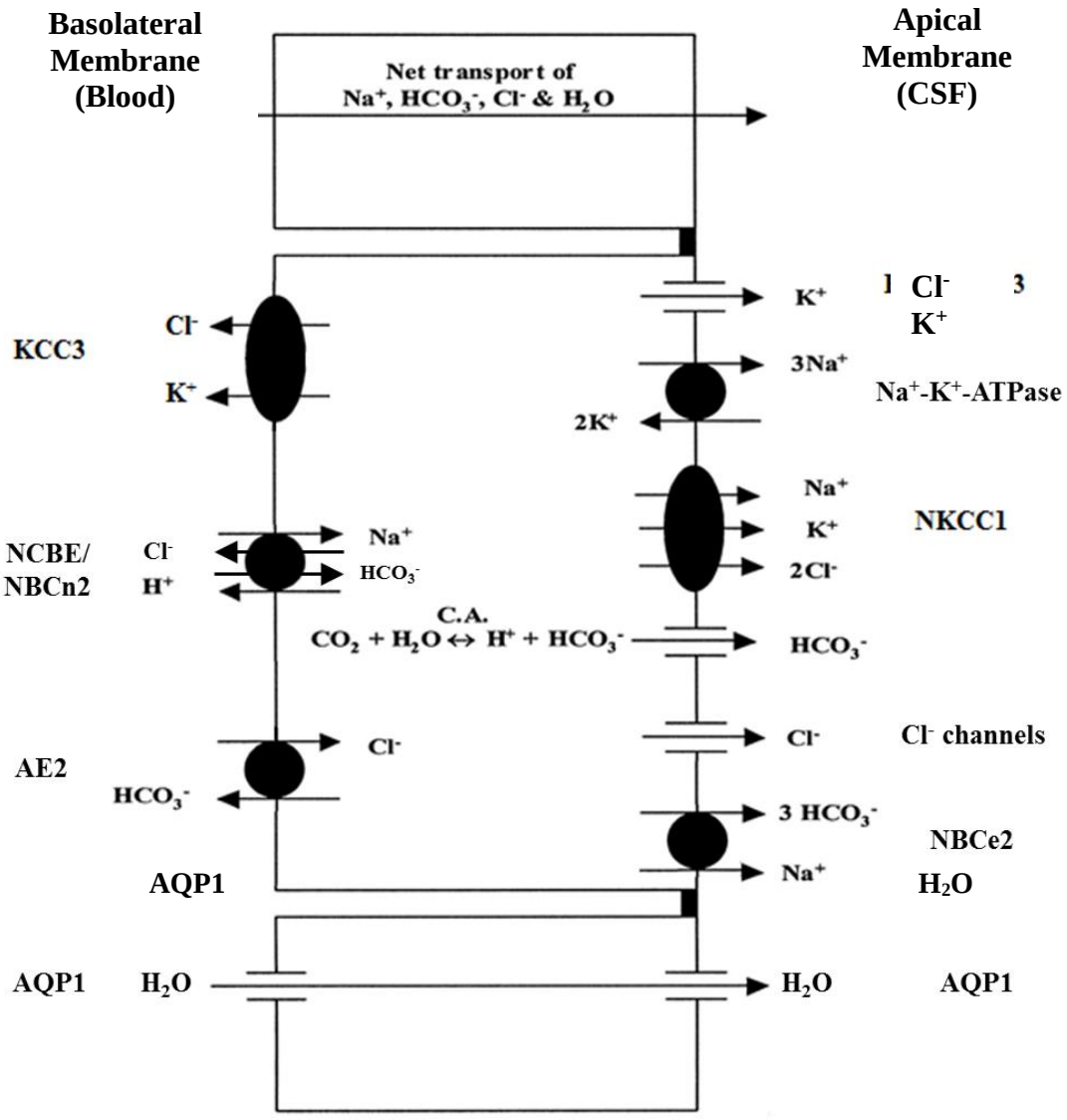

Figure 1.11: Mechanism of CSF secretion within choroid plexus epithelium. The net transport of Na^+, K^+, Cl^-, HCO_3^- and water, from basolateral (blood) to apical (CSF) membranes, with schematic locations of ion transporters. C.A refers to carbonic anhydrase. (Based on diagram by Hladky & Barrand 2016).

1.4.2 Regulation of Na^+ transport

As with other secretory epithelia, the main driving force for fluid movement across the choroid plexus is provided by the Na^+, K^+-ATPase or Na^+-pump (Hladky & Barrand 2016). However, when studying choroid plexus epithelial cells, it is evident that Na^+-K^+-ATPase is located, not in the basal (blood-facing) membrane, but in the apical (CSF-facing) membrane (Figure 1.11) (Speake et al. 2001); driving the efflux of Na^+ into the CSF. The cells build up an ion gradient across the cell monolayer due to the increase in transepithelial resistances and the polar distribution of Na^+-K^+-ATPase at the apical side (Brown et al. 2004). Na^+ ions are then actively transported out of the epithelial cells into CSF thereby reducing intracellular [Na^+] and providing a gradient for Na^+ influx via other transporters. Na^+ entry from the basolateral side occurs by the NBCn2/NCBE Na^+, HCO_3^- cotransporter. Some Na^+ leaves the cell across the apical membrane towards the CSF via NBCe2 (sodium bicarbonate electrogenic transporter number 2) driven outward by the coupled outward flux of 3 HCO_3^- ions (Hladky & Barrand 2016). Regulation of the rate of net Na^+ transport is almost equivalent to regulation of the rate of CSF fluid secretion.

There may also be a net flux of Na^+ that cross the epithelial layer via the paracellular route through tight junctions. The claudins present in these tight junctions are expected to allow passive movement of small univalent cations and water (Hladky & Barrand 2016). Thus there should be observable tracer fluxes of Na^+ in each direction but with a net paracellular flux that is smaller than the transcellular movements (Daneman 2012).

Na^+-K^+-ATPase contains two subunits, α and β, with the α containing the ATP and cardiac glycosides binding sites (the latter being the site for Na^+-K^+-ATPase inhibition by [^{3}H]-ouabain) (Speake et al. 2001). Isoenzymes $\alpha_1\beta_1$ and $\alpha_1\beta_2$ are expressed in the rat lateral ventricle choroid plexuses (Zlokovic et al. 1993), whereas, in most other epithelia only the $\alpha_1\beta_1$ isoform is expressed. The presence of the β_2 subunit may be important in determining the apical localisation of the Na^+-K^+-ATPase in choroid plexus epithelium (Rizzolo 1998).

The Na^+-K^+-ATPase pump is also expressed in the apical membrane in retinal pigmented epithelium (Lobato-Álvarez et al. 2016). As the location of ion channels is similar within the choroid plexus and retinal epithelium, then the molecular mechanisms of fluid secretion pathways might be expected to be analogous. Cortisol is a potent anti-inflammatory and there is evidence that cortisol generation by 11β-hydroxysteroid dehydrogenase type 1 (11β-HSD1) enzyme stimulates serum and glucocorticoid-regulated kinase-1 (SGK1) pathways to increase the movement of Na^+ in the ocular ciliary epithelium (Sinclair et al. 2010) (see Section 1.9 and Figure 1.12). A similar system has also been postulated within the choroid plexus epithelium, in which the up-regulation of SGK1 stimulates movement of Na^+ across the apical membrane, into the CSF, through epithelial sodium channels (ENaC) (Sinclair et al. 2010). The ENaC heterotetramer consists of two α, one β and one γ subunit. Expression of all subunits leads to generation of a small sodium influx across the apical membrane across choroidal epithelium; however an efflux into the CSF could also be seen (Rauz et al. 2003).

1.4.3 Na^+- K^+-ATPase inhibition

Administration of the neurotransmitter serotonin has been shown to decrease the secretion of CSF in porcine choroid plexus. Serotonin binds to the 5-HT receptor on choroid epithelial cells (Pazos et al. 1984) in turn activating phospholipase C (Conn et al. 1986), which forms diacylglycerol, by the cleavage of phospholipids. This leads to the activation of protein kinase C (PKC), which is an enzyme involved in controlling the function of other proteins through the phosphorylation of hydroxyl groups. The Na^+-K^+-ATPase pathway can be inhibited through the activation and phosphorylation of PKC (Fisone et al. 1995), leading to a 50% reduction in activity due to phosphorylation of the Na^+-K^+-ATPase α-subunit. The resulting inhibition of the movement of Na^+ as well as the consequent movement of HCO_3^- and Cl^- into the ventricle has the effect of decreasing the osmotic gradient needed for the diffusion of water across the choroid plexus epithelium (Conn et al. 1986).

Cyclic guanosine monophosphate (cGMP) is shown to reverse the movement of ions in the choroidal epithelium, leading to a reduction in CSF secretion (Kolb et al. 1994). cGMP is a cyclic nucleotide that acts as a second messenger. cGMP-generating agent, atrial natriuretic peptide (ANP) has been shown to activate the guanylate cyclase-cGMP system which caused a decrease in CSF production that correlated with an increase in cGMP production within the choroid plexus (Steardo & Nathanson 1987). In tubular epithelial cells within the kidney, ANP modulates sodium and potassium-activated ATP leading to cGMP-dependent protein kinase G (PKG) inhibition of Na^+-K^+-ATPase (Ellis et al. 2000). There is no evidence of whether this pathway of Na^+-K^+-ATPase inhibition occurs in the choroid plexus epithelial cells**.** However, the increase

in cGMP levels within choroid plexus epithelia could be a possible mechanism in decreasing CSF production through the inhibition of the Na^+-K^+-ATPase transporter.

1.4.4 Na^+-$2Cl^-$-K^+ (NKCC1) transporter

As described in Figure 1.11, the process of CSF production involves the transport of Na^+, Cl^-, K^+ and HCO_3^-. As well as the Na^+-K^+-ATPase transporter, the NKCC1 transporter is also located in the apical membrane of choroidal epithelia (Hladky & Barrand 2016) (Wu et al. 1998). NKCC1 plays a role in regulating cell volume and transepithelial ion transport (Russell 2000) by mediating Na^+, K^+ and Cl^- efflux into the CSF (Keep et al. 1994). However, other studies focused on epithelial cell volume strongly imply that NKCC1 mediates net influx (Crum et al. 2012) (Wu et al. 1998). The results may all correctly reflect the conditions in which they have been measured because the net driving force, derived from the concentrations of Na^+, K^+ and Cl^-, is finely balanced and NKCC1 could be transporting in either direction (Damkier et al. 2013) (Hladky & Barrand 2016).

1.4.5 K^+ transport

The activity of the Na^+-pump increases the concentration of K^+ into the choroid plexus epithelial cells from the CSF. All other routes for K^+ transport mediate net K^+ efflux or in the case of NKCC1 the direction of transport is finely balanced, as mentioned in Section 1.1.4. Almost all of the K^+ that enters the choroid plexus epithelial cells from the CSF is recycled to the CSF via a combination of KCC4, K^+ channels (Kv 1.1, 1.3 and Kir 7.1) and NKCC1, all of which are known to be present in the apical membrane (Hladky & Barrand 2016).

1.4.6 HCO_3^- and Cl^- transport

HCO_3^- enters the choroid plexus epithelial cells via the either the NBCn2 or NCBE transporter (Hladky & Barrand 2016). If this transporter operates with stoichiometry of 1 Na^+ and 1 HCO_3^- moving inwards the name NBCn2 (sodium bicarbonate neutral transporter number 2) is appropriate. Alternatively, if 1 Na^+ and 1 HCO_3^- move inwards and 1 H^+ and 1 Cl^- outwards the name should be NCBE (sodium driven chloride bicarbonate exchanger) which effectively loads the cell with 2 HCO_3^- for each Na^+ transported. A study by Damkier and colleagues describe the sodium bicarbonate transporter rat gene (SLC4a10) when expressed in mouse NIH-3T3 fibroblasts behaves as Ncbe (Damkier et al. 2010) while studies by Parker and colleagues describe the human gene when expressed in *Xenopus laevis* oocytes behaves as NBCn2 (Parker et al. 2008). Therefore, the mode of operation of the transporter is determined by the type of cell in which the gene is expressed or by the species of the gene.

Additional Cl^- uptake on the basolateral surface is increased through the exchange between Cl^- and HCO_3^- (see Figures 1.11 and 1.12). HCO_3^- and H^+ are produced from H_2O and CO_2, in a reaction catalysed by carbonic anhydrase (Haselbach et al. 2001). This enzyme is expressed in the cytoplasm of rat choroid plexus epithelial cells (Masuzawa & Sato 1983). Cl^- channels play a major role in fluid secretion in epithelial cells. In the choroid plexus, a 'CIC-2' named Cl^- anion channel with a high HCO_3^- permeability has been shown to be involved in CSF secretion (Saito & Wright 1984). It is located on the apical membrane and is essential for HCO_3^- and Cl^- efflux into the CSF in the lateral ventricles of the rat brain (Speake et al. 2001). Anion channels are activated by cAMP and protein kinase A (PKA) (Deng & Johanson 1992), and

intravenous injection of forskolin, a cAMP agonist, caused a 17-33% increase in Cl^- movement into the CSF in adult rats (Deng & Johanson 1992).

HCO_3^- leaves the epithelial cell into CSF via NBCe2 as indicated in Figure 1.11 and possibly via anion selective channels (Hladky & Barrand 2016). Coupling of Na^+ entry to influx of one HCO_3^- ion per Na^+ ion (NCBE/NBCn2) implies that more HCO_3^- enters the cell on the basolateral membrane than appears in CSF. The remaining HCO_3^- ion concentration recycled across the basolateral membrane via the Cl^-/HCO_3^- exchanger AE2 (Hladky & Barrand 2016). This is also the only known route for net entry of Cl^- into the choroid plexus epithelial cells from the blood. In addition, a small amount of Cl^- returns to the blood with K^+ via the KCC3 cotransporter (Hladky & Barrand 2016).

Cl^- efflux from the epithelial cells appears to involve both transporters and channels (Keep et al. 1994). On the apical membrane Cl^- leaves the choroid plexus epithelial cells to the CSF by cotransport with K^+ mediated by KCC4 and via anion channels that have been observed functionally but whose molecular identities are as yet unknown (Hladky & Barrand 2016).

1.4.7 Aquaporin-1

Aquaporins are a family of integral membrane proteins that function as water channels. Aquaporins are distributed widely throughout the body including red blood cells, lung and secretory epithelia such as the salivary glands, but most notably in the kidney where they are expressed in higher levels (Speake et al. 2001). Aquaporin 1 (AQP1) protein is expressed in the apical membrane of rat choroid plexus epithelial

cells and may mediate water transport across the membrane during CSF secretion (Figures 1.11 and 1.12) (Wu et al. 1998). A role for AQP1 in CSF secretion is supported by evidence from Oshio and co-workers, who reported reduced CSF production and intracranial pressure (ICP) in mice lacking AQP1 (Oshio et al. 2005). The reduced ICP correlated with the reduction of CSF production in AQP1 null mice.

AQP1 is co-expressed with thyroid transcription factor-1 (TTF-1) protein in rat choroid plexus, which enhances AQP1 gene transcription. Intraventricular injection of antisense TTF-1 oligodeoxynucleotide in rats resulted in a reduction of AQP1 mRNA and protein in the choroid plexus (Kim et al. 2007), resulting in decreased CSF formation. TTF-1 expression is also stimulated by glucocorticoids in the lung (Morrison et al. 2012). In a rat model, prenatal treatment with dexamethasone (a glucocorticoid) increased TTF-1 mRNA expression (Losada et al. 2000). This evidence could provide a further insight with regard to the effects of a specific endogenous glucocorticoid, cortisol (described further in Section 1.9), on CSF secretion rates but more specifically on the idea of glucocorticoids elevating CSF secretion levels through increased TTF1 and hence increased AQP1 expression; reducing CSF drainage and increasing ICP via glucocorticoid receptor-α (GR-α).

In summary, fluid secretion by the choroid plexus epithelial cells involves Na^+- K^+-ATPase, NKCC1, AQP1, ENaC and CIC-2 transporters/channels located on the apical membrane, driving the efflux of Na^+, Cl^-, K^+, HCO_3^- and H_2O into the CSF. Further transporters, AE2, NCBn1 and NCBE, located on the basolateral membrane drive the

accumulation of Na^+, Cl^- and HCO_3^- into the cytoplasm of the choroid plexus epithelial cells, eventually resulting in CSF secretion.

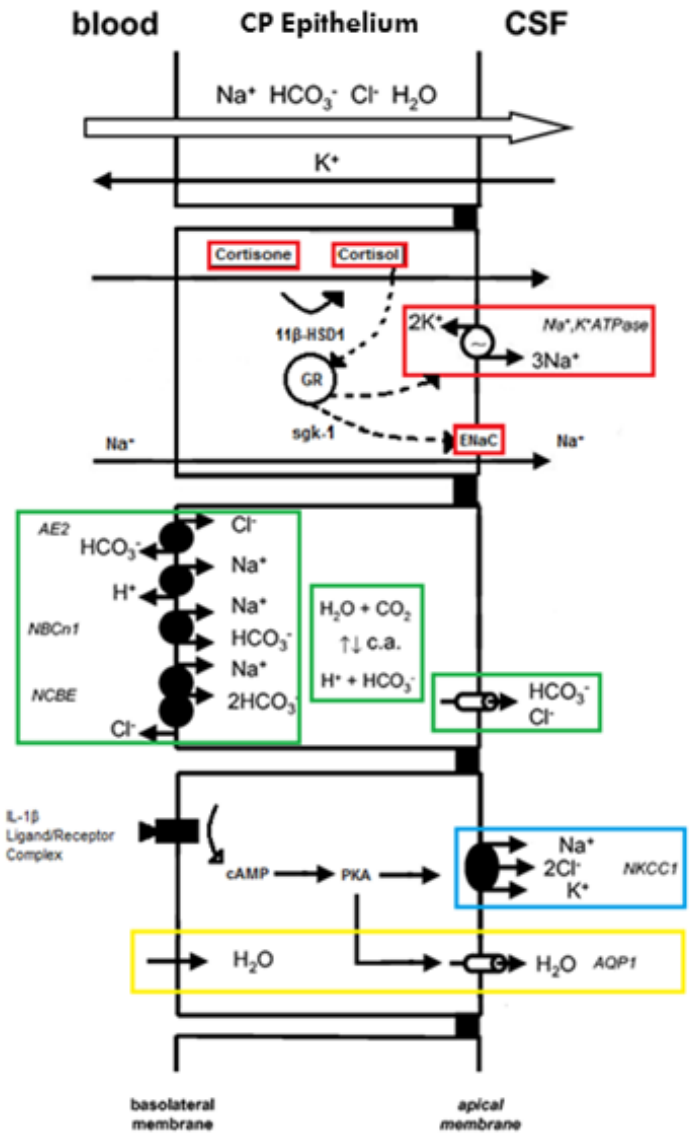

Na^+ Regulation

- Mediates $3Na^+$ and $2K^+$ exchange at the expense of a single ATP molecule.
- 11β-HSD1 generation of cortisol, with subsequent up-regulation of sgk-1. (Sinclair et al., 2010)
- Stimulates epithelial sodium transport.
- Creates an osmotic gradient to drive CSF secretion.

Carbonic Anhydrase

- Catalyzes the production of HCO_3^- and H^+ from H_2O and CO_2.
- Plays a role in CSF secretion as evidence of acetazolamide, carbonic anhydrase inhibitor, decreases CSF secretion. (Vogh et al, 1987)
- Combined action of AE2 and NBCn-1 and NCBE may explain accumulation of Na^+, HCO_3^- and Cl^- in cytoplasm of CP epithelial cells, leading to CSF secretion.

NKCC1

- PKA activation mediates Na^+, $2Cl^-$, K^+ transport.
- IL-1β and TNF-α alter fluid secretion in the gut through NKCC1. (Baniak et al., 2012)
- This transporter is also found in the CP, and is inhibited by bumetanide.

Aquaporin-1

- PKA activation mediates H_2O transport across apical membrane during CSF secretion. (Han and Patil., 2000)
- Evidence of reduced CSF production and ICP in mice lacking CP water channel AQP1. (Oshio et al., 2005)

Figure 1.12: Schematic diagram to illustrate the different transport mechanisms that are involved in regulating ion gradients and CSF secretion across the choroid plexus epithelium (own diagram based on information by Brown et al. 2004 and Hladky & Barrand 2016).

1.5 Molecular mechanisms involved in CSF drainage

As well as increased CSF secretion, a reduction in the absorption of CSF is another potential mechanism that could cause increased CSF pressure in IIH; however, the mode by which this might occur is unclear. The third barrier between the brain and the blood, the arachnoid barrier appears to be the main site of CSF drainage from the human brain, and Glueck and colleagues found microthrombi impeding CSF drainage in the arachnoid villi as a potential cause of altered CSF absorption in women with IIH (Glueck et al. 2005).

Each of the choroid plexuses secretes CSF into the respective brain ventricle (Figure 1.6 and 1.13). The ependymal epithelium, which lines the ventricles is then in contact with the CSF. The CSF and the ISF of the brain parenchyma are separated only by the perivascular space that surrounds the large blood vessels (Szentistványi et al. 1984). There is a constant directional flow of CSF from the lateral ventricles through the foramina of Monro into the third ventricle and through the aqueduct of Sylvius to the fourth ventricle. CSF exits the ventricular system through the foramina of Luschka and Magendie into the SAS (Figure 1.13). Once in the SAS, the CSF is now separated from the outer surface of the brain by the pia mater (the innermost layer of the meninges). The openings of the SAS into the dural venous system are the main sites of CSF drainage back into the blood. CSF returns to venous blood in the brain sinuses through arachnoid granulations and villi (Figure 1.14).

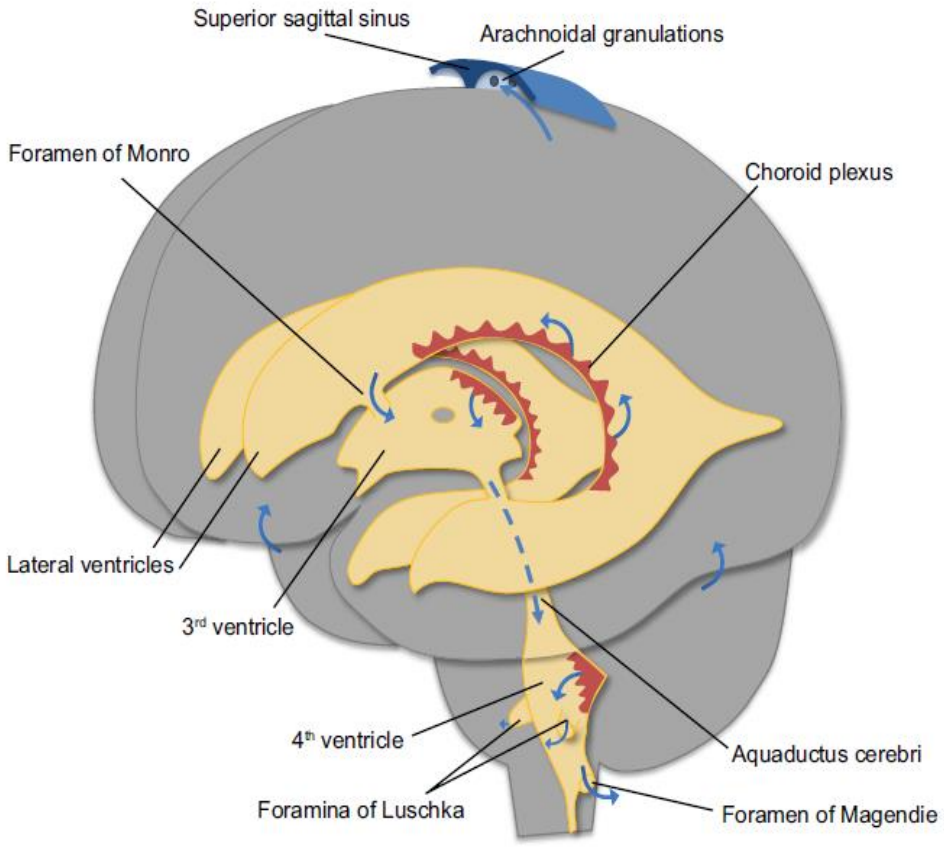

Figure 1.13: Organization of the ventricular system of the brain.
The brain parenchyma (grey), ventricles and aquaducts (yellow), and choroid plexuses (red) are shown. Lateral ventricle CSF joins in the 3rd ventricle (located between the two lateral ventricles) through the foramen of Monro and reaches the 4th ventricle through the aquaductus cerebri. The CSF leaves the 4th ventricle through the foramina of Magendie and Luschka to the CNS. The majority of the fluid is reabsorbed in the arachnoidal granulations draining to the superior sagittal sinus (Damkier et al. 2013).

The arachnoid granulations contain a central core which resembles the SAS. Endothelial cells from the venous layer, and connective tissue and fibroblasts from the dura mater form a capsule which covers the core. An arachnoid layer covers the apical part of the granulation which is in direct contact with the venous lumen (Figure 1.14) (Kida et al. 1988). Evagination of the arachnoid membrane into the lumen of the vein and therefore the dural vessel allows the communication between CSF in the SAS and blood in the dural sinus. Hydrostatic pressure is maintained in the SAS allowing the flow of CSF into the dural sinus. As the opening is valvular, the blood cannot cross in the opposite direction (Hertz et al. 2013) (Davson et al. 1987).

Although arachnoid villi and granulations are prominent in the major venous sinuses associated with the brain and spinal cord in humans, arachnoid villi are very small in rodents and sheep (Figure 1.15a) (Johanson et al. 2008). In rats, small arachnoid villi are associated with veins on the dorsal surface of the olfactory bulbs (Kida et al. 1993).

Studies of the effects of retinol (vitamin A) on IIH has found it to cause morphological abnormalities of the arachnoid villi by increasing resistance in the pia arachnoid cells (Tabassi et al. 2005). Unimpaired arachnoid villi support the flow of CSF from the arachnoid space into the bloodstream. This research also reported CSF retinol levels to be significantly higher in IIH patients (median 575.91 nM) than in 20 controls (median 63.35 nM); however, serum levels of retinol did

not differ between the two groups. These data suggest the possibility of further studies to be carried out on the effects of retinol in IIH.

Recent data suggest a second pathway of CSF drainage occurs at the lymph nodes (Figure 1.14 and 1.15). At least 50% of CSF drains to lymph nodes in rodents (Figure 1.15a) (Cserr & Knopf 1992) and the lymphatic drainage pathways are well developed in humans (Johanson et al. 2008). Injection studies in rodents have shown that CSF passes through the SAS to the inferior aspect of the olfactory bulbs and then drains into nasal lymphatics by passing through the cribriform plate and along channels adjacent to olfactory nerves (Kida et al. 1993) (Johanson et al. 2008). Similar drainage pathways have been demonstrated in humans (Weller et al. 2009), where tracers injected into the CSF, drain from the SAS into sheaths of lymphatics in the nasal mucosa (Figure 1.15b) (Johanson et al. 2008). A third route of fluid clearance through paravenous drainage pathways, the glymphatic pathway, involves the exchange of fluid between the CSF in the SAS and the ISF in the brain parenchyma (Iliff et al. 2012). The arachnoid and lymphatic CSF drainage pathways are summarised in Figure 1.16.

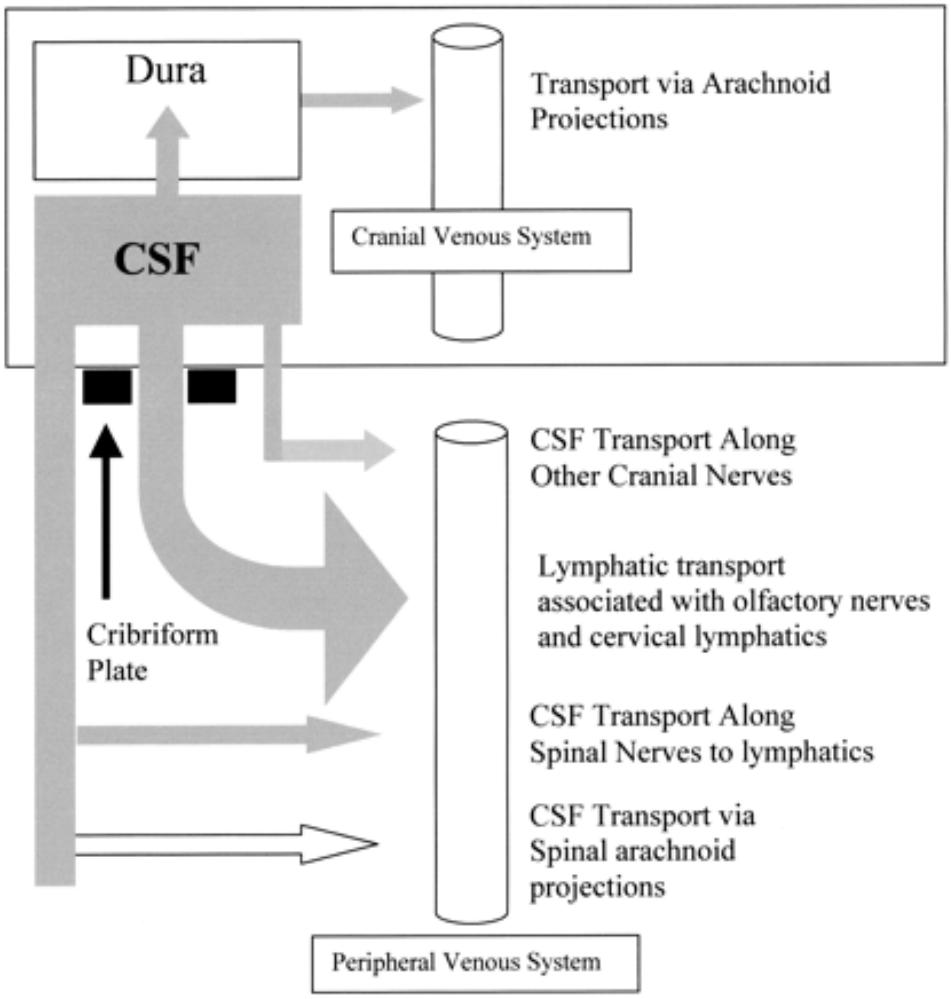

Figure 1.14: Schematic diagram of CSF drainage.
CSF is drained through the arachnoid villi into the venous sinuses of the brain and into the cervical lymphatics through the cribriform plate (Johnston & Papaiconomou 2002).

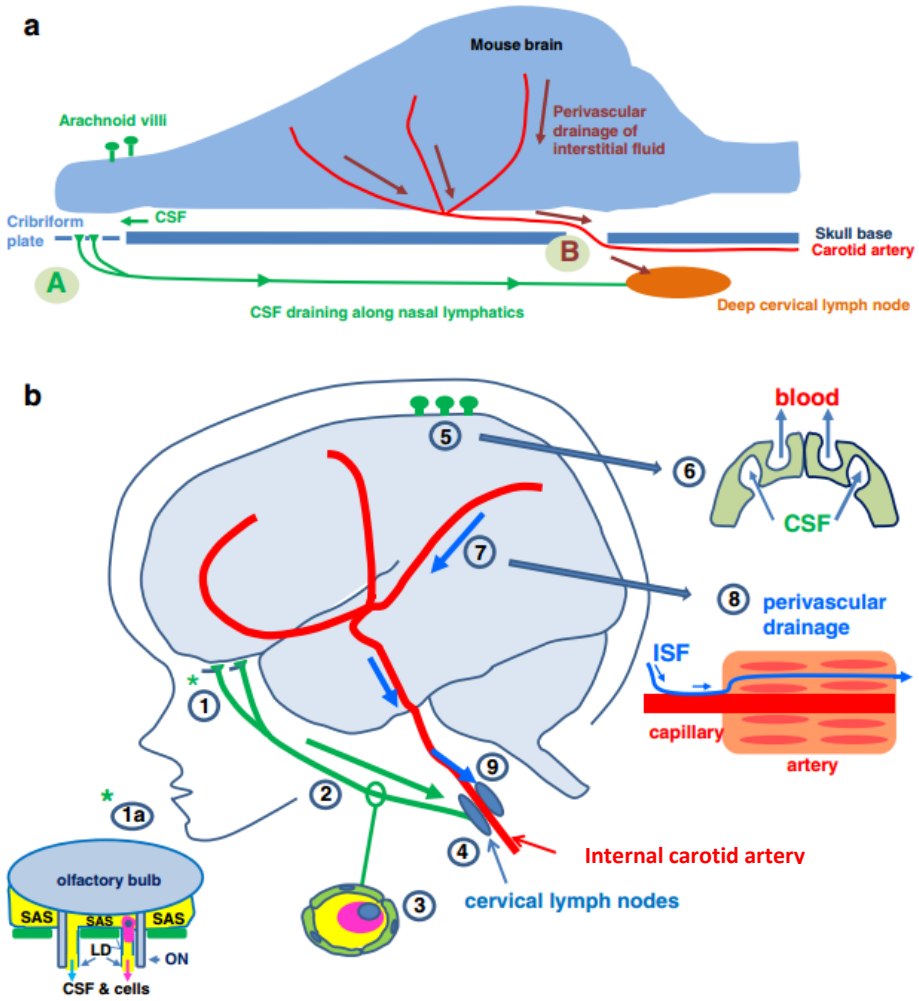

Figure 1.15: Fluid drainage pathways from brain to cervical lymph nodes in rodents and humans.

(a) Lymphatic drainage within the rodent brain. In rodents, the arachnoid villi are smaller than in humans, making the cervical lymph nodes the main site of CSF drainage, via the cribriform plate (A), from the brain. ISF is drained from the brain parenchyma along basement membranes in the walls of capillaries and arteries to the cervical lymph nodes (B). (b) Lymphatic drainage within the human brain. CSF drains from the SAS and into nasal lymphatics (1) via the cribriform plate. CSF passes alongside branches of olfactory nerves (ON) into the nasal mucosa (1a). Lymphatic vessels (2) drain CSF and cells (3) to cervical lymph nodes (4). The arachnoid villi (5) are a major site of CSF drainage from the human brain. Each villus is formed by an outpouching of the arachnoid membrane which allows the SAS to come into close contact with the blood. Hydrostatic pressure creates vacuoles which can elongate to become pores and CSF is transported transcellularly as the arachnoid cells contain tight junctions (6). ISF drains from the brain parenchyma along perivascular pathways (7) by diffusing through extracellular spaces and walls of capillaries (8). ISF also drains to the cervical lymph nodes (9) by passing first along the walls of cerebral arteries (7) and into the internal carotid artery in the neck (Laman & Weller 2013).

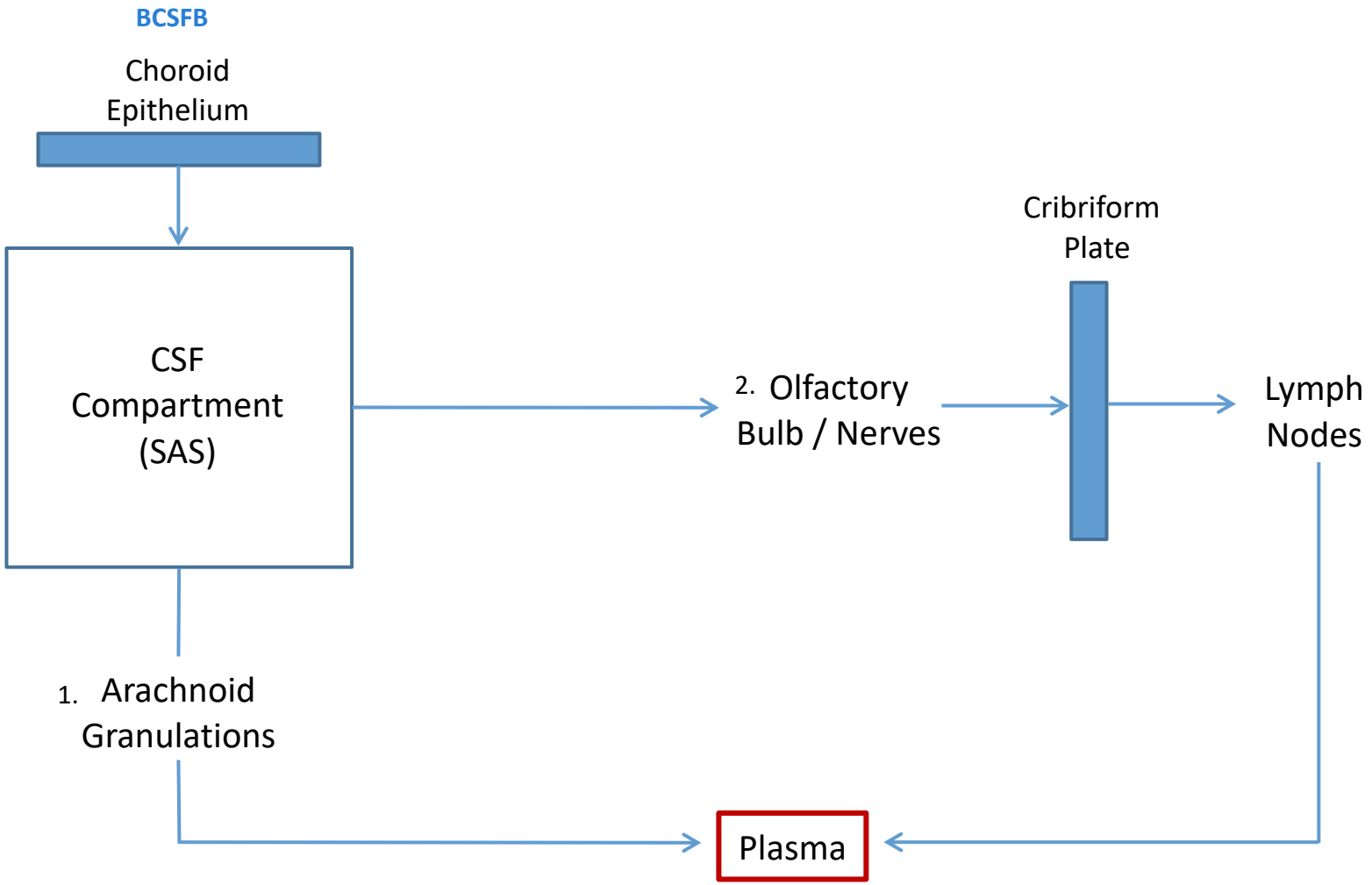

Figure 1.16: Putative pathway of CSF drainage.
Pathway 1: Evagination of the arachnoid membrane into the lumen of the vein and therefore the dural vessel allows the communication between CSF in the subarachnoid space (SAS) and blood. Pathway 2: CSF passes through the SAS to the olfactory bulbs and then drains into nasal lymphatics by passing through the cribriform plate and along channels adjacent to olfactory nerves and into the blood (own diagram based on information by Laman & Weller 2013).

1.6 Clinical features of IIH

Clinical features of IIH include headaches, occurring in 94% of IIH patients, intracranial noises, and dizziness. Headache appeared to be the most common feature in a study comparing 50 IIH patients and 100 controls (Giuseffi et al. 1991).

Visual symptoms usually accompany headache, but may occur in isolation, as found in one study in 19.5% of 77 IIH patients (Galvin & Van Stavern 2004). Visual manifestations include transient visual obscurations in 68% of cases, and papilloedema (swelling of the optic disc causing severe visual loss) (Wall & George 1991). The papilloedema swelling is due to raised ICP in the optic nerve head, or optic disc (Mackenzie & Cioffi 2008). In the absence of papilloedema, further assessment should be carried out on IIH patients in order to confirm diagnosis as IIH can appear to be clinically indistinguishable from chronic daily headaches (Mackenzie & Cioffi 2008) (Dhungana et al. 2009).

The main risk factor of IIH is obesity and the incidence of IIH presents a challenge to countries experiencing an obesity epidemic. In addition, IIH affects a greater proportion of the female population compared to males. Both features regarding obesity and sex in IIH are described further in Section 1.8.

1.7 Diagnosis and treatment of IIH

Correct diagnosis of IIH can only be made using strict criteria guidelines whereby all other causes of intracranial hypertension have been excluded (Friedman & Jacobson 2002). The diagnostic criteria include:

- Signs/symptoms present may highlight the presence of papilloedema.
- ICP is elevated.
- CSF composition is normal in terms of protein and ion content: Na^+ (150 mM), K^+ (2.86 mM), Cl^- (113 mM), HCO_3^- (23.3 mM) (Davson et al. 1987)
- There is no evidence of hydrocephalus (abnormal accumulation of CSF).
- No other cause of intracranial hypertension has been found.

In order to diagnose and manage the symptoms of IIH effectively, combinations of medical, physical and surgical measures are used. Brain imaging, such as magnetic resonance imaging (MRI), is helpful in excluding intracranial abnormalities that may not be evident in a plain computerised tomography (CT) scan. A lumbar puncture is performed to document the raised CSF pressure. These are the two most important investigations needed to make the diagnosis of IIH (Dhungana et al. 2009). The goals of IIH treatment are to reduce the elevated CSF pressure, preserve visual function and relieve symptoms.

Current treatments include, acetazolamide, a carbonic anhydrase inhibitor which decreases the production of CSF by reducing HCO_3^- levels in the choroid plexus epithelium (Dhungana et al. 2009) and thereby decreasing Cl^- uptake through reduced activity of AE2 channels located in the basolateral membrane (Vogh et al. 1987).

Reports of corticosteroid therapy withdrawal, in children with ulcerative colitis (inflammation of the colon) and various neurological disorders, showed a syndrome indistinguishable from IIH. Administering glucocorticoid hydrocortisone (HC) (400 mg) increased blood pressure; however, following withdrawal, papilloedema, a feature of IIH, developed after five days (Neville & Wilson 1970). Patient improvement was recorded following the re-introduction of a different corticosteroid, prednisolone (10 mg). Intravenous methylprednisolone (synthetic corticosteroid) with acetazolamide resulted in an improvement in visual symptoms in 75% of patients IIH, who initially had symptoms of acute severe visual failure (Liu et al. 1994). These data seem to contradict the theory of HC increasing ICP, and the effects of improved visual symptoms in Liu and colleagues' study may have been due to acetazolamide treatment as opposed to the actions of HC alone. Therefore, the mechanism of action of corticosteroids used to treat IIH is still unknown (Goodwin 2003).

Topiramate is another carbonic anhydrase inhibitor and antiepileptic drug that reduces CSF production and causes weight loss. A report on the effectiveness of topiramate vs. acetazolamide in 40 patients with IIH showed significant visual field improvements with either drug (Çelebisoy et al. 2007).

One of the main surgical practices for treatment of IIH is CSF diversion. This involves diverting the CSF from the lumbar SAS to the peritoneal cavity (LP shunt) or from a lateral ventricle to the peritoneal cavity (VP shunt). However, CSF diversion procedures have a high failure rate and can suffer from complications including over-drainage and low pressure headaches, as well as infections (Rosenberg et al. 1993). A review of a total of 73 LP and 9 VP shunts, in 37 patients from 6 US institutions, found that only 14 patients remained symptom free after a single procedure (Rosenberg et al. 1993).

1.8 Epidemiology of IIH

1.8.1 Incidence of IIH

It is possible to state that an underlying inflammatory pathology is present in IIH in terms of abnormal expression of inflammatory mediators. This is because IIH is strongly associated with obesity, a chronic low grade pro-inflammatory state (Lyon et al. 2003). The reported incidence of IIH ranges from 0.6-2.2 per 100,000 persons (Craig et al. 2001), (Dhungana et al. 2009), (Radhakrishnan et al. 1993) (Table 1.1), however these figures vary from country to country, potentially reflecting a variation in the prevalence of obesity and efficiency of diagnosis of the condition (Dhungana et al. 2009).

Region	Incidence (per 100,000 persons)	Reference
Belfast, Northern Ireland	0.6	(Craig et al. 2001)
Iowa, USA	0.9-1.0	(Dhungana et al. 2009)
Louisiana, USA	1.07	(Dhungana et al. 2009)
Benghazi, Libya	2.2	(Radhakrishnan et al. 1993)

Table 1.1: Incidence of IIH per 100,000 persons in various regions of the world.

1.8.2 Epidemiology of obesity and IIH

The evidence linking obesity with IIH is strong, with IIH patients being classified as obese, defined as body mass index (BMI) above 30 kgm^{-2}, in 71% (Radhakrishnan et al. 1993) and 91% (Kesler & Gadoth 2001) of cases. Several studies have reported weight gain in newly diagnosed IIH patients (Rowe & Sarkies 1999) (Radhakrishnan et al. 1993). The incidence of IIH in Iowa, USA grew to 13-14.8 per 100,000 for women aged 20-44 years of age who were 10% or more over ideal weight and 19.3 per 100,000 when 20% overweight (Dhungana et al. 2009). These figures are alarming, especially when taking into account the increasing prevalence of obesity around the world.

The pathophysiological mechanisms behind obesity in IIH remain elusive. One theory suggests that increased ICP is a result of an increase in cardiac filling pressure due to raised abdominal pressure as a result of obesity (Sugerman et al. 1997) as well as an increase in pleural pressures causing an obstruction to cerebral venous outflow via the jugular venous system (Bloomfield et al. 1997). However, this does not take into account the high prevalence of females,

compared to males, suffering from IIH, as females are less likely to have a greater distribution of body fat.

In vitro and *in vivo* studies of serum and adipose tissue have shown obesity to be associated with chronic, low grade inflammation and an abnormal, pro-inflammatory cytokine profile, including interleukin (IL)-8 (IL-8) (Straczkowski et al. 2002) and tumour necrosis factor-α (TNF-α) (Hotamisligil et al. 1995). Increased expression of other mediators, including IL-6, chemokine (CC-motif) ligand 2 (CCL2) and leptin, have also been linked with obesity as adipose tissue (fat cells) are an important source of cytokines (see section 1.10) (Lyon et al. 2003). Levels of serum adipokines (cytokines secreted by white adipose tissue) are elevated in humans and animals with excess adiposity (Lyon et al. 2003).

1.8.3 Epidemiology of gender and IIH

In addition to obesity being a factor in the incidence of IIH, sex hormones may influence patients with IIH as it is found to occur mostly in females. IIH mainly affects obese women between the ages of 15 and 45. It can develop at any age; however, the links to obesity would appear to be weaker in children. From a study by Durcan and co-workers, IIH is mainly found in younger adults with 59% of patients in the third decade of life at diagnosis (Durcan et al. 1988), with a female to male ratio of 8:1 (Dhungana et al. 2009).

Menstrual irregularities (Durcan et al. 1988) (Giuseffi et al. 1991), the use of oral contraceptives (Glueck et al. 2005), and high concentrations of oestrone (an oestrogenic hormone) have been linked with IIH and CSF production,

thought to be through stimulation of the choroid plexus secretory cells (Donaldson & Horak 1982) (Dhungana et al. 2009). However, a more extensive study needs to be carried out as the mechanism by which this occurs is unknown. If oestrone does stimulate CSF production, then the resulting elevated ICP associated with obese female IIH patients may be treated by an oestrone receptor antagonist.

Further studies have revealed high levels of progesterone in females are significant as they can stimulate cortisol production, which alone may cause an increase in CSF secretion, as described further in Section 1.9. Progesterone is a steroid hormone involved in pregnancy and the female menstrual cycle. Cortisol is a glucocorticoid thought to increase Na^+ movement through choroid plexus epithelial cells (Sinclair et al. 2010). As shown by Lucki and co-workers, the initial step in the synthesis of progesterone is the conversion of cholesterol into pregnenolone by the action of 3β-hydroxysteroid dehydrogenase in the adrenal cortex. The enzyme 17α-hydroxyprogesterone catalyzes the conversion of progesterone to 11-deoxycortisol, which in turn undergoes 11β-hydroxylation to produce cortisol (Lucki & Sewer 2008). This mechanism could provide further evidence as to the relationship between sex hormones' influence on patients with IIH.

1.9 Glucocorticoid cortisol (hydrocortisone) and IIH

Cortisol (hydrocortisone) is a potent endogenous anti-inflammatory mediator that regulates hepatic gluconeogenesis and regulates adipocyte differentiation (Tomlinson et al. 2004). Hydrocortisone in general refers to synthetic cortisol.

Cortisol is produced by the adrenal cortex and is synthesized from cholesterol as described in Figure 1.17. The biosynthetic pathway does not differ between humans and rats, however, cortisol is the predominant glucocorticoid in humans, whereas corticosterone is less abundant in humans, but is the dominant glucocorticoid in rodents. However, they both bind to the same glucocorticoid receptor. (Raubenheimer et al. 2006).

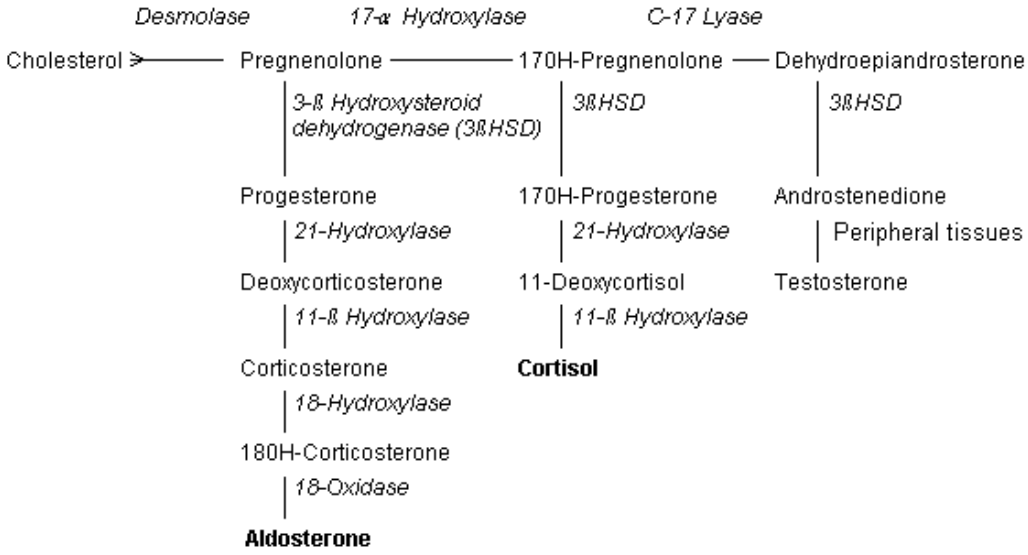

Figure 1.17: Enzymatic pathway for biosynthesis of cortisol and aldosterone, beginning with cholesterol.
Italics denote enzymes (Deaton et al. 1999).

Sinclair and colleagues found links between an increase in cortisol production within choroid plexus epithelial cells and IIH, in obese patients (Sinclair et al. 2010). Elevated levels of cortisol in the choroid plexus epithelium may cause an increased movement of Na^+ into the CSF, which would raise ICP associated with IIH patients. Following brain immunolocalisation studies from New Zealand White Albino rabbits, 11β-hydroxysteroid dehydrogenase (11β-HSD) enzyme was found to be expressed in the choroid plexus epithelial cells and

regulated corticosteroid hormone levels (Sinclair et al. 2007) (Odermatt et al. 1999). One of its two isoforms, 11β-HSD1, controls cortisol availability by converting cortisone into cortisol, a process dependent on the coenzyme NADP(H). The other, 11β-HSD2 is a dehydrogenase that inactivates cortisol to cortisone (NAD-dependent) in the kidney (Sinclair et al. 2010) (Chapman et al. 2013). As outlined previously in Section 1.4.2, in the choroid plexus epithelium, CSF production is dependent on an osmotic gradient created by the Na^+-K^+-ATPase pump and intracellular carbonic anhydrase activity, driving water into the brain ventricles (Speake et al. 2001). Cortisol binds to glucocorticoid receptors in epithelial cells, which activates SGK1 pathways to increase the movement of Na^+ across the cells via apical Na^+ channels, increasing this osmotic gradient and driving water into the CSF (Figure 1.12) (Sinclair et al., 2010). In this way, cortisol could contribute to elevated ICP observed in IIH patients.

As already mentioned, 11β-HSD1 activity can be regulated by sex steroids including progesterone (see Section 1.8.3). In addition, studies by Gomez-Sanchez and colleagues found 11β-HSD1 mRNA and protein are decreased to almost undetectable levels in the kidneys of animals treated with another sex hormone, estradiol (Gomez-Sanchez et al. 2003). This evidence would suggest a possible reduction of 11β-HSD1 enzyme activity, normally seen in women, may be lost in IIH as a result of abnormal sex hormone metabolism (Sinclair et al. 2010), therefore implicating sex hormones as a cause for increased glucocorticoid metabolism leading to an increase in CSF secretion associated with IIH patients.

Studies by Rauz found 11β-HSD1 may affect ICP regulation in a system similar to the trabecular meshwork (Rauz et al. 2003). This is an area of tissue, near the ciliary body, involved in the drainage of aqueous humour from the eye through the anterior chamber. As mentioned previously, 11β-HSD1 catalysed synthesis of cortisol in the ocular ciliary epithelium, the site of aqueous humour drainage, stimulates aqueous humour production and increased intraocular pressure through induction of corticosteroid regulated target genes. Sinclair and colleagues stated that a similar system could be found in the choroid plexus contributing to CSF production and ICP (Sinclair et al. 2008).

Studies by Tomlinson et al. showed 11β-HSD1 activity is up-regulated by TNF-α and IL-1β through the secretion of PLA2 (Tomlinson et al. 2004), an enzyme that increases cytokine production involved in inflammatory responses in glomerular mesangial cells (GMC) (Escher et al. 1997).

As well as TNF-α, IL-6 (see section 1.10.3) is associated with obesity and may also regulate 11β-HSD1 activity (Park et al. 2005). Within this same study of obese and non-obese adults free from inflammatory disease, TNF-α levels were higher in obese (2.69 pg/ml) compared with non-obese patients (1.72 pg/ml). IL-6 levels were also elevated in obese patients (2.00 pg/ml) when compared with lean controls (1.58 pg/ml). This provides a theory that 11β-HSD1 activation may be due to the dysregulation of these cytokines.

1.10 Cytokines levels are increased in IIH patients

Cytokines are small, non-structural proteins that are synthesized by most nucleated cells. Cytokines include interleukins (IL), interferons (IFN) and colony stimulating factors. Cytokines and chemokines (a sub-group of cytokines that direct chemotaxis in responsive cells) are involved in regulating inflammatory responses through coordination of cell movement to sites of infection in the immune system (Dhungana et al. 2009). Chemokines facilitate the passage of leukocytes from the circulation and into the tissues (Dinarello 2000).

Examples of pro-inflammatory cytokines implicated in IIH are listed in Table 1.2, along with an indication of the change in the levels of these factors in the CSF and serum (plasma where indicated) in IIH patients compared to controls. Changes in levels of HC are also considered.

Treatment	CSF	Serum	Reference
Hydrocortisone	**-**	↑	(Sinclair et al. 2010)
Leptin	↑	↑	(Ball et al. 2009)
CCL2*	↑	**-**	(Dhungana et al. 2009)
IL-6**	↑	↑	(ReihaniKermani et al. 2008) (Singhal et al. 2002) **(plasma)**
IL-17***	↑	**-**	(Edwards et al. 2013)
TNF-α**	↑	↑	(Hayakata et al. 2004) (Edwards et al. 2013)
IL-1β**	↑	↑	(Hayakata et al. 2004) (Dhungana et al. 2009)

Table 1.2: A summary of the differences observed of endogenous CSF and blood serum (plasma indicated) cytokine and hydrocortisone levels between IIH patients and controls. *against tension type headache patient controls; **against ICP following Traumatic Brain Injury (TBI) patient controls; ***against multiple sclerosis (MS) patient controls; (–) indicates no change between IIH patients and controls (see section 1.10.4). Actual treatment concentrations can be found in Table 6.2 of Appendix Section 6.1, page 267.

Infection and immune-activated T cells initiate a pro-inflammatory response which is mediated by cytokines. Cytokines IL-1 and TNF-α induce endothelial adhesion molecules, involved in the binding of leukocytes to the endothelial surface, and initiate a cascade of inflammatory mediators, through the activation of genes including phospholipase A2 (PLA2), cyclooxygenase (COX)-2, and inducible nitric oxide (NO) synthase, by targeting the endothelium (Dinarello 2000).

In response to inflammation, adipose tissue secretes pro-inflammatory cytokines, chemokines and various hormones. Once activated, adipose tissue recruits macrophages which secrete inflammatory mediators (Weisberg et al. 2003). These mediators bind to specific membrane receptors, for example IL-1 receptor (IL-1R) in the case of IL-1. This binding results in a number of intracellular signalling events, such as protein phosphorylations and activation of phosphatases (Dinarello 2000), which cause the induction of certain genes that mediate the activities of cytokines (Zdanov & Wlodawer 2008).

Due to its links with obesity, IIH could be associated with increased expression of adipokines and cytokines (see section 1.8.2). Pro-inflammatory cytokines could serve as important diagnostic markers of molecular pathways that may serve as targets for therapeutic intervention (Dhungana et al. 2009) if they are found to cause elevated ICP and therefore be a cause of IIH.

1.10.1 CCL2

C-C Motif Chemokine Ligand 2 (CCL2) belongs to the CC chemokine family and is involved in the recruitment of monocytes and memory T cells to sites of

inflammation. CCL2 is involved in the production of cytokines by these monocytes.

CCL2 is also involved in the pathogenesis of several diseases including neuroinflammation (Ramesh et al. 2013) (Ransohoff 2002), ischaemic stroke (Wolinski et al. 2013), and Alzheimer's disease (Azizi et al. 2014) and produces its biological effects through interaction with its CCR2 receptor, which belongs to the G-protein coupled receptor superfamily (Murphy et al. 2000).

During peripheral inflammation of the choroid plexus, expression levels of CCL2 were found to be increased (Mitchell et al. 2009). Szymydynger-Chodobska et al. found that CCL2 is secreted at the apical membrane of the choroidal epithelium in adult male Long-Evans rats. In addition, there is evidence of this chemokine secretion promoting leukocyte migration across epithelial barriers in patients following traumatic brain injury (TBI) (Szmydynger-Chodobska et al. 2012).

Further studies have been performed by Dhungana and colleagues on the detectable level of CSF and serum cytokine and chemokine profiles amongst IIH patients compared to controls of multiple sclerosis and tension-type headache patients. The results showed significantly elevated levels of CCL2 ($P \leq 0.01$) in the CSF of IIH patients compared with controls (Dhungana et al. 2009). Within the BBB, Gerhardt and co-workers found monocyte infiltration in endothelial and smooth muscle cells which also highlighted CCL2 expression (Gerhardt et al. 2001).

Other studies found that CCL2 is synthesised by a variety of epithelial cells in response to pro-inflammatory cytokines IL-1β and TNF-α (see section 1.10.5) (Paine et al. 1993) (Prodjosudjadi et al. 1995) (Szmydynger-Chodobska et al. 2012). Within these studies, the choroidal production of CCL2 appeared to reach its maximum capacity when the rat choroid plexus monolayers were incubated with IL-1β at a concentration of 1ng/ml.

As CCL2 aids in the recruitment of monocytes, these data suggest that the BCSFB not only contributes to the post-traumatic invasion of monocytes, but possibly to the pathogenesis of IIH as the choroid plexus is the site of CSF production.

1.10.2 Leptin

Leptin and adiponectin are cytokines most secreted in the highest concentrations by the adipose tissue (see section 1.8.2) and were also found to be present at increased levels in the CSF of IIH patients (Ball et al. 2009). These results imply that the transfer of leptin across the BCSFB in IIH may be increased.

Leptin is an adipocyte-derived hormone (adipokine) that circulates in serum at levels proportionate to body fat. Its major role is in the modulation of appetite and energy balance (Klok et al. 2007). Leptin is a product of the Obese (Ob) gene and when absent, results in profound obesity in mice (Tartaglia et al. 1995). When exogenously supplied, leptin can reduce food intake and body weight in a variety of rodent models (Tartaglia et al. 1995). Various studies

have shown that leptin could also be sourced in the brain (Wilkinson et al. 2000) (Morrison 2009); plays a role in obesity and starvation through its action on the BBB (Banks 2008); and that it is also secreted by the epithelial cells of the stomach (Sobhani et al. 2000) and placenta (Lepercq et al. 2001).

Concentrations of serum leptin have also been shown to be higher in females compared to males, independent of body mass (Baumgartner et al. 1999) (Ruhl & Everhart 2001). The fact that higher testosterone levels are associated with lower leptin levels could be a reason for this (Söderberg et al. 2001).

Obese people are shown to have increased serum levels of leptin (Buyukbese et al. 2004). A radioimmunoassay by Considine and colleagues found that the concentration of leptin in the peripheral circulation is about four-fold higher in obese individuals compared with lean (Considine et al. 1996). However, the rate of leptin uptake into the CSF does not increase in obese individuals with high serum leptin levels, due to the saturation of available transport carriers (Caro et al. 1996). This would explain the lower CSF/serum ratios for leptin and apparent leptin resistance of obese individuals. The increased levels of serum leptin in obesity are due to a resistance to its appetite suppressing effects, mainly due to impaired transport of leptin across the BBB (Flier 2004).

The effect of exogenous leptin on CSF secretion rate has not been previously studied. However, increased exogenous concentrations of leptin have been shown to elevate sodium excretion rate, two-fold ($P \leq 0.01$), in kidneys of anaesthetised rats (Jackson & Li 1997), through the activation of Janus kinase

(JAK) pathways which phosphorylate signal transducers and activators of transcription (STATS). STATS bind to promoter regions of genes, in turn altering their expression (Jackson & Li 1997). Concentrations of leptin within the CSF may be attributed to its movement across the choroid plexus. There is evidence of an increased affinity (K_m 0.5nM) for net leptin uptake from the blood to the CSF across the choroid plexus than the levels measured at the basolateral membrane (K_m 16nM) (Thomas et al. 2001). The study by Thomas and colleagues, found that secretion of new CSF by the choroid plexuses was significantly decreased with leptin present and that leptin transport at the BCSFB is via a saturable transport mechanism (where unlabelled leptin competes with [^{125}I]leptin for uptake sites) and non-saturable mechanisms and that the choroid plexus is involved in the regulation of leptin availability to the brain (Thomas et al. 2001).

Leptin has also been found to increase plasma corticosterone levels as compared with controls in male Long-Evans rats following infusion into the third cerebral ventricle, suggesting that leptin activates the hypothalamo-pituitary-adrenal (HPA) axis (van Dijk et al. 1997). The HPA axis is a set of feedback interactions among the hypothalamus, pituitary and adrenal glands. The adrenal cortex is a key element of the HPA axis, and produces cortisol in humans through the stimulation of adrenocorticotropic hormone (ACTH) (Schwartz et al. 1996). These results could explain the possible leptin:glucocorticoid levels and their effects on fluid production within the choroid plexus epithelium.

The increased levels of leptin in obese and female individuals, which coincide with the epidemiology of IIH; as well as its increased association within the CSF of IIH patients, suggest a possible role of leptin in the pathogenesis of this disease.

1.10.3 IL-6

IL-6 is a pro-inflammatory cytokine that stimulates the body's own immune system. It is produced in a number of cell types in response to pro-inflammatory stimuli, including IL-1 and TNF-α (Akira et al. 1993).

IL-6 roles include the regulation of immune and inflammatory responses, acute-phase protein production, bone metabolism, and hematopoiesis (Leonard et al. 1999). This study by Leonard and colleagues, also showed the presence in primary mesangial and proximal tubular cells from human kidney tissues of both the P38 mitogen-activated protein kinases and mitogen-activated protein kinases/extracellular signal-regulated kinases (MAPK/ERK) pathways, which regulate the production of IL-6 from the proximal tubular (duct system of the kidney leading from the Bowman's capsule to the loop of Henle) and glomerular mesangial (network of capillaries) regions of the nephron. Activation was confirmed by the SB203580 (1-30 μM) and PD98059 (0.01-10 μM) inhibitors abolishing TNF-α-stimulated IL-6 production by p38 MAPK activity, and phosphorylation of ERK1,2 pathway, respectively. These data may suggest a similar regulatory pathway for IL-6 within the choroid plexus epithelium.

Studies by Reihani-Kermani and colleagues found IL-6 to be elevated in the CSF (23.6 pg/ml) of IIH patients when compared to healthy controls (1.8 pg/ml) (Reihani-Kermani et al. 2008). In addition, as with leptin, circulating IL-6 stimulates the HPA axis; activation of which is associated with central obesity and cortisol production (Yudkin et al. 2000).

Protein and mRNA levels of IL-6 are increased in human peripheral blood mononuclear cells (PBMCs) following nitric oxide (NO) stimulation at low concentrations (<10 μM) (Siednienko et al. 2011). The effects of NO on IL-6 expression are cGMP dependent. The cGMP-dependent pathway is initiated when NO binds to the heme moiety of cytosolic guanylyl cyclase (GC) and stimulates its enzymatic activity (Siednienko et al. 2011). These results show NO may play a stimulatory role in IL-6 expression, in human PBMCs, involving the GC/cGMP/PKG pathway. As already mentioned in section 1.3.2, cGMP is shown to reverse the movement of ions in the choroidal epithelium, leading to a reduction in CSF secretion (Kolb et al. 1994) through protein kinase inhibition of Na^+-K^+-ATPase. The pathway of initial increased cGMP stimulation, increased IL-6 expression, and reversed ion movement across the choroid plexus, may suggest a link between IL-6 and a potential decrease in CSF secretion.

A link between the elevated levels of leptin, CCL2 and IL-6 in the CSF of IIH patients; and potential increases in CSF secretion rate, could provide a theory as to the cause of raised ICP associated with IIH patients.

1.10.4 IL-17

There is evidence of another pro-inflammatory cytokine, IL-17, with increased levels in the CSF of IIH patients (Edwards et al. 2013). IL-17 is a cytokine secreted exclusively by activated T-cells. The IL-17 receptor (IL-17R) is expressed in all tissues examined to date (Das Sarma et al. 2009). Activation of Th17 cells releases IL-17, which then activates IL-17R and results in the induction of other pro-inflammatory cytokines and chemokines, such as IL-1β, TNF-α and IL-6, through activation of transcription factor nuclear factor-kappa-light-chain-enhancer of activated B cells (NF-κB) (Hershko et al. 2002) from parenchymal cells and macrophages (Jovanovic et al. 1998).

Other studies have found IL-17 to act synergistically with TNF-α (Griffin et al. 2012); however, there are conflicting reports with regards to whether TNF-α is elevated in the CSF of IIH patients (Dhungana et al. 2009) (Ball et al. 2009) (Hayakata et al. 2004).

Findings by Zúñiga implicate IL-17 as a negative regulator of adipogenesis and glucose metabolism in mice, and show that it delays the development of obesity (Zúñiga et al. 2010). The onset of adipogenesis is essential for the secretion of leptin; a cytokine found in elevated levels in the CSF of IIH patients (Ball et al. 2009) (see Table 2.2 and section 1.10.2). This could suggest an opposing theory of reduced CSF secretion, involved in the pathogenesis of IIH, caused by increased IL-17 levels leading to decreased CSF leptin levels. Therefore, if no effect in CSF secretion rates is seen following exogenous leptin stimulation *in vivo*, it may be due to the increased levels of endogenous IL-17.

1.10.5 IL-1β and TNF-α

IL-1 is a pro-inflammatory cytokine that is secreted from monocytes and macrophages and stimulates the activation of resting T-cells, in turn producing more cytokines. IL-1 has two isoforms, IL-1α and IL-1β, both of which induce TNF-α expression. There is evidence of IL-1 having effects in various neuroinflammatory diseases such as cerebral ischaemia (Tuttolomondo et al. 2008), Alzheimer's disease (Van Everbroeck et al. n.d.) and Parkinson's disease (Pott Godoy et al. 2008) by acting on type 1 IL-1 receptors on target cells.

Links between IL-1 and leptin have been shown, as administration of IL-1 produces a dose-dependent increase in human serum leptin levels (Simons et al. 2005).

TNF-α is a transmembrane protein located in the plasma membrane, from which a soluble form of TNF-α is released into the extracellular space through the actions of TNF-α converting enzyme (TACE). During increased stress-induced kinase signalling, various cells can produce TNF-α such as microglia, astrocytes, immune cells, and brain endothelial cells (McCoy & Tansey 2008). TNF-α produces an immune response via activation of macrophages and T lymphocytes (Boehm et al. 1997), similar to the effects associated with IL-17 in Section 1.10.4. TNF receptors type 1 and type 2, found in brain endothelium (Lombardi et al. 2009), mediate the biological roles of TNF-α. At the BBB, TNF-α increases the passage of inflammatory cells into the CNS by upregulating adhesion molecules on the endothelium (Wosik et al. 2007).

Baniak and co-workers studied the effects of IL-1β and TNF-α on fluid secretion by swine airway submucosal glands (Baniak et al. 2012). It was found that both IL-1β and TNF-α, simultaneously, increased fluid secretion and that this effect was dependent on cAMP and PKA elevation. The increased action of cAMP and PKA involved a conformation change of the NKCC1 transporter (Na^+-K^+-$2Cl^-$) which drove the movement of ions into the CSF. This mechanism was suggested on the basis that there was a reduction in fluid secretion following treatment with bumetanide, an NKCC1 inhibitor.

As mentioned in section 1.9, 11β-HSD1 activity is up-regulated by TNF-α and IL-1β (Tomlinson et al. 2004), and TNF-α levels were found to be higher in obese individuals (Park et al. 2005). Interestingly, in obese individuals, diet-induced weight loss resulted in reduced TNF-α, IL-6, and leptin concentrations (Lyon et al. 2003). Therefore, the roles of these cytokines in epithelial fluid secretion, and reduced concentrations following weight loss, is consistent with the association of obesity and increased ICP in IIH where these cytokines are present at elevated levels.

1.11 Aim

The potential roles of cytokines and HC in modulating CSF secretion in IIH are summarised in Figure 1.18. The four potential mediators that have been shown to be elevated in the CSF of IIH patients – leptin, CCL2, IL-6 and IL-17 (Ball et al. 2009) (Dhungana et al. 2009) (Reihani-Kermani et al. 2008) (Edwards et al. 2013) - are highlighted. IL-17 has been shown to trigger the release of cytokines IL-1β and TNF-α from macrophages (Jovanovic et al. 1998). These three cytokines are involved in the production of the 11β-HSD-1 enzyme which

activates the conversion of cortisone to cortisol (HC), possibly driving Na^+ secretion through the ENaC pathway across choroid plexus epithelial cells (Sinclair et al. 2008). IL-1β and TNF-α also bind in a ligand-receptor complex, activating the NKCC1 transporter and PKA pathways (which also activates AQP1 water channels) to drive the movement of ions (Na^+, K^+, $2Cl^-$), and water respectively, across the choroid plexus epithelium. Leptin activates the hypothalmo-pituitary-adrenal (HPA) axis. The adrenal cortex of the axis produces cortisone through stimulation of adrenocorticotropic hormone (ACTH). Nitric oxide (NO) stimulates an increase in IL-6 in peripheral blood mononuclear cells (PBMCs) which increases intracellular cGMP. cGMP reverses the movement of ions across epithelia which is the opposite to cAMP. This would indicate that IL-6 could possibly decrease CSF secretion rates. IL-1β and TNF-α are also known to increase the expression of CCL2 which may also increase CSF secretion through an unknown pathway (Figure 1.18). Studying CSF secretion rates in response to treatment with these cytokines may explain the cause of increased levels of CSF, and in turn, ICP in patients with IIH.

In addition to increased CSF secretion, the resistance to CSF drainage may also contribute to increased ICP levels in IIH patients. However, the potential mechanisms of altered CSF drainage pathways involved with cytokines, found to be elevated in the CSF of IIH patients, and HC, is unknown. A potential blockage of the CSF drainage sites; the arachnoid villi and lymph nodes, associated with the cytokines of interest may explain their possible role of increased ICP in IIH patients.

Therefore, the overall aim is to investigate CSF secretion and resistance to CSF drainage as the main cause of IIH by investigating the effects selected mediators and pro-inflammatory cytokines, found to be elevated within the CSF, have on CSF secretion and resistance to CSF drainage.

1.11.1 Objectives:

1. Measure the effects of leptin, CCL2, IL-6, IL-17, IL-1β, TNF-α and HC on CSF secretion rates *in vivo* in both normal and high-fat diet fed male and female rat models, using ventriculo-cisternal perfusion.

2. Measure the effects of leptin, CCL2, IL-6, IL-17, IL-1β, TNF-α and HC on the resistance to CSF drainage *in vivo* in both normal and high-fat diet fed male and female rat models, using a variable rate infusion technique.

3. Perform a transcriptome analysis to confirm the mRNA composition of human choroid plexus epithelial cells (hCPEPiC) following 24h incubation *in vitro* with the cytokines that affected CSF secretion rates *in vivo*.

1.11.2 Hypothesis

A combination of a high-fat diet and elevated cytokines IL-17, IL-6, TNF-α, IL-1β, leptin, and the glucocorticoid hydrocortisone stimulate CSF secretion rates and/or increase resistance to CSF drainage in IIH patients.

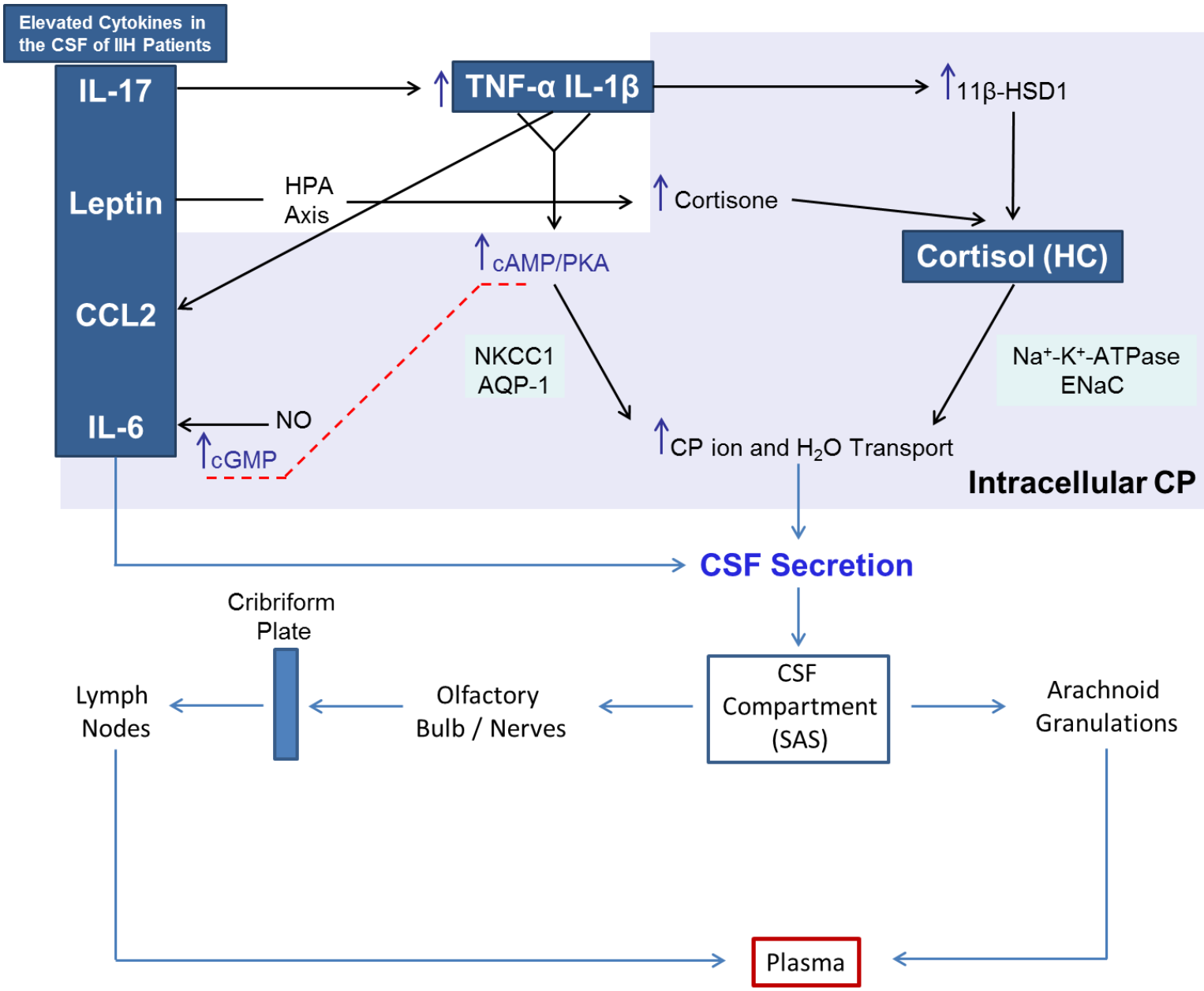

Figure 1.18: Putative CSF secretion and drainage pathways underlying IIH factors to be tested within this project.

Dashed red lines indicate the opposite action of cAMP and cGMP on ion movement across the choroid plexus epithelial cells. Own diagram based on references cited in the introduction.

2 Materials and Methods

2.1 Materials

A complete table of all chemicals, solutions and reagents used, including suppliers and catalogue numbers, are provided in Table 6.1 of Appendix Section 6.1.

2.2 Methods

2.2.1 Preparation of artificial CSF with blue dextran

Artificial cerebrospinal fluid (aCSF) containing 0.5% (w/v) blue dextran (Sigma-Aldrich Ltd, Dorset, UK, Cat No. D5751) was used for the *in vivo* perfusion experiments. The aCSF (with blue dextran) was made up using the compounds listed in Table 2.1.

Compound	MW (g/mol)	g/l	mM
Sodium chloride (NaCl)	58	7.076	122
Potassium chloride (KCl)	74	0.296	4
Calcium chloride ($CaCl_2$)	111	0.111	1
Magnesium chloride ($MgCl_2$)	95	0.095	1
Sodium bicarbonate ($NaHCO_3$)	84	1.26	15
HEPES	238	3.57	15
Disodium phosphate (Na_2HPO_4)	142	0.071	0.5
Glucose	180	3.15	17.5
Blue dextran	2,000,000	5	0.0025

Table 2.1: Molecular composition of aCSF with blue dextran, including the MW (g/mol) and concentration in the solution, (g/l and mM).
Ion concentrations followed those described in the rat CSF by (Davson 1967).

2.2.2 *In vivo* CSF secretion - the ventriculo-cisternal perfusion technique

The ventriculo-cisternal perfusion technique allowed for perfusion of the aCSF (containing blue dextran) with the treatment of interest through the two ventricles in the brain in anaesthetised live rats. The method is based on the collection of CSF samples from the cisterna magna and further analysis of these by spectrophotometry, which allows the CSF secretion rate, steady states and initial CSF volume to be determined.

The experiment was carried out in 11 week old male and female Wistar rats, 250-300 g, in accordance with Home Office project licence ("Cerebrovascular changes in the aged and disease brain", PPL number: 70/8507; ICV injections and perfusions under Protocol 3 "dynamics of ISF and CSF drainage"). The animals were housed in standard polypropylene cages (three rats/cage) and maintained under controlled room temperature (22 ± 2 ^{0}C) and humidity (55 ± 5%) with 12:12 h light and dark cycle.

The animals were first anaesthetised using a 100% isofluorane (Merial Animals Health, Essex, UK) inhalation vapour, administered within an inhalation chamber for 5 min. A single intraperitoneal (i.p.) injection of 'Domitor' (medetonidine hydrochloride) at 20 µl/100 g weight and 'Vetalar' (ketamine) at 50 µl/100 g weight of animal (both supplied by the Home Office Named Veterinary Surgeon, Red Kite Veterinary Consultants Centaur Services, Castle Cary, UK) was then given. After checking for lack of reflexes, the head was held in position using a stereotaxic frame and a midline cutaneous incision was made from forehead to neck to expose the top

of the skull. The lateral ventricles were located 0.8 mm posterior to the bregma and 1.5 mm laterally either side for each lateral ventricle. A 0.65 mm hand-chuck drill bit (Farnell Element, Leeds, UK, eclipse 121 pin vice, Cat No. 146443) bore holes in the skull for insertion of metal cannulae to a depth of 4 mm. The cannulae were attached to a water manometer; a fall in pressure as the cannulae was inserted confirmed correct positioning within the ventricle.

A 1 mm diameter needle was inserted into the cisterna magna for collection of perfusion outflow (Figure 2.1). Entry into the cisterna magna was obtained by locating the base of the occipital bone, found at the back of the rat skull, before piercing the arachnoid membrane, below the bone, and inserting the needle into the subarachnoid space (SAS) of the cisterna magna. Correct positioning of the needle was evident following immediate visualisation of aCSF (containing blue dextran) perfusion through the needle and into the 1 mm bore tubing (Altec Products Ltd, St Austell, UK, Cat No. 01-93-1407/30).

2.2.2.1 Schematic diagram of ventriculo-cisternal perfusion

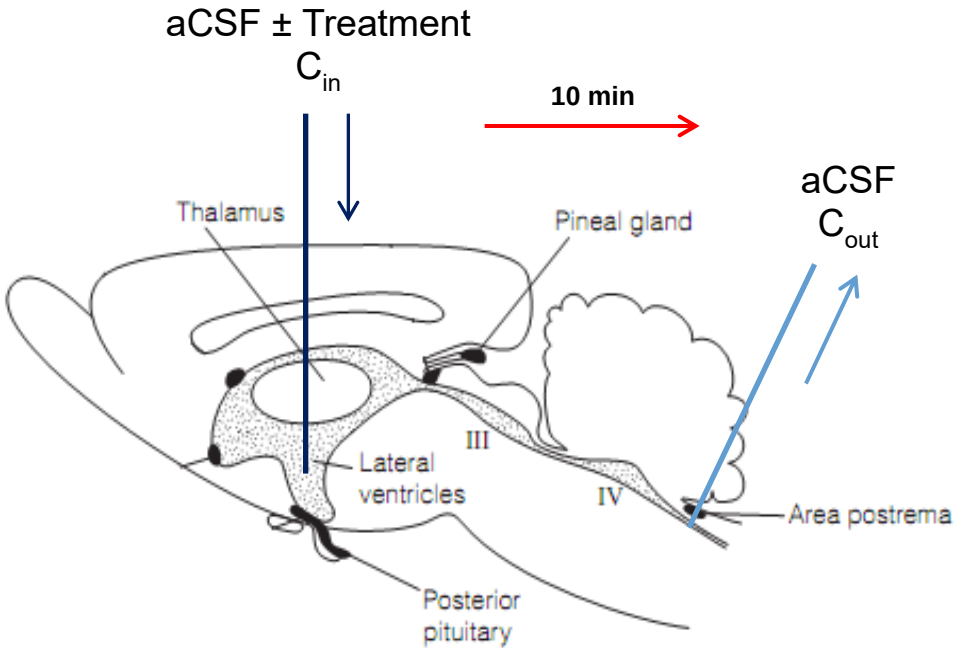

Figure 2.1: *In vivo* model of ventriculo-cisternal perfusion in adult Wistar rats.
The treatment of interest was perfused with the aCSF (containing blue dextran) into each lateral ventricle of the rat brain (C_{in}). The solutions were collected every 10 min for a period of 90 min from the cisterna magna (C_{out}) and the absorbance was read on a spectrophotometer at a 625 nm wavelength. The increase in dilution of the blue dextran within the aCSF for each sample indicates an increase in CSF secretion over the course of experiment.

Two 10 ml plastic syringes (Medicina, Bolton, UK, Cat No. FWC347) were filled with aCSF (containing blue dextran) (see Section 2.2.1) with or without the treatment of interest at the concentrations shown in Table 2.2:

Treatment	Supplier	Dose (ng/ml)	Reference based on reported levels in IIH patients
Hydrocortisone	Sigma-Aldrich, Dorset, UK, (H0135)	500	Sinclair et al. 2010
Leptin	Sigma-Aldrich, Dorset, UK, (L4146)	100	Dhungana et al. 2009
CCL2	Cambridge Bioscience, Cambridge, UK, (00220-0-100)	50	Dhungana et al. 2009
IL-6	Life Technologies, Paisley, UK, (10398-H08H-5)	0.1	Reihani-Kermani et al. 2008
IL-17	Miltenyi Biotech Ltd, Woking, UK, (130-093-959)	0.1	Li et al. 2012
TNF-α	Sigma-Aldrich, Dorset, UK, (H8916)	0.1	Hayakata et al. 2004
IL-1β	Miltenyi Biotech Ltd, Woking, UK, (130-093-897)	0.1	Hayakata et al. 2004

Table 2.2: Concentrations of the treatment of interest added to the aCSF (containing blue dextran) for ventriculo-cisternal perfusion.

In some experiments, rats were administered the same treatments via i.p injections 90 minutes prior to the start of the experiment, at the concentrations shown in Table 2.3:

Treatment	Dose	Reference based on reported levels in IIH patients
Hydrocortisone	100 µg/ml	Sinclair et al. 2010
Leptin	25 µg/ml	Dhungana et al. 2009
CCL2	10 µg/ml	Dhungana et al. 2009
IL-6	25 ng/ml	Singhal et al. 2002
IL-17	25 ng/ml	Li et al. 2012
TNF-α	25 ng/ml	Ball et al. 2009
IL-1β	25 ng/ml	Dhungana et al. 2009

Table 2.3: Concentration of the treatment of interest in i.p injections 90 minutes prior to ventriculo-cisternal perfusion.

The concentrations given for both aCSF (with blue dextran) and i.p administration were higher than those detected in the CSF and serum of IIH patients from other studies shown in Table 6.2 of Appendix Section 6.1.

Both lateral ventricles of the brain were perfused with aCSF (containing blue dextran) with or without treatment using a Harvard slow-drive syringe pump (Harvard Apparatus UK, Cambridge, UK, Cat No. 703007INT) for a total period of time of 90 min (Figure 2.1). Two 10 ml syringes with a diameter of 14.5 mm were used. Perfusion inflow rate of aCSF was 20 µl min^{-1} for each ventricle for the first 20 min and 10 µl min^{-1} for the remaining 70 minutes. The choice of perfusion rate was made to remove possible clots resulting from cannulae insertion and to rapidly flush out endogenous CSF, which was flushed out over the first 40 minutes. The need to

reduce clot accumulation was an observation that was determined during the initial experiments. Cisternal CSF samples were collected over 10 min time periods during the entire 90 min perfusion period. For measurement of CSF secretion rate, blue dextran was included in the aCSF. The levels of the blue dye in the collected perfusate samples was determined using spectrophotometry (FLuostar Optima, BMG labtech, Aylesbury, UK) at 625 nm wavelengths. The CSF secretion rate was calculated by the dilution of the blue dextran as shown in Equation 2.1:

Equation 2.1:

$$\textbf{CSF Secretion Rate } (\mu\textbf{l min}^{-1}) = \frac{\mathbf{C_{in} - C_{out}}}{\mathbf{C_{out}}} \times \textbf{Perfusion Rate } (\mu\textbf{l min}^{-1})$$

Where C_{in} is the absorbance value of the initial aCSF (containing blue dextran) that was perfused into each of the lateral ventricles (concentration in) and C_{out} is the absorbance value of aCSF (containing blue dextran) that was perfused out of the cisterna magna (concentration out) for a particular perfusion period. The perfusion rate was the result of the two syringes used, i.e 2x10 µl min^{-1}.

The average CSF secretion rate reading was calculated from each collected sample at steady state; i.e. from 40-90 min, once the animal's own initial endogenous CSF had been removed during the first perfusion time period (0-40 min).

The initial *in vivo* CSF volume was calculated as shown in Equation 2.2:

Equation 2.2:

$$\textbf{Initial CSF Volume } (\mu\textbf{l}) =$$
$$\textbf{Total volume secreted during whole experiment}(\mu\textbf{l})^{*} -$$
$$(\textbf{Average CSF Secretion Rate} \times \textbf{90 min}(\mu\textbf{l}/\textbf{90 min}))$$

***Calculated by multiplying the CSF secretion rate (µl min^{-1}) by the number of minutes the animal was perfused for, at each time period (i.e. 10 min), before adding up the values from each time period to one another.**

The steady states were calculated by dividing the absorbance value of aCSF, containing blue dextran, that was perfused out of the cisterna magna (C_{out}) after each 10 minute interval by the absorbance value of the initial aCSF, containing blue dextran, that was perfused into each of the lateral ventricles (C_{in}) (Equation 2.3):

Equation 2.3:

$$\textbf{aCSF Sample Steady State} = \frac{\mathbf{C_{out}(Abs)}}{\mathbf{C_{in}(Abs)}}$$

Examples of all calculations are shown in Appendix Section 6.2.

2.2.3 *In vivo* resistance to CSF drainage – variable rate infusion technique

The variable rate infusion technique, described by Jones and co-workers, measures the resistance to drainage of the CSF in the rat (Jones et al. 1987). According to this technique, flow infusion of aCSF into the lateral ventricle at a known flow rate would

cause CSF pressure to rise to a plateau level. The resistance to drainage of the CSF, in $mmH_2O \cdot min/\mu l$ can then be calculated from the gradient of CSF pressure at plateau level (recorded over four increasing rates) plotted against the infusion rate.

The variable rate infusion technique is similar to the ventriculo-cisternal perfusion method in that it allows for perfusion of the aCSF with the treatment of interest but through only one lateral ventricle of the brain in live anaesthetised rats. The other lateral ventricle is inserted with a cannula attached to a pressure transducer (PATCOSHH Ltd, Kent, UK, Cat No. 00015027), and pressure readings are taken at 10 min intervals at increasing perfusion rates.

Just as in the ventriculo-cisternal perfusion experiment, the variable rate infusion technique was carried out in male Wistar rats, 250-300 g, in accordance with Home Office project licence (PPL number: 70/8507). The animals were anaesthetised as in Section 2.2.2, with a 100% isofluorane inhalation vapour for 5 min and a single i.p. injection of 'Domitor' (medetonidine hydrochloride) at 20 µl/100 g weight and 'Vetalar' (ketamine) at 50 µl/100 g weight of animal, before being positioned into the stereotaxic frame, and the lateral ventricles located as also described in Section 2.2.2.

One 10ml plastic syringe (Medicina, Bolton, UK, Cat No. FWC347) was placed in the Harvard slow-drive syringe pump (Harvard Apparatus UK) (filled with aCSF with or without the treatment of interest) (Figure 2.2). Only treatments that had an effect

on either CSF secretion rates or initial CSF volumes (as determined in the ventriculo-cisternal perfusion experiments) were selected for investigation here. The concentrations of these treatments were the same as those used in ventriculo-cisternal perfusion experiments, as described in Table 2.2 and Table 2.4.

Treatment	Dose	Reference
Hydrocortisone	500 ng/ml	Sinclair et al., 2010
CCL2	50 ng/ml	Dhungana et al., 2009
IL-6	0.1 ng/ml	Reihani-Kermani et al., 2008
IL-17	0.1 ng/ml	Li et al., 2012
TNF-α	0.1 ng/ml	Hayakata et al., 2004

Table 2.4: Concentrations of the treatment of interest added to the aCSF for variable rate infusion.

For i.p injections 90 min prior to the start of the experiment (where performed), the concentrations of the treatments were the same as those used in the ventriculo-cisternal perfusion experiments, as described in Table 2.3 and Table 2.5.

Treatment	Dose	Reference
Hydrocortisone	100 µg/ml	Sinclair et al., 2010
CCL2	10 µg/ml	Dhungana et al., 2009
IL-6	25 ng/ml	Singhal et al., 2002
IL-17	25 ng/ml	Li et al., 2012
TNF-α	25 ng/ml	Ball et al., 2009

Table 2.5: Concentrations added of the treatment of interest for i.p injections 90 minutes prior to variable rate infusion.

One lateral ventricle of the brain was perfused using a slow-drive syringe Harvard pump for 10 min at each increasing perfusion rate (5, 10, 16 and 20 µl min^{-1}) using a 10 ml plastic syringe with a diameter of 14.5 mm. Pressure readings (mmH_2O) after

each 10 min were recorded using a pressure transducer which was attached to a separate cannula inserted into the other lateral ventricle. The cannulae were glued in place using Loctite Liquid Super Glue (RS Components, UK, Cat No. 425927) to create a closed system. Changes in pressure recordings at plateau level at each increasing perfusion rate over those found in control animals would indicate whether the treatment of interest could modulate the resistance to CSF drainage.

2.2.3.1 Schematic diagram of variable rate infusion

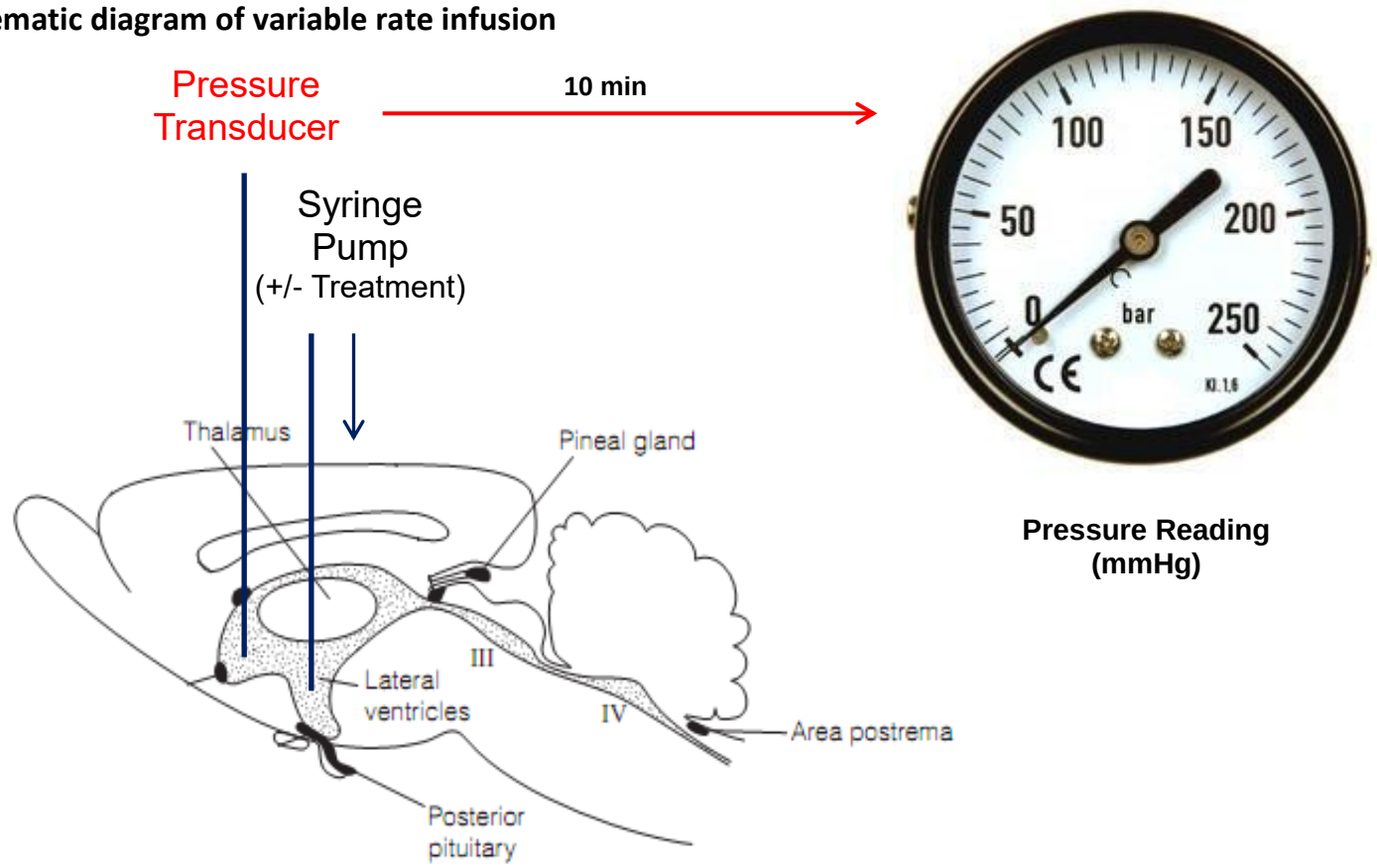

Adult Rat Brain: Site of injection into each lateral ventricle

Figure 2.2: *In vivo* model of variable rate infusion in adult Wistar rats.
The treatment of interest was perfused with the aCSF into one lateral ventricle of the rat brain at increasing perfusion rates. A separate cannula, attached to a pressure transducer, was inserted into the other lateral ventricle and pressure readings were taken every 10 min at both increasing and then decreasing perfusion rates.

2.2.4 High-fat and normal control diets

Male Wistar rats were ordered at 4 weeks of age and maintained on either a normal pellet or high-fat (HF) diet. Rat weights ranged between 250-350 g at the onset of experiments. The HF diet male rats were fed a 'Rodent Maintenance (RM) Atwater Fuel Energy (AFE) 45% Fat, 20% Crude Protein (CP) and 35% Carbohydrate (CHO)' diet which was purchased from Special Diet Services (SDS), Essex, UK (Table 2.6).

45% AFE High-Fat Diet (Male Wistar Rats)	
Ingredient	**g% (w/w)**
Fat	22.6
Carbohydrates	39.8
Protein	23
Fibre	4.6
Minerals	4.3
Vitamins	1.2
Total	**95.5**

Table 2.6: Ingredients contained within % (w/w) of SDS 45% AFE HF diet.

The HF diet female rats were provided with a 'Western Rodent HF Diet' also purchased from SDS, Essex, UK (Table 2.7).

Western RD High-Fat Diet (Female Wistar Rats)	
Ingredient	**g% (w/w)**
Fat	21.4
Carbohydrates	50
Protein	17.5
Fibre	3.5
Minerals	3.5
Vitamins	1
Total	**96.9**

Table 2.7: Ingredients contained within % (w/w) of SDS Western RD HF diet.

The screening control male rats were fed a commercially available 14% Protein Rodent Maintenance Diet, normal pellet diet (NPD), purchased from Envigo Teklad Diets, Huntingdon, UK as shown in Table 2.8.

Normal Control Diet (Male Screening Rats)	
Ingredient	**g% (w/w)**
Fat	4
Carbohydrates	48
Protein	14.3
Fibre	4.1
Minerals	2.8
Vitamins	0.2
Total	**73.4**

Table 2.8: Ingredients contained within % (w/w) of Teklad 14% protein rodent maintenance normal control diet.

The control male and female rats were provided with a 'Rat and Mouse No. 1 Maintenance (RM1) normal diet purchased from SDS, Essex, UK, as shown in Table 2.9.

Normal Control Diet (Male and Female OU)	
Ingredient	**g% (w/w)**
Fat	2.7
Carbohydrates	45
Protein	14.3
Fibre	4.7
Minerals	3.3
Vitamins	0.1
Total	**70.1**

Table 2.9: Ingredients contained within % (w/w) of SDS RM1 rodent maintenance normal control diet.

The rats were fed ad-libitum and the diets were administered as pellets for a period of seven weeks. Control rats and those receiving the high-fat diet (HF rats) were weighed every week from the onset of diet.

2.2.5 Cytology of female oestrous cycle

Vaginal smear analysis was performed, according to methods by Cora and co-workers, on female Wistar rats prior to ventriculo-cisternal perfusion and variable rate infusion experiments to determine the stage of their oestrous cycle (Cora et al. 2015). 200 µl dH_2O was inserted into the vaginal orifice, using a Pasteur pipette at a depth of 5-10 mm, and flushed into the vagina and back out 2-3 times. A small drop of the sample was placed evenly on a microscope slide (Marienfeld, Germany, Cat No. 1320102) before imaging under a Bresser LCD Micro light microscope (Meade Instruments, Germany). It was only once analysis confirmed the female Wistar rats were on the diestrus phase of the cycle (quiescence between periods of sexual activity, therefore levels of estradiol are low), and was determined by the presence of leucocytes but few nucleated cells (Cora et al. 2015), that ventriculo-cisternal perfusion and variable rate perfusion experiments could be performed.

2.2.6 Cholesterol assay

To compare the plasma concentration of cholesterol in male and female adult Wistar rats on a normal and HF diet, a colorimetric Cholesterol Assay Kit (Abcam, Cambridge, UK, Cat No. ab65390) was used to measure total cholesterol, HDL and LDL/VLDL fractions from plasma samples. All of the reagents used were supplied by Abcam within the assay kit unless stated otherwise. Plasma was collected by intracardiac withdrawal from the left ventricle of the heart from each animal (11 weeks of age) immediately after the completion of the experiment and prior to perfusion for brain fixation (see Section 2.2.7). 3ml of blood was collected using a 20 gauge; 1.5 inch sized needle and was slowly

extracted into a 5 ml syringe so as not to exert excess pressure which could sheer the cell walls and cause haemolysis of the blood sample. The blood was transferred into a 15 ml tube and left to clot at room temperature for 60 mins. The samples were then centrifuged (1300 x *g* for 10 mins) before the plasma was collected and stored at -20^{0}C until needed.

2.2.6.1 Preparation of standard

A fresh standard was prepared for each analysis to generate a standard dilution curve. 250 µl of 0.2 µg/µl cholesterol standard was prepared by diluting 25 µl of cholesterol standard (2 µg/µl) in 225 µl of Cholesterol Assay Buffer. Using the 0.2 µg/µl Cholesterol Standard, five standards were produced by serial dilution ranging from 1-5 µg cholesterol in microcentrifuge tubes before being transferred into a 96-well plate. Each dilution had enough amount of standard to set up duplicate readings (2x50 µl).

2.2.6.2 Sample preparation - quantification of total cholesterol

The plasma samples were used directly and no preparation step was required. A volume of 20 µl of each normal diet and high-fat diet plasma sample was added into each well and labelled as the 'Total Cholesterol' sample wells.

2.2.6.3 Separation of HDL and LDL/VLDL

First, 100 µl of the plasma sample was mixed with 100 µl of 2x Precipitation Buffer in microcentrifuge tubes. The mixed samples were then incubated at RT for 10 min before being centrifuged at 2,000 x *g* for 10 min. The supernatant

was then transferred to new microcentrifuge tubes and labelled as the 'HDL fraction'. The precipates contained the LDL/VLDL fraction, which were then centrifuged again at 2,000 x *g* for 10 min. Any remaining trace amount of HDL supernatant was carefully removed before the precipitate was resuspended in 200 µl phosphate buffered saline (PBS) and labelled as the 'LDL/VLDL fraction'. 20 µl of each HDL and LDL/VLDL fraction was added into separate wells of the 96-well assay plate and labelled accordingly as 'free cholesterol' sample wells.

2.2.6.4 Cholesterol reaction mix

All of the reagents were equilibrated to room temperature prior to use. The cholesterol probe however was warmed in a 37 ^{0}C water bath for 3 min to thaw the DMSO within the vial. The Enzyme Mix and the Cholesterol Esterase were each reconstituted in 220 µl of Cholesterol Assay Buffer before use. Sufficient volumes of these mixes were made up to allow 50 µl per assay sample. The 50 µl Reaction Mix was prepared for each reaction as shown in Table 2.10.

Component	Total Cholesterol Reaction Mix (µl)	Free Cholesterol Reaction Mix (µl)
Cholesterol Assay Buffer	44	46
Cholesterol Probe	2	2
Enzyme Mix	2	2
Cholesterol Esterase	2	0

Table 2.10: Volumes in µl of components added in both a Total Cholesterol Reaction Mix, and Free Cholesterol Reaction Mix which were used to obtain total cholesterol as well as HDL and LDL/VLDL concentration in the plasma samples, respectively.

A 50 µl volume of Total Cholesterol Reaction Mix was then added into each 50 µl Standard well and 20 µl Total Cholesterol (whole plasma) sample wells. 50 µl of

Free Cholesterol Reaction Mix was added into each of the 20 µl HDL and 20 µl LDL/VLDL sample wells. The samples were then protected from light and incubated at 37 ^{0}C for 60 min. The absorbance was then measured on a FLuostar Optima microplate reader at a wavelength of 570 nm.

The duplicate readings for each standard were averaged before the mean absorbance value of the blank (standard no. 1) was subtracted from all standard and sample readings. This obtained the corrected absorbance. The corrected absorbance values were then plotted. The standard curve and trendline equation was constructed using the points of the corrected absorbance values.

The concentration of cholesterol in the test samples was then calculated as described in Equation 2.4.

Equation 2.4:

$$\textbf{Cholesterol Concentration} = \frac{\mathbf{A}}{\mathbf{V}} \times \mathbf{D}$$

A = amount of cholesterol in the sample well calculated from the standard curve (µg).

V = volume of sample added to the sample reaction well (i.e 20 µl for Total cholesterol; HDL and LDL/VLDL fractions).

D = dilution factor. For total cholesterol, D = 1; for HDL and LDL/VLDL fractions, D = 2.

2.2.7 Intracardiac perfusion in adult Wistar rats

For each animal, a 200 ml volume of 4% (w/v) *p*-formaldehyde (PFA) (Sigma-Aldrich, Dorset, UK, Cat No. P6148) in 0.1 M PBS (Sigma-Aldrich, Dorset, UK, Cat No. P4417) was heated at 60 ^{0}C until the powder dissolved, pH adjusted to 7.4 using NaOH, and stored at 4 ^{0}C until needed. On the day of the experiment, 0.5% (v/v) glutaraldehyde (Agar Scientific, Essex, UK, Cat No. R1311) was added before use.

The anaesthetized rat [single i.p. injection of 'Domitor' (medetonidine hydrochloride) at 20 µl/100g weight and 'Vetalar' (ketamine) at 50 µl/100g weight of animal] was positioned flat on its back and secured on an oblique surface to enable draining of fluids. The peristaltic pump (Harvard Apparatus UK, Cambridge, UK, Cat No. 702027) was switched on and a 0.1 M PBS solution was run through the tubing in a circular system at 5 µl/min with the addition of a butterfly needle (Becton Dickinson Valve Set, Belliver Industrial, UK, Cat No. 387412) to make sure there was no air in the system.

The skin underneath the rib cage was pinched and a small incision was made with large scissors before opening wide the thorax diaphragm to the armpits in order to expose the heart. The sternum was then clamped back and held in place. The lower heart was grasped (gently but firmly). The peristaltic pump was briefly switched off before the cannula (butterfly needle) was inserted into the left ventricle and pushed up into aorta. The pump was then switched on at the same speed of 5 µl/min. The right atrium was incised with fine scissors to drain out fluids and avoid excessive pressure. After 2 min the 0.1 M PBS solution was

switched to PFA 4% + glutaraldehyde 0.5% and 100 ml was run for 5 min while checking stiffness of the tail, which would indicate progress of the fixation.

At the end of the perfusion the cannula was withdrawn and the animal was decapitated using a guillotine. The skull was opened using scissors and the brain was dissected out. The brain was stored in 4% (w/v) PFA + 0.5% (v/v) glutaraldehyde fixative at 4 ^{0}C. The brain was then placed in a 50 ml tube of 30% sucrose solution at 4 ^{0}C to drain it of water. The brain was fully drained when it sank to the bottom of the tube and was then stored at 4 ^{0}C until sectioning.

2.2.8 Adult male Wistar rat brain vibratome sectioning

The adult Wistar rat brains were washed 3x for 1 h in 0.2 M phosphate buffer (PB) (6.2g sodium dihydrogen orthophosphate (BDH Chemicals Ltd, Poole, UK, Cat No. 10245) and 22.6g di-sodium hydrogen orthophosphate anhydrous (Fisher Scientific, Loughborough, UK, Cat No. S/4520/53) in 1 litre dH_2O, pH 7.5 in order to clean the brain of sucrose. The cerebellum was cut off each brain and the cerebra allowed to air dry for 5 min. The caudal (posterior) side of the brain was then glued onto the vibratome (Leica VT, Leica Microsystems Ltd, Milton Keynes, UK, Cat No. 10005) plate and was then placed into the water bath in a horizontal position. A fresh blade was used for every brain and cleaned with acetone under the hood before being fixed onto the vibratome. The water bath was filled with 0.2 M PB until the brain was covered. The vibratome settings were set at a frequency of 70 Hz and a cutting speed of 1.5 mm s^{-1}. The blade was then lowered to the level of the brain surface and sections were cut to a size of 50 µm

thickness continuously before being collected in glass containers containing 0.2% (v/v) glutaraldehyde and stored at 4 ^{0}C until electron microscopy analysis.

2.2.9 Electron microscopy analysis

Following vibratome sectioning, the brain sections were placed into a petri dish containing 0.1 M PB (pH 7.4) before two sections were selected randomly and transferred to a 7 ml glass vial containing 0.1M PB. The sections were washed 3x for 10 minutes in 0.1 M PB. After making sure that the sections were flat inside the glass vials, they were covered in 1% osmium tetroxide (Agar Scientific, Cat No. R1017) diluted in 0.1 M PB for 1h at RT. It was important that the sections remained flat as they would become brittle when osmium tetroxide was added. The sections were then washed again 3x in 0.1 M PB for 10 min before being dehydrated in a series of solutions as follows: 30% ethanol for 5 min, 50% ethanol for 5 min, 70% ethanol for 10 min, 90% ethanol for 10 min, 100% molecular sieve prepared ethanol for 10 min and 100% molecular sieve prepared acetone 3x for 10 min. Molecular sieves are zeolite compounds used to adsorb water and have carefully controlled pore sizes. All of the washes and dehydration steps were performed at room temperature.

The sections were then placed in a 50:50 pre-made acetone:resin mixture for 1h at RT. The resin mixture was made by mixing 22.5 ml araldite (Agar Scientific, Cat No. R1040), 22.5 ml Agar 100 resin (Epon) (Agar Scientific, Cat No. R1043) and 60 ml dodecenyl succinic anhydride (DDSA) (Agar Scientific, Cat No. R1051) solutions for 1h at RT. A 0.6 ml 2,4,6-tris dimethylaminomethyl phenol (DMP-30) (Agar Scientific, Cat No. AGR1065) solution was then added before mixing

overnight at RT to produce epoxy resin. All of the resin solutions were ordered from Agar Scientific Ltd, Essex, UK. Finally, 1.5 ml of epoxy resin was then mixed with 1.5 ml acetone and added to the sections for 1 h at RT.

A drop of acetone:resin mixture for each section was placed onto a clean sheet of Aclarfilm (used to keep epoxy resin in contact with each section) that had been cleaned with acetone and removed of static using a Zerostat anti-static instrument (Sigma-Aldrich, Dorset, UK, Cat No. Z108812-1EA). Each brain section was placed down on top of the Aclarfilm into the drop and cut into three pieces (two pieces contained each lateral ventricle and the middle piece contained the third ventricle of the rat brain) as shown in Figure 2.3. Another drop of acetone:resin mixture was then added to each cut section before the excess was collected using filter paper. A few drops of epoxy resin were then added on to each section before the second piece of Aclarfilm was placed on top. Weights were then positioned on top of the second piece of Aclarfilm, and then everything was placed into a 60 ^{0}C oven for 48 h.

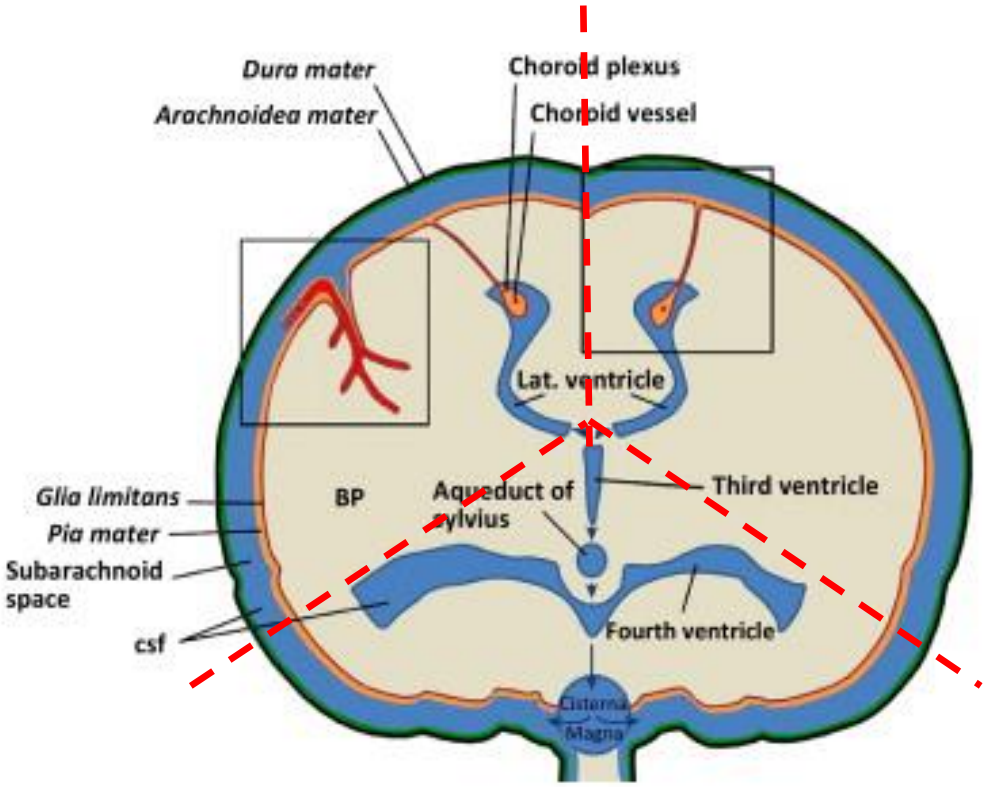

Figure 2.3: Diagram of sections of adult male rat brain cut for EM analysis.
Red dashed lines indicate the areas cut to separate the two lateral ventricles and the 3rd ventricle of the male rat brain that was then used to analyse the choroid plexus ultrastructure by electron microscopy.

A gelatin capsule (Agar Scientific, Essex, UK, Cat No. G29218) for each cut section was filled with epoxy resin before also being placed face down on the flat surface of the rubber mould and polymerized in the oven at 60 ^{0}C for 48 h. The sections and the capsules were then removed from the oven before the top layer of Aclarfilm was peeled off the sections. A drop of epoxy resin was then added on top of each section before each epoxy resin filled capsule was placed on top of each section, followed by polymerization at 60 ^{0}C for 48 h.

The sections were then allowed to cool before being cut at 1 µm using a glass knife mounted on to a Leica EM UC7 ultramicrotome (Leica Microsystems Ltd, Milton Keynes, UK). The sections were then stained with 1% (w/v) toluidine blue

in 5% (w/v) sodium borate and imaged on a Nikon Eclipse 80i light microscope (Nikon UK Ltd, Surrey, UK). The sections were then cut at 0.1 µm using a Diatome Ultra 45^0 diamond knife (Leica Microsystems, Milton Keynes, UK, Cat No. 16DIA.DU4530). Sections were collected on copper TEM slots with carbon coated piolorform film, and then counterstained in 3.5% aqueous uranyl acetate and lead citrate (Reynolds recipe) (Reynolds 1963). After that the sections were imaged on the JEOL JEM 1400 transmission electron microscope (JEOL (UK) Ltd, Welwyn Garden City, UK) and AMT XR60Z camera (Deben UK Ltd, London, UK). Magnification of x3000 and x4000 montaging method was used. Frames were adjusted for brightness/contrast in ImageJ software and montages were combined in Adobe Photoshop.

2.2.10 Culture of human choroid plexus epithelial cells (hCPEpiC)

The human choroid plexus epithelial cell line (hCPEpiC) (Caltag Medsystems, Milton Keynes, UK, Cat No. SC-1310) was cultured on 2 µg/cm^2 poly-l-lysine (Sigma-Aldrich, Dorset, UK, Cat No. P4707)-coated flasks. Coating was achieved by the addition of 10 ml of sterile water (Sigma-Aldrich, Dorset, UK, Cat No. W3500) and 500 µl of 0.1 mg/ml poly-l-lysine solution, into a T75 flask, and incubation at 37 ^{0}C for 1 h. The coating solution was then removed before the flask surfaces were washed 3x with Hank's Balanced Salt Solution (HBSS) with Ca^{2+} (Sigma-Aldrich, Dorset, UK, Cat No. H6648) before the cells were seeded straight away. The cells were brought up from frozen stock and seeded at a density of 5000 cells/cm^2 in complete hCPEpiC medium (Caltag Medsystems, Milton Keynes, UK, Cat No. SC4101) containing 2% foetal bovine serum (FBS), 1% (v/v) epithelial cell growth supplement (EpiCGS), and 1% (v/v)

penicillin/streptomycin solution (P/S). Once seeded, the cells were not disturbed for at least 16 h before the medium was changed the following day to remove any dimethyl sulfoxide (DMSO) (Sigma-Aldrich, Dorset, UK, D2438), from the initial freezing medium, and unattached cells that were present. The medium was then replaced every 48 h thereafter. The cell numbers doubled after 2-3 days in culture (DIC) and were then either frozen down or passaged when they reached 90% confluency. Cells were cultured and used for experiments from passage 1-5.

2.2.11 RNA extraction and mRNA analysis of hCPEpiC following 24h incubation with HC, TNF-α and IL-6

hCPEPiC were grown to confluence and used for this experiment from passage 2-5 on sterile 6-well plates (Greiner Bio-One, Stonehouse, UK, Cat No. 657160) and treated with 1 ng/ml of TNF-α, 1 ng/ml of IL-6 and 500 ng/ml HC for 24 h. The cell medium was removed and cells were washed once with pre-warmed HBSS without Ca^{2+} (Sigma-Aldrich, Dorset, UK, Cat No. H8264). Total RNA was isolated using the RNeasy mini kit (Qiagen, Crawley, West Sussex, UK, Cat no. 217004) according to the manufacturer's protocol. Cell homogenization was achieved by adding 700 µl of QIAzol lysis reagent into each well and pipetting up and down several times. The cell lysate was transferred to 1.5 ml microfuge tube (Greiner Bio-One, Stonehouse, UK, Cat No. 616201) and left at RT for 5 min.

For the separation phase, 140 µl of chloroform (Sigma-Aldrich, Dorset, UK, Cat No. C2432) was added to each tube and mixed vigorously for 15 sec. The cells were then incubated for 3 min at RT before centrifugation (12,000 x *g*, 15 min,

4^0C). The upper aqueous phase containing RNA was transferred to a new 1.5 ml microfuge tube.

To precipitate the RNA, 525 µl of 100% ethanol was added into each tube and mixed vigorously by pipetting up and down several times. The RNA-ethanol sample was then added in to the RNeasy mini spin column and centrifuged at 8,000 x *g* for 15 sec at RT. The flow through was discarded before the column was washed twice with RWT buffer and once with RPE buffer (solutions supplied by Qiagen in the RNeasy mini kit). The flow through was then again discarded. The column was dried by centrifugation at full speed for 1 min and RNase-free water was added directly onto the column membrane.

To elute the RNA, the column was centrifuged at 8,000 x *g* for 1 min at RT and the RNA pellet was collected in a new Eppendorf tube. The column and supernatant were removed and the pellet was washed in 1 ml 75% ethanol and centrifuged at 8,000 x *g*, 5 min, 4 ^{0}C. The supernatant was again removed and the pellet air-dried at RT before being dissolved in 20-50 µl DNase/RNAse-free water.

To determine the concentration and purity of RNA, 2 µl of each sample was dissolved in 500 µl of 10 mM Tris/HCl solution (pH 7.5) and analysed using UV spectrophotometry at 260 and 280 nm using a GeneQuantpro spectrophotometer (Amersham Biosciences, Buckinghamshire, UK, Cat No. 80-2114-98).

The RNA destined for mRNA profiling was performed by Cambridge Genomic Services, University of Cambridge. The RNA was assessed for concentration and quality using a SpectroStar (BMG Labtech, Aylesbury, UK) and a Bioanalyser (Agilent Technologies, Cheadle, UK) and the mRNA profile was described as follows from the Cambridge Genomic Service Microarray Gene Expression Report. Microarray experiments were performed using the HumanHT-12 v4 Expression BeadChip (Illumina, Chesterford, UK) according to the manufacturer's instructions. Briefly, 200 ng of Total RNA underwent linear amplification using the Illumina TotalPrep RNA Amplification Kit (Life Technologies, Paisley, UK) following the manufacturer's instructions. The concentration, purity and integrity of the resulting cRNA were measured by SpectroStar and Bioanalyser. Finally cRNA was hybridised to the HumanHT-12 v4 BeadChip overnight followed by washing, staining and scanning using the Bead Array Reader (Illumina).

After scanning, these data were loaded in Illumina proprietary software, GenomeStudio. No background correction or normalisation was applied at this stage. A final report was generated, creating a text file containing the sample probe profile and the control probe information. The report was then processed in R software (version 3.2.2) using the Lumi package (Du et al. 2008) and the Limma package (Ritchie et al. 2015). These data were loaded and divided into subsets according to the groups being compared; only the samples involved in a given comparison were used. Subsets were then filtered to remove any non-expressed probes using the detection p-value from Illumina. Across all samples, probes for which the intensity values were not significantly different from the negative controls (P>0.01) were removed from the analysis. Following filtering,

these data were transformed using the Variance Stabilization Transformation (VST) (Du et al. 2008) from Lumi and then normalised to remove technical variation between arrays using quantile normalisation. Comparisons were performed using the Limma package with results corrected for multiple testing using False Discovery Rate (FDR) testing. Finally, the quality of these data was assessed and the correlation of the samples in the groups compared.

2.2.11.1 Bioinformatic analysis

ClueGO, a cytoscape plug-in, was used to create a visualization map from microarray analysis by integrating Gene Ontology (GO) terms, KEGG/Biocarta pathways and DAVID Bioinformatics. The software was used for comparison analysis between the mRNA expression profiles of hCPEpiC and published experimental data of genes involved in specific biological processes.

2.2.12 RT-qPCR analysis

cDNA was synthesized by the High Capacity cDNA Reverse Transcription kit (Life Technologies, Applied Biosystems division, Paisley, UK, Cat No. 4368814) using random primers according to the manufacturer's protocol. This included adding 1.3 ng/µl of RNA to a 2X Reverse Transcription (RT) Master Mix as described in Table 2.11:

Reagent	Volume (µl)/Reaction
10X Reverse Transcription Buffer	2.0
25X dNTP Mix (100mM)	0.8
10X RT Random Primers	2.0
Multiscribe^{TM} Reverse Transcriptase	1.0
RNase Inhibitor	1.0
RNase-free H_2O	3.2

Table 2.11: Volumes in µl of reagents used to prepare 10 µl of a 2X Reverse Transcription Master Mix.

A volume of 10 µl of 2X RT Master Mix was pipetted into individual tubes before adding 10 µl of each RNA sample to each specific Master Mix tube, after mixing. The tubes were briefly centrifuged to eliminate any air bubbles that may have formed. Each sample was then placed in a Bio-Rad thermal cycler (Bio-Rad iCycler, Bio-Rad Laboratories Ltd, Hertfordshire, UK) at 25 ^{0}C for 10 min, 37 ^{0}C for 120 min and 85 ^{0}C for 5 min before being cooled to 4 ^{0}C.

TaqMan® gene expression real-time q-PCR kit (Fischer Scientific, Loughborough, UK) was used to determine the relative levels of cDNAs that correspond to the mRNAs transcribed from the genes of interest. Specific TaqMan® gene expression assay primer/probe set, also provided by Fischer Scientific, Loughborough, UK, were used to determine Sjogren's Syndrome Antigen A2 (Ssa2, also known as TROVE-2) (Hs00190252_m1), Sperm Associated Antigen 16 (SPAG16) (Hs00226005_m1), Neurochondrin (NCDN) (Hs00379444_m1) and Cerebral Cavernous Malformation 2 (CCM2) (Hs01123855_m1) mRNA levels, whereas Eukaryotic 18s rRNA (Hs99999901_s1) was used as an internal control.

A PCR Reaction Mix was made as described in Table 2.12.

Reagent	Volume (µl)/Reaction
TaqMan Gene Expression Master Mix (2X)	10.0
TaqMan Gene Expression Assay (Primer) (20X)	1.0

Table 2.12: Volumes in µl of reagents used to set up a PCR Reaction Mix.

The PCR Reaction Mix was added to each well of an optical plate along with 3 ng cDNA replicates and RNase-free H_2O to create a final volume of 20 µl per well. 3 ng cDNA was used as it was the maximum amount of cDNA obtainable from the samples in order to perform replicates. The plate was covered with a MicroAMP^{TM} Optical Adhesive Film (Fischer Scientific, Loughborough, UK, Cat No. 4311971) and centrifuged briefly to remove any air bubbles from the solution. The plate was run on a DNA Engine Opticon 2 Continuous Fluorescence Detector (MJ Research, Quebec, Canada). The thermal cycling conditions were set as shown in Table 2.13.

Step	AmpliTaq Gold, UP Enzyme Activation	PCR	
	HOLD	CYCLE (40 Cycles)	
		Denature	Anneal/Extend
Time	10 minutes	15 seconds	1 minute
Temperature (^{0}C)	95	95	60

Table 2.13: Thermal cycling conditions.

2.2.13 Immunocytochemistry

Immunocytochemistry was used to view the expression of Transthyretin (TTR), Zonula Occludens-1 (ZO-1) and Claudin-1 tight junctional proteins; Na^+-K^+-

ATPase, NKCC1, AQP1, and ENaC transporters/channels; and CCR2, IL-17Rα, TNF-R1, and IL-6R receptors on hCPEpiC.

2.2.13.1 Preparation of solutions

A 4% (w/v) PFA (Sigma-Aldrich, Dorset, UK, Cat No. P6148) solution was made by dissolving 4 g PFA powder in 100 ml PBS (Sigma-Aldrich, Dorset, UK, Cat No. P4417) before adjusting the pH to 7.4 using drops of NaOH. A 0.5% (w/v) bovine serum albumin (BSA) (Sigma-Aldrich, Dorset, UK, Cat No. A9085) solution was made by dissolving 0.5 g BSA in 100 ml PBS. A 0.025% Tween-20 (Sigma-Aldrich, Dorset, UK, Cat No. P7949) solution was made by adding 2.5 µl Tween-20 into 10 ml PBS.

2.2.13.2 Incubation with primary antibodies

The hCPEpiC were grown to confluence on Lab-Tek II Glass Chamber Slides (ThermoFisher Scientific, Loughborough, UK, Cat No. 154917). All of the solutions were added at a volume of 300 µl/well of chamber slide and the slides were placed on a shaker for 5-10 min each time unless stated otherwise.

The medium was removed and the cells were washed twice with pre-warmed HBSS (with Ca^{2+}). The cells were then fixed for 10 min with 4% PFA solution at RT. The cells were then washed once in PBS and then once in 0.5% (w/v) BSA for 30 min. The cells were then incubated with the primary antibodies overnight at 4 ^{0}C at the concentrations shown in Table 2.14.

Primary Antibody	Supplier	Working Conc.	Volume Added
Prealbumin (TTR) Sheep Polyclonal IgG	Abcam, Cambridge, UK, Cat No. ab9015	1:100 (196 µg/ml)	1 µl of stock (19.6 mg/ml) into 100 µl 0.5% BSA
ZO-1 Rabbit Polyclonal IgG	Life Technologies, Paisley, UK, Cat No. 61-7300	1:80	1.25 µl of stock into 100 µl 0.5% BSA
Claudin-1 Rabbit Polyclonal IgG	Thermo Fisher Scientific, Hemel Hempstead, UK, Cat No. 51-9000;	1:50	2 µl of stock into 100 µl 0.5% BSA
Na^+K^+ATPase Rabbit Polyclonal IgG	Abcam, Cambridge, UK, Cat No. ab58475	1:100	1 µl of stock into 100 µl 0.5% BSA
NKCC1 Rabbit Polyclonal IgG	Abcam, Cambridge, UK, Cat No. ab58475	1:1000	0.1 µl of stock into 100 µl 0.5% BSA
Aquaporin-1 Rabbit Polyclonal IgG	Abcam, Cambridge, UK, Cat No. ab15080	1:500	0.2 µl of stock into 0.5% BSA
ENaC Rabbit Polyclonal IgG	Abcam, Cambridge, UK, Cat No. ab65710	1:200	0.5 µl of stock into 100 µl0.5% BSA
CCR2 Rabbit Polyclonal IgG	Abcam, Cambridge, UK, Cat No. ab21667	1:50 (20 µg/ml)	2 µl of stock into 100 µl 0.5% BSA
IL-17Rα Rabbit Polyclonal IgG	St John's Laboratory Ltd, London, UK, Cat No. STJ93683	1:1000 (1 µg/ml)	0.1 µl of stock into 100 µl 0.5% BSA
TNF-R1 Rabbit Polyclonal IgG	Abcam, Cambridge, UK, Cat No. ab19139	1:1000 (1 µg/ml)	0.1 µl of stock (1 mg/ml) into 100 µl 0.5% BSA
IL6R Rabbit Polyclonal IgG	Abcam, Cambridge, UK, Cat No. ab85105	1:500 (1 µg/ml)	0.2 µl of stock (0.5 mg/ml) into 100 µl 0.5% BSA

Table 2.14: Volumes in µl and working concentrations of primary antibodies used in ICC analysis of hCPEpiC proteins, transporters/channels and receptors.

2.2.13.3 Incubation with secondary antibodies

The cells were then washed three times in PBS and twice with 0.025% Tween-20 for 5-10 min each time before being incubated with the corresponding fluoresceinisothiocynate (FITC)/Alexa secondary antibodies for 1 h at RT at the concentrations shown in Table 2.15.

Secondary Antibody	Supplier	Working Conc.	Volume Added
Donkey anti-sheep IgG (FITC conjugated)	Abcam, Cambridge, UK, Cat No. ab9015	1:200 (10 µg/ml)	2.5 µl of stock (2 mg/ml) into 500 µl 0.5% (w/v) BSA
Goat anti-rabbit IgG (Alexa 488 conjugated)	Life Technologies, Paisley, UK, Cat No. A11008	1:200	2.5 µl stock into 500 µl 0.5% (w/v) BSA

Table 2.15: Volumes in µl and working concentrations of secondary antibodies used in ICC analysis of hCPEpiC proteins, transporters/channels and receptors.

The cells were again washed twice with 0.025% Tween-20 and three times with PBS for 5-10 min each time. The slide holder was then placed in between the rubber gasket of the slide partitions and the chamber walls in order to peel off the walls leaving the slide and rubber gasket intact. Each partition on the slide was stained with one drop of DAPI nuclei stain (Southern Biotech, Alabama, USA, Cat no. 0100-20) before the rubber gasket was peeled off and a 22x50 mm coverslip was placed on top. The images were viewed using a Leica SP-5 confocal microscope (Leica Microsystems, Milton Keynes, UK).

2.2.14 Flow cytometry analysis

Flow cytometry was used to confirm the expression as seen with immunocytochemistry of TTR protein; Na^+-K^+-ATPase, NKCC1 Aquaporin-1, and ENaC transporters/channels; and CCR2, IL-17Rα, TNF-R1, IL6R receptors on hCPEpiC. The concentrations of the primary and secondary antibodies used were the same as in Tables 2.14 and 2.15, respectively. In addition, a separate experiment was performed to measure the expression levels of the hCPEpiC transporters/channels following a 24 h incubation with HC, TNF-α, and IL-6 treatments at the same concentrations as seen in Table 2.2.

A 1x PBS solution and a 2% (w/v) PFA solution was made by dissolving 2 g PFA powder in 100 ml PBS before adjusting the pH to 7.4 using drops of NaOH.

hCPEpiC were grown to confluence in 6 well tissue culture plates (total = $5x10^5$ cells per well). Two wells were used for the untreated control transporter antibody and two were incubated with the cytokine/mediator of interest, with the transporter antibody, 24 h prior to the start of the experiment which would equate to the treated transporter reading. The treated transporter reading would show if there was an increase in hCPEpiC transporter expression following treatment with the cytokine/mediator of interest against the untreated transporter antibody control.

The cells were harvested by removing the medium and washing them once with HBSS (without Ca^{2+}) before incubation at 37 ^{0}C for 2-3 min. The solution was then aspirated before 1 ml of Trypsin + EDTA solution (Sigma-Aldrich, Dorset, UK, Cat No. T3924) was added before incubation again at 37 ^{0}C for 1-2 min. The cells were checked under the microscope to determine if they had detached from the wells before 2 ml of 10% FBS was added to block the action of the trypsin solution.

All of the following stages were carried out on ice. The cells from each well were transferred into separately labelled 15 ml tubes and were then centrifuged (1000 x *g* for 5 min) and the supernatant removed before washing the pellet in 10 ml HBSS (with Ca^{2+}) and then again in 10 ml PBS. The cells were then fixed in 1 ml of 2% PFA solution for 30 min at RT. After fixing, two further washes in PBS were

carried out before the cells from each corresponding well were re-suspended in antibody diluent (0.5% (w/v) BSA) at a volume of 500,000 cells per 1.5 ml Eppendorf tube. The primary antibodies were then added at the concentrations shown in Table 2.14. The samples were then placed at 4 ^{0}C on a shaker overnight.

After incubation with the primary antibody, the cells were washed twice with PBS microfuged (Hettich Zentrifugen EBA IZR) at 1000 x *g* for 5 min before being re-suspended in 100 µl 0.5% (w/v) BSA containing their corresponding FITC/Alexa secondary antibodies (as shown in Table 2.15) for 2 h at 4 ^{0}C on a shaker.

After incubation, the cells were again washed twice in 1 ml PBS/tube and microfuged at 1000 x *g* for 5 min. Following the final wash, each cell pellet was re-suspended in 300 µl HBSS (with Ca^{2+}) and transferred to separate BD Falcon 5 ml polystyrene round bottom fluorescence activated cell sorting (FACS) tubes (Becton Dickinson, Cat No. 352052) before being analysed using a FACS Calibur flow cytometer (Becton Dickinson, Franklin Lakes, NJ, USA) with Cell Quest software (Pro BD Biosciences). The results were expressed as a median fluorescence for each 10,000 cell sample in arbitrary units.

2.2.15 Statistical analysis

All data are presented as mean ± standard error of the mean and are the result of a number of independent experiments (n) with replicates specified in each figure or legend. Calculations were performed using GraphPad Prism 7 software (GraphPad Software, La Jolla, USA). A one-way ANOVA was used for comparison

of initial control *in vivo* CSF secretion and resistance to CSF drainage experiments against treatment groups. A two-way ANOVA was used for comparison of *in vivo* control CSF secretion rates and resistance to drainage experiments for both diets, respectively. A three-way ANOVA tested *in vivo* CSF secretion rates and resistance to drainage experiment values of each treatment against control for both diets, respectively. In all cases, ANOVAs were followed by an unpaired t test with Welch-correction (one-way ANOVA) or Sidak's multiple comparison post hoc test (two- and three-way ANOVA) to determine a significant difference among groups. The significant multiple comparison results following the post-hoc test is shown in each graph. Positive/negative results refers to an increase/decrease in CSF secretion rates over controls, respectively. Correlation r^2 analysis was performed for all *in vivo* control experiment values against weight gain; total cholesterol; and LDL/VLDL cholesterol readings. Statistically significant differences are presented as probability levels of $P < 0.05$ (*), $P < 0.01$ (**), $P < 0.001$ (***).

3.0 Results

3.1 CSF secretion rate

A ventriculo-cisternal perfusion method, adapted from studies by Oreskovic et al. 2003, was used to investigate the *in vivo* effects of exogenous cytokines/treatments, that have been reported to be elevated in the CSF of IIH patients, on CSF secretion rates, as a possible mechanism contributing to raised intracranial pressure. Male Wistar rats, 250-300g were perfused with aCSF, (with or without the treatment of interest) through both lateral ventricles for 90 min. The concentration of blue dextran in the perfusate collected from the cisterna magna relative to that in the aCSF (C_{out}/C_{in}) versus time, which was used to calculate CSF secretion rate, is shown in Fig. 3.1. Following initiation of the perfusion of aCSF, there was a sharp increase in the relative concentration of blue dextran in the perfusate, which reached steady state after 20-40 min, depending on the treatment. Control, IL-6, CCL2 and HC treatments reached steady state after 20 min aCSF perusion. TNF-α, leptin and IL-1β reached steady state after 30 min and IL-17 after 40 min perfusion.

3.1.1 Cytokine administration in perfused aCSF

The values obtained from the mean steady state results (Fig. 3.1) were used to calculate the CSF secretion rates for each treatment from the ventriculo-cisternal perfusion experiments.

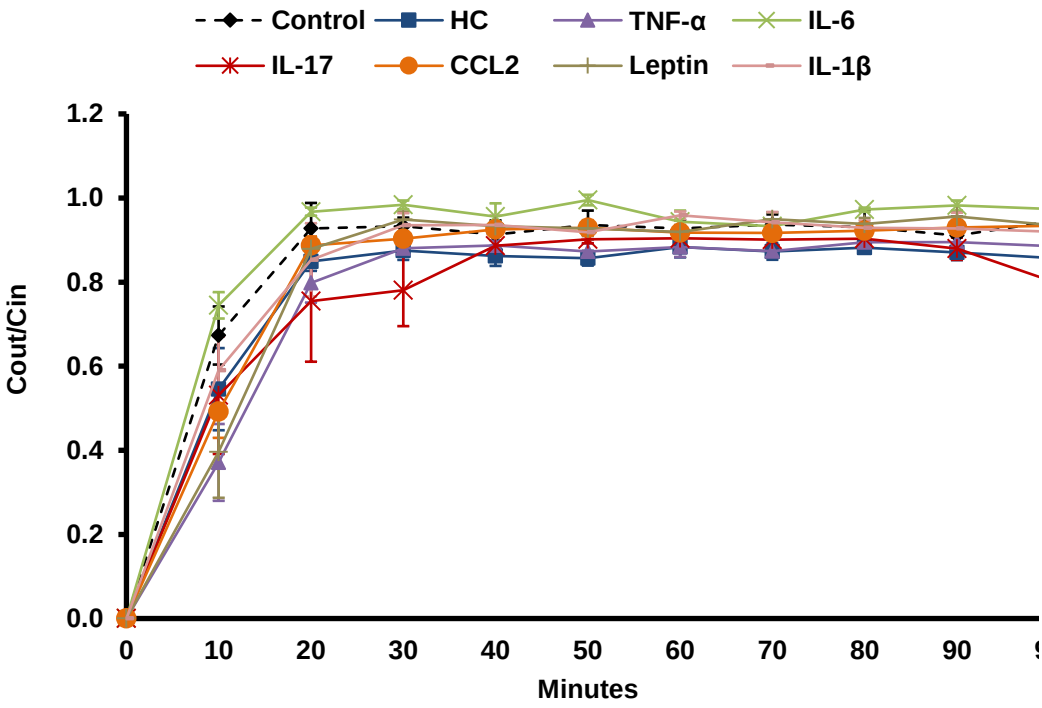

Figure 3.1: Mean steady state values (C_{out}/C_{in}) of the perfused aCSF ventriculo-cisternal perfusion experiments.
Mean steady states were calculated from the concentration of blue dextran in the perfusate collected from the cisterna magna relative to that in the aCSF C_{out}/C_{in}. Concentrations of treatments in aCSF, perfused for 90 min: HC (0.5 µg/ml, n=4), TNF-α (0.0001 µg/ml, n=3), IL-17 (0.0001 µg/ml, n=4), IL-6 (0.0001 µg/ml, n=3), CCL2 (0.05 µg/ml, n=4), leptin (0.1 µg/ml, n=4), IL-1β (0.0001 µg/ml, n=3). Samples were averaged (±SEM) and compared to controls (n=5). C_{out}/C_{in} values from each treatment were averaged from 40-94 mins and extrapolated to the y-axis. Individual treatment results are shown in Appendix Section 6.3, page 270.

Steady state C_{out}/C_{in} values differed between treatments. Control steady state C_{out}/C_{in} values (0.93 ±0.03) were similar to those obtained previously in the adult rat (Harnish & Samuel 1988). Treatment with HC or TNF-α showed the lowest average steady state C_{out}/C_{in} values (0.88 ±0.02 and 0.87 ±0.03, respectively), suggesting an increase in CSF secretion rate compared to controls. By contrast, IL-6 showed the highest average steady state C_{out}/C_{in} values (0.97 ±0.07), suggesting a lower CSF secretion rate compared to controls. No significant changes in steady state C_{out}/C_{in} were observed following treatment with CCL2, leptin and IL-1β

compared to controls. The C_{out}/C_{in} values at steady state were then used to calculate the CSF secretion rates for each treatment, according to the formula described in the Methods Section 2.2.2 (Equation 2.1), as shown in Fig. 3.2.

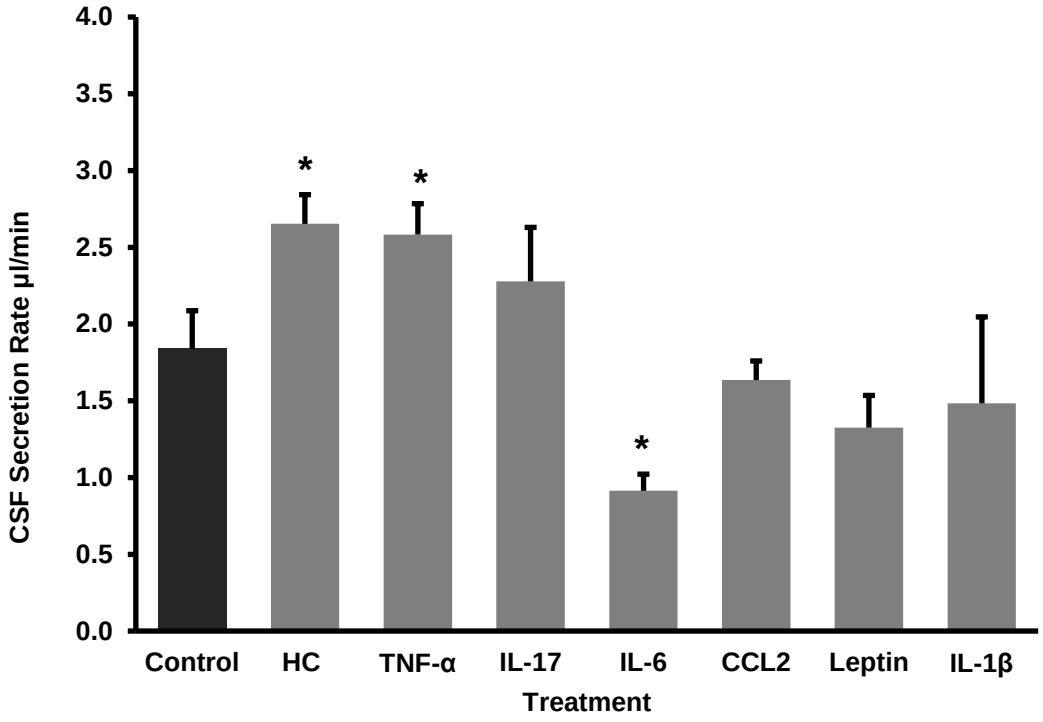

Figure 3.2: CSF secretion rates for each treatment using ventriculo-cisternal perfusion.
Each experiment was carried out by perfusing aCSF with each treatment through both lateral ventricles of the rat brain. CSF secretion rates were obtained once at steady state (40-90 min) and averaged ±SEM and compared to controls (n=5). Concentrations of treatments in aCSF, perfused for 90 min: HC (0.5 µg/ml, n=4), TNF-α (0.0001 µg/ml, n=3), IL-17 (0.0001 µg/ml, n=4), IL-6 (0.0001 µg/ml, n=3), CCL2 (0.05 µg/ml, n=4), leptin (0.1 µg/ml, n=4), IL-1β (0.0001 µg/ml, n=3). A one-way ANOVA was used to analyse the statistical significance. The significant results are shown following an unpaired t test with Welch-correction and was made against the control in expectation of positive (increased CSF secretion)/negative (decreased CSF secretion) results *P = ≤0.05.

The *in vivo* measurements of CSF secretion rates where treatments were added to perfused aCSF, displayed in Fig. 3.2, show that HC (2.65 ±0.19 µl/min) and TNF-α

(2.58 ±0.20 µl/min) significantly increased CSF secretion rates ($P \leq 0.05$), and IL-6 (0.91 ±0.11 µl/min) showed a significant decrease in CSF secretion rate when compared to controls (1.84 ±0.25 µl/min, $P \leq 0.05$). Treatment with CCL2 (1.64 ±0.12 µl/min), leptin (1.33 ±0.21 µl/min) and IL-1β (1.48 ±0.56 µl/min) showed a slight decrease in CSF secretion, although these were not statistically significant. IL-17 treatment (2.28 ±0.35 µl/min) increased the CSF secretion rate compared to controls but this effect was also not statistically significant.

3.1.2 Cytokine peripheral administration

The effect of peripheral (i.p) administration of the different treatments on CSF secretion was also assessed as some of the cytokines are reported to be increased in the plasma of IIH patients as well as in the CSF. The i.p. administered dose of each treatment was in addition to the perfused aCSF dose as performed earlier in Fig. 3.2. The C_{out}/C_{in} values obtained from the mean steady state results (Fig. 3.3) were used to calculate the CSF secretion rates for each treatment from the i.p. ventriculo-cisternal perfusion experiments shown in Fig. 3.4. CSF secretion rates from all treatments reached steady state after 20 mins perfusion.

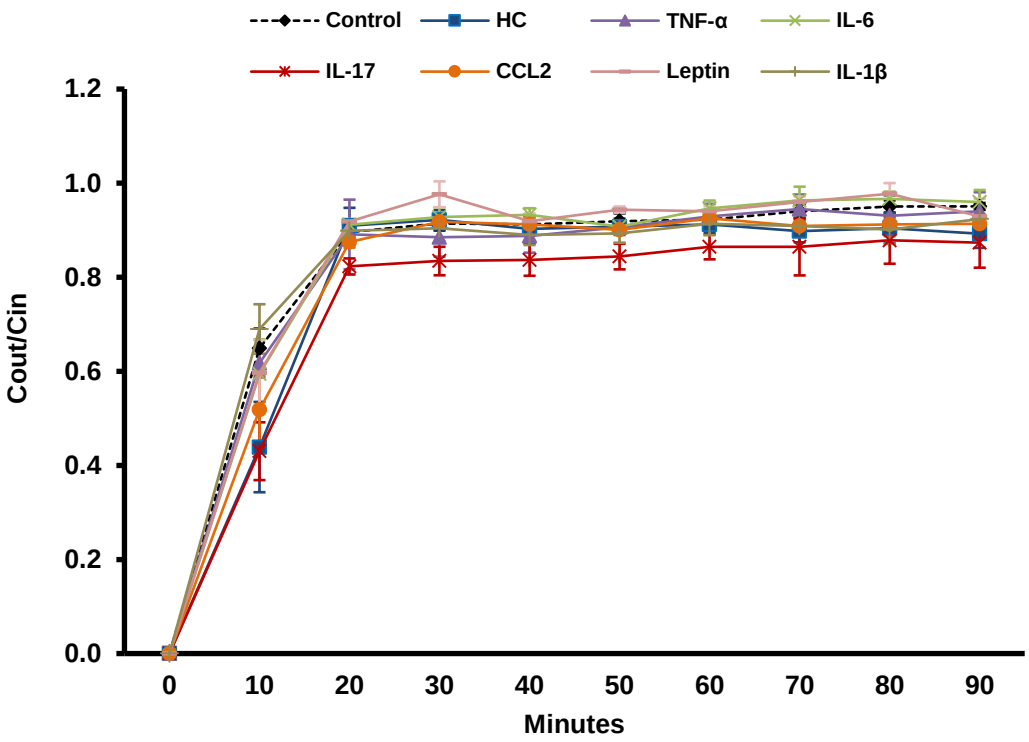

Figure 3.3: Mean steady state values (C_{out}/C_{in}) of the perfused aCSF following i.p. injection of treatment for the ventriculo-cisternal perfusion experiments. Complete mean steady states were calculated from the concentration of blue dextran in the perfusate collected from the cisterna magna relative to that in the aCSF C_{out}/C_{in}. Concentrations of treatments in aCSF, perfused for 90 min: HC (aCSF 0.5 µg/ml, i.p. 100 µg/ml, n=3), TNF-α (aCSF 0.0001 µg/ml, i.p. 0.025 µg/ml, n=3), IL-17 (aCSF 0.0001 µg/ml, i.p. 0.025 µg/ml, n=3), IL-6 (aCSF 0.0001 µg/ml, i.p. 0.025 µg/ml, n=3), CCL2 (aCSF 0.05 µg/ml, i.p. 10 µg/ml, n=5), leptin (aCSF 0.1 µg/ml, i.p. 25 µg/ml, n=3), IL-1β (aCSF 0.0001 µg/ml, i.p. 0.025 µg/ml, n=4). Samples were averaged (±SEM) and compared to controls (n=4). C_{out}/C_{in} values from each treatment were averaged from 40-90 mins and extrapolated to the y-axis. Individual treatment results against the control are shown in Appendix Section 6.4, page 274.

IL-17 treatment showed the lowest average steady state value (0.88 ±0.04) indicating an increase in CSF secretion rate, although it was not statistically significant when compared with control (0.92 ±0.04). Treatment with HC (0.92 ±0.02), TNF-α (0.92 ±0.05), IL-6 (0.92 ±0.06), CCL2 (0.92 ±0.03), leptin (0.94 ±0.06) and IL-1β (0.92 ±0.03) showed no change in steady state values when compared with control. These results correspond to the calculated CSF secretion rates following i.p injection plus treatments in perfused aCSF results in Fig. 3.4.

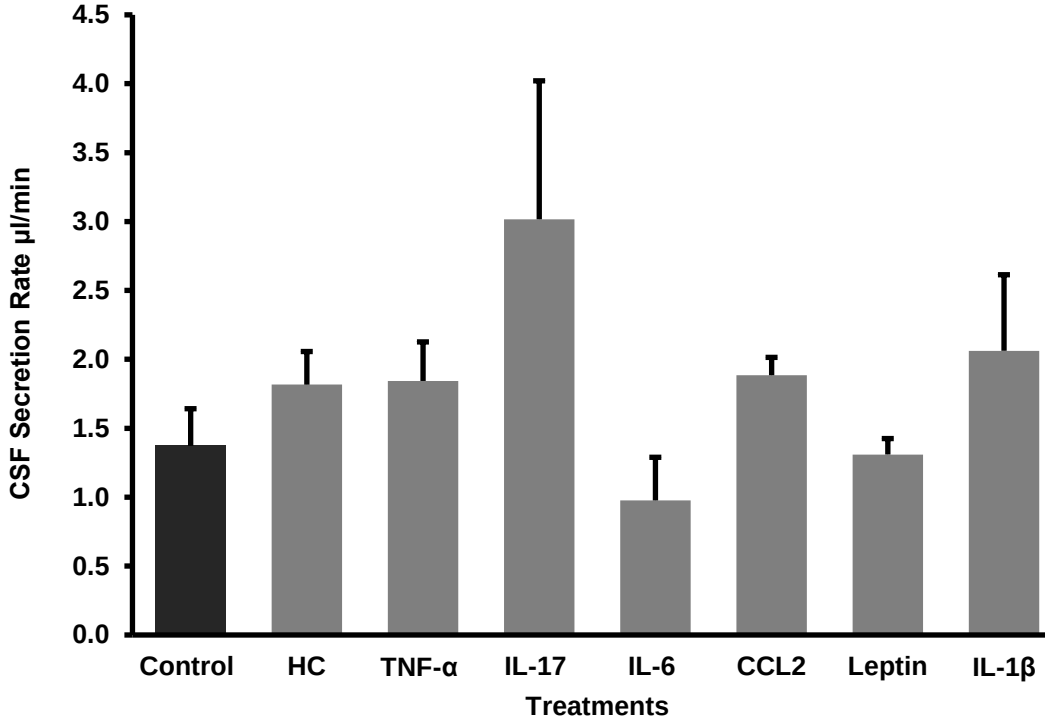

Figure 3.4: CSF secretion rates using ventriculo-cisternal perfusion following intraperitoneal injection of each treatment 90 min prior to perfusion.
Each experiment was carried out by perfusing aCSF with a treatment through both lateral ventricles of the rat brain following i.p. injection of the same treatment 90 min prior to perfusion. CSF secretion rates were obtained from each animal once at steady state (40-90 min) and averaged ±SEM before comparing to controls (n=4). Concentrations of treatments in aCSF, perfused for 90 min: HC (aCSF 0.5 µg/ml, i.p. 100 µg/ml, n=3), TNF-α (aCSF 0.0001 µg/ml, i.p. 0.025 µg/ml, n=3), IL-17 (aCSF 0.0001 µg/ml, i.p. 0.025 µg/ml, n=3), IL-6 (aCSF 0.0001 µg/ml, i.p. 0.025 µg/ml, n=3), CCL2 (aCSF 0.05 µg/ml, i.p. 10 µg/ml, n=5), leptin (aCSF 0.1 µg/ml, i.p. 25 µg/ml, n=3), IL-1β (aCSF 0.0001 µg/ml, i.p. 0.025 µg/ml, n=4). A one-way ANOVA was used to analyse the statistical significance. No significant results were shown following an unpaired t test with Welch-correction which was made against the control in expectation of positive (increased CSF secretion)/negative (decreased CSF secretion) results.

The *in vivo* measurements of CSF secretion where treatments were injected intraperitoneally into male adult Wistar rats 90 min prior to perfusion of the same treatment into the lateral ventricles are displayed in Fig. 3.4. There were no significant changes in CSF secretion rates for any treatments compared to control (1.37 ±0.27 µl/min) values; HC (1.82 ±0.24 µl/min), TNF-α (1.84 ±0.28 µl/min), IL-

6 (0.98 ±0.31 µl/min), IL-17 (3.02 ±1.00 µl/min), CCL2 (1.89 ±0.13 µl/min), leptin (1.31 ±0.12 µl/min), IL-1β (2.06 ±0.55 µl/min).

No effect on CSF secretion rates was observed following the addition of an i.p. pre-injection with any mediator. This may be due to the effect of each mediator becoming transient over time. As the i.p. dose was injected 90 min prior to perfusion, this may have been too long for an effect to be seen.

3.2 Initial CSF volume

IIH is characterised by an increase in intracranial pressure, thought to be due to an increase in CSF secretion rates, altered CSF drainage pathways leading to an increase in resistance to CSF drainage, or a combination of both of these. Having tested the CSF secretion rate effects of each mediator, it was important to test their effects on initial CSF volume following an i.p. pre-injection 90 mins prior to ventriculo-cisternal perfusion. The initial CSF volume was calculated as in method section 2.2.2 Equation 2.3, where the sum of the average CSF secretion rate over 90 min perfusion (µl/90min) was subtracted from the total volume of CSF secreted throughout the whole experiment (µl), and displayed in Fig. 3.5.

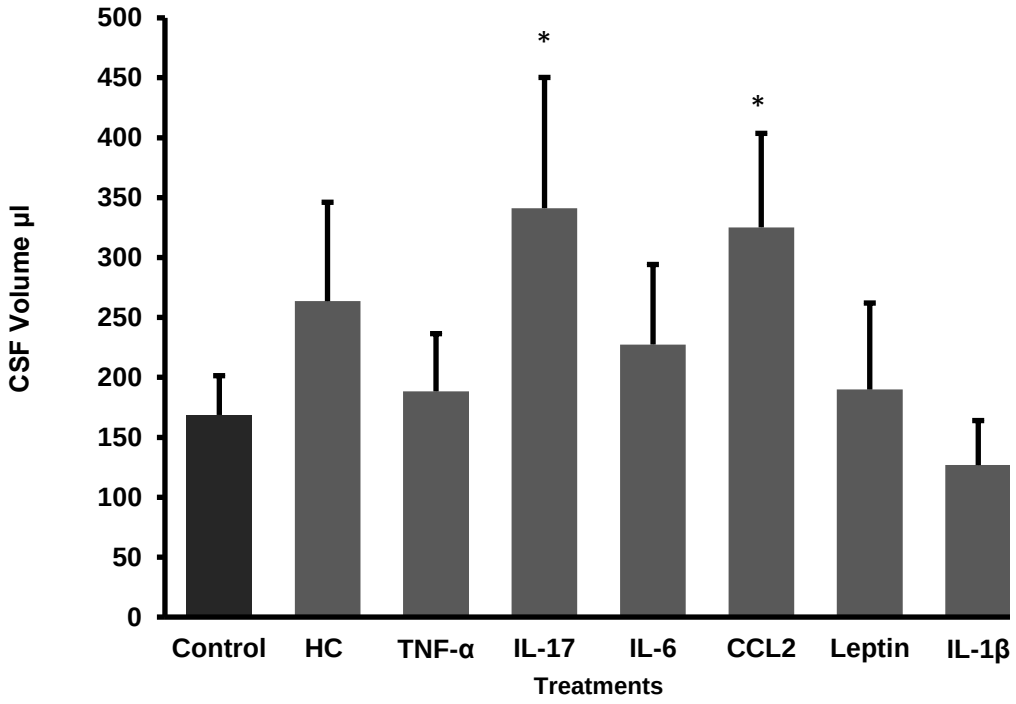

Figure 3.5: Initial CSF volumes (µl).
Each experiment was carried out by an i.p. injection of each treatment 90 min prior to perfusion. The mean volume of CSF obtained within that window (±SEM) for each treatment is indicated and was compared to controls (n=4). Concentrations of treatments in aCSF, perfused for 90 min: HC (aCSF 0.5 µg/ml, i.p. 100 µg/ml, n=3), TNF-α (aCSF 0.0001 µg/ml, i.p. 0.025 µg/ml, n=3), IL-17 (aCSF 0.0001 µg/ml, i.p. 0.025 µg/ml, n=3), IL-6 (aCSF 0.0001 µg/ml, i.p. 0.025 µg/ml, n=3), CCL2 (aCSF 0.05 µg/ml, i.p. 10 µg/ml, n=5), leptin (aCSF 0.1 µg/ml, i.p. 25 µg/ml, n=3), IL-1β (aCSF 0.0001 µg/ml, i.p. 0.025 µg/ml, n=4). A one-way ANOVA was used to analyse the statistical significance. The significant results are shown following an unpaired t test with Welch-correction and was made against the control in expectation of positive (increased CSF secretion)/negative (decreased CSF secretion) results. * P = ≤0.05.

Treatment with CCL2 (325.2 ±78.41 µl) and IL-17 (341.17 ±109.10 µl) showed a significantly increased initial CSF volume following i.p injection and 90 min aCSF perfusion (Fig. 3.5) when compared with controls (168.63 ±28.40 µl) (P≤0.05). Due to the significant increase in initial CSF volume but no significant change in overall CSF secretion for CCL2 and IL-17, this could indicate impairment within CSF drainage associated with these cytokines.

3.3 Resistance to CSF drainage

The variable rate infusion method was used to determine the resistance to CSF drainage of the three treatments that significantly increased CSF secretion rates from Fig. 3.2 (HC, TNF-a and IL-6), as well as IL-17 and CCL2, which caused a significant increase in initial CSF volumes (Fig. 3.5), which were administered over four increasing infusion rates (5, 10, 16, 20 µl/min) as described in Fig. 3.6a and b.

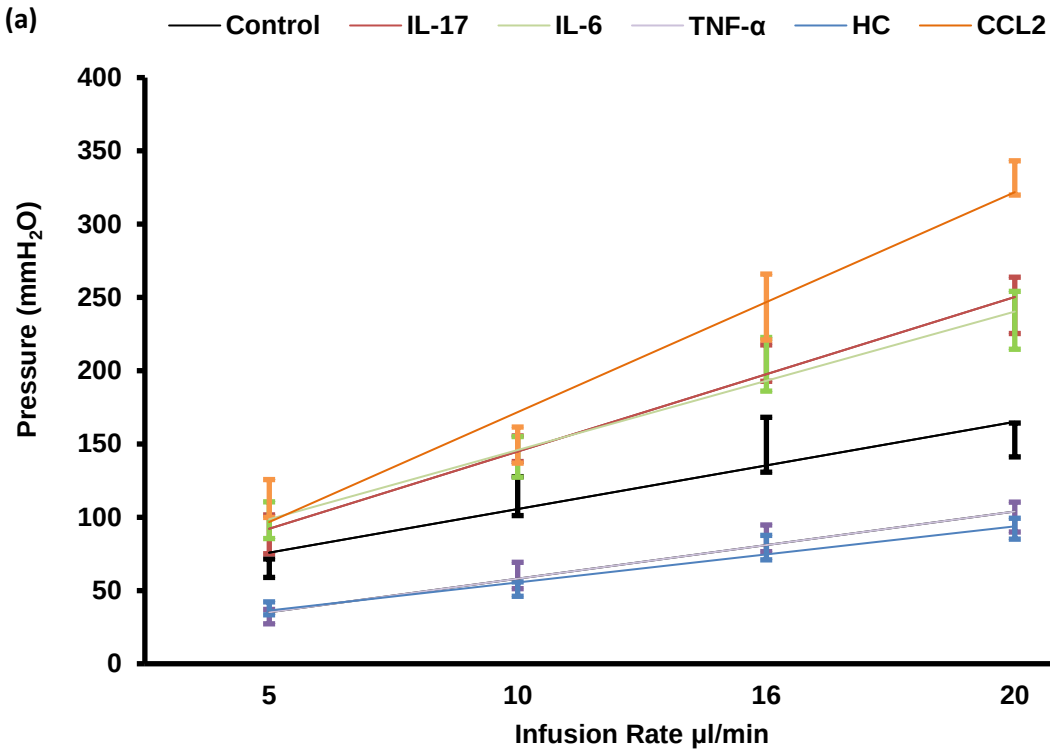

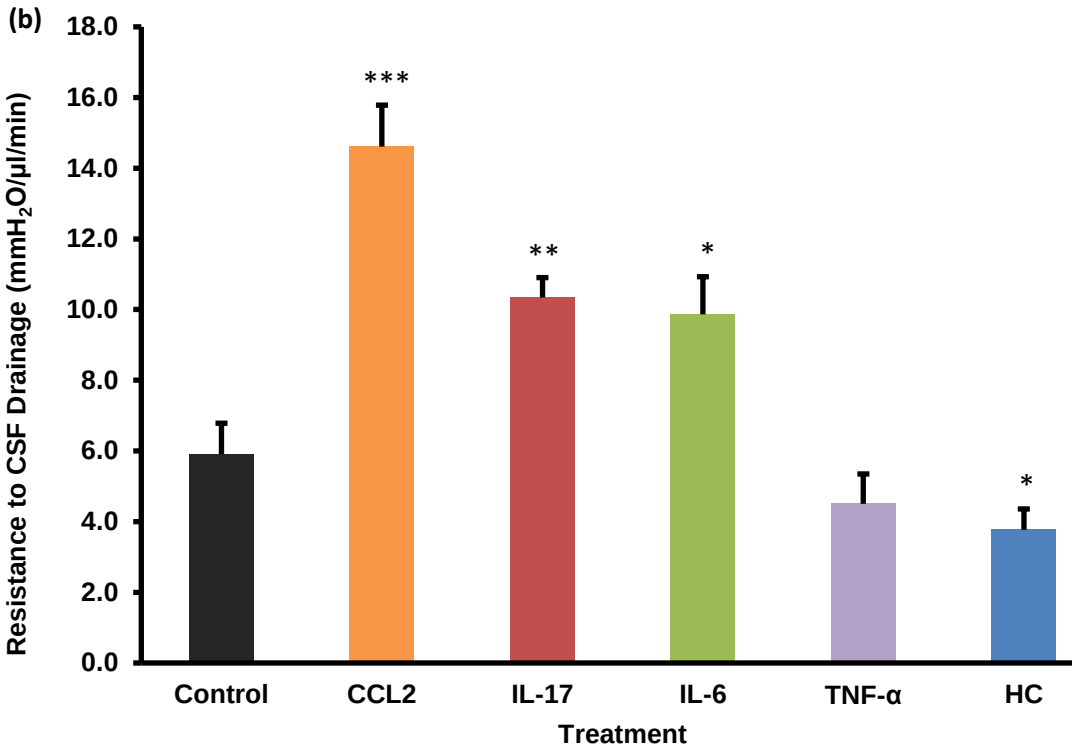

Figure 3.6: Resistance to CSF drainage values ($mmH_2O \cdot min/\mu l$) following variable rate infusion.

Each experiment was carried out by perfusing aCSF with each treatment through one lateral ventricle plus the addition of a single dose i.p treatment injection minutes prior to perfusion. Concentrations of treatments in i.p injection and aCSF perfused for 90 min: HC (i.p. 100 µg + aCSF 0.5 µg/ml, n=3) CCL2 (i.p 10 µg + aCSF 0.005 µg/ml, n=3), IL-6 (i.p 0.025 µg + aCSF 0.0001 µg/ml, n=4), IL-17 (i.p 0.025 µg + aCSF 0.0001 µg/ml, n=3), TNF-α (i.p 0.025 µg + aCSF 0.0001 µg/ml, n=3). Samples from each group were averaged (±SEM). The graphs show the linear pressure readings (mmH_2O) at each infusion rate (a); averaged resistance to CSF drainage readings ($mmH_2O \cdot min/\mu l$) (b). A one-way ANOVA was used to analyse the statistical significance. The significant results are shown following an unpaired t test with Welch-correction and was made against the control in expectation of positive (increased resistance to CSF drainage) / negative (decreased resistance to CSF drainange) results *P = ≤0.05; ** P = ≤0.01, *** P = ≤0.001.

CCL2 (14.61 ±1.17 $mmH_2O \cdot min/\mu l$), IL-17 (10.34 ±0.56 $mmH_2O \cdot min/\mu l$) and IL-6 (9.87 ±1.06 $mmH_2O \cdot min/\mu l$) administration caused a significantly higher resistance to CSF drainage (n=3-5; P≤0.05) when compared with controls (5.91 ±0.87 $mmH_2O \cdot min/\mu l$, n=3), suggesting an impairment to the absorption of CSF in the presence of these cytokines. HC (3.77 ±0.59 $mmH_2O \cdot min/\mu l$, n=3) caused a

significant decrease when compared with controls, however TNF-α (4.51 ±0.84 $mmH_2O \cdot min/\mu l$, n=3) showed no change in resistance to CSF drainage.

3.4 Summary of initial investigation on CSF secretion rates and resistance to CSF drainage

Mediator	Initial CSF Volume	CSF Secretion Rate	Resistance to CSF Drainage
IL-17	↑	n/s	↑↑
CCL2	↑	n/s	↑↑↑
IL-6	n/s	↓	↑
HC	n/s	↑	↓
TNF-α	n/s	↑	n/s
IL-1β	n/s	n/s	n/d
Leptin	n/s	n/s	n/d

Table 3.1: Summary of in vivo results.
A summary of the results from initial CSF volumes, CSF secretion rates and resistance to CSF drainage, following mediator treatment, from ventriculo-cisternal perfusion and variable rate infusion experiments. Red arrow = significant increase, blue arrow = significant decrease, n/s = not significant, n/d = not determined.

Table 3.1 summarises results obtained in sections 3.1 through to 3.3. Out of the seven mediators tested, five appear to regulate CSF dynamics but in different directions. HC and TNF-α treatment appeared to increase CSF secretion rates but also to decrease resistance to CSF drainage (although in the case of TNF-α this was not significant for the resistance to CSF drainage results). Hence the initial CSF volume appeared unchanged following administration of HC and TNF-α. Similarly, IL-6 showed no effect on initial CSF volume but, in this case the effect on CSF secretion and resistance to CSF drainage appeared to be in the opposite direction to that observed with HC, that is, IL-6 induced a decrease in CSF secretion rate and an increase in resistance to CSF drainage. The opposing effects of HC compared to IL-6 on CSF secretion rate and resistance to CSF drainage suggest a possible

compensatory mechanism taking effect so that no change in CSF volume was observed.

By contrast, CCL2 and IL-17 results showed no effect upon CSF secretion rates, for both *in vivo* perfused aCSF and i.p injection in conjunction with perfused aCSF; but statistically significant increases in initial CSF volume within the rat brain and in resistance to CSF drainage. This could indicate a link between increased levels of CCL2 and IL-17 and increased resistance to CSF drainage leading to an increase in intracranial pressure observed in patients with IIH.

The changes observed in CSF dynamics with these five treatments provided a rationale to test their effects in conjunction with diet and sex, in further experiments on CSF secretion rates (Section 3.6) and on resistance to CSF drainage (Section 3.7) in male and female Wistar rats.

3.5 Sex and diet effects on CSF dynamics: Physiological and biochemical parameters

Due to the incidence of IIH increasing in the obese population (Radhakrishnan et al. 1993) (Kesler & Gadoth 2001) (Dhungana et al. 2009) and several studies reporting weight gain in newly diagnosed IIH patients (Rowe & Sarkies 1999) (Radhakrishnan et al. 1993), it was important to test the effects of the treatments of interest on CSF secretion rates and resistance to CSF drainage in high-fat (HF) diet animal models compared to those raised on a normal diet. Male and female Wistar rats were ordered at four weeks of age and raised on either a normal pellet or HF diet for seven weeks. Separate diets were provided for both the normal and

HF diet animal groups as shown in Methods Section 2.2.4; Tables 2.6, 2.7 and 2.8. Rat weights ranged between 250-350 g at the onset of experiments. Male rats on both diets were slightly heavier when compared to the female rats at the onset of experiments with an average difference of 78.7g in the normal diet groups, and 49.1g in the HF diet groups (results not shown).

Characterisation of food and water intake, average percentage weight gain, and cholesterol levels were initially recorded in the normal diet and HF diet groups (Sections 3.5.2-3.5.4). Further ventriculo-cisternal perfusion and variable rate infusion experiments were performed in order to determine the effects diet, in conjunction with the treatments of interest, have on CSF secretion rates (Section 3.6) and resistance to CSF drainage (Sections 3.7) in male Wistar rats.

As the incidence of IIH is greater in the female population and mainly affects obese women between the ages of 15-45, with a female to male ratio of 8:1 (Dhungana et al. 2009), we examined the effects of the treatments of interest and diet have on CSF secretion rates and resistance to CSF drainage in female Wistar rats. This would allow us to compare and contrast any differences seen with the male models.

As with the male Wistar rats, characterisation of diet and water intake, average percentage weight gain, and cholesterol levels were initially recorded between the normal diet and HF diet female Wistar rat groups (Sections 3.5.2-3.5.4). Ventriculo-cisternal perfusion and variable rate infusion experiments were again performed in order to determine the effects diet, in conjunction with the

treatment of interest, has on CSF secretion rates (Section 3.6) and resistance to CSF drainage (Section 3.7) in female Wistar rats.

3.5.1 Determination of female Wistar rat oestrous cycle phase

It was important to determine first at what stage of the oestrous cycle the female rats were on at during the experiment in order to eliminate variables introduced by hormonal cycling. Vaginal smears from female rats were taken prior to ventriculo-cisternal perfusion and variable rate infusion and viewed under a light microscope in order to select the same stage in the oestrous cycle for further experiments. The results shown in Fig. 3.7 describe the four main stages of the female rat cycle; proestrus, oestrous, metestrus and diestrus.

Round and nucleated cells are the epithelial cells (E); smaller rounded cells depict the leukocytes (L); irregular needle shaped are the cornified cells (C). A proestrus smear consists of an abundance of nucleated cells with cornified cells starting to appear, but few leucocytes are described in Fig. 3.7a and 3.7b. In the oestrous phase there are many cornified cells that take on the appearance of needle-shapes (Fig. 3.7c and 3.7d). Some nucleated cells may remain, but they have lost their swollen appearance as seen in proestrus. As oestrous progresses, leucocytes begin to infiltrate the smear as metestrus begins (Fig. 3.7e, 3.7f). In diestrus, you see parts of every cell type mentioned, with leucocytes being the most abundant. It is the stage where the smallest number of cells is seen, and there is often some mucous present, which can clump some cells (usually leucocytes) together (Fig. 3.7g, 3.7h). All ventriculo-cisternal perfusion and variable rate infusion experiments on female Wistar rats were performed during the female rat diestrus stage.

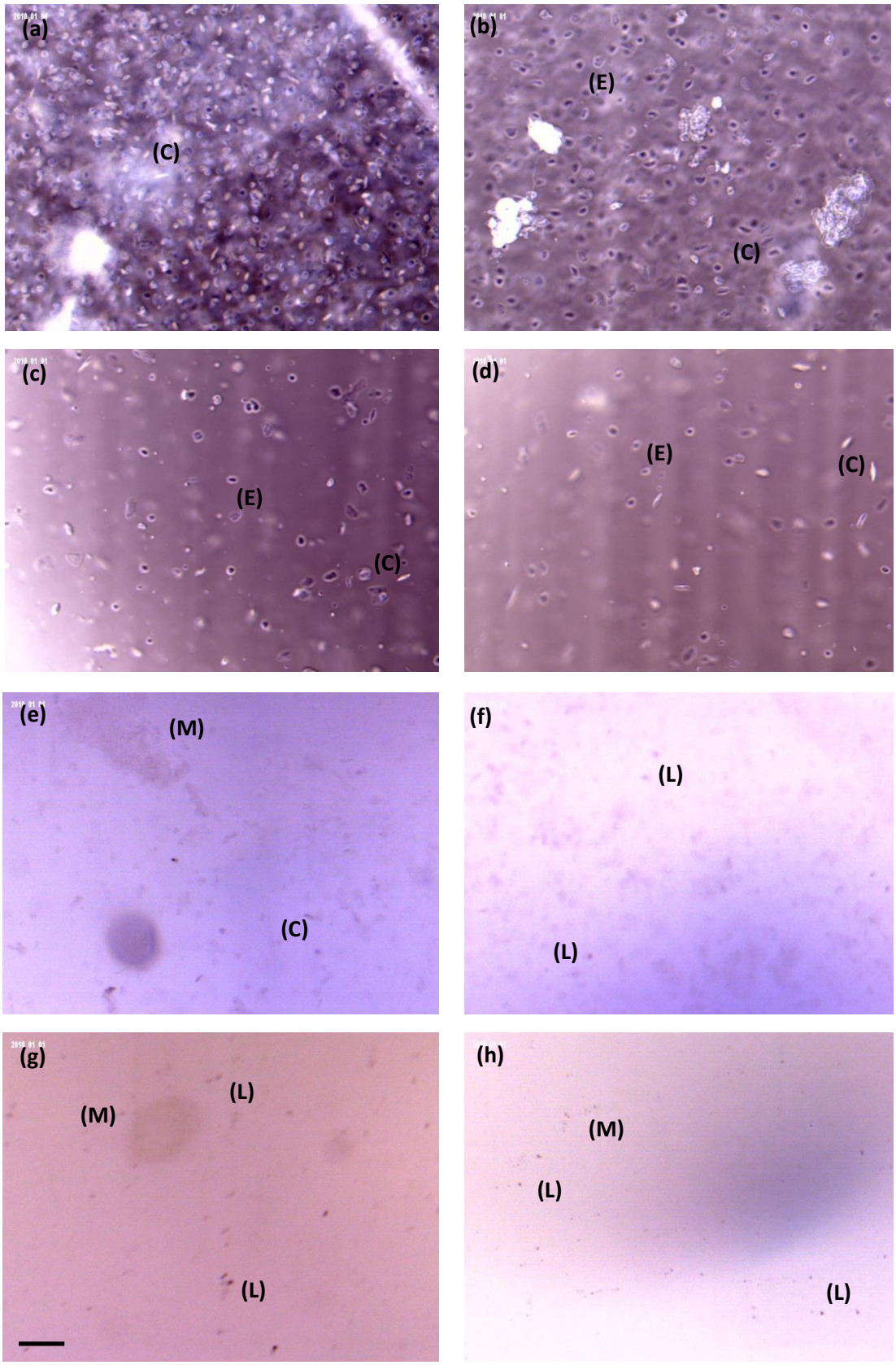

Figure 3.7: Photomicrographs of unstained vaginal smear from female Wistar rats. (a,b) Proestrus, (c,d) Oestrous, (e,f) Metestrus, (g,h) Diestrus, (E) Epithelial Cells, (L) Leukocytes, (C) Cornified Cells, (M) Mucus. Images were observed and taken on a light microscope. Scale bar represents 90 µm.

3.5.2 Food and water intake

Food and water intake was monitored daily in order to determine the amount of nutrients the rats on each diet were obtaining, and whether food intake would affect the rat's water intake. Food and water intake are shown in Fig. 3.8 (a) and (b), respectively.

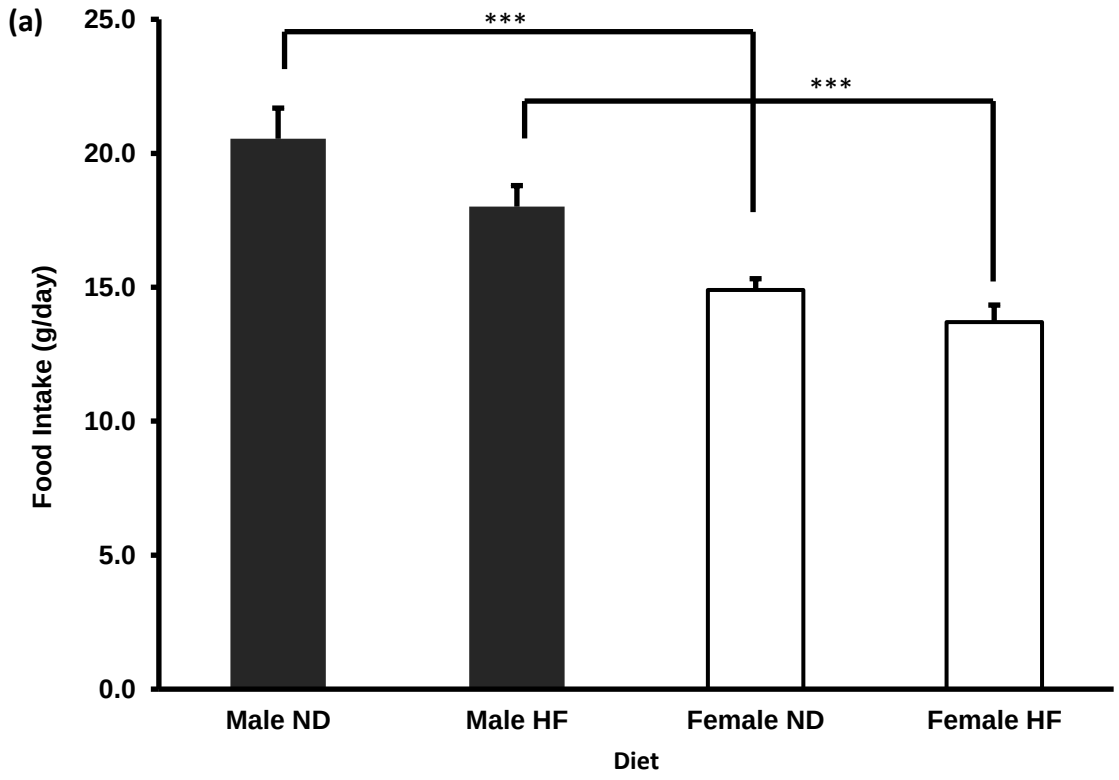

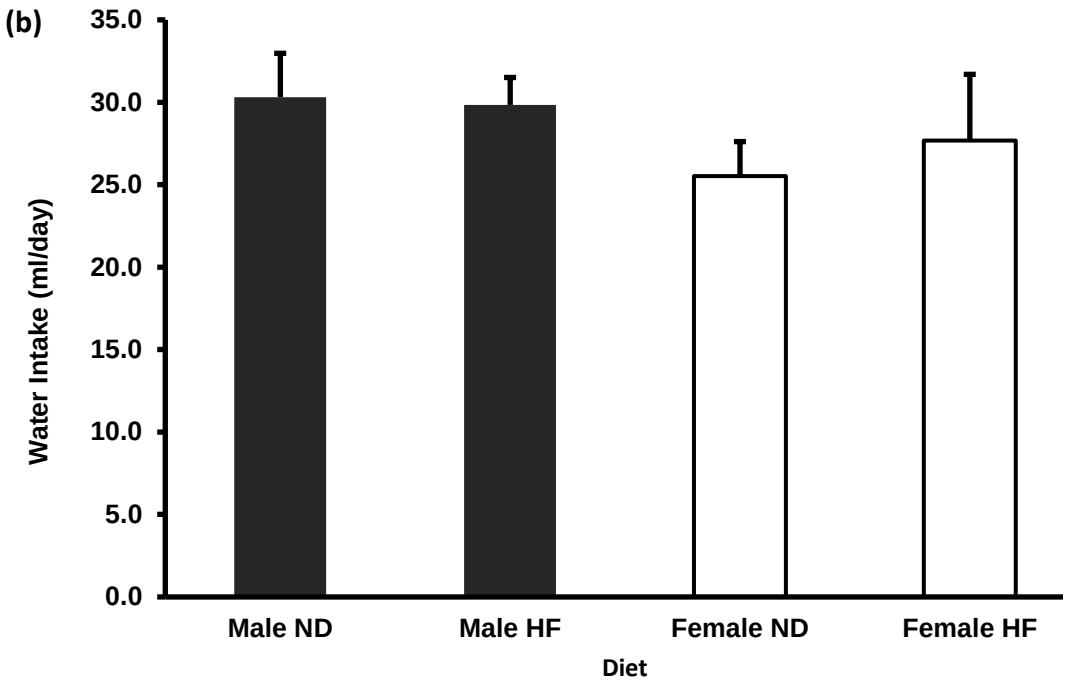

Figure 3.8: Normal and high-fat (HF) diet food (g/day) and water (ml/day) intake of male and female Wistar rats.

Graphs for food (a) and water (b) intake of male and female Wistar rats raised on either a normal or high fat diet are displayed. Normal diet rats in both sexes were fed the Teklad Global 14% Protein Rodent Maintenance Diet (n=3, respectively). HF males were raised on the Western RD High Fat Diet (n=4). HF females (n=3) were fed the 45% AFE High Fat Diet. Food and water intake were recorded as cage averages (±SEM) as the rats were not housed singly. A two-way ANOVA was used to analyse the statistical significance. The significant results are shown following Sidak's multiple comparison test against each diet and treatment variables. *** $P \leq 0.001$.

Food intake was slightly higher in the male (20.5 ±1.14 g/day) and female (14.9 ±0.42 g/day) rats on a normal diet compared to the HF diet (18.0 ±0.78 g/day and (13.7 ±0.63 g/day, respectively) (Fig. 3.8a). The slightly lower average food intake for the HF diet rats could be due to their initial diet intake being lower for the first week as they did not take to eating it as readily as the normal pellet diet. Water intake in males fed on the male normal diet and those on the HF diet was similar (30.0 ±2.66 ml/day and 29.8 ±1.66 ml/day, respectively) (Fig. 3.8b). However, the HF diet females displayed a higher water intake (27.7 ±4.02 ml/day) compared

with the normal diet females (25.5 ±2.09 ml/day), although this was not significant. Female Wistar rats displayed an overall lower water intake, but significantly lower food intake for both the normal and HF diets (P=≤0.001), when

compared with the male Wistar rats. Note however that HF diets of males and females were different as described in Methods Section 2.2.4.

3.5.3 Average percentage weight gain

The average percentage weight gain between normal diet and HF diet was monitored to confirm that the HF diet induced weight gain in both male (Fig. 3.9) and female (Fig. 3.10) Wistar rats.

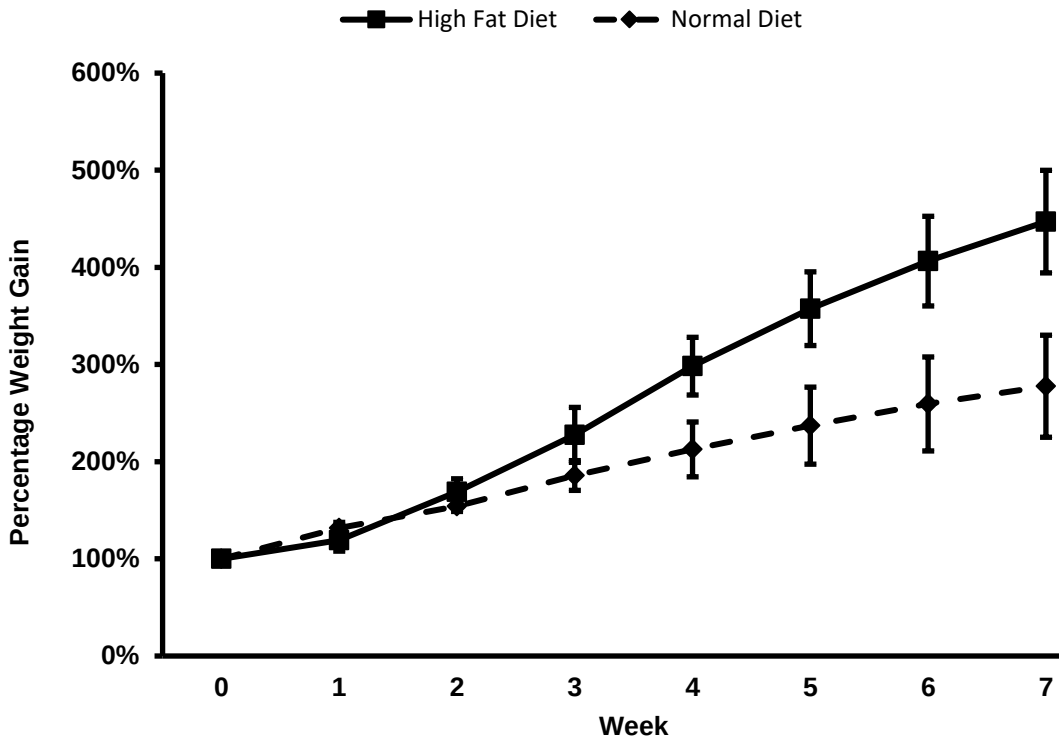

Figure 3.9: Average percentage weight gain of male Wistar rats on a normal and HF diet over a seven week period.

Readings were recorded weekly over a seven week period (from 4 weeks of age) for both ND and HF diet male Wistar rats. Average percentage weight gain was monitored prior to ventriculo-cisternal perfusion and variable rate infusion experiments which were performed at 11 weeks of age. Normal diet (dashed line), HF diet (solid line).

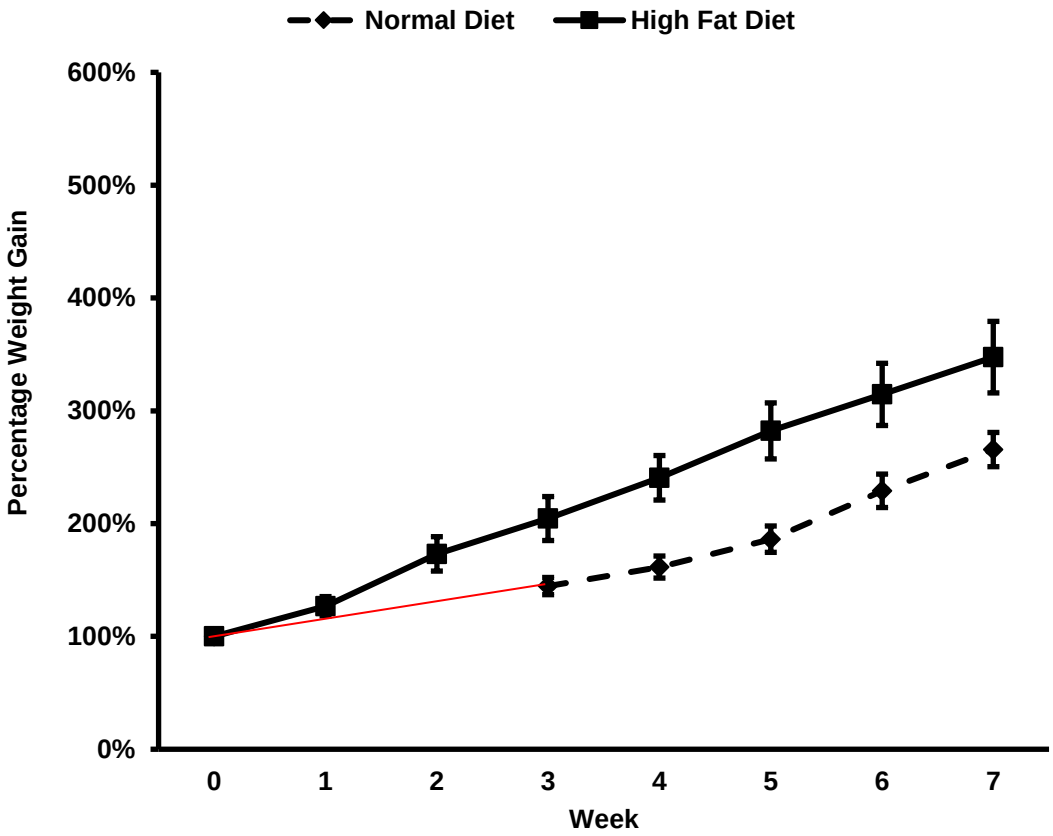

Figure 3.10: Average percentage weight gain of female Wistar rats on a normal and HF diet over a seven week period.
Readings were recorded weekly over a seven week period (from 4 weeks of age) for HF diet rats and four week period (from 7 weeks of age) for normal diet rats (extrapolated over literature female rat weights at week 0 (red line)). Average percentage weight gain was monitored prior to ventriculo-cisternal perfusion and variable rate infusion experiments which were performed at 11 weeks of age. Normal diet (dashed line), HF diet (solid line).

The average percentage weight gain was much higher for the male HF diet rats (447.14%) when compared to the normal diet (277.68%), as shown in Fig. 3.9. The same correlation was seen, although at lower levels, with the HF diet females (347.57%) when compared with normal diet female rats (265.65%) (Fig. 3.10).

3.5.4 Plasma cholesterol levels

A cholesterol assay was used to characterise the effect of a normal and HF diet on total cholesterol, high-density lipoprotein (HDL) and low-density lipoprotein/very-

low density lipoprotein (LDL/VLDL) cholesterol levels in both male (Fig. 3.11a) and female (Fig. 3.11b) Wistar rats.

(a)

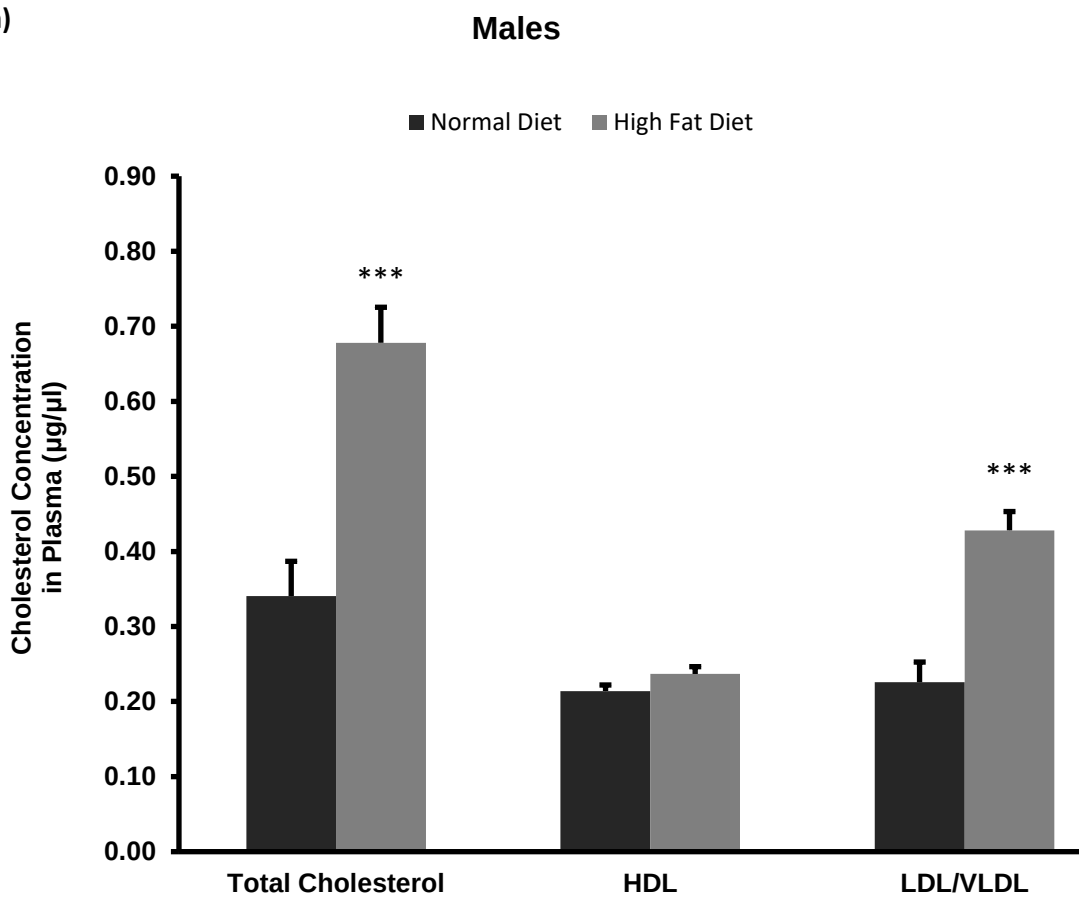

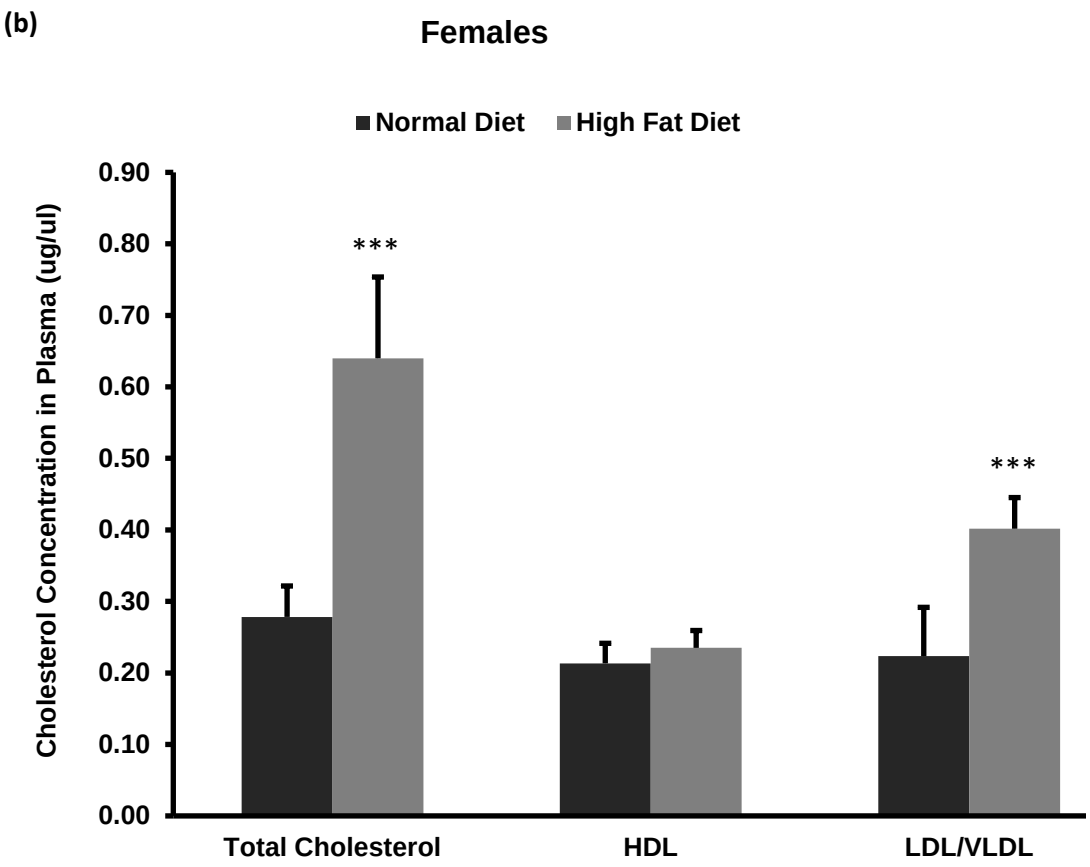

Figure 3.11: Total cholesterol, HDL, and LDL/VLDL from plasma samples. Analysis was performed using a cholesterol assay kit in plasma samples from male (a) and female (b) Wistar rats on normal or HF diets. A two-way ANOVA was used to analyse the statistical significance. The significant results are shown following Sidak's multiple comparison test between normal (n=6) and HF (n=6) diet values (±SEM). ****P* = ≤0.001.

Total cholesterol concentrations were significantly higher in the HF diet groups in both male (0.68 ±0.06 µg/µl, *P*≤0.001) and female (0.64 ±0.11 µg/µl, *P*≤0.001) Wistar rats when compared to normal diet controls (0.34 ±0.06 µg/µl and 0.38 ±0.04 µg/µl, Fig. 3.11a. and b., respectively). The LDL/VLDL levels in the HF diet groups of both males (0.43 ±0.03 µg/µl, *P*≤0.001) and females (0.40 ±0.04 µg/µl, *P*≤0.001) is significant when compared to the normal diet rats (0.23 ±0.03 µg/µl and 0.22 ±0.07 µg/µl, respectively) and high levels of VLDL cholesterol have been associated with the development of plaque deposits on artery walls, which narrow the passage and restrict blood flow. There were no significant differences between the two groups within the HDL cholesterol measurement. From the

results of the average percentage weight gain (Fig. 3.9 and 3.10) and cholesterol levels (Fig. 3.11), it is possible to show a difference between rats on a HF diet when compared with a normal pellet diet, confirming the validity of the HF-fed animals as a model of obesity.

3.6 Sex and diet effects on CSF dynamics: CSF secretion rates

The values obtained from the control mean steady state C_{out}/C_{in} (Fig. 3.12) were used to calculate the CSF secretion rates for each treatment from the ventriculo-cisternal perfusion experiments (Fig. 3.13).

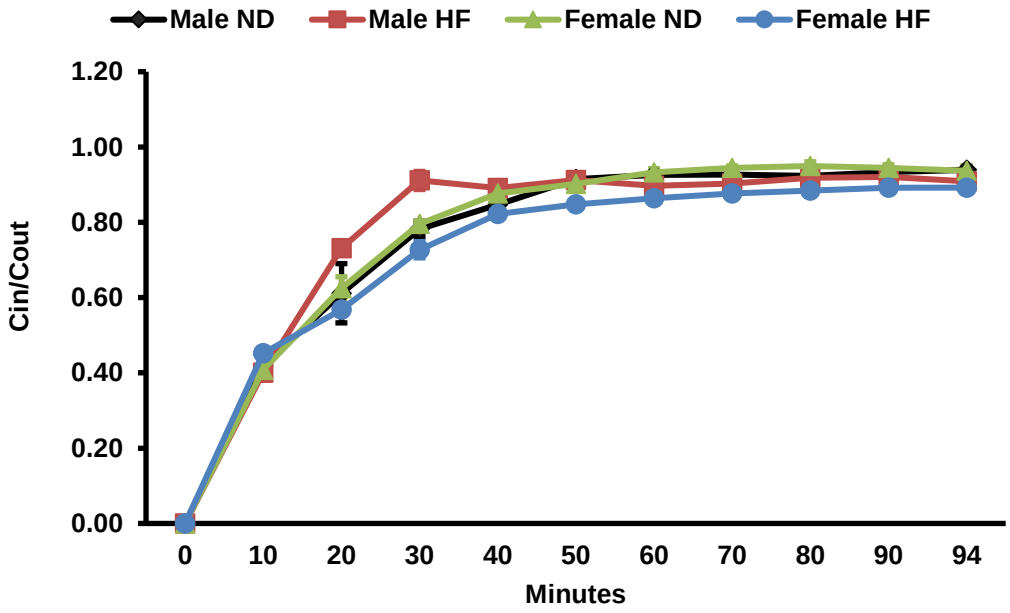

Figure 3.12: Mean control steady state values (C_{out}/C_{in}) following ventriculo-cisternal perfusion experiments in both male and female Wistar rats fed a normal or HF diet.
Complete mean steady states were calculated from the concentration of blue dextran in the perfusate collected from the cisterna magna relative to that in the aCSF C_{out}/C_{in}. Samples from control male ND (n=3), male HF (n=4, female ND (n=3), female HF (n=3) rats were averaged (±SEM) and compared to one another. C_{out}/C_{in} values from each group were averaged from 40-94 mins and extrapolated to the y-axis.

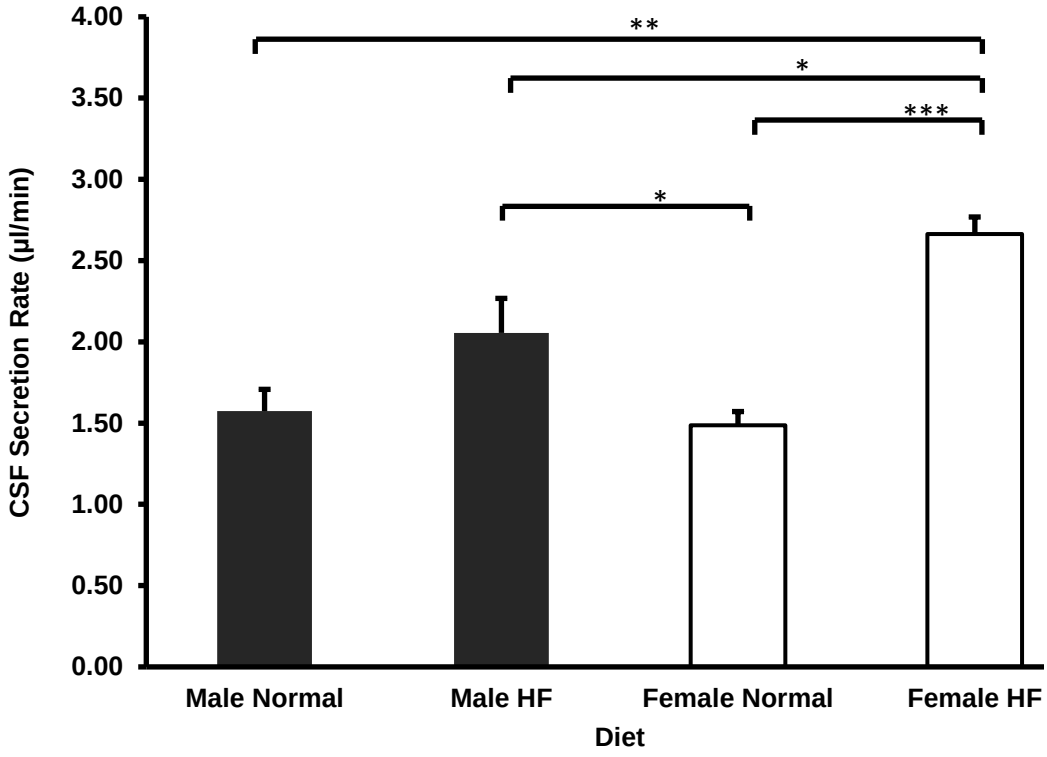

Figure 3.13: CSF secretion rates in normal diet and HF diet male and female Wistar rats determined using ventriculo-cisternal perfusion.
Each experiment was carried out by perfusing aCSF through both lateral ventricles of the rat brain. CSF secretion rates were obtained once at steady state (40-90 min) and averaged ±SEM. Samples from male ND (n=3), male HF (n=4), female ND (n=3), female HF (n=3) rats were averaged (±SEM) and compared to one another. A two-way ANOVA was used to analyse the statistical significance. The significant results are shown following Sidak's multiple comparison test A two-tailed equal variance t-test comparison each diet and sex variable. * P = ≤0.05, ** P = ≤0.01, ***P = ≤0.001.

The control mean steady state values (Fig. 3.12) reflect the CSF secretion rates of male and female Wistar rats raised on a normal or HF diet. CSF secretion rates of female rats raised on a HF diet (2.66 ±0.10 µl/min) were significantly higher than in males fed on normal (1.57 ±0.13 µl/min, P≤0.01) and HF diets (2.06 ±0.21 µl/min, P≤0.05), as well as females fed a normal diet (2.21 ±0.08 µl/min, P≤0.001) rates. The male 'HF diet' rats also showed higher CSF secretion rates when compared with the female rats raised on a normal diet (P≤0.05). There was no

difference between the sexes when comparing CSF secretion rates in animals fed the normal diet; or between males on different diets, which suggests that HF diet could play a more prominent role in increasing CSF secretion than just gender alone.

3.6.1 Association between *in vivo* CSF secretion rates and physiological parameters

In order to investigate the association of the physiological diet-induced effects (percentage weight gain, total cholesterol and LDL/VLDL levels) with CSF secretion rate, correlations were performed for both males and females as shown in Fig. 3.14-3.16.

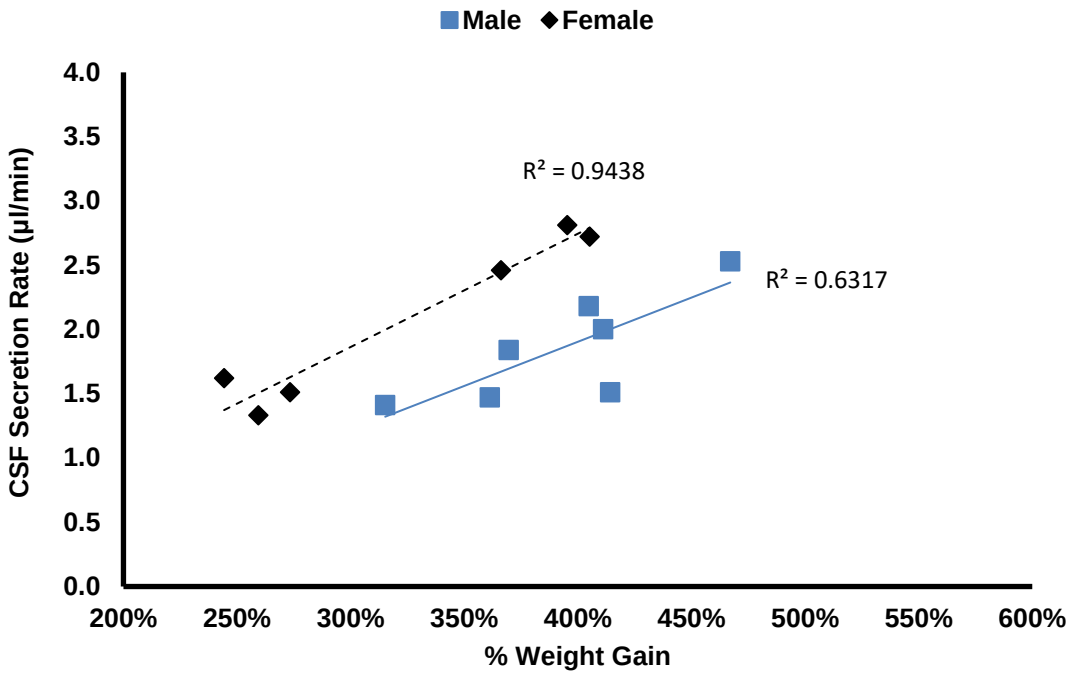

Figure 3.14: Association between control percentage weight gain and CSF secretion rates in male and female Wistar rats.
Normal diet rats in both groups were fed the Teklad Global 14% Protein Rodent Maintenance Diet (n=3). HF males were raised on the Western RD High Fat Diet (n=4). HF females (n=3) were fed the 45% AFE High Fat Diet. R^2 analysis confirmed the strength of correlation and a Pearson correlation coefficient test was performed to determine significance.

The results show that a significant association between percentage weight gain of female Wistar rats and increased CSF secretion rates may exist ($R^2 = 0.94$, $P \leq 0.01$). This association was also noticeable with the male Wistar rats, however at a slightly weaker level ($R^2 = 0.63$, $P \leq 0.05$) (Fig. 3.14).

Similar results are observed when comparing the total cholesterol level effects upon CSF secretion rates as shown in (Fig. 3.15). Female Wistar rats again show a strong association ($R^2 = 0.86$, $P \leq 0.01$) between the two variables, with males again

displaying a weaker relationship with increased CSF secretion rates (R^2 = 0.57, $P \leq 0.05$).

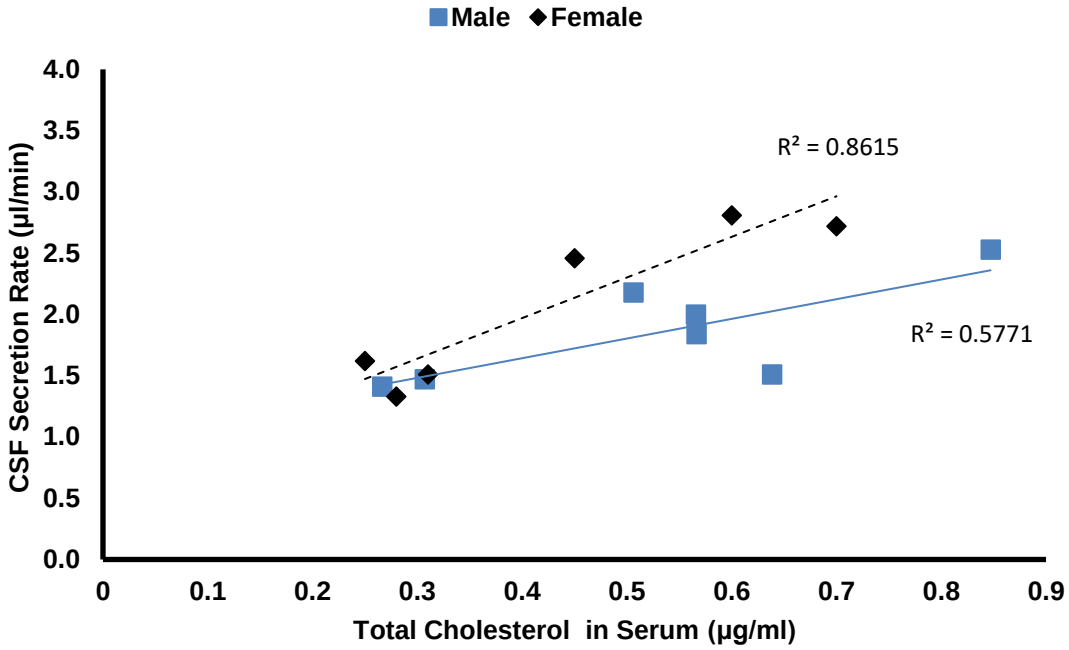

Figure 3.15: Association between control total cholesterol level and CSF secretion rates in male and female Wistar rats.
Normal diet rats in both groups were fed the Teklad Global 14% Protein Rodent Maintenance Diet (n=3). HF males were raised on the Western RD High Fat Diet (n=4). HF females (n=3) were fed the 45% AFE High Fat Diet.

An association between LDL/VLDL cholesterol level and CSF secretion was noticeable in female Wistar rats (R^2 = 0.78, $P \leq 0.05$), which was not observed with the males (R^2 = 0.49), as shown in (Fig. 3.16).

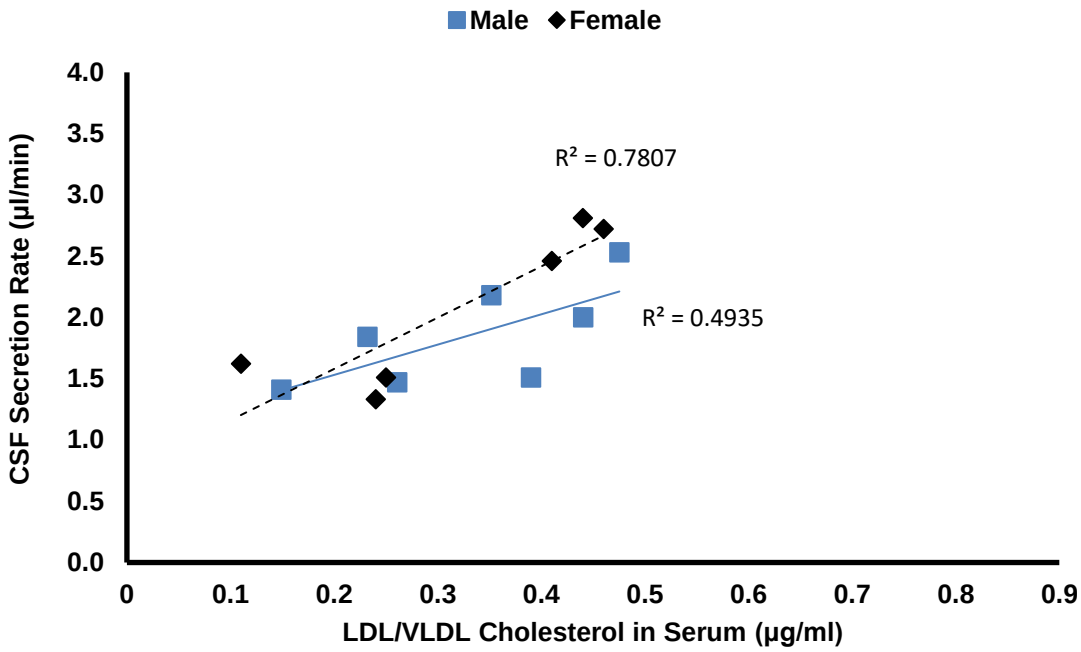

Figure 3.16: Association between control LDL/VLDL cholesterol level and CSF secretion rates in male and female Wistar rats.
Normal diet rats in both groups were fed the Teklad Global 14% Protein Rodent Maintenance Diet (n=3). HF males were raised on the Western RD High Fat Diet (n=4). HF females (n=3) were fed the 45% AFE High Fat Diet.

When summarising the values of percentage weight gain, total, and LDL/VLDL cholesterol effects on CSF secretion rate; there appears to be an association between the different physiological parameters of a HF diet in female Wistar rats and CSF secretion. This could imply that not only treatment alone but sex hormones along with percentage weight gain could play a significant role in increased CSF secretion. This is even more evident as the male Wistar rats showed a weak association between CSF secretion rate and the three physiological parameters.

However, even though this analysis grouped both normal and HF diet rats, it is important to note the HF diet differences between the male and female rats. As stated in Methods Section 2.2.4, the HF male rats were fed on the Western RD High Fat diet and the females on the 45% AFE High Fat Diet, which differ slightly in protein and carbohydrate content. Therefore, the differences in the three different diets make it difficult to interpret the differences observed with the associations in the different sexes.

3.6.2 Sex and diet effects on hydrocortisone and TNF-α-modulated *in vivo* CSF secretion rates

The HC and TNF-α mean steady state values (C_{out}/C_{in}) (Fig. 3.17a. and b., respectively) were used to calculate the CSF secretion rates for each treatment from the ventriculo-cisternal perfusion experiments (Fig. 3.18).

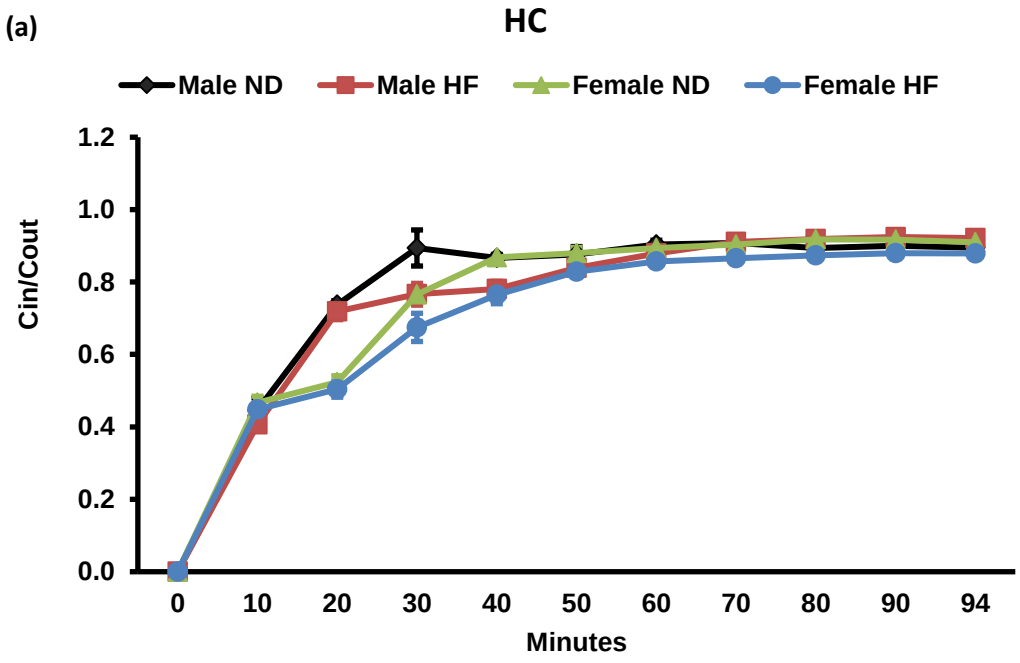

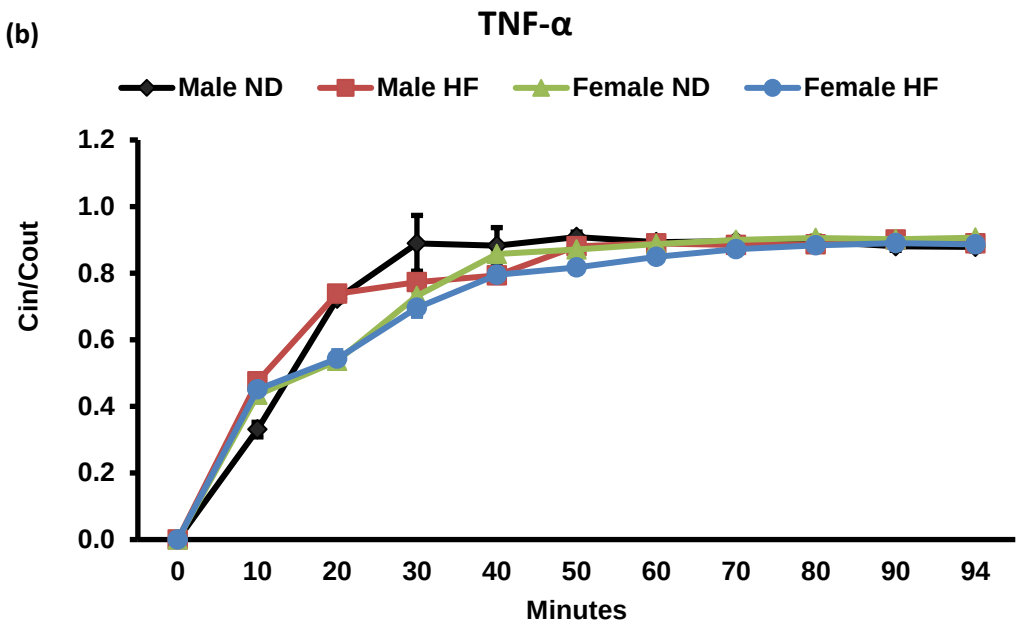

Figure 3.17: Mean HC and TNF-α steady state values (C_{out}/C_{in}) following ventriculo-cisternal perfusion experiments in both male and female Wistar rats fed a normal or HF diet. Complete mean steady states were calculated from the concentration of blue dextran in the perfusate collected from the cisterna magna relative to that in the aCSF; C_{out}/C_{in}. Concentrations of treatments in aCSF, perfused for 90 min: HC (0.5 µg/ml, n=3-4), TNF-α (0.0001 µg/ml, n=3). Samples were averaged (±SEM) and compared to one another. C_{out}/C_{in} values from each treatment were averaged from 40-94 mins and extrapolated to the y-axis.

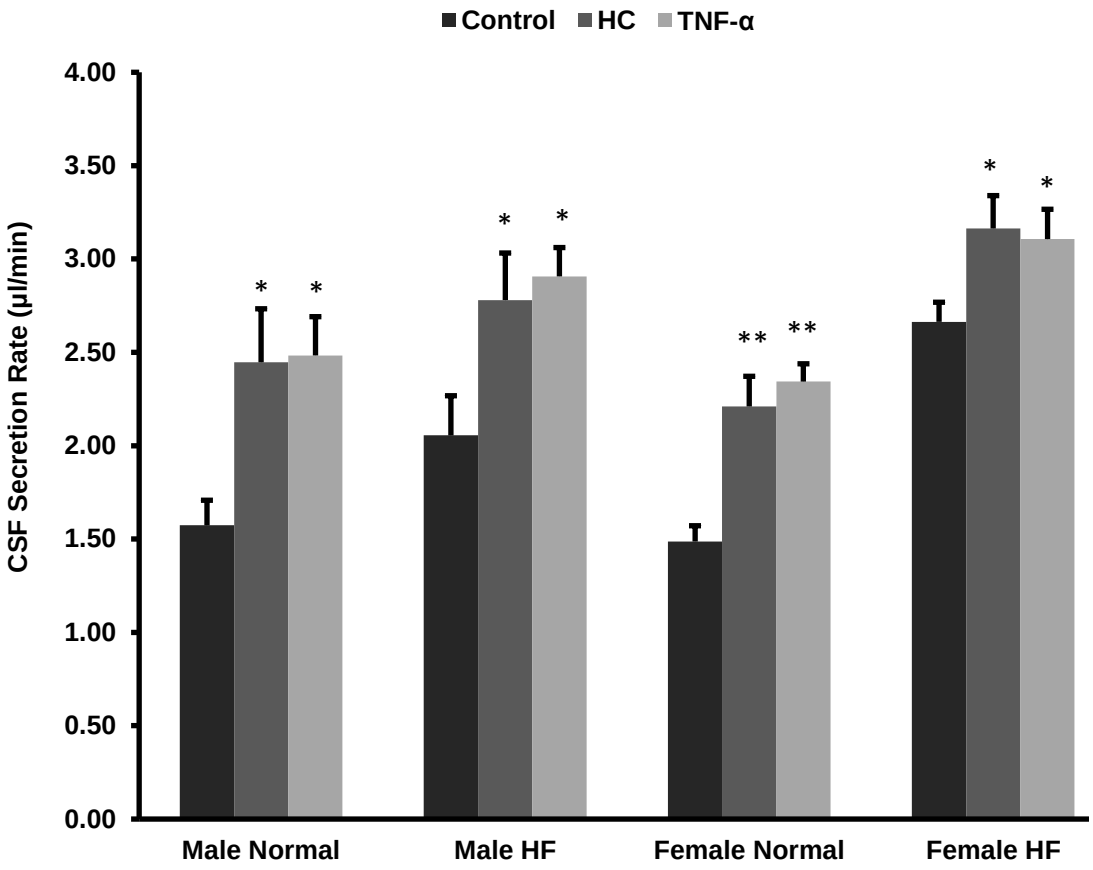

Figure 3.18: HC and TNF-α CSF secretion rates on normal diet and HF diet male and female Wistar rats using ventriculo-cisternal perfusion.
Each experiment was carried out by perfusing aCSF with each treatment through both lateral ventricles of the rat brain. CSF secretion rates were obtained once at steady state (40-90 min) and averaged (±SEM) before being compared to controls (n=3-4). Concentrations of treatments in aCSF, perfused for 90 min: HC (0.5 µg/ml, n=3-4), TNF-α (0.0001 µg/ml, n=3). A three-way ANOVA was used to analyse the statistical significance. The significant results are shown following Sidak's multiple comparison test and was performed for each diet, sex and treatment variable. * P = ≤0.05, ** P = ≤0.01.

The mean steady state values of HC and TNF-α (Fig. 3.17) correspond to the CSF secretion rates with each treatment of male and female Wistar rats raised on a normal or HF diet (Fig. 3.18). A two sample t-test comparison showed that HC and TNF-α significantly increased CSF secretion rates compared to the appropriate untreated controls in male and female Wistar rats raised on both types of diet. HC (2.45 ±0.29 µl/min, n=3) and TNF-α (2.48 ±0.21 µl/min, n=3) treated male 'ND rats' showed significantly increased CSF secretion rates compared to the corresponding

control (1.57 ±0.13 µl/min, n=3, $P \leq 0.05$). The same effect was seen with the male 'HF diet' group where treatment with HC (2.78 ±0.25 µl/min, n=4) and TNF-α (2.91 ±0.15 µl/min, n=3) displayed increasing CSF secretion over the control (2.06 ±0.21 µl/min, n=4, $P \leq 0.05$). Female 'ND rats' treated with HC (2.21 ±0.16 µl/min, n=3) and TNF-α (2.34 ±0.10 µl/min, n=3) also showed higher CSF secretion rates over controls (1.49 ±0.08 µl/min, n=3) ($P \leq 0.01$). The same pattern was seen with the female 'HF diet' rats where HC (3.16 ±0.09 µl/min, n=3) and TNF-α (3.11 ±0.08 µl/min, n=3) treatment increased CSF secretion rates against the female 'HF diet' control (2.66 ±0.10 µl/min, n=3, $P \leq 0.05$).

Both HC and TNF-α female HF diet treatments displayed higher CSF secretion rates over their corresponding treatments in the both male ($P \leq 0.05$) and female ($P \leq 0.01$) normal diet animals. In addition, male HF diet TNF-α CSF secretion rates were higher than the TNF-α female normal diet treatment ($P \leq 0.05$).

These results show that females on a HF diet have the highest basal CSF secretion rate and (like all diet/sex groups) still showed a significant increase in CSF secretion with HC or TNF-α treatment.

3.6.3 Sex and diet effects on IL-6-modulated *in vivo* CSF secretion rates

The values obtained from the IL-6 mean steady state analysis (Fig. 3.19) were used to calculate the CSF secretion rates for each treatment from the ventriculo-cisternal perfusion experiments (Fig. 3.20).

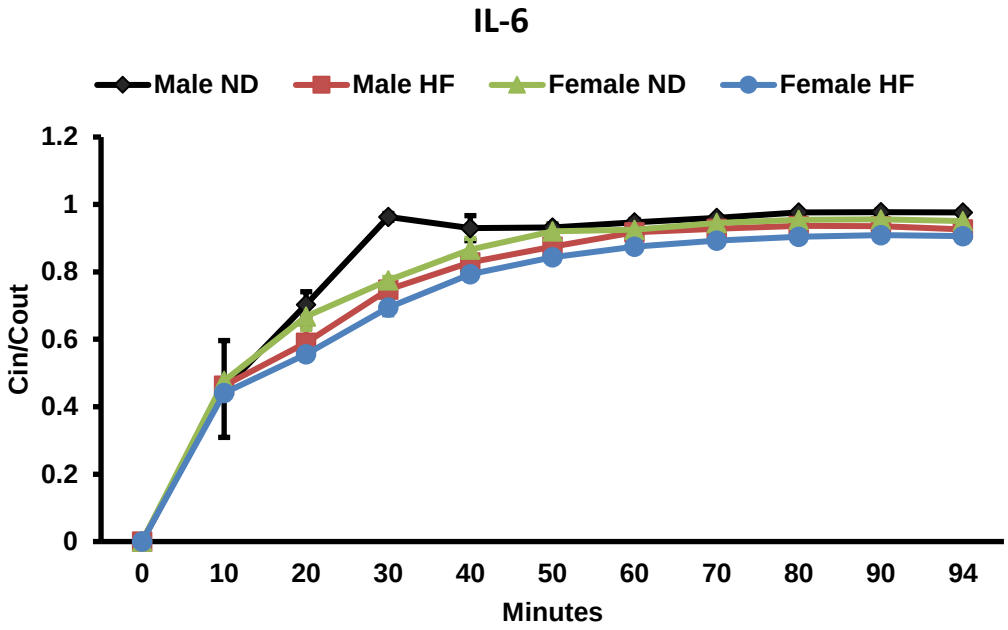

Figure 3.19: Mean IL-6 steady state values (C_{out}/C_{in}) following ventriculo-cisternal perfusion experiments in both male and female Wistar rats fed a normal or HF diet. Complete mean steady states were calculated from the concentration of blue dextran in the perfusate collected from the cisterna magna relative to that in the aCSF C_{out}/C_{in}. Concentrations of treatments in aCSF, perfused for 90 min: IL-6 (0.0001 µg/ml, n=3-4). Samples were averaged (±SEM) and compared to one another. C_{out}/C_{in} values from each treatment were averaged from 40-94 mins and extrapolated to the y-axis.

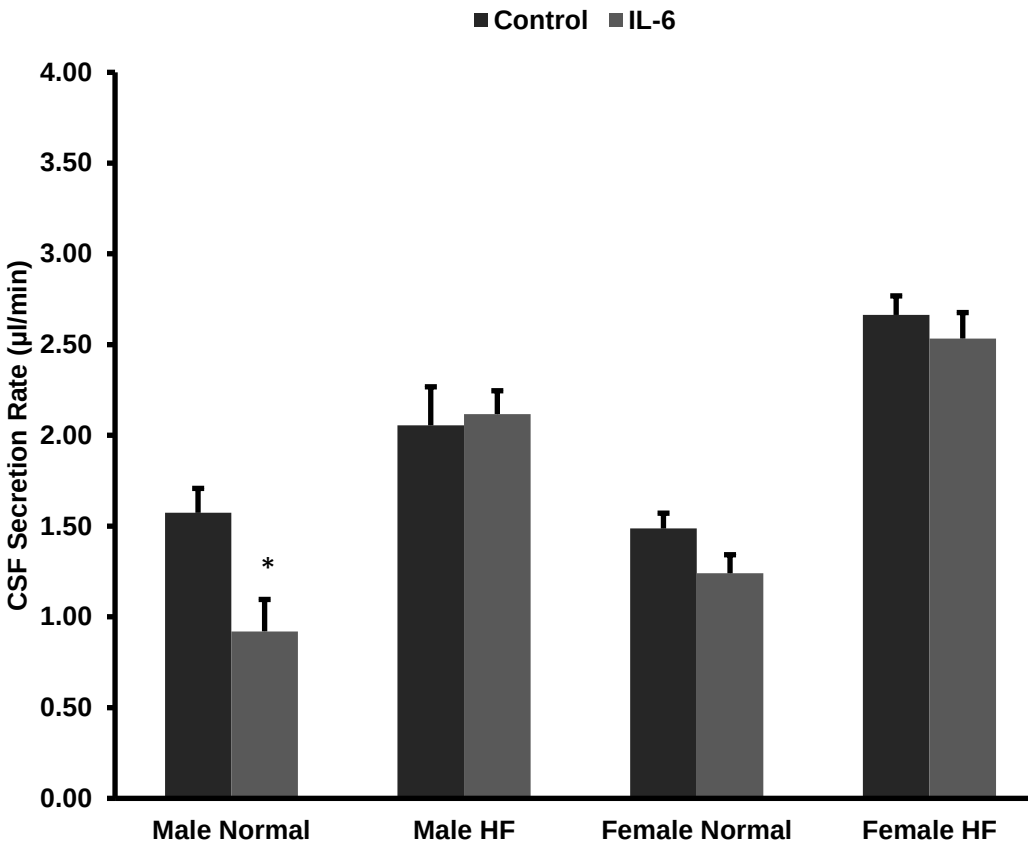

Figure 3.20: IL-6 CSF secretion rates on normal diet and HF diet male and female Wistar rats using ventriculo-cisternal perfusion.
Each experiment was carried out by perfusing aCSF with each treatment through both lateral ventricles of the rat brain. CSF secretion rates were obtained once at steady state (40-90 min) and averaged (±SEM) before being compared to controls (n=3-4). Concentrations of treatments in aCSF, perfused for 90 min: IL-6 (0.0001 µg/ml, n=3-4). A three-way ANOVA was used to analyse the statistical significance. The significant results are shown following Sidak's multiple comparison test and was performed for each diet, sex and treatment variable. * $P = \leq 0.05$.

A two-tailed t-test comparison showed IL-6 treated male 'ND rats' (0.92 ±0.18 µl/min, n=3) showed decreased CSF secretion rates and was the only treatment that showed a significant change against its corresponding control (1.57 ±0.13 µl/min, n=3, $P \leq 0.05$). This treatment also caused a significant decrease in CSF secretion against 'HF diet' male (2.12 ±0.13 µl/min, n=4, $P \leq 0.05$) and female rats (2.53 ±0.07 µl/min, n=3, $P \leq 0.01$). IL-6-treated females on the HF diet also showed a higher rate of CSF secretion compared to all other IL-6-treated groups: male

normal diet (0.92 ±0.18 µl/min, n=3, $P \leq 0.001$), male HF diet (2.12 ±0.13 µl/min, n=4, $P \leq 0.05$) and female normal diet rats (1.24 ±0.10 µl/min, n=3, $P \leq 0.001$). These results suggest IL-6 may only significantly reduce CSF secretion rates in male Wistar rats raised on a normal diet. Female rats do not appear to show this IL-6 effect whereas and HF diets in both sexes seem to abolish any effect IL-6 may have on decreasing CSF secretion rates.

IL-6 caused no change in CSF secretion over controls following a three-way ANOVA analysis, however sex ($P \leq 0.05$), and diet ($P \leq 0.001$) alone did show a significant increase in CSF secretion rate over controls, mostly evident with the female rats raised on a HF diet over males fed a normal diet.

3.6.4 Sex and diet effects on IL-17 and CCL2-modulated *in vivo* CSF secretion rates

The C_{out}/C_{in} values obtained from the IL-17 and CCL2 mean steady state analysis (Fig. 3.21a and b, respectively) were used to calculate the CSF secretion rates for each treatment from the ventriculo-cisternal perfusion experiments (Fig. 3.22).

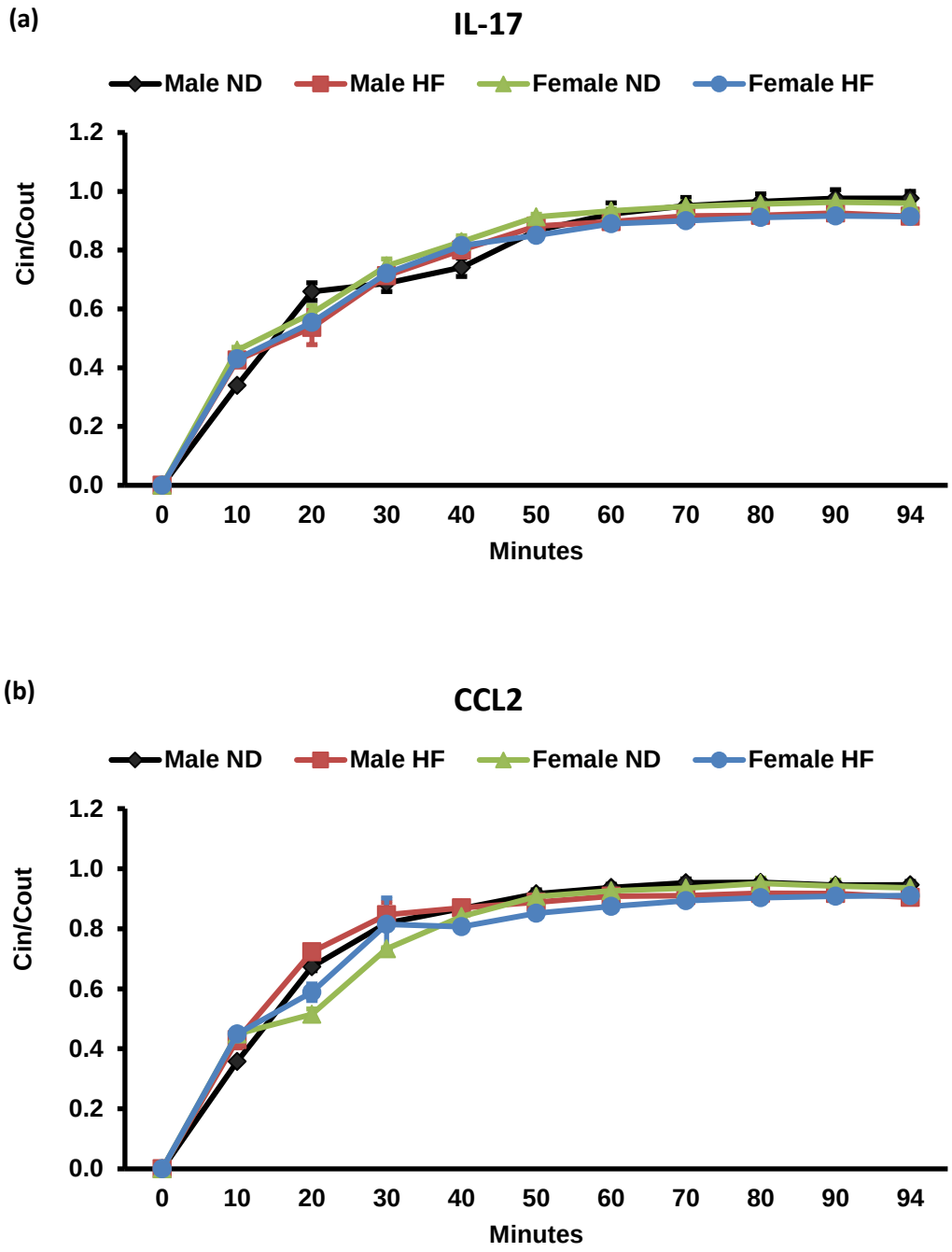

Figure 3.21: Mean IL-17 and CCL2 steady state values (C_{out}/C_{in}) following ventriculo-cisternal perfusion experiments in both male and female Wistar fed a normal or HF diet.

Complete mean steady states were calculated from the concentration of blue dextran in the perfusate collected from the cisterna magna relative to that in the aCSF C_{out}/C_{in}. Concentrations of treatments in aCSF, perfused for 90 min: IL-17 (0.0001 µg/ml, n=3-4), CCL2 (0.05 µg/ml, n=3-4). Samples were averaged (±SEM) and compared to one another. C_{out}/C_{in} values from each treatment were averaged from 40-94 mins and extrapolated to the y-axis.

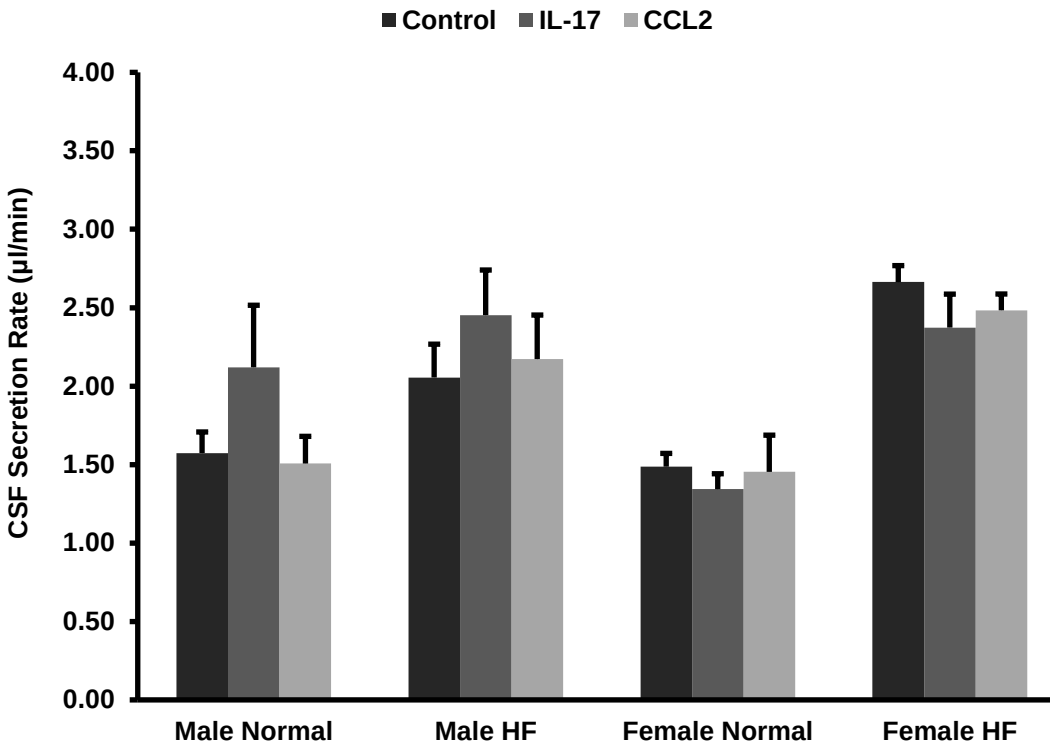

Figure 3.22: IL-17 and CCL2 CSF secretion rates on normal diet and HF diet male and female Wistar rats using ventriculo-cisternal perfusion.
Each experiment was carried out by perfusing aCSF with each treatment through both lateral ventricles of the rat brain. CSF secretion rates were obtained once at steady state (40-90 min) and averaged (±SEM). Concentrations of treatments in aCSF, perfused for 90 min: IL-17 (0.0001 µg/ml, n=3-4), CCL2 (0.05 µg/ml, n=3-4). A three-way ANOVA was used to analyse the statistical significance. No significant results are shown following Sidak's multiple comparison test which tested against each diet, sex and treatment variable.

Using a two-tailed t-test, treatment with IL-17 and CCL2 caused no significant changes in CSF secretion rates in either male or female Wistar rats raised on both normal and HF diets compared to their respective untreated controls. However CCL2-treated females on the HF diet (2.48 ±0.05 µl/min, n=3) showed higher CSF secretion rates than both CCL2-treated males (1.51 ±0.30 µl/min, n=3) and females fed a normal diet (1.45 ±0.23 µl/min, n=3) ($P \leq 0.01$). In addition, IL-17-treated groups in both male (2.45 ±0.29 µl/min, n=4, $P \leq 0.05$) and female (2.37 ±0.11 µl/min, n=3, $P \leq 0.01$) rats fed a HF diet displayed a significant increase in CSF

secretion rates over IL-17 treated females on a normal diet (1.34 ±0.10 µl/min, n=3). These results could show a trend of a HF diet in females increasing CSF secretion rates over both sexes on normal diets. Sex differences in response to IL-17 treatment are not as clear which may suggest that in animals on any diet, IL-17 may not play a role in increasing CSF secretion rates.

3.6.5 Summary of sex and diet effects on CSF secretion rates

When comparing controls it was evident that female Wistar rats raised on a HF diet had a significantly increased CSF secretion rates over female rats on a normal diet and male rats on both diets. This would indicate that a combination of a HF diet and female sex hormones could be an important factor in elevated intracranial pressures associated with IIH patients through increased CSF secretion.

As with the initial studies on male Wistar rats (Section 3.1.1); HC and TNF-α were found to increase CSF secretion rates in both diets and sexes over controls. This would indicate that these two treatments may be a factor in elevated intracranial pressures, associated with IIH patients, regardless of diet and sex.

IL-6 treatment in male normal diet rats decreased CSF secretion rates, as with the initial results in Section 3.1.1. However, this effect was not seen in females and HF diet rats.

IL-17 and CCL2 caused no significant change upon CSF secretion when compared with controls; however a HF diet in females had a significant effect on secretion rate, increasing it when compared to normal diets on both treatments. These results would again suggest that a HF diet could be an important factor increasing CSF secretion rates.

3.7 Sex and diet effects on CSF dynamics: resistance to CSF drainage

The variable rate infusion method was used to test the *in vivo* effects each treatment had on the resistance to CSF drainage over four increasing infusion rates (5, 10, 16, 20 µl/min). Fig. 3.23 shows the resistance to CSF drainage values of untreated animals (male and female) on normal and HF diets. An increase in resistance to CSF drainage was observed when male Wistar rats were perfused with CCL2, IL-17, and IL-6, suggesting an impairment of the absorption of CSF in the presence of these cytokines (Fig. 3.28 and 3.29). However, a decrease in resistance to CSF drainage was seen following HC and TNF-α treatment in certain groups (Fig. 3.27), which could indicate a compensatory mechanism taking effect against the increased CSF secretion rate associated with these two treatments. The same observation, with regards to a compensatory mechanism, could be made of IL-6 due to its effect on decreasing CSF secretion rates (as shown in Fig. 3.2) and increasing resistance to CSF drainage (Fig. 3.28).

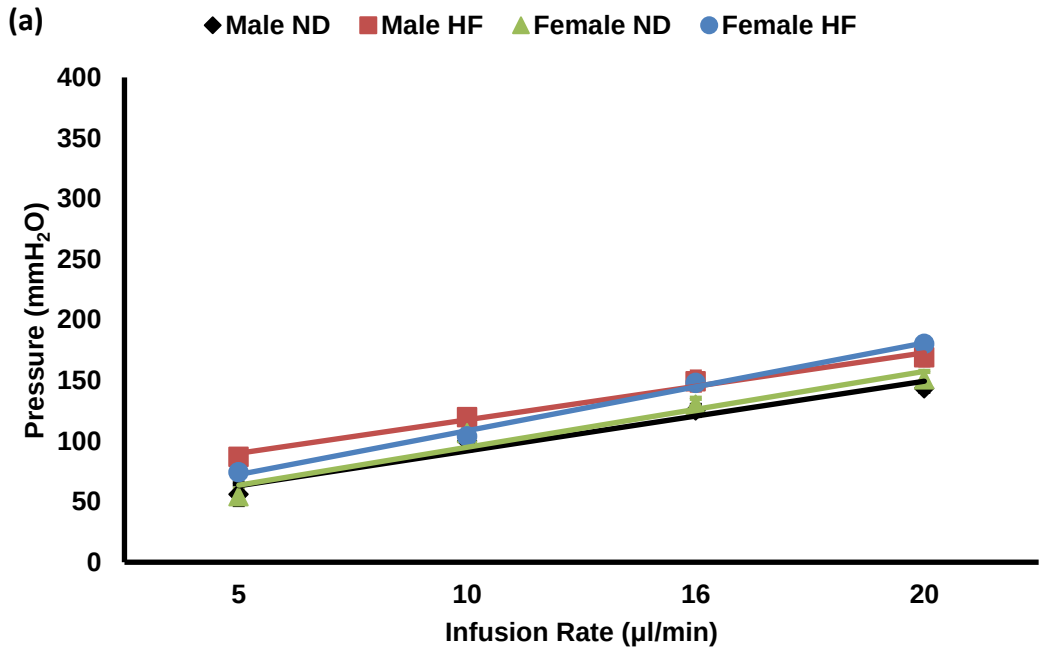

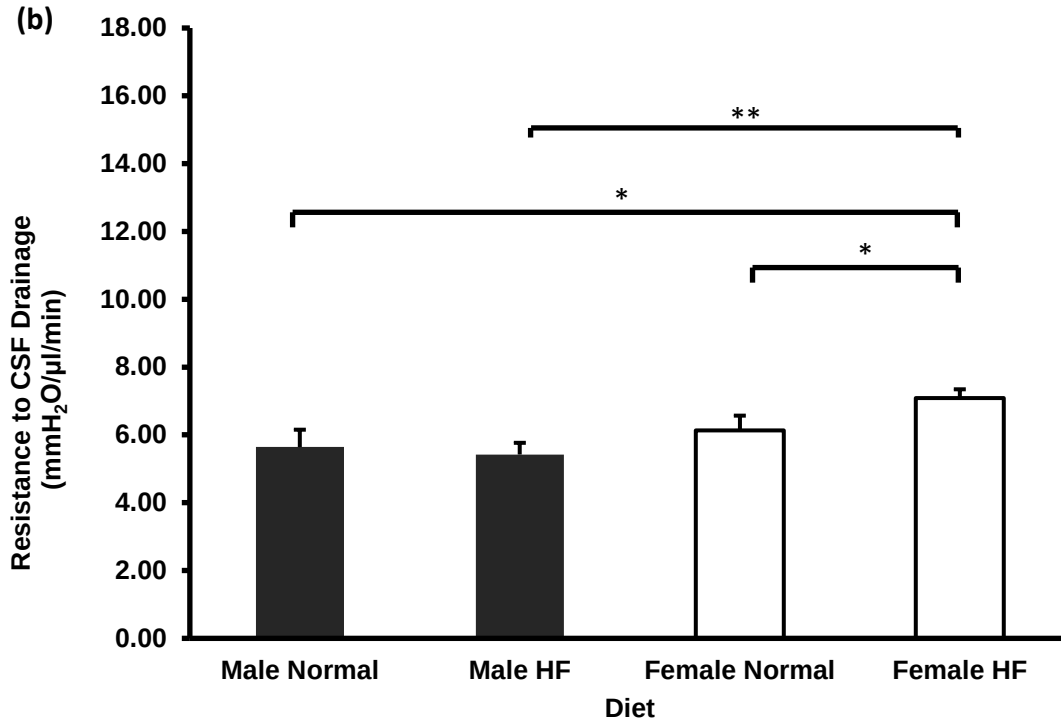

Figure 3.23: Control resistance to CSF drainage values in male and female Wistar rats on a normal and high-fat diet.

Each experiment was carried out by perfusing aCSF with each treatment through one lateral ventricle plus the addition of a single dose i.p injection of PBS 90 minutes prior to perfusion. Samples from each group were averaged (±SEM); male ND (n=3), male HF (n=3), female ND (n=3), female HF (n=3) and compared to one another. The graphs show the linear pressure readings (mmH_2O) at each infusion rate (a); averaged resistance to CSF drainage readings ($mmH_2O{\cdot}min/\mu l$) (b). A two-way ANOVA was used to analyse the statistical significance. The significant results are shown following Sidak's multiple comparison test and was performed against each diet and sex variable. * P = <0.05; ** P = <0.01.

The resistance to CSF drainage was compared in untreated animals (male and female) on normal and HF diets (Fig. 3.23). The results show female Wistar rats raised on a HF diet (7.09 ±0.26 $mmH_2O{\cdot}min/\mu l$) had significantly higher resistance values when compared with males on the HF diet (5.42 ±0.34 $mmH_2O{\cdot}min/\mu l$, $P \leq 0.01$), as well as males (5.64 ±0.51 $mmH_2O{\cdot}min/\mu l$, $P \leq 0.05$) and females fed a normal diet (6.13 ±0.44 $mmH_2O{\cdot}min/\mu l$, $P \leq 0.05$). These results could imply that

females on a HF diet could be most at risk in developing the raised intracranial pressures, due to the increased resistance to CSF drainage, associated in patients with IIH.

3.7.1 Correlation between in vivo resistance to CSF drainage and physiological parameters

As with CSF secretion, the association between diet and resistance to CSF drainage was analysed using graphs of percentage weight gain, total cholesterol and LDL/VLDL cholesterol levels, against resistance to CSF drainage, for each individual animal in grouped normal and HF diets as shown in Fig. 3.24-3.26.

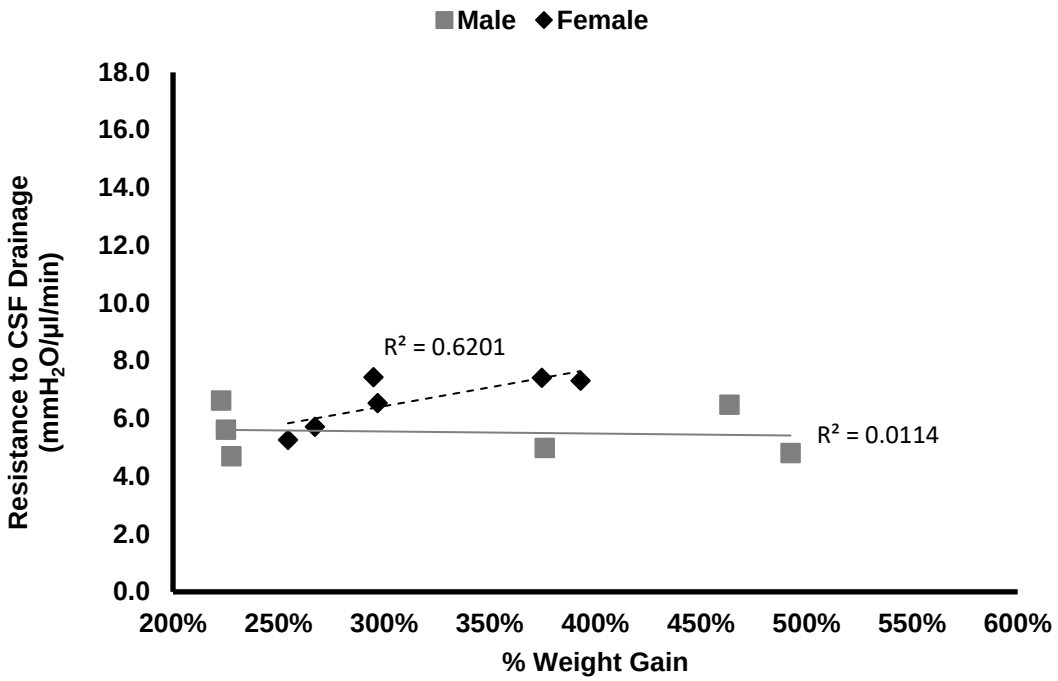

Figure 3.24: Association between control percentage weight gain and resistance to CSF drainage in male and female Wistar rats.
Normal diet rats in both groups were fed the Teklad Global 14% Protein Rodent Maintenance Diet (n=3). HF diet rats were fed the 45% AFE High Fat Diet (n=3). R^2 values were calculated as a measure of the level of correlation between weight gain and resistance to CSF drainage.

The results in Fig. 3.24 show that there is a weak relationship between percentage weight gain and resistance to CSF drainage in female (R^2 = 0.62) Wistar rats, although not significant. However, there was no association observed in the male group (R^2 = 0.01). In addition, there was no association between total cholesterol levels and resistance to CSF drainage in both male (R^2 = 0.08) and female (R^2 = 0.45) Wistar rats (Fig. 3.25).

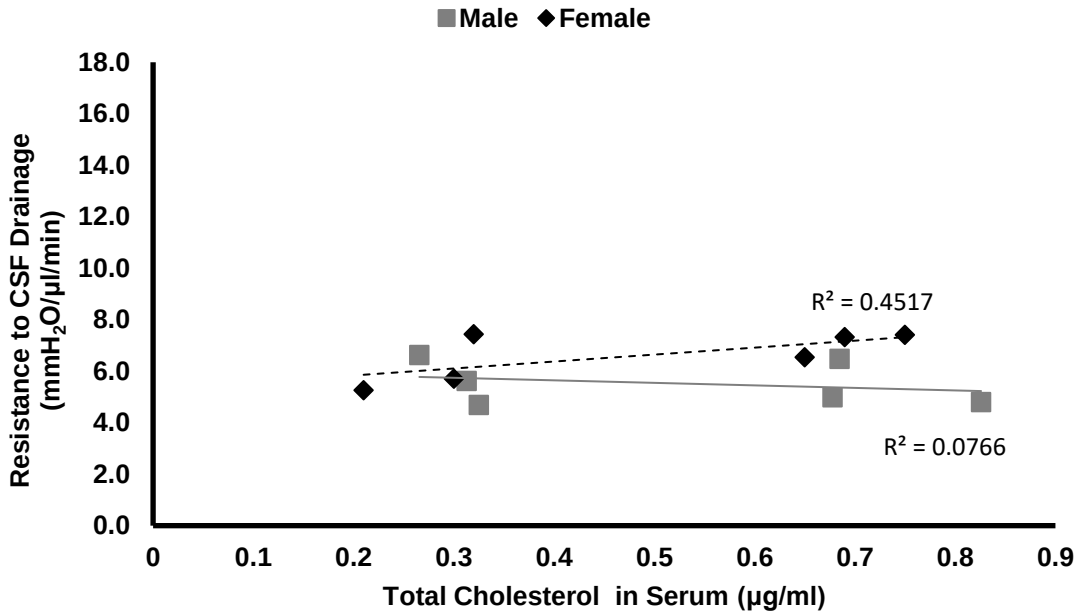

Figure 3.25: Association between total cholesterol level correlation and resistance to CSF drainage in male and female Wistar rats.
Normal diet rats in both groups were fed the Teklad Global 14% Protein Rodent Maintenance Diet (n=3). HF diet rats were fed the 45% AFE High Fat Diet (n=3). R^2 values were used to calculate the level of correlation between weight gain and resistance to CSF drainage.

Similar results were observed with LDL/VLDL cholesterol levels (Fig. 3.26) as with percentage weight gain where female Wistar rats showed a significant association between LDL/VLDL cholesterol levels and increased resistance to CSF drainage (R^2 = 0.66, $P \leq 0.05$), which was not evident in the male group (R^2 = 0.14).

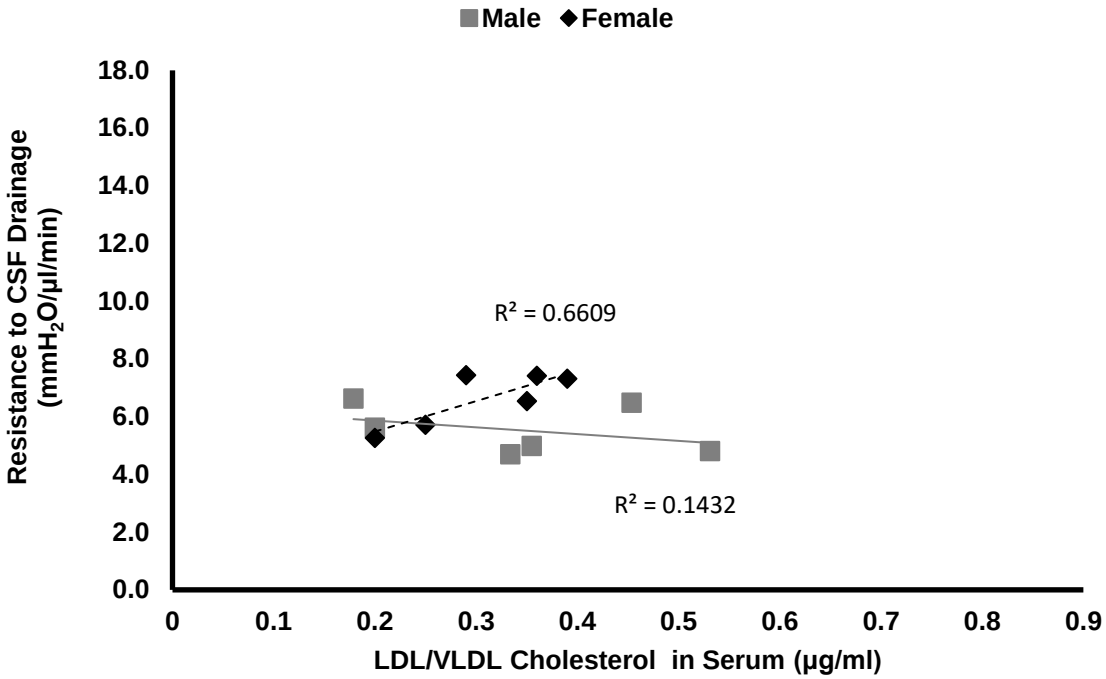

Figure 3.26: Association between LDL/VLDL cholesterol level correlation and resistance to CSF drainage in male and female Wistar rats.
Normal diet rats in both groups were fed the Teklad Global 14% Protein Rodent Maintenance Diet (n=3). HF diet rats were fed the 45% AFE High Fat Diet (n=3). R^2 values were used to calculate the level of correlation between weight gain and resistance to CSF drainage.

In summary, there appears to be an association between one of the physiological parameters of a HF diet (LDL/VLDL cholesterol levels) and resistance to CSF drainage, but only with female Wistar rats. There was no evident association with percentage weight gain, total cholesterol levels and resistance to CSF drainage in either male or female Wistar rats.

3.7.2 Sex and diet effects on hydrocortisone and TNF-α-modulated resistance to CSF drainage

The variable rate infusion method was used to test the *in vivo* effects HC and TNF-α modulation (in male and female Wistar rats raised on either a normal or HF diet) had on the resistance to CSF drainage over four increasing infusion rates (5, 10, 16, 20 µl/min). The linear pressure readings (mmH_2O) at each infusion rate following HC and TNF-α treatment are shown in Fig. 3.27a and b, respectively. The averaged resistance to CSF drainage readings (mmH_2O/µl/min) are described in Fig. 3.27c.

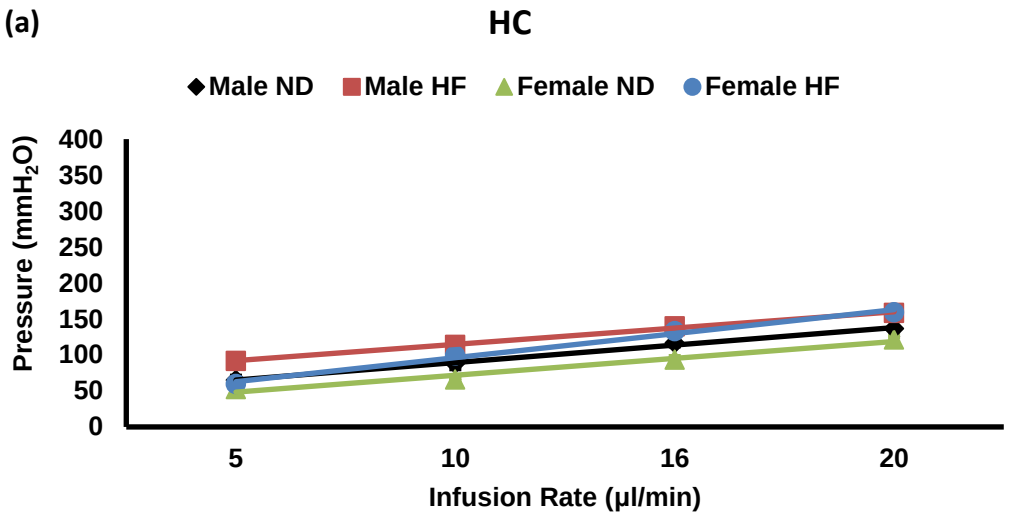

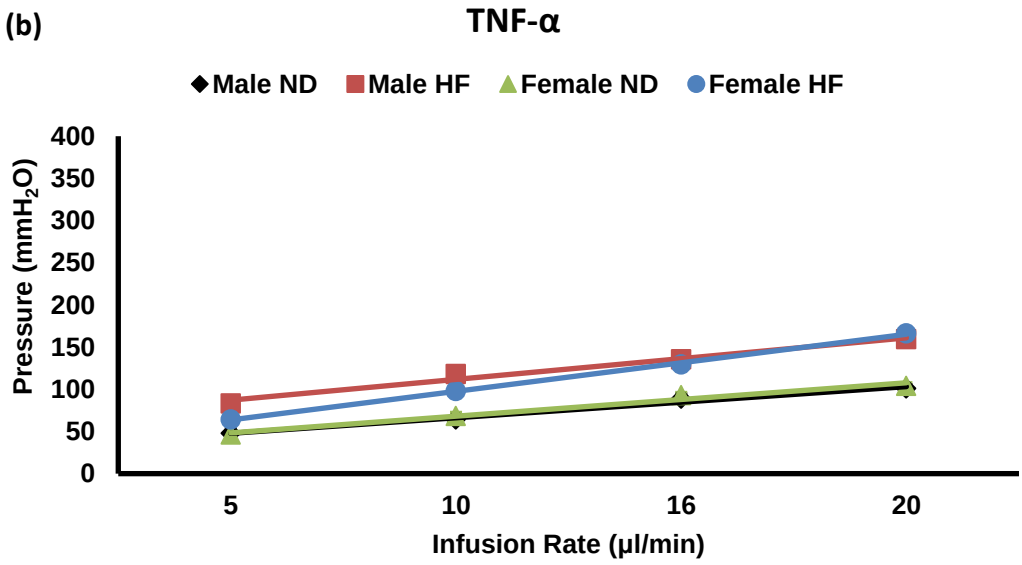

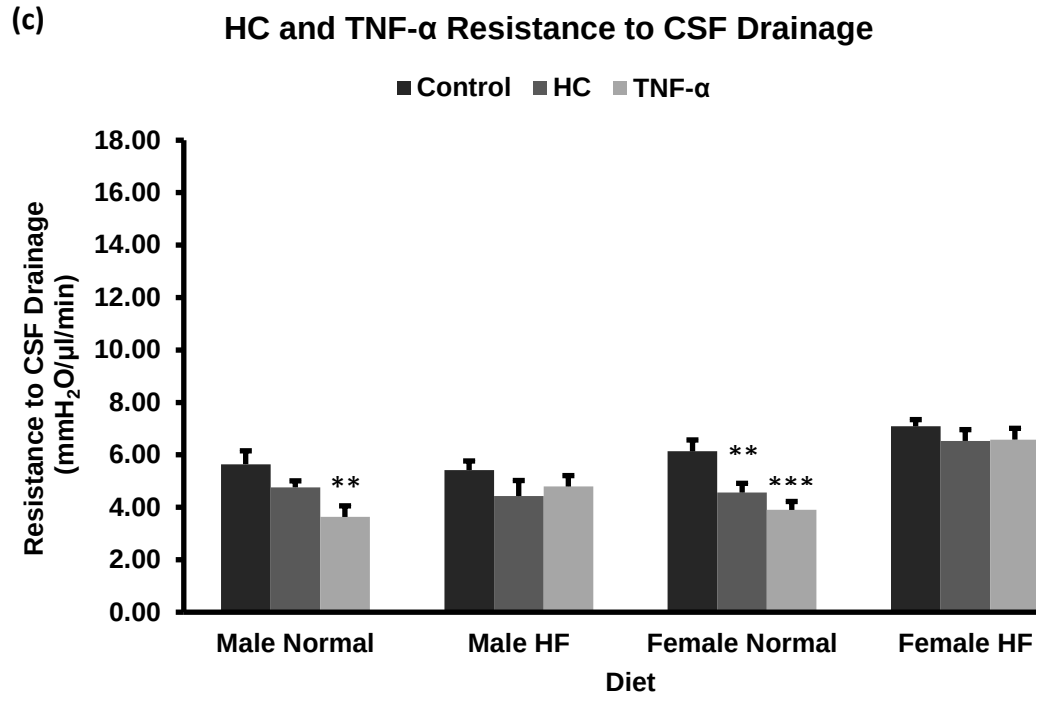

Figure 3.27: HC and TNF-α resistance to CSF drainage values in male and female Wistar rats on a normal and high-fat diet.
Each experiment was carried out by perfusing aCSF with each treatment through one lateral ventricle plus the addition of a single dose i.p injection of either HC or TNF-α 90 minutes prior to perfusion. Samples from each group were averaged (±SEM); male ND (n=3), male HF (n=3), female ND (n=3), female HF (n=3) and compared to one another. The graphs show the linear pressure readings (mmH_2O) at each infusion rate of HC (a); TNF-α (b); averaged resistance to CSF drainage readings ($mmH_2O \cdot min/\mu l$) (c). A three-way ANOVA was used to analyse the statistical significance. The significant results are shown following Sidak's multiple comparison test and was performed for each diet, sex and treatment variable. * $P = \leq 0.05$; ** $P = \leq 0.01$, *** $P = \leq 0.001$.

A two-tailed equal variance t-test described significant decreases in resistance to CSF drainage in male and female normal diet variables. TNF-α-treated males on a normal diet (3.63 ±0.42 $mmH_2O \cdot min/\mu l$) showed a significant decrease in resistance to CSF drainage when compared with controls (5.64 ±0.51 $mmH_2O \cdot min/\mu l$, $P \leq 0.01$). Female Wistar rats raised on a normal diet showed a significant decrease in resistance to CSF drainage following treatment with TNF-α

(3.90 ±0.32 $mmH_2O \cdot min/\mu l$, $P \leq 0.01$) and HC (4.56 ±0.35 $mmH_2O \cdot min/\mu l$, $P \leq 0.01$) when compared with controls (6.13 ±0.44 $mmH_2O \cdot min/\mu l$).

Following a three-way ANOVA analysis, the results of HC and TNF-α treatment effects show that there is a significant difference between the treatments (HC $P \leq 0.01$; TNF-α $P \leq 0.0001$) in decreasing the resistance to CSF drainage over controls. This decrease is mostly evident with HC in female normal diet rats ($P \leq 0.01$) and TNF-α in both male ($P \leq 0.01$) and female ($P \leq 0.001$) normal diet fed rats when compared with controls.

There was a significant difference between males and females, following both treatments, upon resistance to CSF drainage (HC $P \leq 0.01$; TNF-α $P \leq 0.0001$), which is mostly evident by the increase in pressure of the HC treated HF diet females when compared to the HF diet males. A significant effect is also seen between the diets (HC $P \leq 0.05$; TNF-α $P \leq 0.001$) as the decrease in resistance to CSF drainage associated with normal diet rats is not evident in the HF diet animals.

3.7.3 Sex and diet effects on IL-6-modulated resistance to CSF drainage

The variable rate infusion method tested the *in vivo* effects IL-6 had on the resistance to CSF drainage over four increasing infusion rates (5, 10, 16, 20 µl/min). The graphs show the linear pressure readings (mmH_2O) at each infusion rate (Fig. 3.28a) and averaged resistance to CSF drainage readings ($mmH_2O \cdot min/\mu l$) (Fig. 3.28b).

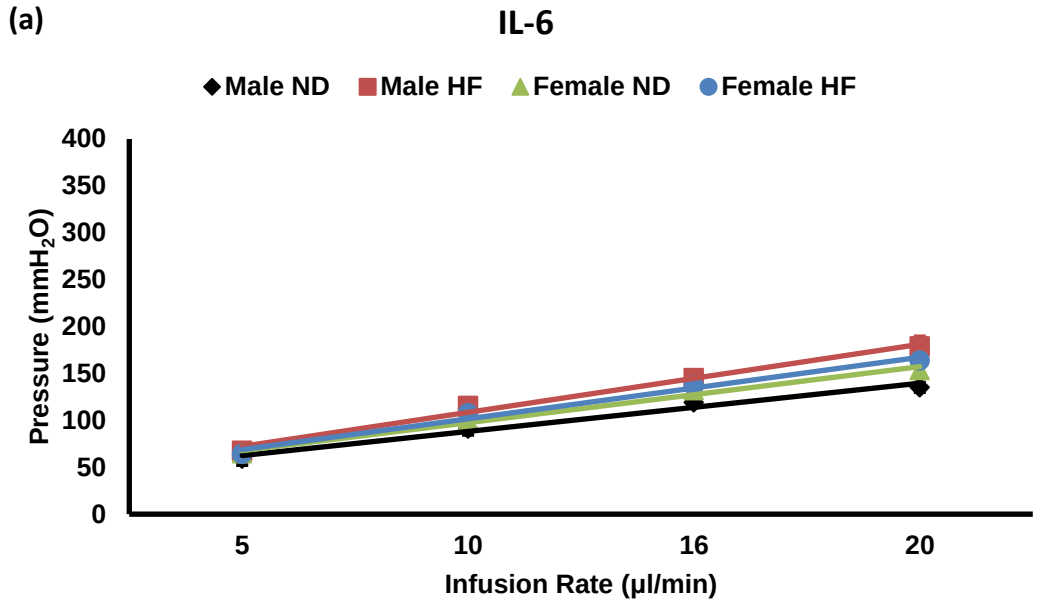

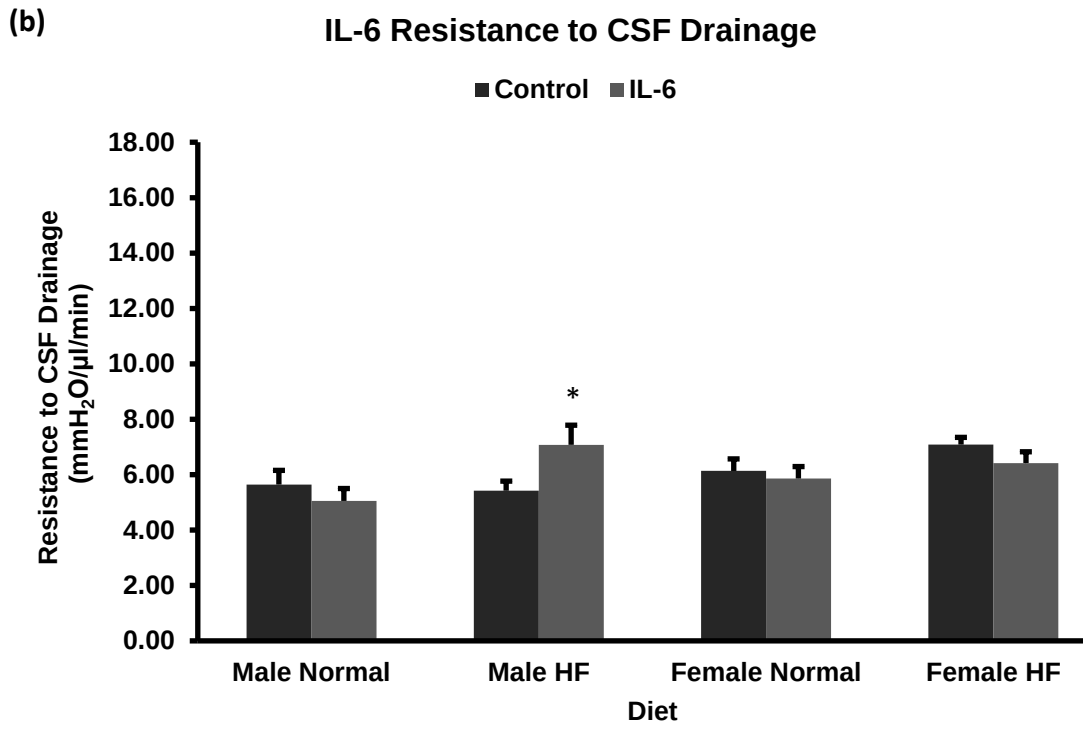

Figure 3.28: IL-6 resistance to CSF drainage values in male and female Wistar rats on a normal and high fat diet.
Each experiment was carried out by perfusing aCSF with each treatment through one lateral ventricle plus the addition of a single dose i.p injection of IL-6 90 minutes prior to perfusion. Samples from each group were averaged (±SEM); male ND (n=3), male HF (n=3), female ND (n=3), female HF (n=3) and compared to one another. The graphs show the linear pressure readings (mmH_2O) at each infusion rate (a); averaged resistance to CSF drainage readings ($mmH_2O \cdot min/\mu l$) (b). A three-way ANOVA was used to analyse the statistical significance. The significant results are shown following Sidak's multiple comparison test and was performed against each diet, sex and treatment variable. * $P = \leq 0.05$.

The only increased change in resistance to CSF drainage significant with IL-6, was with the male rats raised on a HF diet (7.08 ±0.71 $mmH_2O \cdot min/\mu l$) when compared with controls (5.42 ±0.34 $mmH_2O \cdot min/\mu l$, $P \leq 0.05$).

A three way ANOVA showed a significant difference between the normal and HF diets (P=<0.05). However, this could just be due to the difference in increased resistance to CSF drainage between males raised on a HF diet and normal diet.

There were no difference between any of the other variables, which also lead to a significant difference between treatment, sex and diet ($P \leq 0.05$), due to the one significant result in increasing resistance to CSF drainage, associated with IL-6, being observed only in the male HF diet group.

3.7.4 Sex and diet effects on CCL2 and IL-17-modulated resistance to CSF drainage

The variable rate infusion method was used to test the *in vivo* effects CCL2 and IL-17 modulation had on the resistance to CSF drainage over four increasing infusion rates (5, 10, 16, 20 µl/min). The graphs show the linear pressure readings (mmH_2O) at each infusion rate of CCL2 (Fig. 3.29a); IL-17 (Fig. 3.29b) and averaged resistance to CSF drainage readings ($mmH_2O \cdot min/\mu l$) (Fig. 3.29c).

(a)

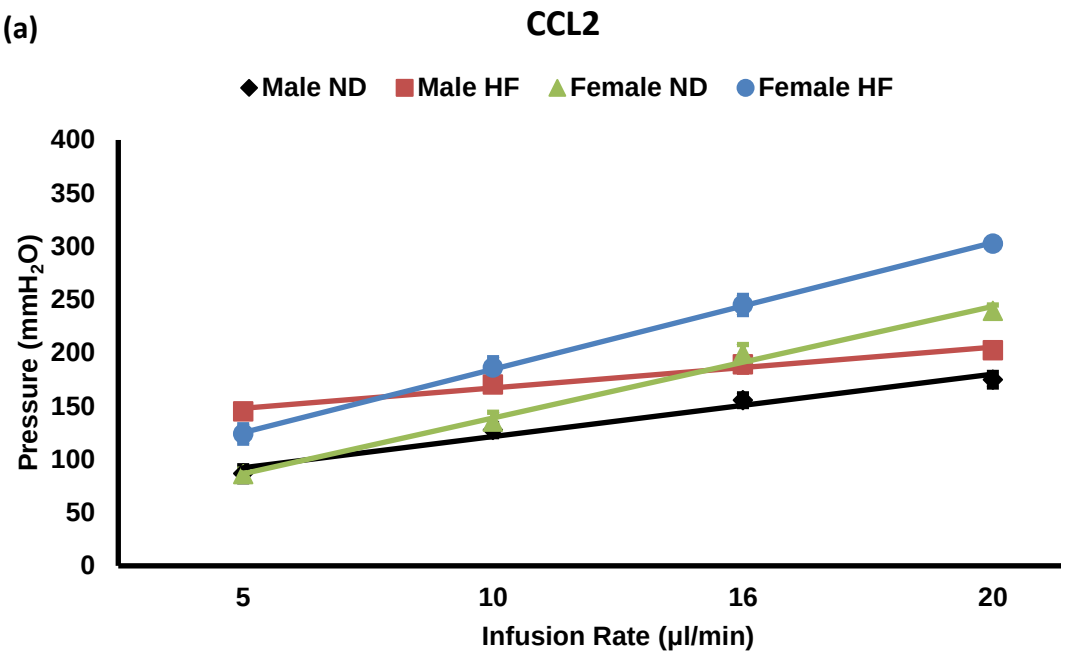
CCL2
Male ND
Male HF
Female ND
Female HF
Pressure (mmH2O)
400
350
300
250
200
150
100
50
0
5
10
16
20
Infusion Rate (µl/min)

(b)

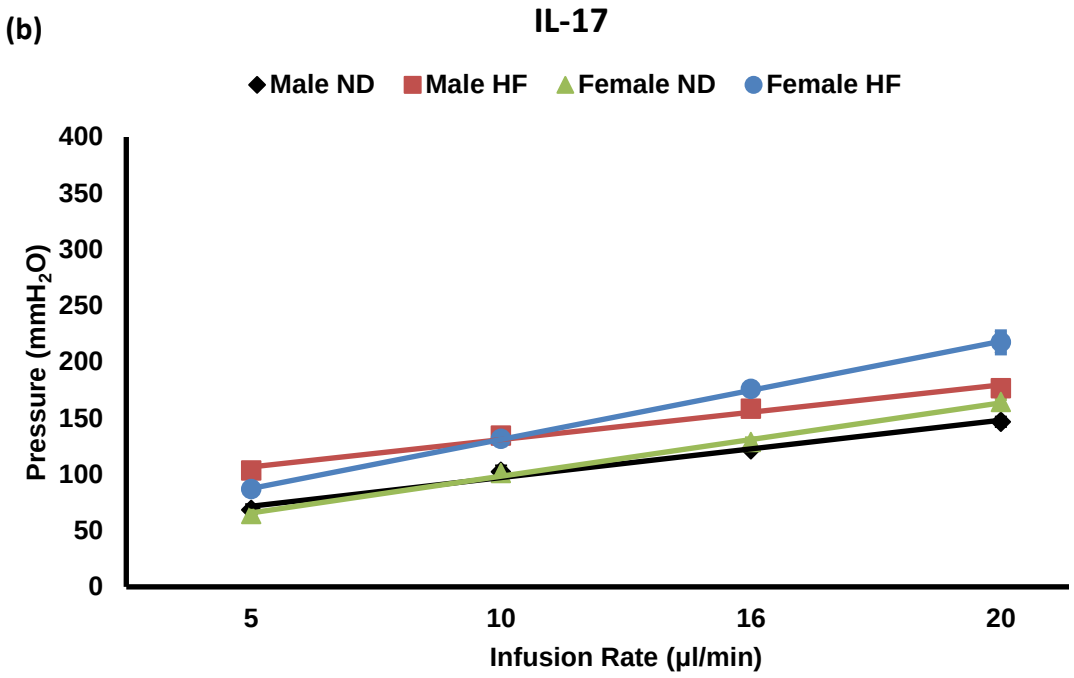
IL-17
Male ND
Male HF
Female ND
Female HF
Pressure (mmH2O)
400
350
300
250
200
150
100
50
0
5
10
16
20
Infusion Rate (µl/min)

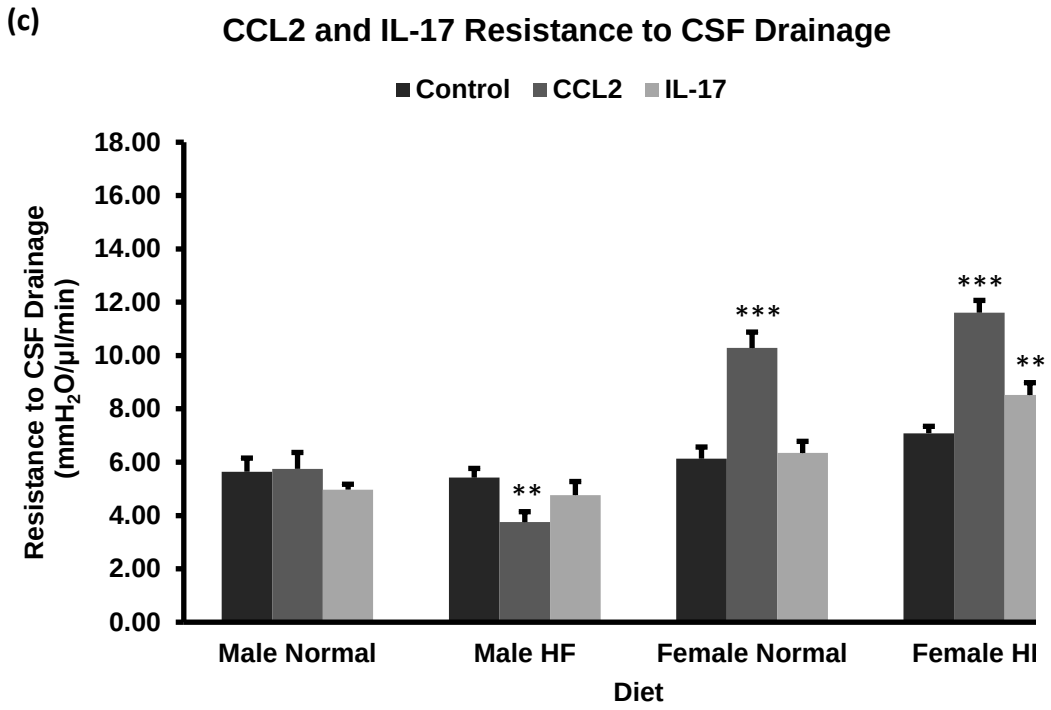

Figure 3.29: CCL2 and IL-17 resistance to CSF drainage values in male and female Wistar rats on a normal and high fat diet.
Each experiment was carried out by perfusing aCSF with each treatment through one lateral ventricle plus the addition of a single dose i.p injection of either CCL2 or IL-17 90 minutes prior to perfusion. Samples from each group were averaged (±SEM); male ND (n=3), male HF (n=3), female ND (n=3), female HF (n=3) and compared to one another. The graphs show the linear pressure readings (mmH_2O) at each infusion rate (CCL2) (a); IL-17 (b); averaged resistance to CSF drainage readings (mmH_2O/µl/min) (b). A three-way ANOVA was used to analyse the statistical significance. The significant results are shown following Sidak's multiple comparison test and was performed against each diet, sex and treatment variable. * P = ≤0.05; ** P = ≤0.01, *** P = ≤0.001.

CCL2 treatment in male rats on a normal diet (3.75 ±0.61 $mmH_2O{\cdot}min/\mu l$, n=3) decreased resistance to CSF drainage when compared with controls (5.42 ±0.51 $mmH_2O{\cdot}min/\mu l$, P≤0.01). However, interestingly, the opposite effect was seen in the female groups where CCL2 showed a significant increase in females fed a normal diet (10.28 ±0.60 $mmH_2O{\cdot}min/\mu l$) when compared with controls (6.13 ±0.44 $mmH_2O{\cdot}min/\mu l$, P≤0.001). The 'HF diet' females displayed a significant increase in resistance to CSF drainage following both CCL2 (11.61 ±0.46

$mmH_2O \cdot min/\mu l$, $P \leq 0.001$) and IL-17 (8.52 $mmH_2O \cdot min/\mu l$, $P \leq 0.01$) treatment when compared with controls (7.09 ±0.26 $mmH_2O \cdot min/\mu l$).

A three-way ANOVA analysis showed only CCL2, and not IL-17 treatment, resulted in a significant increase in resistance to CSF drainage over controls ($P \leq 0.0001$). This is seen with the normal diet and HF diet female rats.

However, there was a significant difference between the two sexes (IL-17 $P \leq 0.0001$; CCL2 $P \leq 0.0001$), which is shown by the increase in resistance to CSF drainage of the HF diet females when compared to the HF diet males, as well as in the normal diet equivalents. Only IL-17 caused a significant increase in resistance to CSF drainage between the diets ($P \leq 0.05$) as evident between the HF female and normal diet female rats.

3.7.5 *In vivo* sex and diet differences on initial pressure readings

Initial pressure readings following a 5 µl/min infusion rate were recorded to measure the effect of the i.p pre-injection effect of each treatment. Graphs of initial pressure differences for male (a) and female (b) Wistar rats raised on either a normal diet or HF diet are displayed in Fig. 3.30.

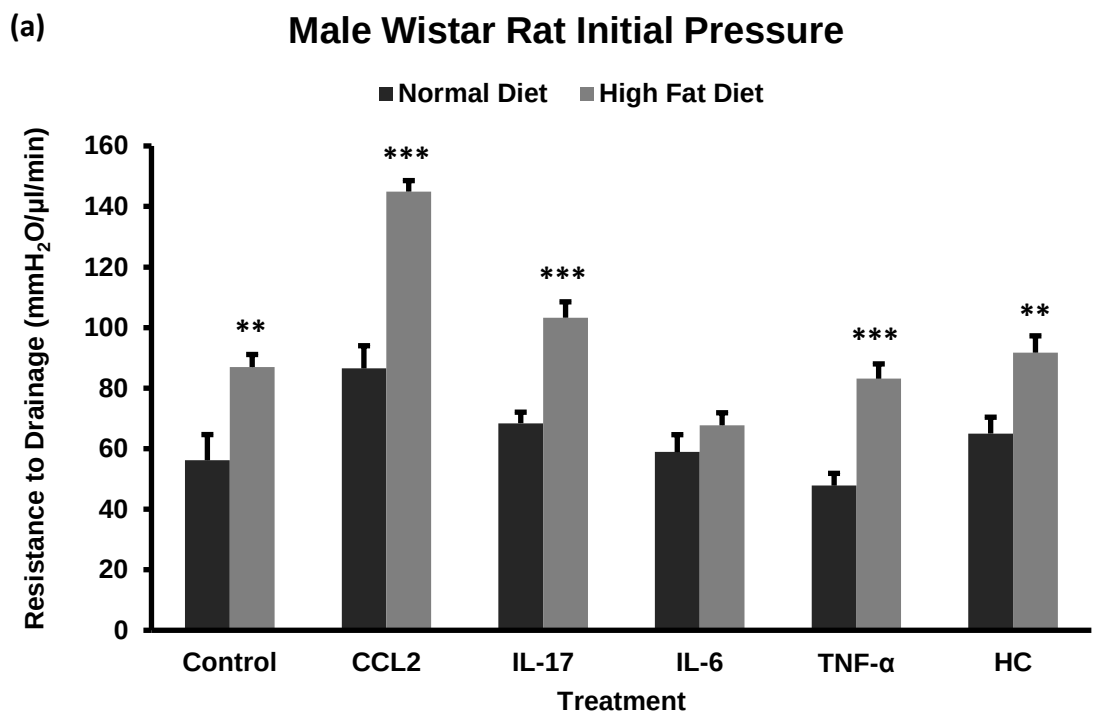

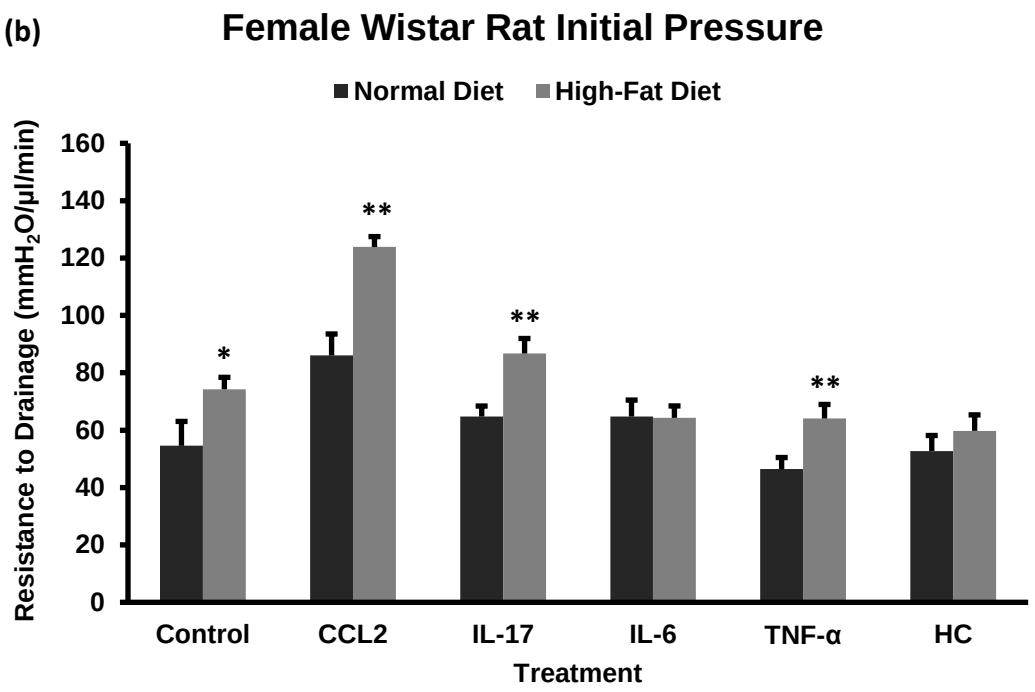

Figure 3.30: Initial pressure comparison of female Wistar rats on a normal and high-fat diet.
Normal diet readings are shown in dark grey; high-fat diet readings shown in light grey for each separate treatment in both male (a) and female (b) Wistar rats. Readings were taken following the first 5 µl/min variable rate infusion. Samples from diet and sex group were averaged (±SEM); HC (n=3), TNF-α (n=3), IL-6 (n=3), IL-17 (n=3), CCL2 (n=3) in both male and female ND and HF diets and compared accordingly. A two-way ANOVA was used to analyse the statistical significance. The significant results are shown following Sidak's multiple comparison test was used to test the significance of the initial pressure for each treatment and diet variables. * P = ≤0.05; ** P = ≤0.01, *** P = ≤0.001.

Each treatment in the HF diet groups in both sexes (excluding IL-6 in both sexes and HC in females) showed significant increases in initial pressures when compared to the corresponding treatment in the normal diet group (Fig. 3.30). In addition, a two-way ANOVA analysis described, that across all the treatments, the initial intracranial pressure readings of rats raised on a HF diet, in both sexes, increased when compared to rats fed on a normal diet (P≤0.001). These results highlight that as well as treatments with CCL2, IL-17 and TNF-α, even control animals raised on a HF diet show increasing initial CSF pressures, regardless of sex.

This correlates with the findings of CSF secretion and resistance to CSF drainage that a HF diet may be the biggest risk factor in raising intracranial pressures associated with IIH patients.

3.7.6 Summary of sex and diet effects on CSF dynamics (resistance to CSF drainage)

The slope pressures for each separate VRI experiment on both normal diet and HF diet rats show the effects each treatment has on the resistance to CSF drainage. The results of the initial experiments in which male Wistar rats were used, show that CCL2, IL-17 and IL-6 all significantly increase resistance to CSF drainage, whilst HC causes a significant decrease in resistance to CSF drainage (Fig. 3.6).

When comparing the male rats in both normal and HF diets it is evident that there is a lack of significance between the two groups and the pattern of results does not match the initial screening significances. The reason for this could be due to a change of cannula that was attached to the syringe that perfused the aCSF into the one lateral ventricle of the rat brain. Whilst a metal cannula had been used in the initial experiments, a plastic cannula was used in later experiments where the effects of diet and sex were investigated. The plastic cannula was chosen for these experiments to reduce the risk of a tear in the tubing, which if it occurred, would cause a decrease in pressure readings. However, over time the plastic cannula may have expanded, therefore decreasing the pressure readings, which would not be seen with a metal cannula that was used during the initial experiments.

A metal cannula was again fitted for the female VRI experiments and the resistance to CSF drainage pressures showed similar results towards the initial screening results in male Wistar rats. It is evident that in the 'normal diet' females, resistance to CSF drainage was increased by CCL2 and decreased by HC and TNF-α treatments. No effect was observed in these animals on treatment with IL-17 or IL-6. When comparing these results to the female Wistar rats on the HF diet, it is evident that the control resistance to CSF drainage values are significantly higher than in the normal diet females. CCL2 and IL-17 both increased the resistance to CSF drainage (Fig. 3.29), which matched the initial preliminary results (Fig 3.6). However, IL-6, HC and TNF-α showed no change when compared with controls. These results suggest that females on a HF diet have an overall increase in resistance to CSF drainage when compared with females on a normal diet. In addition, the effect HC and TNF-α have on decreasing the resistance to CSF drainage in normal diet females is abolished in the HF diet females (Fig 3.27). This would lead to a conclusion that in female animals on a HF diet, where basal CSF secretion (Fig. 3.18) and resistance to CSF drainage (Fig. 3.27) are elevated, the compensatory mechanism associated with HC and TNF-α treatments in animals fed a normal diet are absent or ineffective.

Graphs for each individual treatment's resistance to CSF drainage results, following variable rate infusion, of normal diet against a HF diet are shown in Appendix Section 6.9, page 290. In addition, the findings of CSF secretion and resistance to CSF drainage of animals raised on a HF diet correlate with the results of initial pressure readings (Fig. 3.30) and indicates that a HF diet may be the

biggest risk factor in raising intracranial pressures, which are synonymous with patients suffering from IIH.

3.8 Diet effects on rat choroid plexus ultrastructure by electron microscopy

The choroid plexuses are located in the inferior horn (temporal horn) of the lateral ventricles and the cuboidal epithelium lines the ventricular cavities (Fig. 3.31-3.44). The ependymal cells present microvilli and cilia on the apical surface and a basal lamina separates these cells from the collagen fibre connective tissue and blood vessels. The cuboidal epithelial cells are joined by tight junctions at the apical surfaces.

Cilia numbers, which are known to play an increased role in CSF secretion (Albee & Dutcher 2012), appeared to be similar in both normal and HF diet rats. The images show all of the characteristics associated with choroid plexus brain tissue including the cuboidal epithelial cells; tight junctions at the apical membranes; and microvilli and cilia on the surface of the epithelial cells, in the ventricular lumen, into which the CSF is secreted from the choroid plexus epithelium.

Due to no quantitative analysis being performed, it was not possible to ascertain whether an increase in cilia numbers in the HF diet rats may have presented an added explanation of the increased CSF secretion associated within this group. It is known that motile cilia in choroid plexus epithelial cells are involved in direct CSF movement. Studies by Albee and Ducher found cilia can be motile as on the epithelial surface of respiratory tract, the oviduct, and the fourth ventricle of the brain, where each cell has multiple cilia (Albee & Dutcher 2012). However, only

confirmation of the typical characteristics associated with lateral ventricle choroid plexus ultrastructure was possible due to no quantitative analysis being performed between male rats on a normal diet and those on a HF diet.

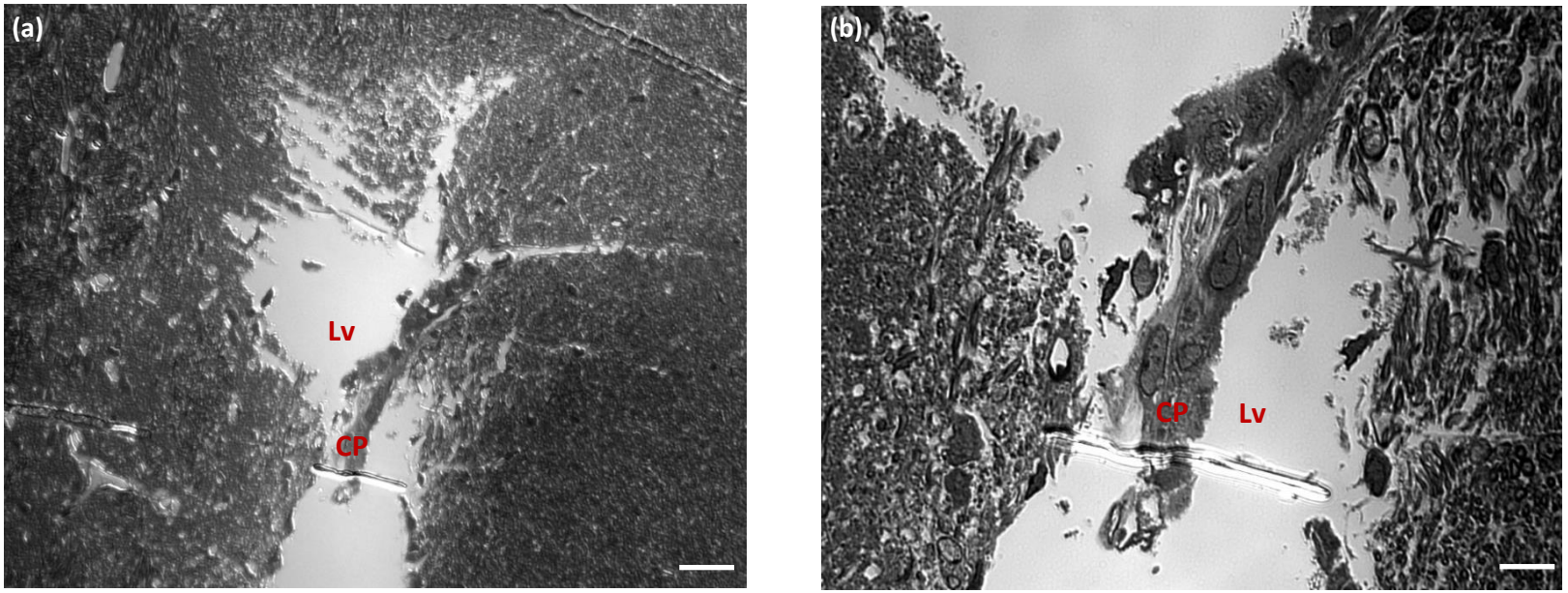

Figure 3.1: 1 µm thick sections of ultrastructure images on normal diet male Wistar rat lateral ventricle choroid plexus. Images obtained on a Leica DMI 6000B Microscope. Scale bar represents 40 µm (a) and 125 µm (b).

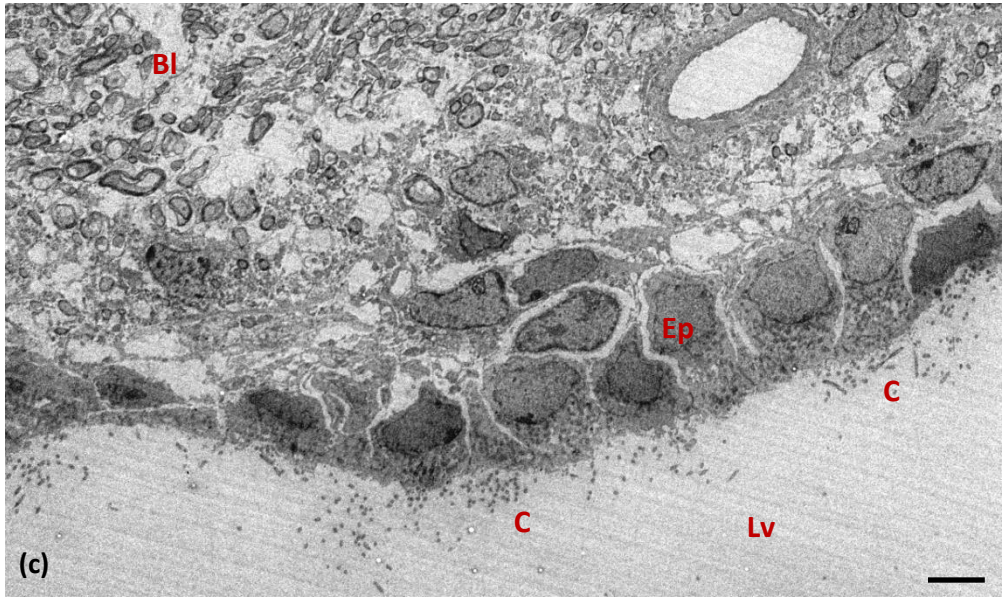

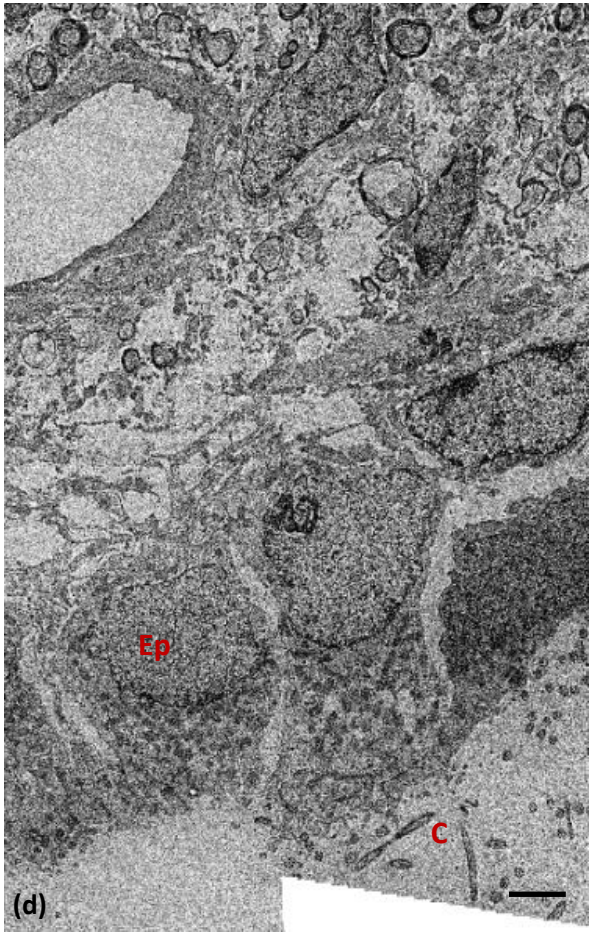

Figure 3.2: Electron micrographs of 0.1 µm thick sections from male Wistar rat lateral ventricle choroid plexus raised on a normal diet. Animals were perfusion fixed with 4% (w/v) PFA + 0.5% (v/v) glutaraldehyde at 11 weeks of age. (c) (d) Cuboidal epithelial cell (Ep); Cilia (C); ventricular lumen (Lv); basal lamina (Bl) Scale bar represents 800nm (c) and 600nm (d).

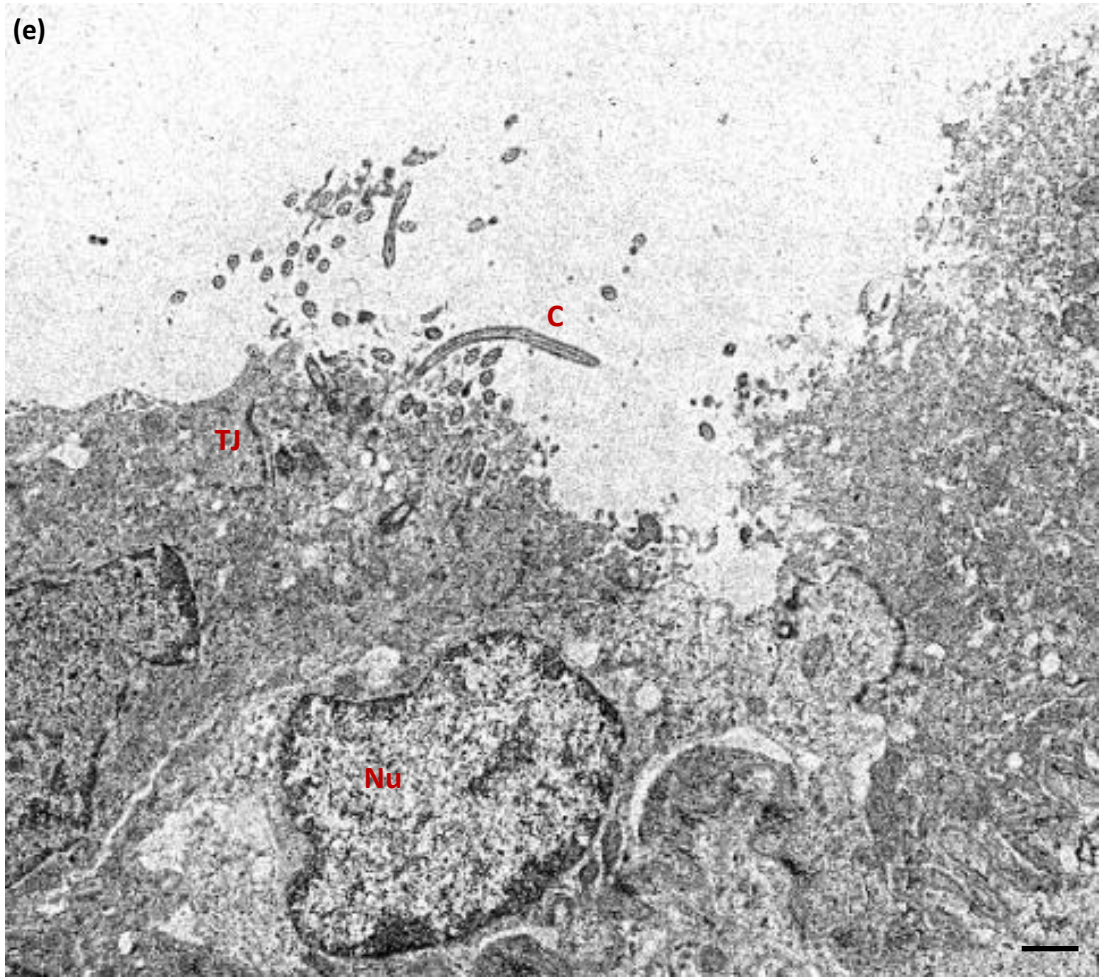

Figure 3.3: Electron micrographs of 0.1 µm thick sections from male Wistar rat lateral ventricle choroid plexus raised on a normal diet.

(e) Cilia (C); Tight junction (TJ); Nucleus (Nu). Scale bar represents 600nm.

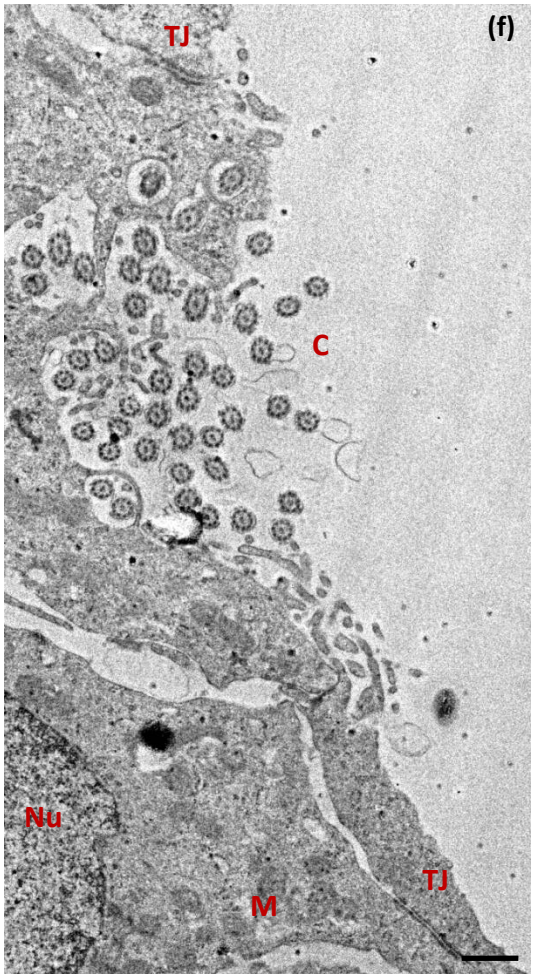

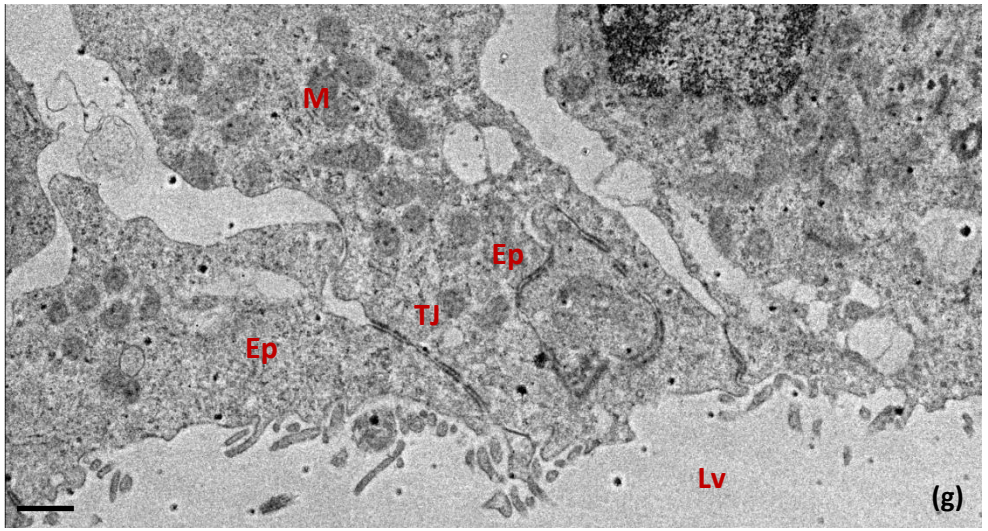

Figure 3.4: Electron micrographs of 0.1 µm thick sections from male Wistar rat lateral ventricle choroid plexus raised on a normal diet.

(f), (g) Cuboidal epithelial cell (Ep); Cilia (C); ventricular lumen (Lv); Tight junction (TJ); Nucleus (Nu); Mitochondria (M). Scale bar represents 600nm.

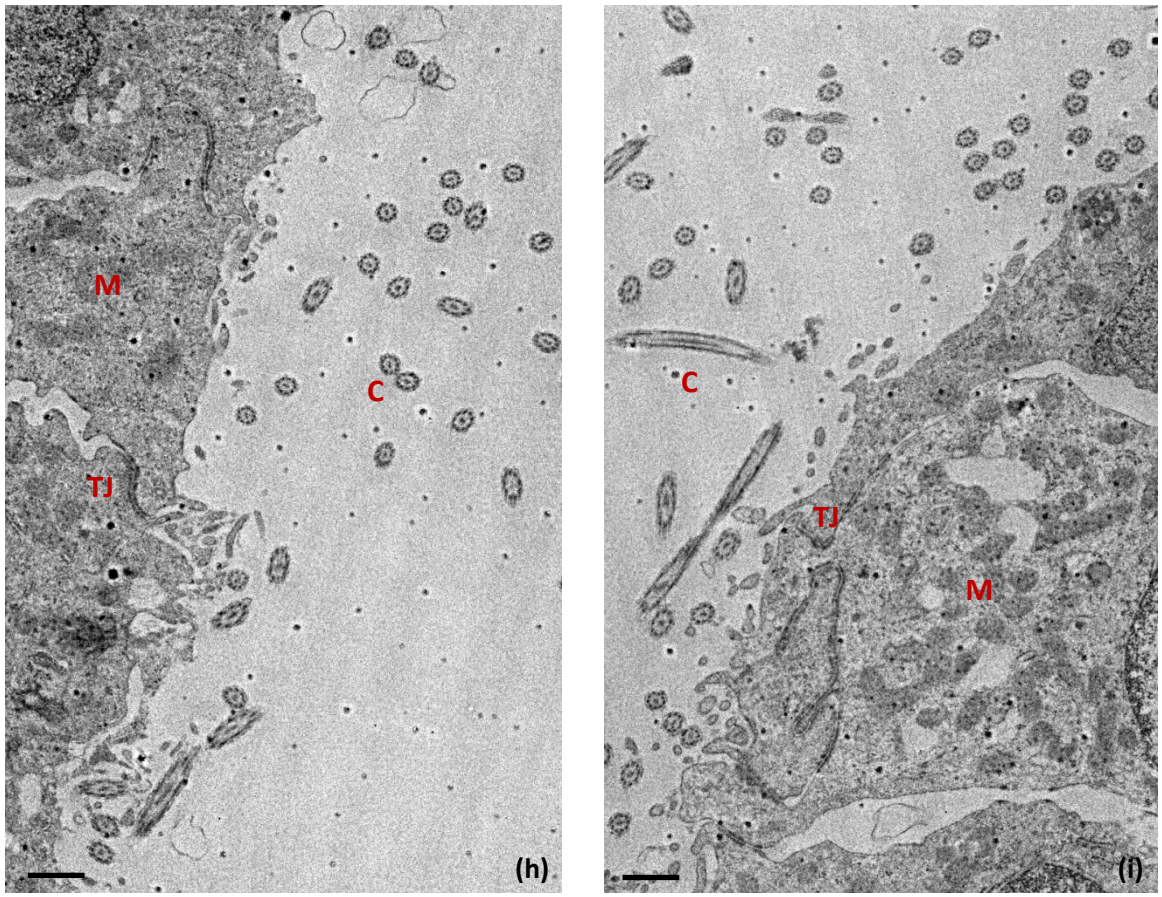

Figure 3.5: Electron micrographs of 0.1 µm thick sections from male Wistar rat lateral ventricle choroid plexus raised on a normal diet.
(h), (i) Cilia (C); tight junction (TJ); mitochondria (M). Scale bar represents 600nm.

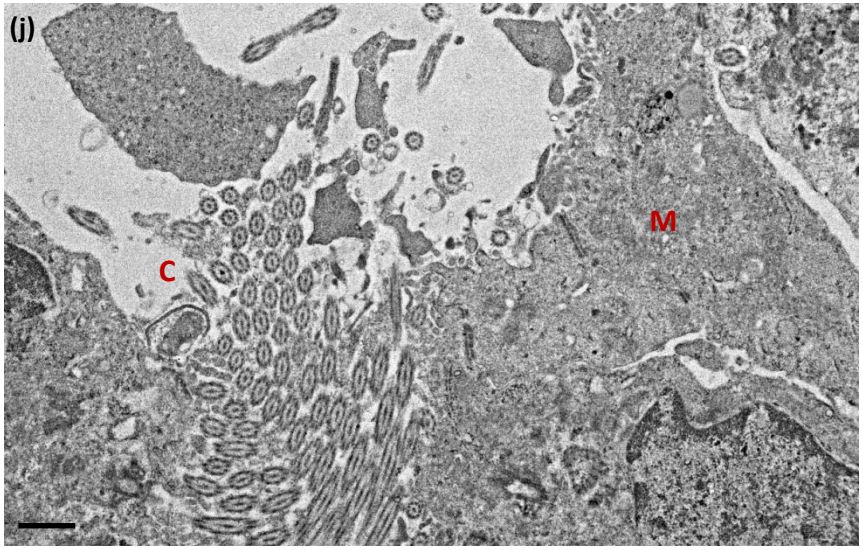

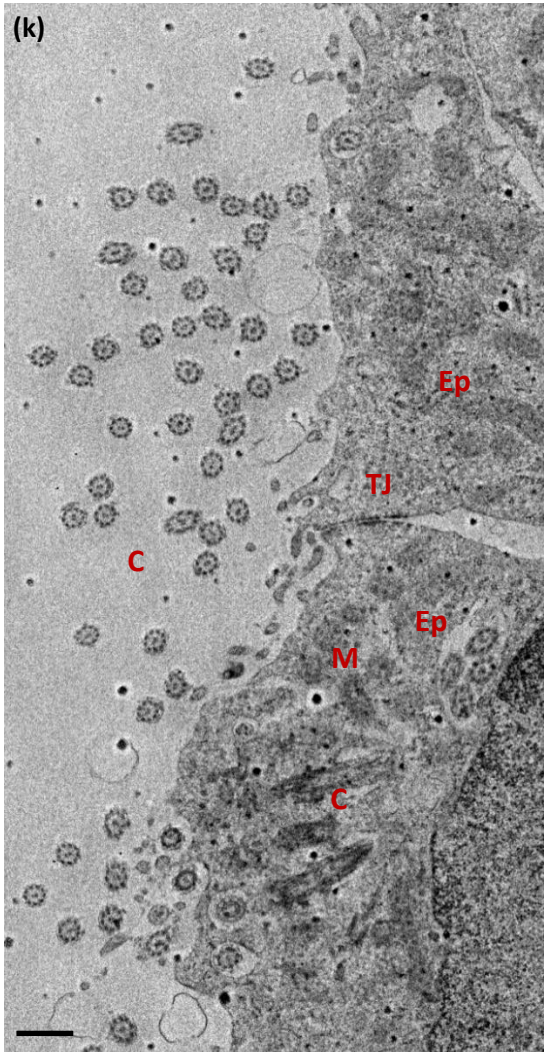

Figure 3.6: Electron micrographs of 0.1 µm thick sections from male Wistar rat lateral ventricle choroid plexus raised on a normal diet.

(j), (k) Cuboidal epithelial cell (Ep); Cilia (C); tight junction (TJ); mitochondria (M). Scale bar represents 600nm.

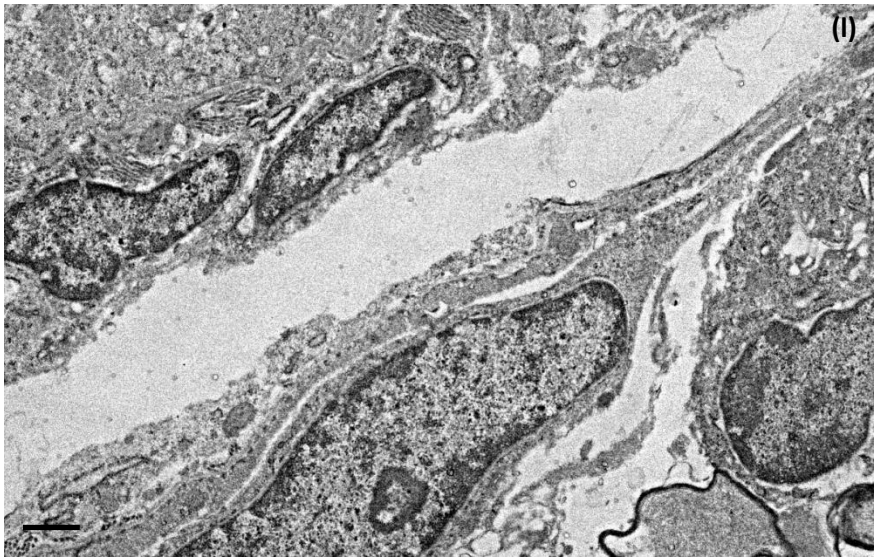

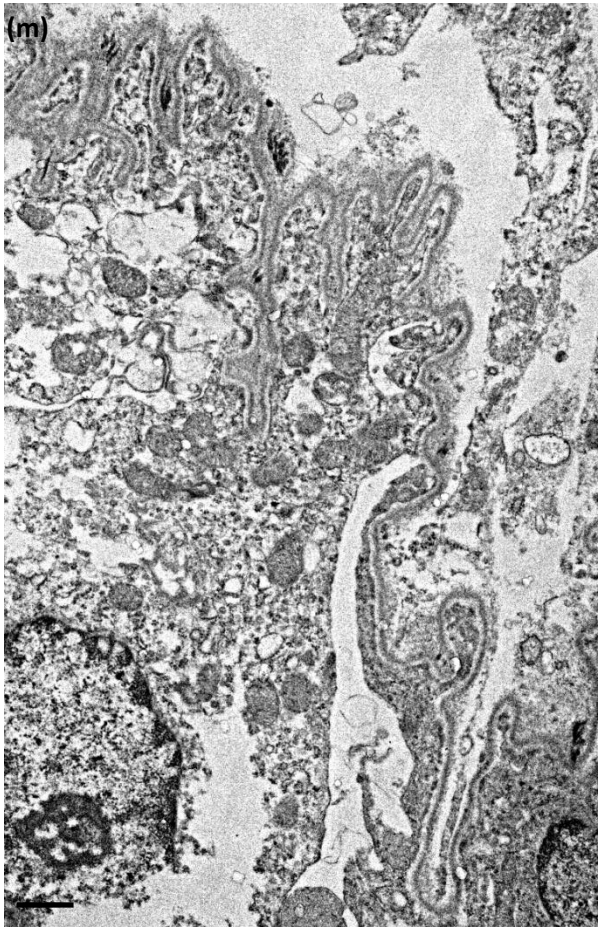

Figure 3.7: Electron micrographs of 0.1 µm thick sections from male Wistar rat lateral ventricle choroid plexus raised on a normal diet.

(l), (m) Choroid plexus epithelia. Scale bar represents 600nm.

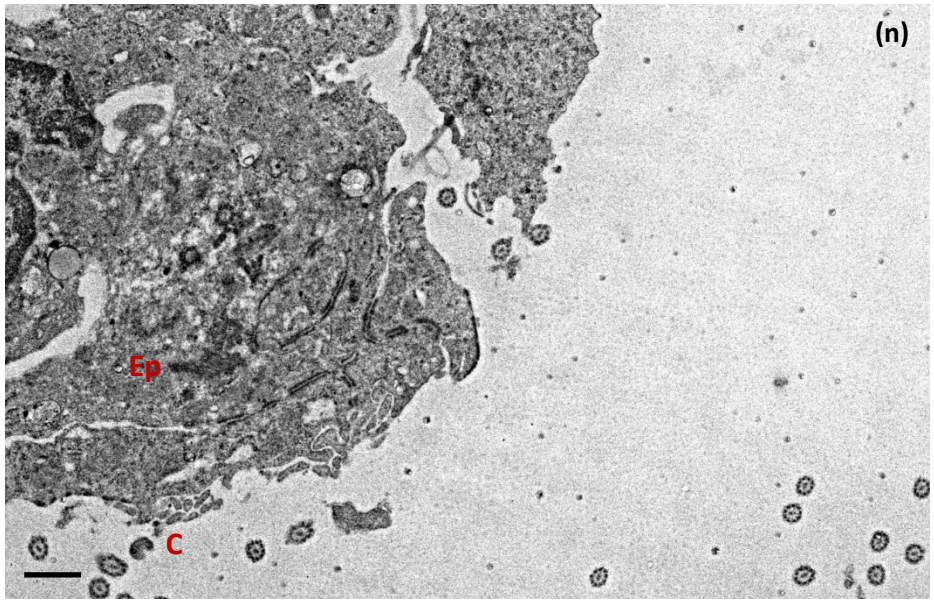

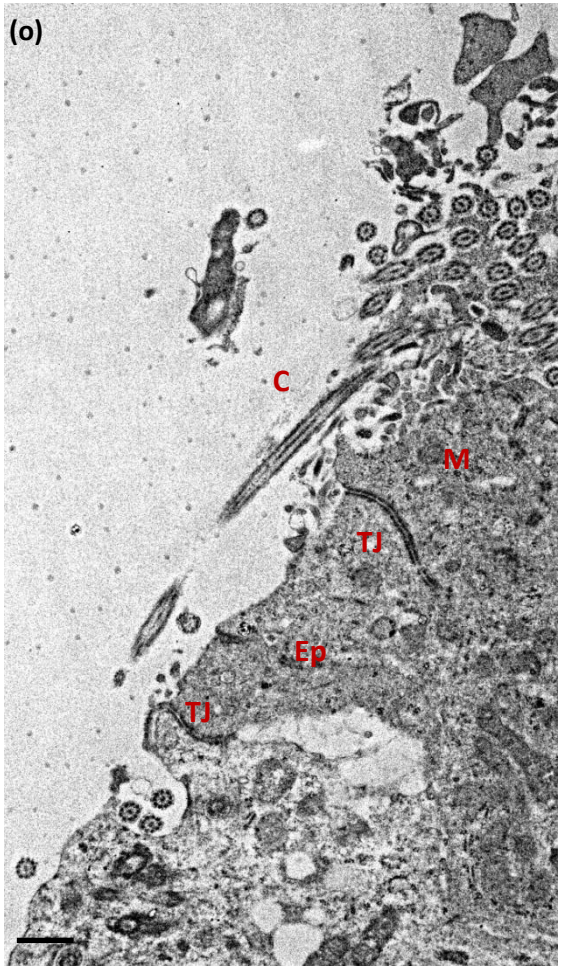

Figure 3.8: Electron micrographs of 0.1 µm thick sections from male Wistar rat lateral ventricle choroid plexus raised on a normal diet.

(n), (o) Cuboidal epithelial cell (Ep); Cilia (C); Tight junction (TJ); Mitochondria (M). Scale bar represents 600nm.

Figure 3.9: Electron micrographs of 1 µm thick sections from male Wistar rat lateral ventricle choroid plexus raised on a high-fat diet.

Animals were killed by perfusion with 4% (w/v) PFA + 0.5% (v/v) glutaraldehyde at 11 weeks of age. Images obtained on a Leica DMI 6000B Microscope. (a) Choroid plexus (Cp); ventricular lumen (Lv). Scale bar represents 125 µm.

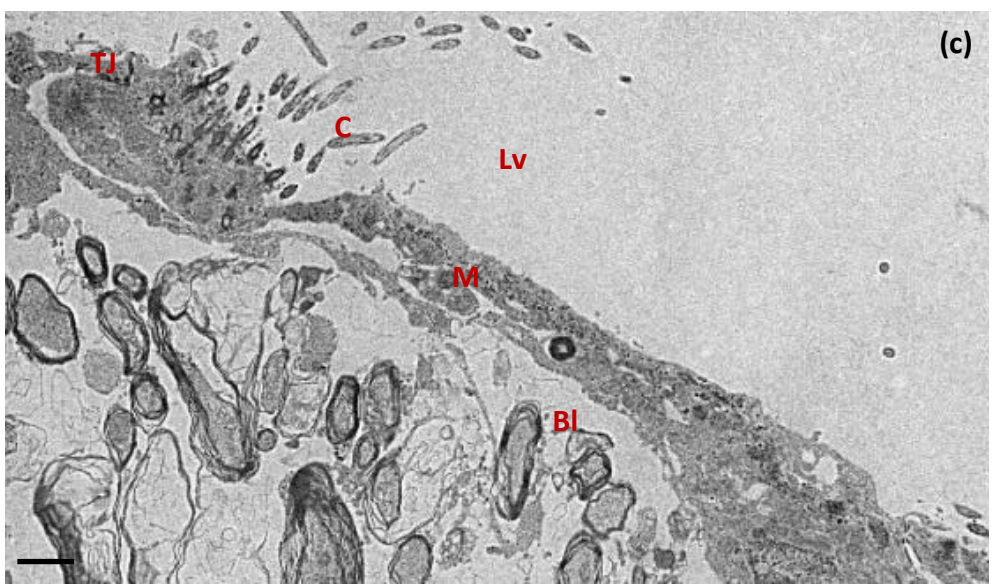

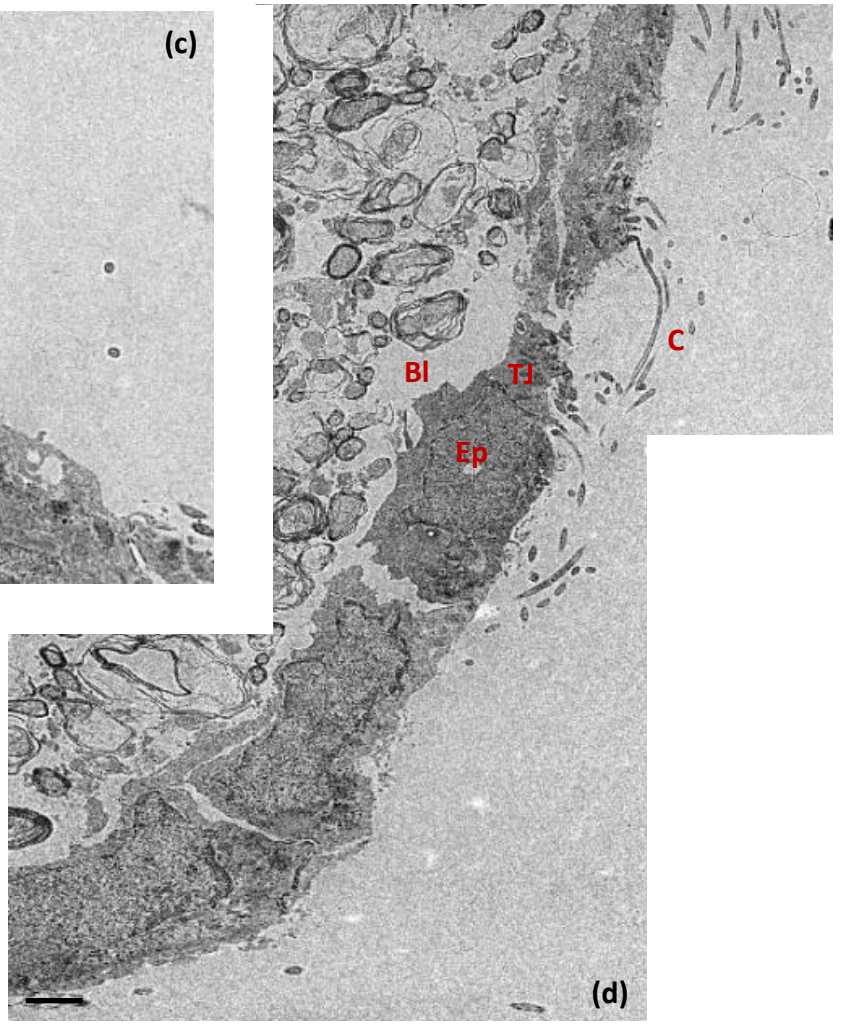

Figure 3.10: Electron micrographs of 0.1 µm thick sections from male Wistar rat lateral ventricle choroid plexus raised on a high-fat diet.

(c), (d) Cuboidal epithelial cell (Ep); cilia (C); ventricular lumen (Lv); tight junction (TJ); mitochondria (M); basal lamina (Bl). Scale bar represents 800nm.

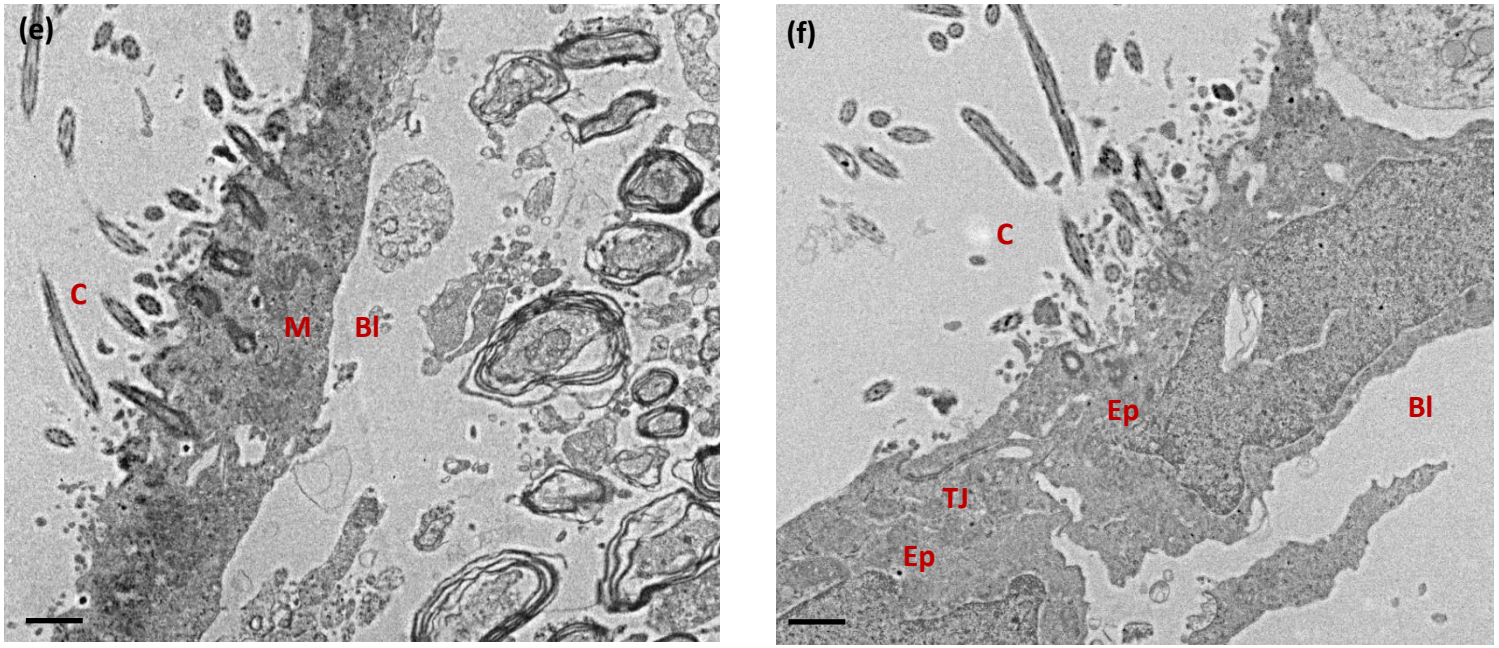

Figure 3.11: Electron micrographs of 0.1 µm thick sections from male Wistar rat lateral ventricle choroid plexus raised on a high-fat diet.

(e), (f) Cuboidal epithelial cell (Ep); cilia (C); ventricular lumen (Lv); tight junction (TJ); mitochondria (M); basal lamina (Bl). Scale bar represents 600nm.

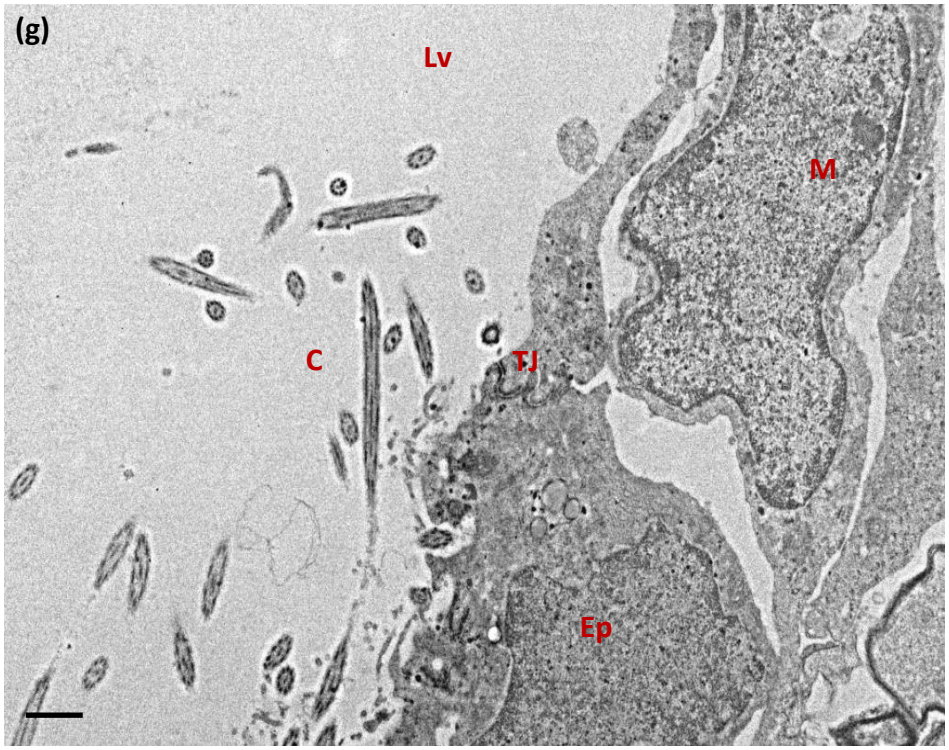

Figure 3.12: Electron micrographs of 0.1 µm thick sections from male Wistar rat lateral ventricle choroid plexus raised on a high-fat diet.

(g) Cuboidal epithelial cell (Ep); cilia (C); ventricular lumen (Lv); tight junction (TJ); mitochondria (M). Scale bar represents 600nm.

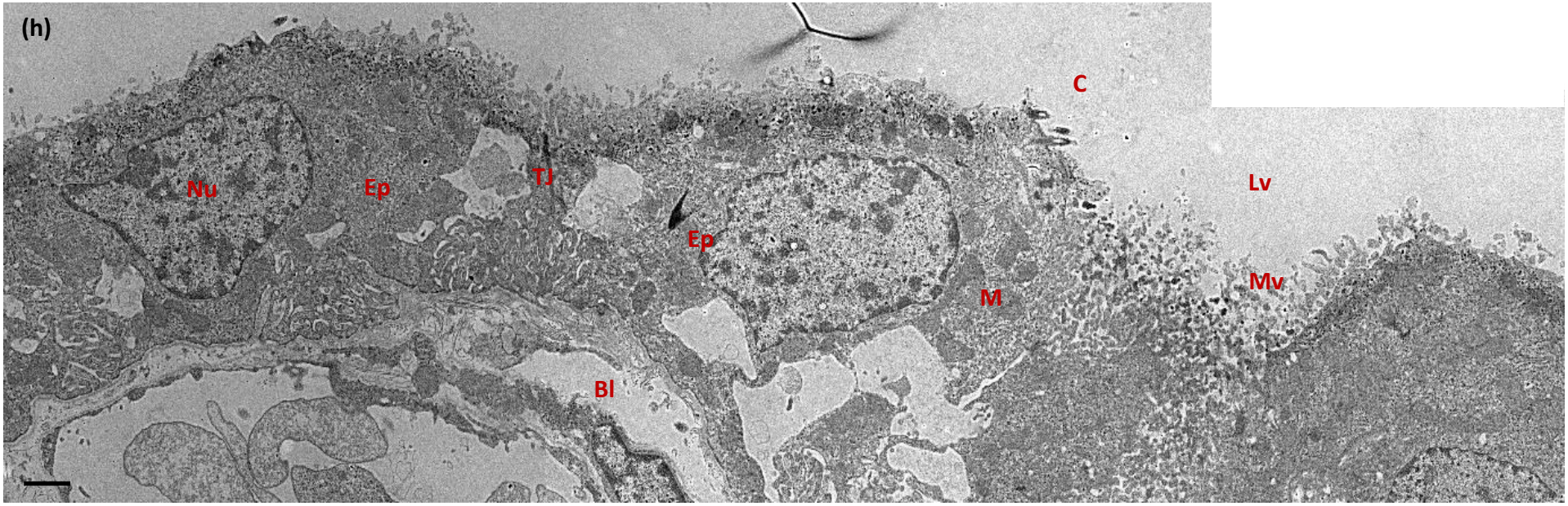

Figure 3.13: Electron micrographs of 0.1 µm thick sections from male Wistar rat lateral ventricle choroid plexus raised on a high-fat diet.
(h) Cuboidal epithelial cell (Ep); cilia (C); ventricular lumen (Lv); tight junction (TJ); mitochondria (M); nucleus (N); microvilli (Mv); basal lamina (Bl). Scale bar represents 1000nm.

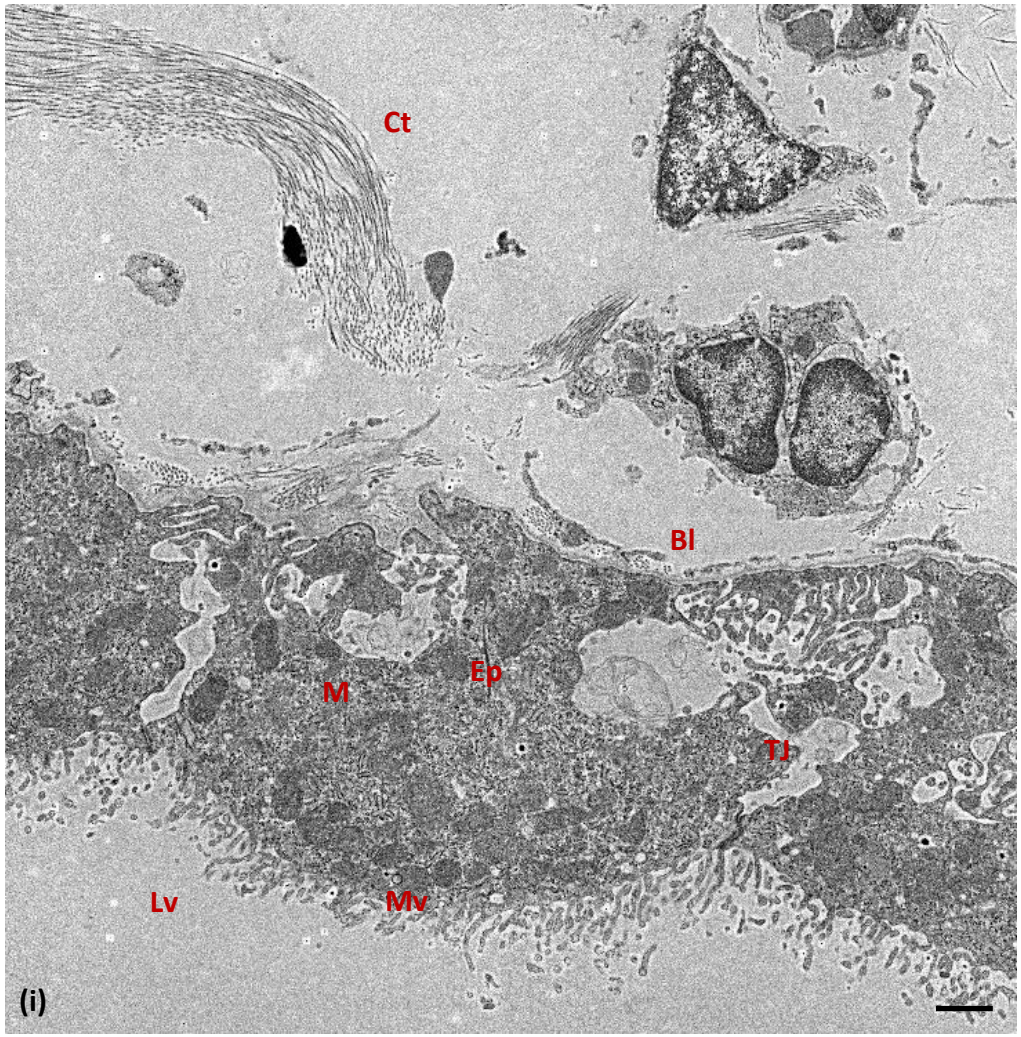

Figure 3.14: Electron micrographs of 0.1 µm thick sections from male Wistar rat lateral ventricle choroid plexus raised on a high-fat diet.
(i) Cuboidal epithelial cell (Ep); ventricular lumen (Lv); tight junction (TJ); mitochondria (M); microvilli (Mv); connective tissue (collagen fibres) (Ct); basal lamina (Bl). Scale bar represents 1000nm.

3.9 Characterisation of human choroid plexus epithelial cells (hCPEpiC)

Having established that HC, TNF-α and IL-6 modulated CSF secretion rates; and IL-17 and CCL2 modulated resistance to CSF drainage *in vivo*, *in vitro* experiments were performed to investigate the molecular mechanisms through which these treatments may influence CSF secretion and thereby intracranial pressure. To this end immunocytochemistry and flow cytometry were used to test the expression of hCPEpiC transporters/channels and cytokine receptors.

3.9.1 hCPEpiC morphology

Primary hCPEpiC displayed spindle shaped cells before growing towards confluence after 8 days in culture (DIC), where they formed polygonal shaped confluent monolayers with some degree of cell-cell overlap.

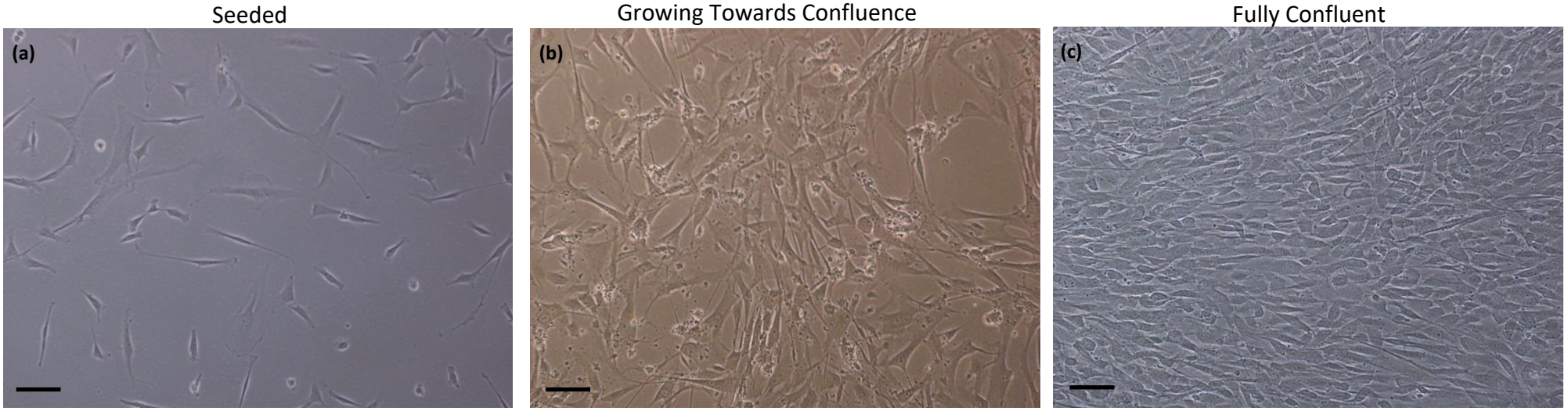

Figure 3.15: Morphology of hCPEpiC viewed by phase contrast microscopy (P1).
The cells were seeded at a density of 5000 cells/cm^2 in complete hCPEpiC medium. Freshly isolated primary hCPEpiC formed confluent monolayers with polygonal shaped colonies of cells after 8 DIC. All further experiments were performed at passages 1-5. Images were taken with a Nikon Eclipse TS100 camera. Scale bar represents 20 µm.

3.9.2 Expression of choroid plexus epithelial markers by hCPEpiC by immunocytochemistry

Characterisation of hCPEPiC proteins, known to be expressed in choroid plexus epithelial cells (Abbott et al. 2010) (Ballabh et al. 2004) (Allt & Lawrenson 2001) (Redzic & Segal 2004) was performed initially by immunocytochemistry. It was important to confirm whether the hCPEpiC would be effective in testing the effect of the modulators of interest on the possible *in vitro* molecular mechanisms of CSF secretion. Transthyretin (TTR) protein was distributed uniformly at the cell surface of hCPEpiC. ZO-1 and Claudin-1 tight junctional proteins were not found to be expressed at the apical tight junction sites associated with choroid plexus epithelial cells (Fig. 3.46). Reviews by Redzic also found this to be the case in many studies using primary hCPEpiC (Redzic 2013). These data suggest that the hCPEpiC cells are not a suitable blood-CSF barrier (BCSFB) *in vitro* model to study CSF secretion assays but are a good model to study the increase/decrease in expression of transporters/channels involved in CSF secretion across the choroid plexus epithelium. The characterisation of the transporters involved in CSF secretion is described in Sections 3.10.3 and 3.11.

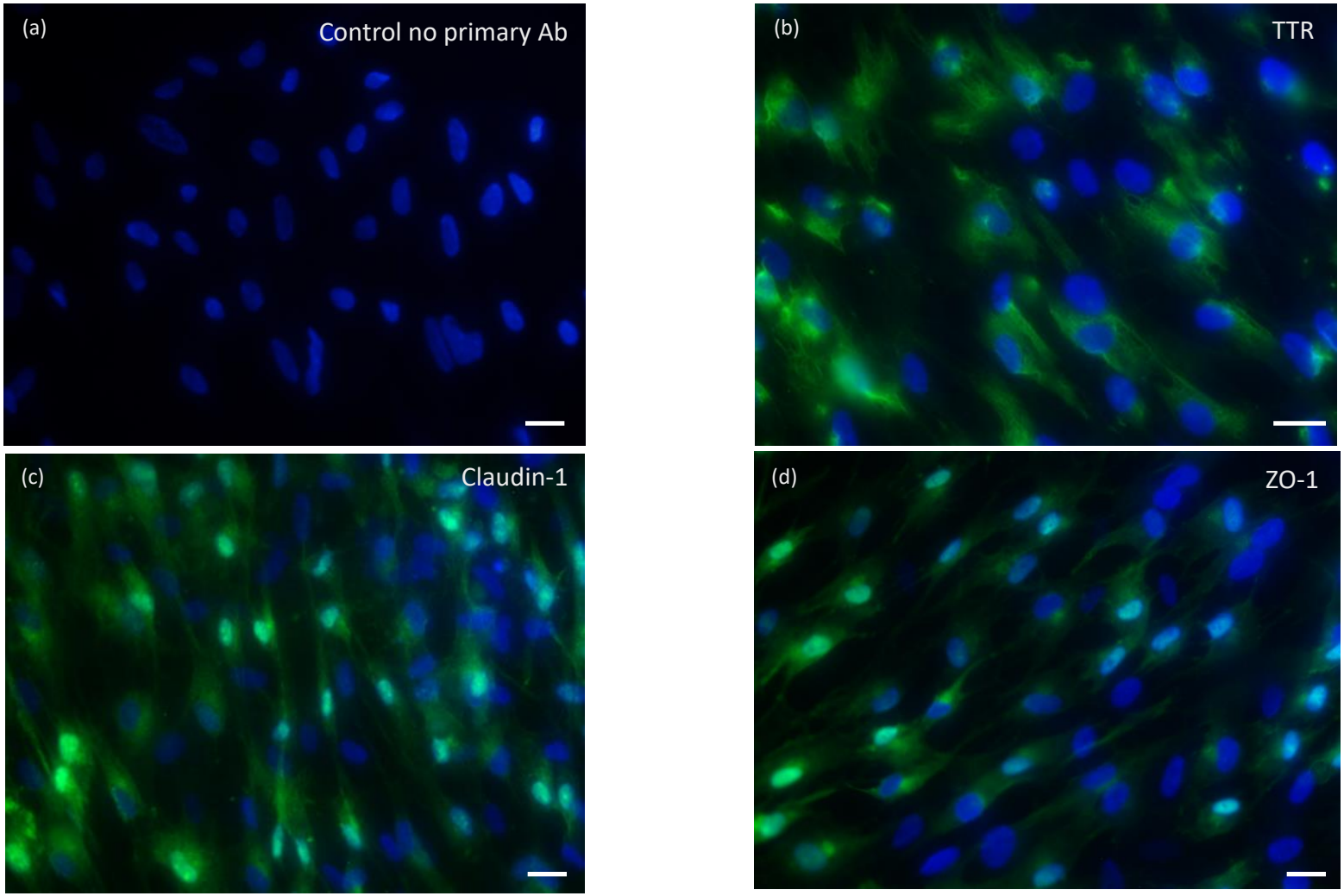

Figure 3.16: Expression of pre-albumin Transthyretin (TTR), Claudin-1 and ZO-1 proteins on hCPEpiC as viewed by confocal microscope. hCPEpiC cells were grown on poly-l-lysine coated Ibidi chambers until confluent. The cells were fixed in 4% PFA and stained for (a) control (no primary Ab), (b) anti-prealbumin (TTR) (sheep polyclonal IgG), (c) claudin-1 (rabbit polyclonal IgG), or (d) ZO-1 (rabbit polyclonal IgG) primary antibodies. The secondary antibodies used included (a) polyclonal sheep anti-mouse IgG FITC conjugated, (b) donkey anti-sheep IgG FITC conjugated, (c,d) goat anti-rabbit IgG Alexa 488. The cells were counterstained with DAPI and viewed via a confocal microscope. Images are a representation of hCPEpiC cells at P2 (n=3). Scale bar represents 125 µm.

3.9.3 Expression of transporters and channels by hCPEpiC by immunocytochemistry

In order to analyse the effect of HC, TNF-α, IL-6 and IL-17 on the expression of hCPEpiC transporters (Na^+-K^+-ATPase, NKCC1, AQP1 and ENaC), identifying whether the hCPEpiC express the transporters/channels that mediate the molecular mechanisms of CSF secretion across the BCSFB was performed first. Immunocytochemistry (Fig. 3.47) and flow cytometry analysis (Fig. 3.50) show Na^+-K^+-ATPase, NKCC1, AQP1 and ENaC transporters/channels, and CCR2, IL17α, TNFR1 and IL-6R receptors are expressed on hCPEpiC. From the results in Fig. 3.47, it is evident that Aquaporin-1 and Na^+-K^+-ATPase are expressed on the cell membrane, whereas NKCC1 and ENaC were detected in the cytosol.

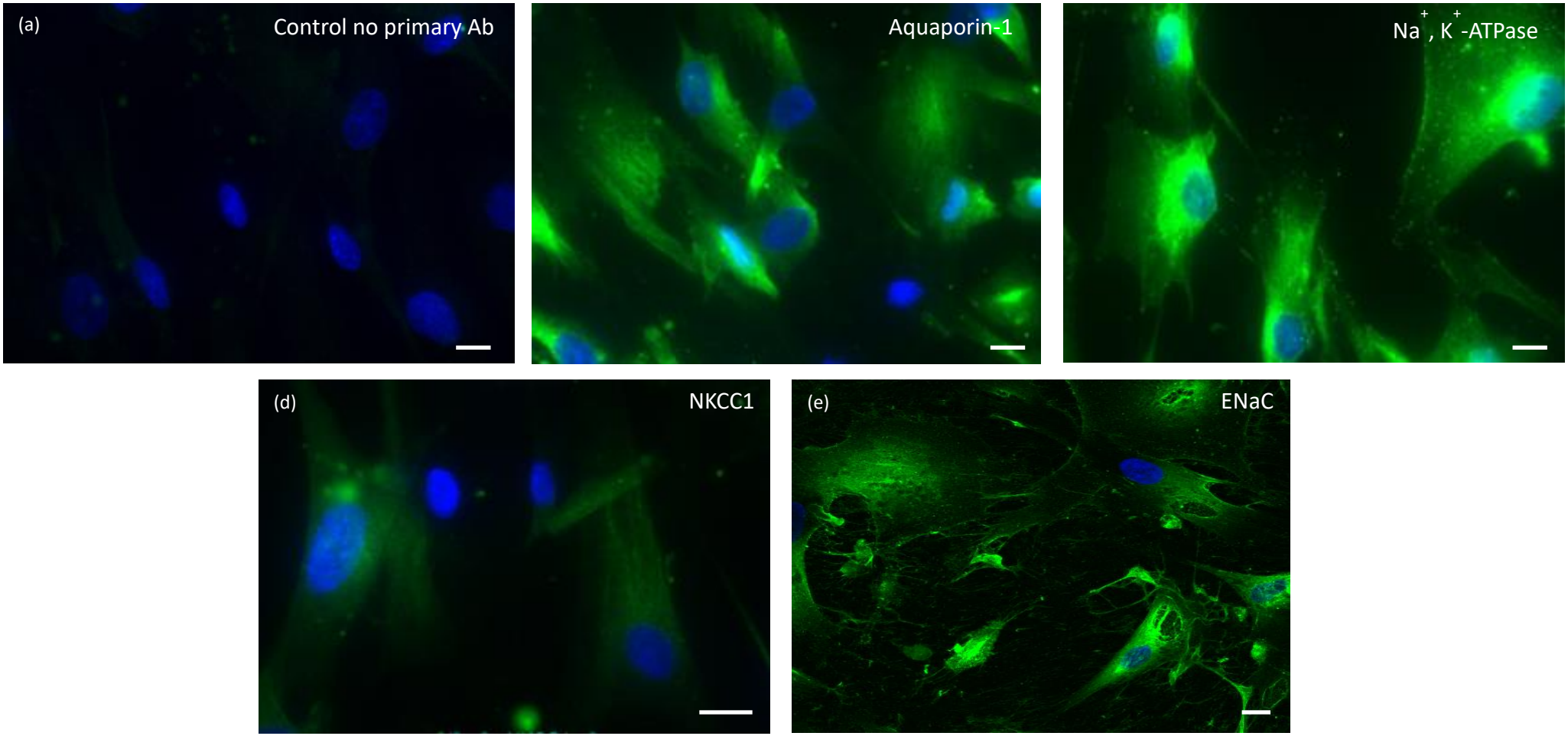

Figure 3.17: Expression of Aquaporin-1 water channel, Na^+-K^+-ATPase, NKCC1 and ENaC transporters on hCPEpiC as viewed by confocal microscope. hCPEpiC cells were grown on poly-l-lysine coated Ibidi chambers until confluent. The cells were fixed in 4% PFA and stained for (a) control (no primary Ab), (b) aquaporin-1 rabbit polyclonal IgG, (c) Na^+-K^+-ATPase rabbit polyclonal IgG, (d) NKCC1 rabbit polyclonal IgG, or (e) ENaC rabbit polyclonal IgG primary antibodies. The secondary antibodies used included (a) polyclonal sheep anti-mouse IgG FITC conjugated, (b,c,d,e) goat anti-rabbit IgG alexa 488. The cells were counterstained with DAPI and viewed via a confocal microscope. Images are a representation of hCPEpiC cells at P2 (n=3). Scale bar represents 80 µm.

3.9.4 Expression of cytokine receptors by hCPEpiC by immunocytochemistry

The receptors of cytokines CCL2, IL-17, TNF-α and IL-6 that could be involved in mediating the biological functions of CSF secretion across the BCSFB were identified. To determine the subcellular distribution of cytokine receptors, hCPEpiC were fixed and the expression of CCR2, IL17Rα, TNFR1 and IL-6R was analysed by immunocytochemistry (Fig. 3.48-3.49) using confocal microscopy and also flow cytometry (Fig. 3.51). Under normal conditions, CCR2 (Fig. 3.48b), IL-17Rα (Fig. 3.48c) and TNFR1 (Fig. 3.49b) were distributed uniformly at the cell surface of hCPEpiC. By contrast, IL-6R staining appeared as a punctate pattern on the plasma membrane of the hCPEpiC, suggesting that IL-6R is located in clusters (Fig. 3.49c).

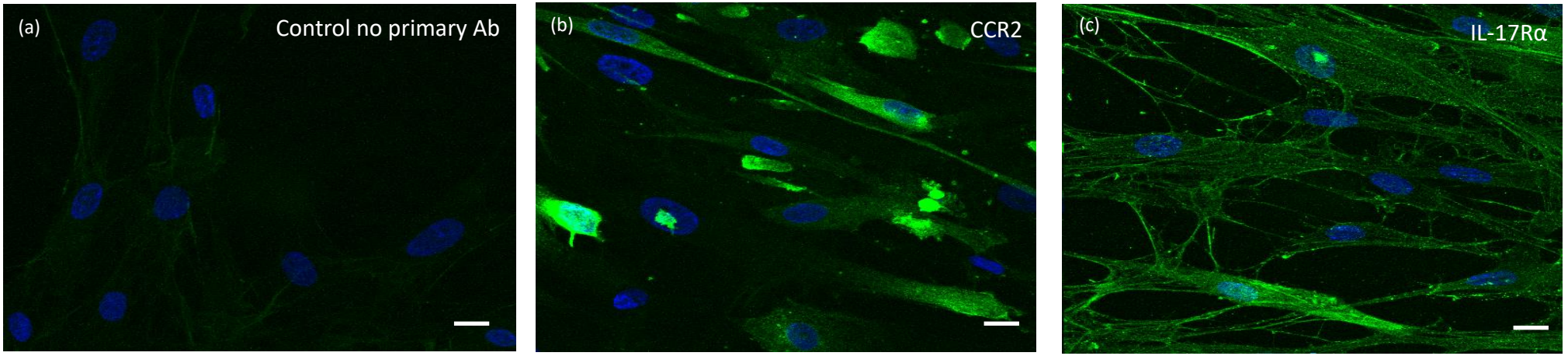

Figure 3.18: Expression of CCR2 and IL-17Rα receptors on hCPEpiC as viewed by confocal microscope. hCPEpiC cells were grown on poly-l-lysine coated Ibidi chambers until confluent. The cells were fixed in 4% PFA and stained for (a) control (no primary Ab), (b) CCR2 rabbit polyclonal IgG, (c) IL-17Rα rabbit polyclonal IgG primary antibodies. The secondary antibodies used included (a) polyclonal sheep anti-mouse IgG FITC conjugated, (b,c) goat anti-rabbit IgG alexa 488. The cells were counterstained with DAPI and viewed via a confocal microscope. Images are a representation of hCPEpiC cells at P4 (n=3). Scale bar represents 80 µm.

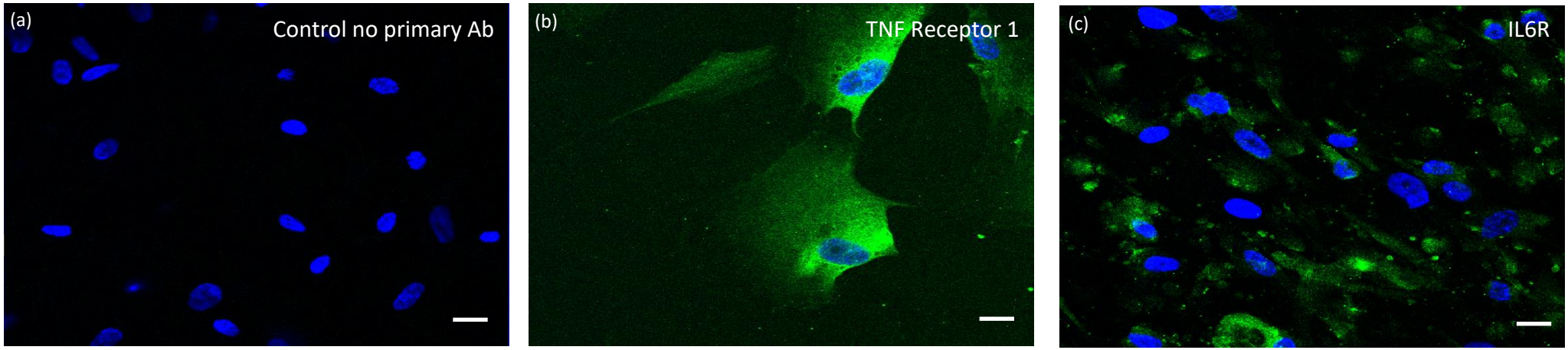

Figure 3.19: Expression of TNF Receptor 1 and IL6R receptors on hCPEpiC as viewed by confocal microscope. hCPEpiC cells were grown on poly-l-lysine coated Ibidi chambers until confluent. The cells were fixed in 4% PFA and stained for (a) control (no primary Ab), (b) TNF receptor 1 rabbit polyclonal IgG, (c) IL6R rabbit polyclonal IgG primary antibodies. The secondary antibodies used included (a) polyclonal sheep anti-mouse IgG FITC conjugated, (b,c) goat anti-rabbit IgG alexa 488. The cells were counterstained with DAPI and viewed via a confocal microscope. Images are a representation of hCPEpiC cells at P4 (n=3). Scale bar represents 125 µm (control and IL-6R) and 80 µm (TNF receptor 1).

3.10 Expression of transporters/channels and cytokine receptors by hCPEpiC by flow cytometry

The expression of hCPEpiC transporter/channels and cytokine receptors by immunocytochemistry was confirmed with flow cytometry analysis as shown in Figures 3.50-3.51.

(a) Na^+-K^+-ATPase

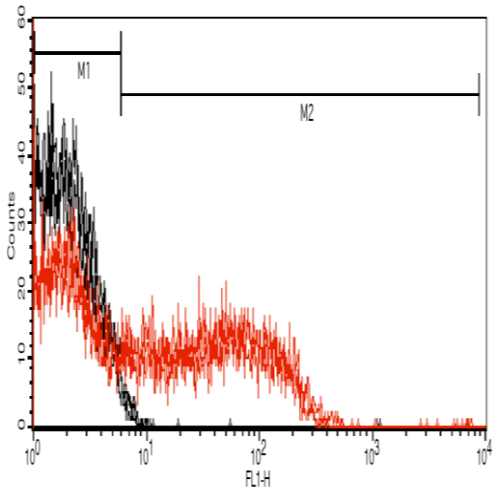

(b) NKCC1

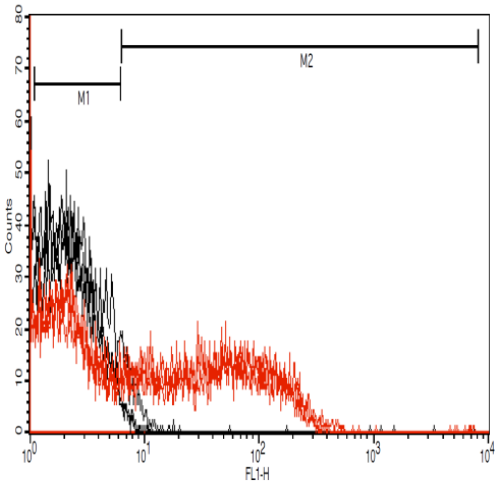

(c) Aquaporin-1

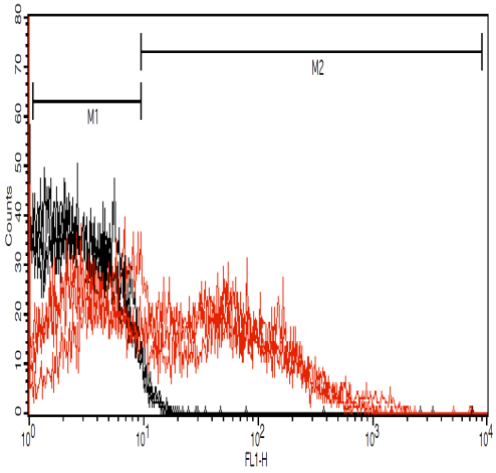

(d) ENaC

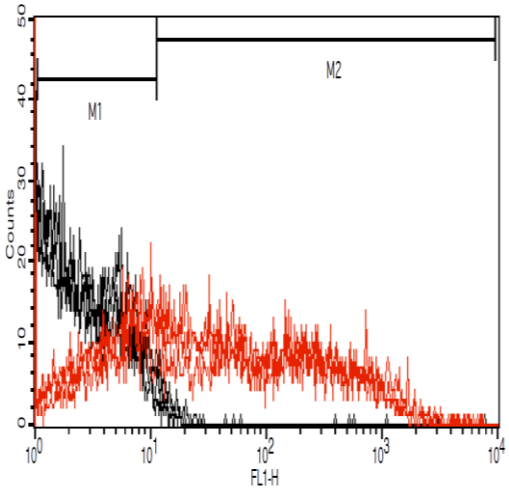

Figure 3.20: The expression of Na^+-K^+-ATPase, NKCC1, Aquaporin-1, and ENaC transporters on hCPEpiC by flow cytometry. Fully confluent hCPEpiC (P3) were fixed in 2% PAF and stained with antibodies for (a) Na^+-K^+-ATPase rabbit polyclonal IgG, (b) NKCC1 rabbit polyclonal IgG, (c) Aquaporin-1 rabbit polyclonal IgG, or (d) ENaC rabbit polyclonal IgG (red) against the control (no primary Ab) (black) and analysed via flow cytometry. Data represents the mean ±SEM, n = 12-13 with duplicate samples. ***P*<0.01 using Paired t test.

,

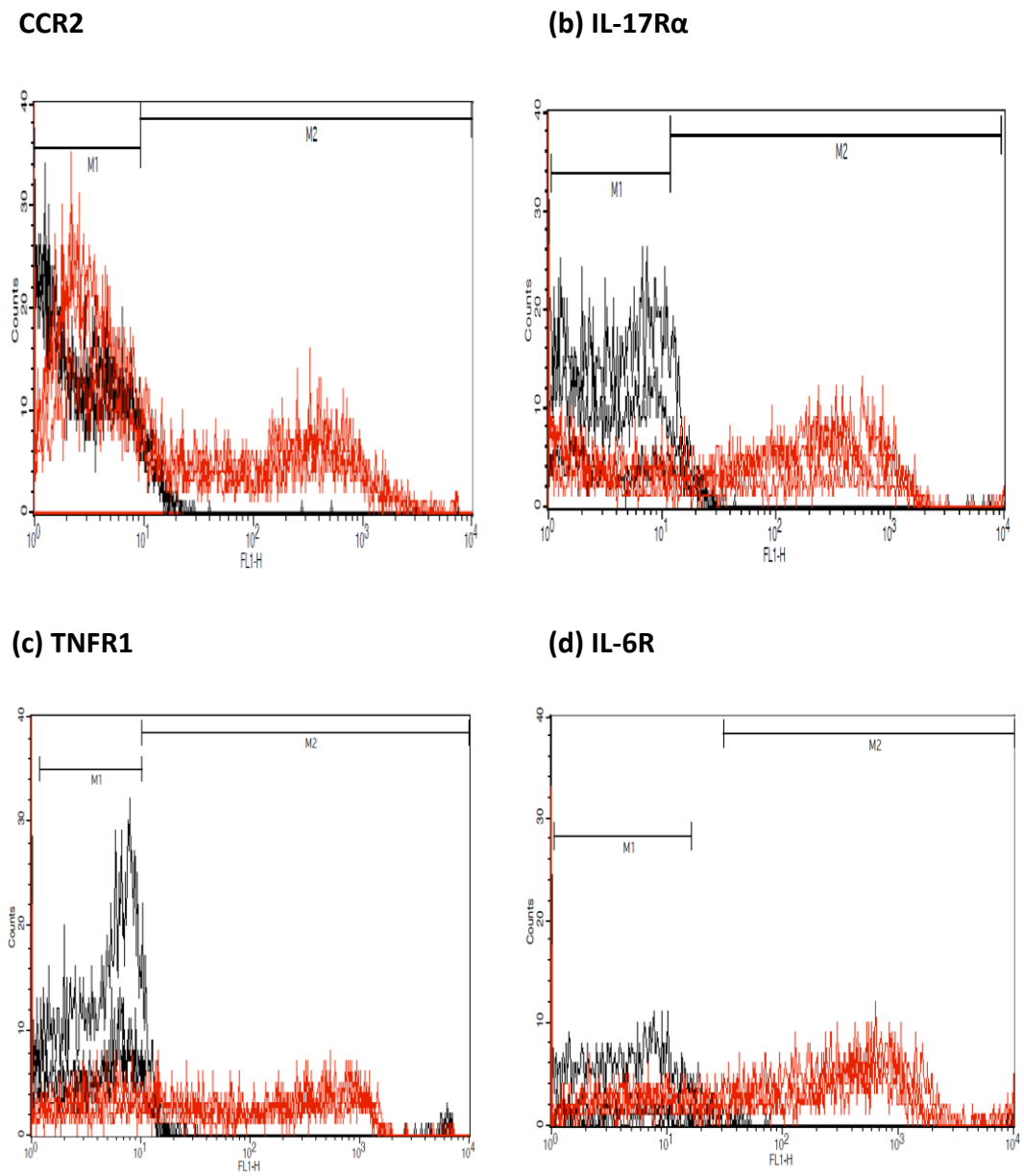

Figure 3.21: The expression of TNF-R1, IL-6R, IL-17Rα and CCR2 receptors on hCPEpiC by flow cytometry. Fully confluent hCPEpiC (P3) were fixed in 2% PAF and stained with antibodies for (a) TNF-R1 rabbit polyclonal IgG, (b) IL-6R rabbit polyclonal IgG, (c) IL-17Rα rabbit polyclonal IgG, or (d) CCR2 rabbit polyclonal IgG (red) against the control (no primary Ab) (black) and analysed via flow cytometry. Data represents the mean ±SEM, n = 12-13 with duplicate samples. ***P*<0.01 using Paired t test.

3.11 Modulation of transporters/channels by cytokines in hCPEpiC

Further FACS analysis on increases/decreases in transporter/channel expression following 24h incubation with either HC, TNF-α, IL-6 or IL-17 on hCPEpiC is shown in Fig. 3.52-3.55. The results show evidence that the three main cytokines that were found to either modulate CSF secretion rates in both male and female rats *in vivo* (TNF-α, HC, IL-6, Fig. 3.2, 3.18, 3.20), as well as IL-17 which was initially found to increase the resistance to CSF drainage (Fig. 3.5, 3.29), have no effect *in vitro* on the expression of the transporters and channels, involved in the movement of ions into the CSF (Fig. 1.10 and 1.11 of Introduction Section 1.4).

3.11.1 Na^+-K^+-ATPase

(a) Na^+-K^+-ATPase with TNF-α

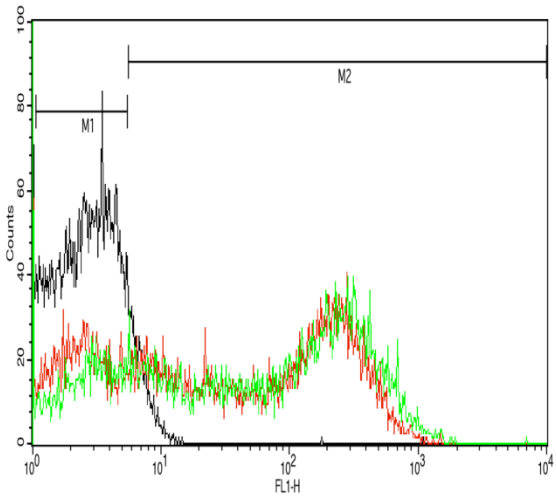

(b) Na^+-K^+-ATPase with IL-17

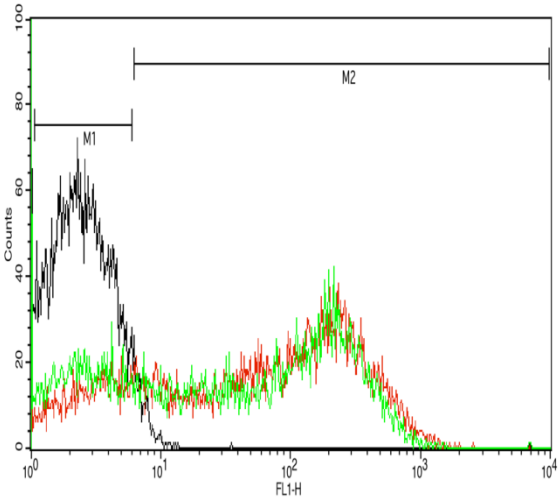

(c) Na^+-K^+-ATPase with IL-6

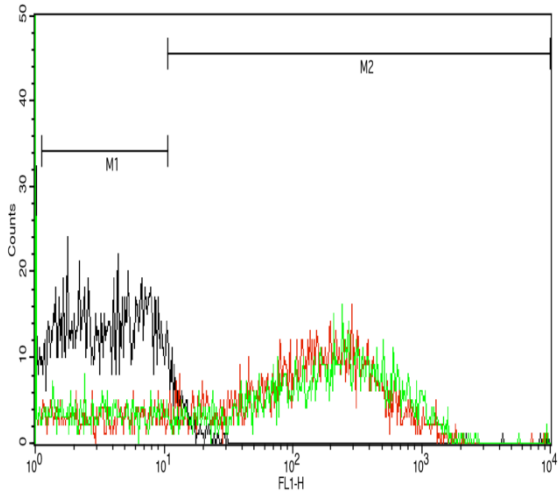

(d) Na^+-K^+-ATPase with HC

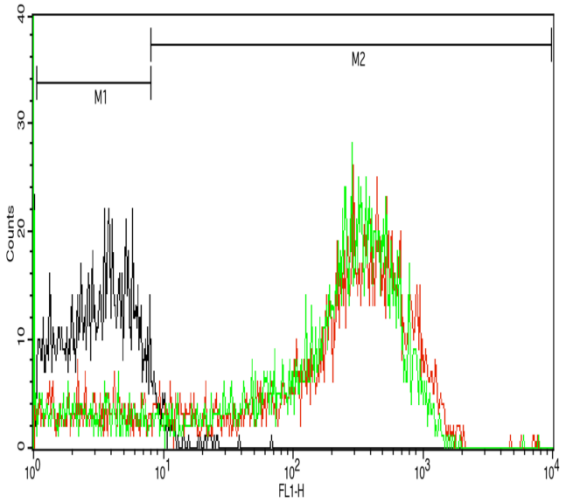

Compound	% Difference Median Fluorescence against Transporter Control	SEM Median Fluorescence of Treated cells
TNF- α	-5.7	3.70
IL-17	-6.4	124.43
IL-6	-2.1	43.56
HC	+5.1	50.52

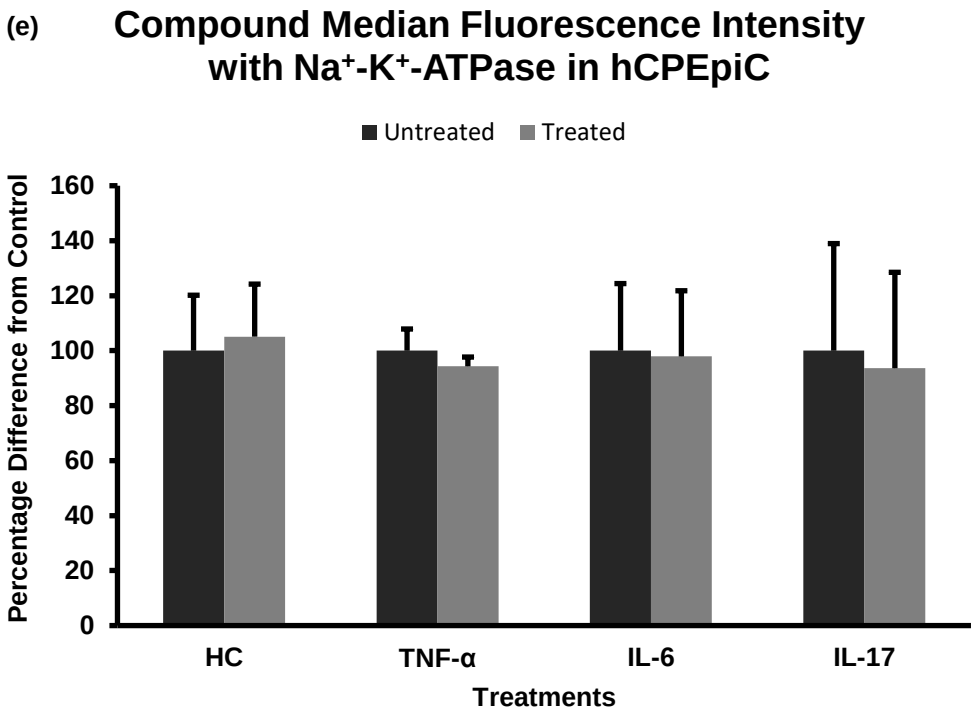

Figure 3.22: The expression of Na^+-K^+-ATPase with TNF-α, IL-17, IL-6 cytokines and glucocorticoid HC on hCPEpiC by flow cytometry. Fully confluent hCPEpiC (P3) were treated with the (a) TNF-α (0.1 ng/ml), (b) IL-17 (0.1 ng/ml), (c) IL-6 (0.1 ng/ml) and (d) HC (500 ng/ml) 24h prior to fixing in 2% PAF and stained with antibodies for Na^+-K^+-ATPase rabbit polyclonal IgG (red) (treated) against the control (no primary Ab) (black) and transporter control Na^+-K^+-ATPase rabbit polyclonal IgG alone (green) (untreated), including table of median fluorescence, before being analysed via flow cytometry. (e) Bar chart to show the median fluorescence intensity of the Na^+-K^+-ATPase transporter with the compound of interest (treated) against untreated control. Data represents the mean ±SEM, n=3 with duplicate samples. A two-way ANOVA was used to analyse the statistical significance. No significant results were shown following Sidak's multiple comparison test between treatments against their corresponding control.

3.11.2 NKCC1

(a) NKCC1 with TNF-α

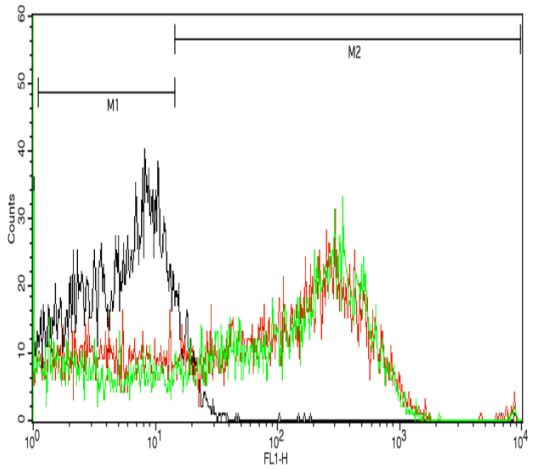

(b) NKCC1 with IL-17

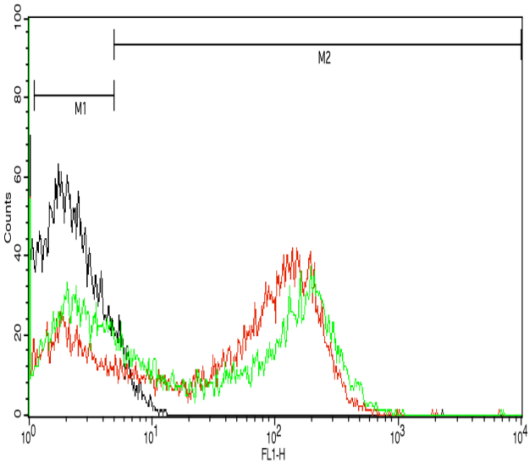

(c) NKCC1 with IL-6

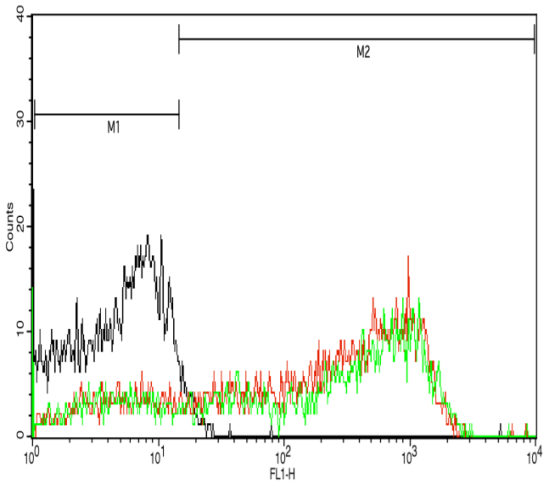

(d) NKCC1 with HC

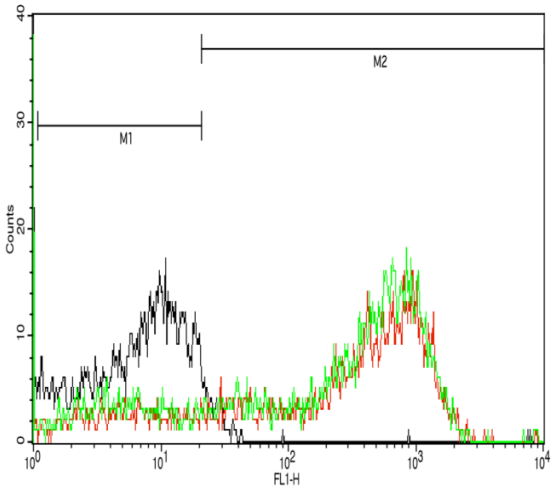

Compound	% Difference Median Fluorescence against Transporter Control	SEM Median Fluorescence of Treated cells
TNF- α	+9.0	109.51
IL-17	-7.7	98.81
IL-6	+12.7	68.44
HC	-13.5	38.30

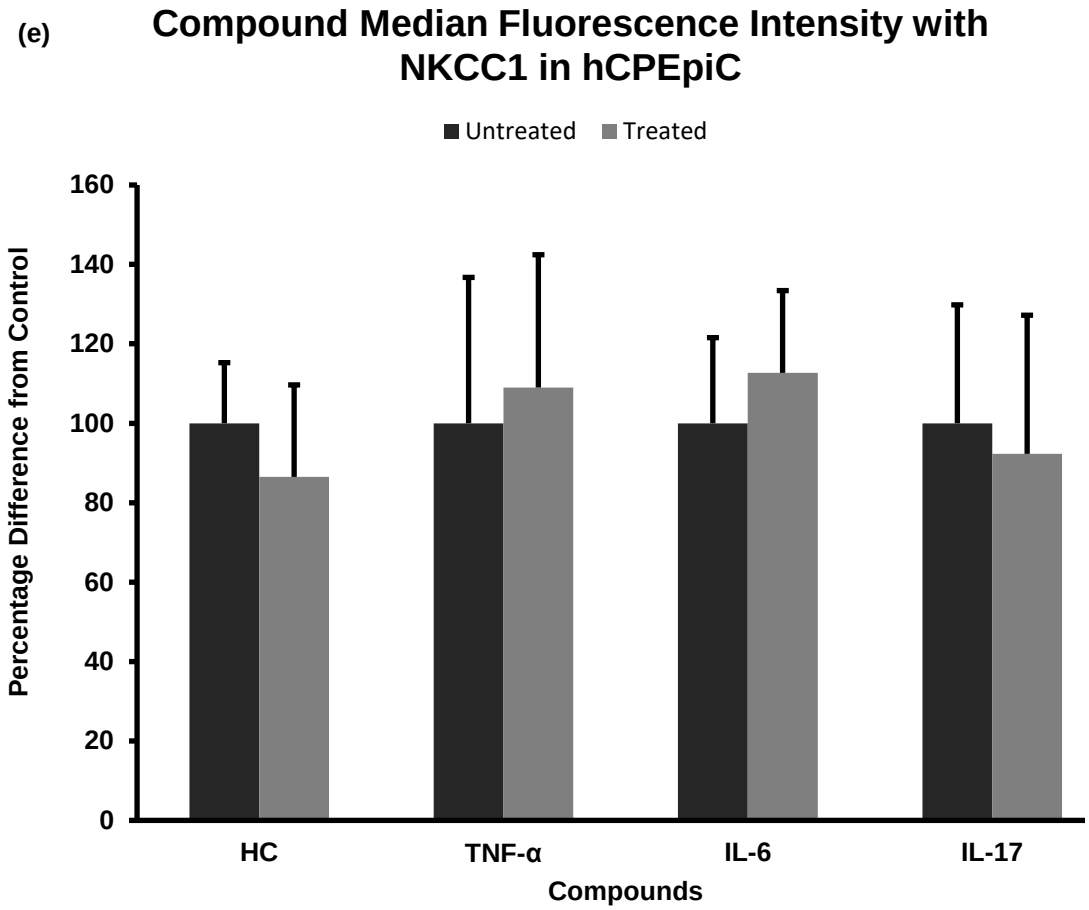

Figure 3.23: The expression of NKCC1 with TNF-α, IL-17, IL-6 cytokines and glucocorticoid HC on hCPEpiC by flow cytometry. Fully confluent hCPEpiC (P3-4) were treated with the (a) TNF-α (0.1 ng/ml), (b) IL-17 (0.1 ng/ml), (c) IL-6 (0.1 ng/ml) and HC (500 ng/ml) 24h prior to fixing in 2% PAF and stained with antibodies for NKCC1 rabbit polyclonal IgG (red) (treated) against the control (no primary Ab) (black) and transporter control NKCC1 rabbit polyclonal IgG alone (green) (untreated), including table of median fluorescence, before being analysed via flow cytometry. (e) Bar chart to show the median fluorescence intensity of the NKCC1 transporter with the compound of interest (treated) against untreated control. Data represents the mean ±SEM, n=3 with duplicate samples. A two-way ANOVA was used to analyse the statistical significance. No significant results were shown following Sidak's multiple comparison test between treatments against their corresponding control.

3.11.3 Aquaporin-1

(a) Aquaporin-1 with TNF-α

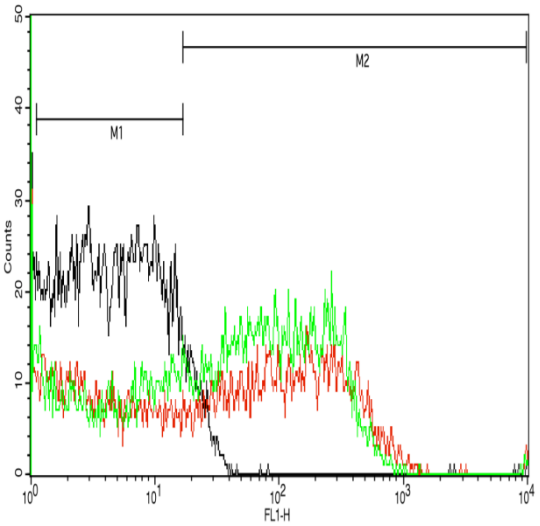

(b) Aquaporin-1 with IL-17

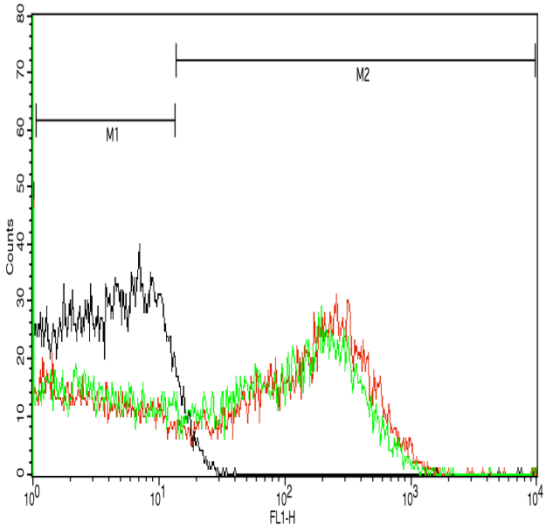

(c) Aquaporin-1 with IL-6

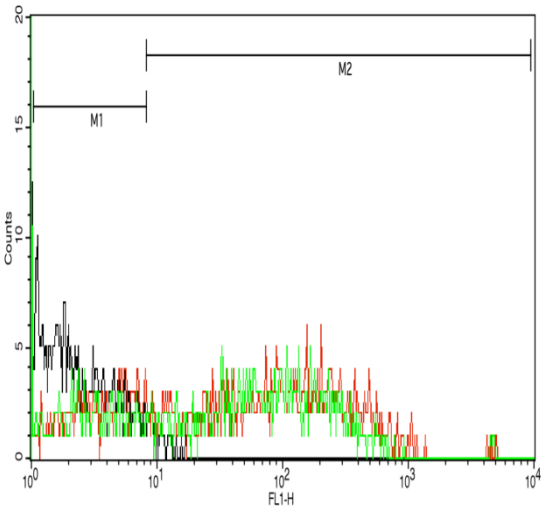

(d) Aquaporin-1 with HC

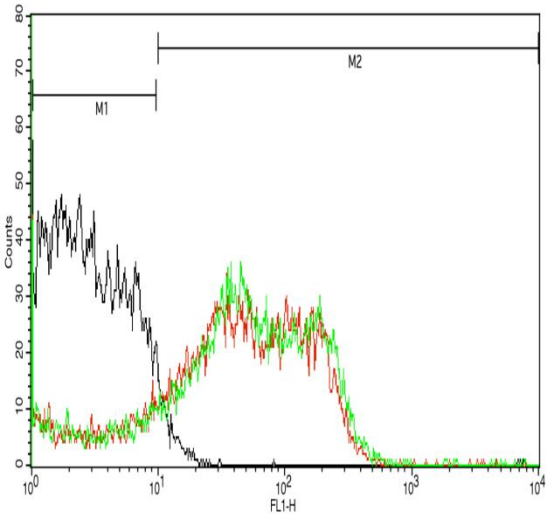

Compound	% Difference Median Fluorescence against Transporter Control	SEM Median Fluorescence of Treated cells
TNF- α	+33.0	29.06
IL-17	-29.0	38.60
IL-6	+7.8	2.03
HC	-29.0	20.56

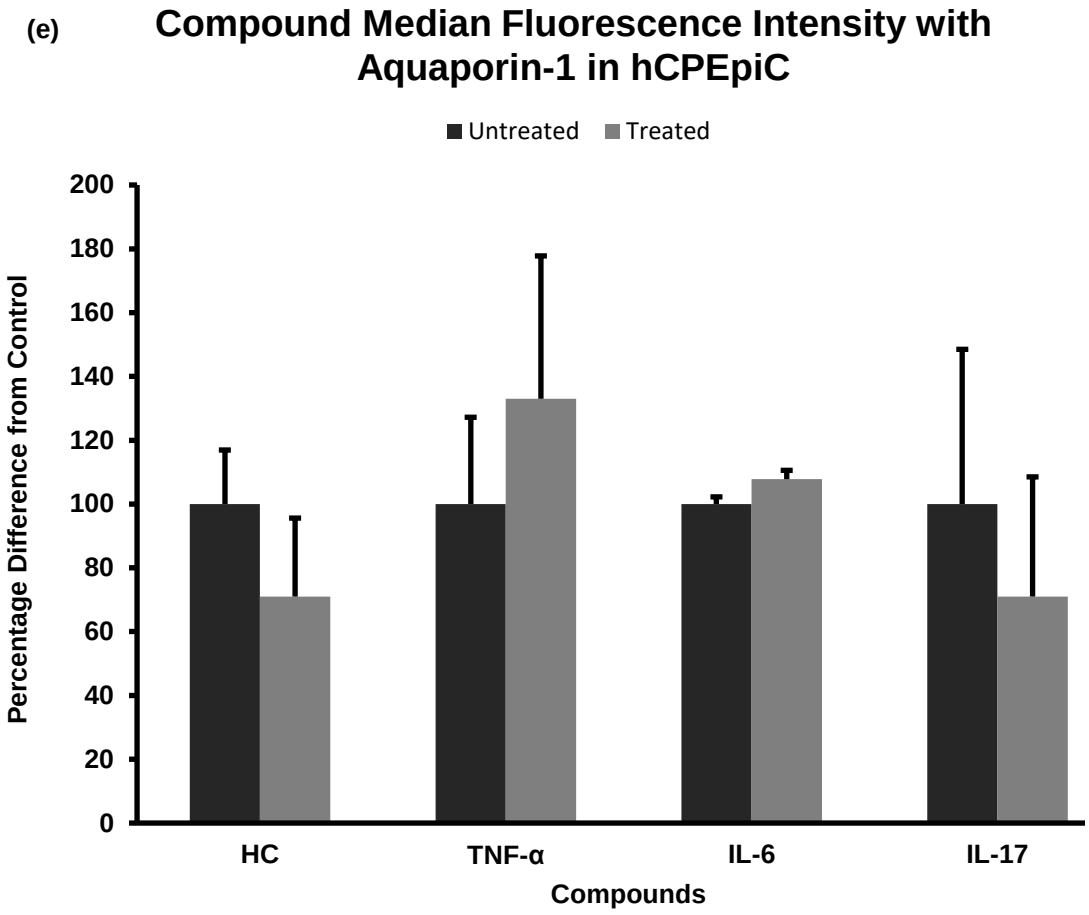

Figure 3.24: The expression of Aquaporin-1 with TNF-α, IL-17, IL-6 cytokines and glucocorticoid HC on hCPEpiC by flow cytometry. Fully confluent hCPEpiC (P4) were treated with the (a) TNF-α (0.1 ng/ml), (b) IL-17 (0.1 ng/ml), (c) IL-6 (0.1 ng/ml) and HC (500 ng/ml) 24h prior to fixing in 2% PAF and stained with antibodies for Aquaporin-1 rabbit polyclonal IgG (red) (treated) against the control (no primary Ab) (black) and transporter control Aquaporin-1 rabbit polyclonal IgG alone (green) (untreated), including table of median fluorescence, before being analysed via flow cytometry. (e) Bar chart to show the median fluorescence intensity of the aquaporin-1 water channel with the compound of interest (treated) against untreated control. Data represents the mean ±SEM, n=3-4 with duplicate samples. A two-way ANOVA was used to analyse the statistical significance. No significant results were shown following Sidak's multiple comparison test between treatments against their corresponding control.

3.11.4 ENaC

(a) ENaC with TNF-α

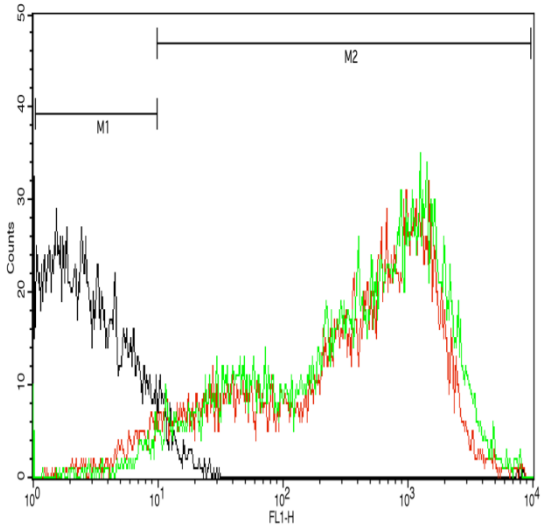

(b) ENaC with IL-17

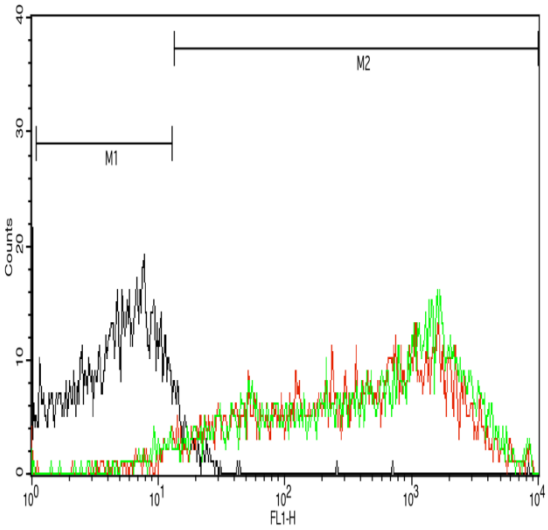

(c) ENaC with IL-6

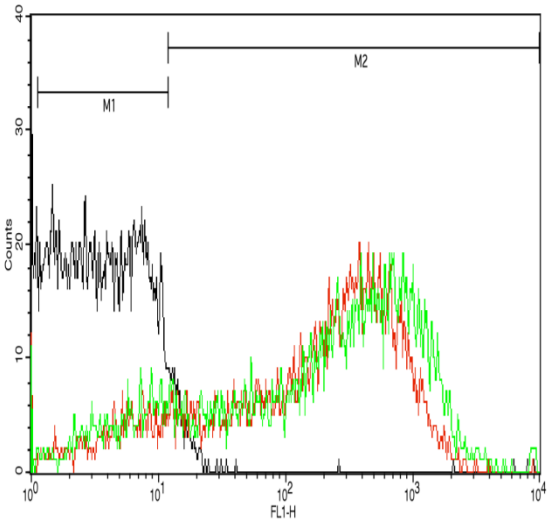

(d) ENaC with HC

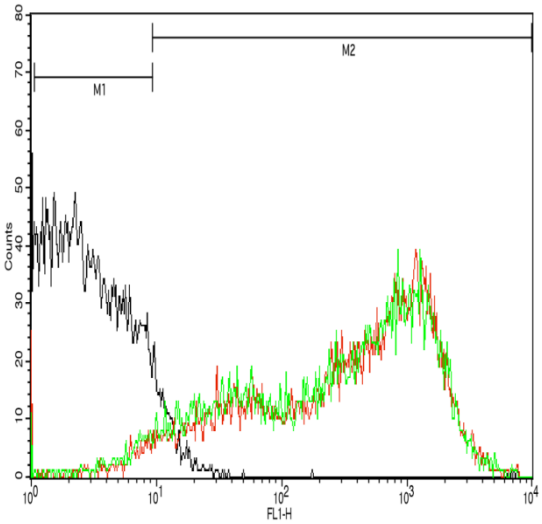

Compound	% Difference Median Fluorescence against Transporter Control	SEM Median Fluorescence of Treated cells
TNF- α	-2.3	97.14
IL-17	-0.2	111.26
IL-6	-18.1	83.60
HC	-0.4	105.55

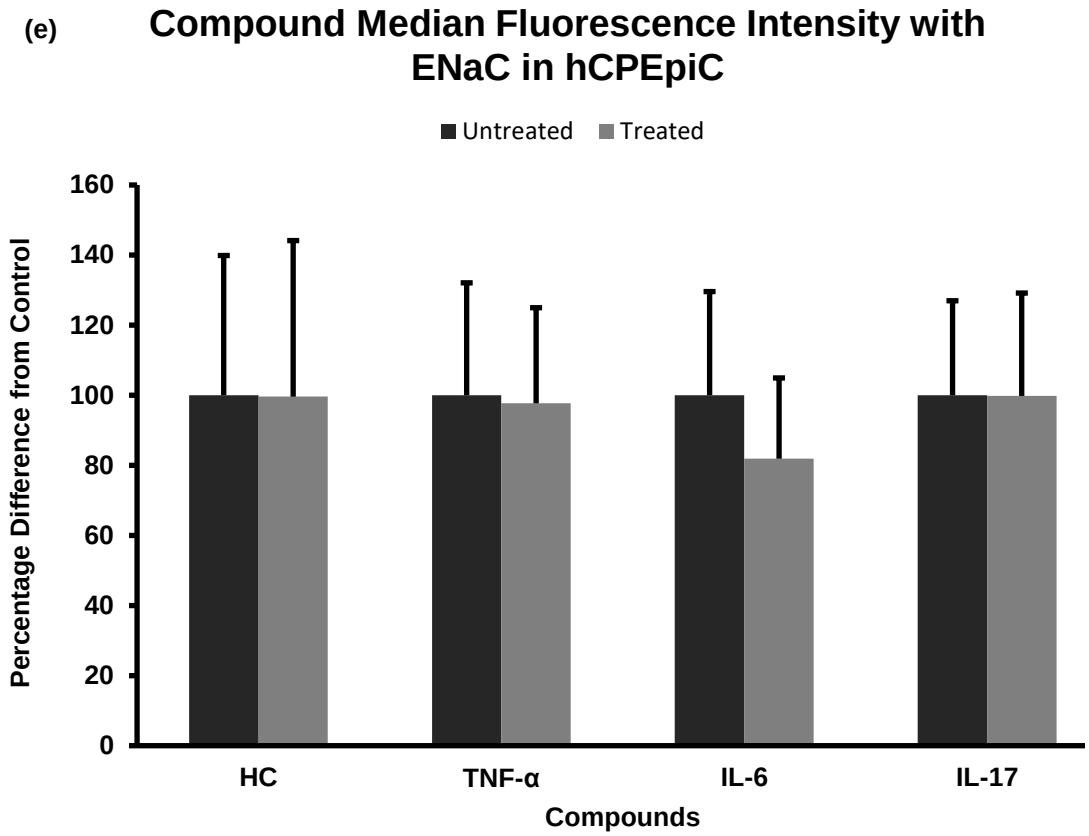

Figure 3.25: The expression of ENaC with TNF-α, IL-17, IL-6 cytokines and glucocorticoid HC on hCPEpiC by flow cytometry. Fully confluent hCPEpiC (P3-5) were treated with the (a) TNF-α (0.1 ng/ml), (b) IL-17 (0.1 ng/ml), (c) IL-6 (0.1 ng/ml) and HC (500 ng/ml) 24h prior to fixing in 2% PAF and stained with antibodies for ENaC rabbit polyclonal IgG (red) (treated) against the control (no primary Ab) (black) and transporter control Aquaporin-1 rabbit polyclonal IgG alone (green) (untreated), including table of median fluorescence, before being analysed via flow cytometry. (e) Bar chart to show the median fluorescence intensity of the aquaporin-1 water channel with the compound of interest (treated) against untreated control. Data represents the mean ±SEM, n=3-4 with duplicate samples. A two-way ANOVA was used to analyse the statistical significance. No significant results were shown following Sidak's multiple comparison test between treatments against their corresponding control.

The lack of an effect in all transporter expression (Na^+-K^+-ATPase, NKCC1, Aquaporin-1, ENaC) may be a consequence of the *in vitro* time-frame of 24h for the treatment being too short for an effect to occur. However, the time-frame may also have been too long as, *in vivo*, the rats were exposed to the cytokines for a 90 min period and an effect in both CSF secretion rates and resistance to

CSF drainage had occurred. Allowing for a 24h exposure, *in vitro*, may have been too long and resulted in the increased expression of transporters peaking at an earlier time-point.

In addition, the pathways used by these cytokines in affecting the CSF secretion/drainage rates may not occur through increased transporter expression but through a different molecular pathway. It is also important to note the species differences, between the *in vitro* human choroid plexus cells and the Wistar rats used *in vivo*, may have also caused the difference in the significance of the experimental results.

3.12 Blood cerebrospinal fluid barrier (BCSFB) enriched transcripts in hCPEpiC

It is important to identify barrier-specific gene expression within the BCSFB in order to understand the physiological properties that are involved in CSF secretion. Recently, Marques and co-workers performed a transcriptome gene analysis of choroid plexus (CP) tissue from normal adult mice (Marques et al. 2011). They compared their CP (BCSFB-enriched) transcripts with the control group transcripts of CP expression (obtained from the GEO database) in B10.pl WT mice (GSE11443) and the gene expression profile of the mouse 4th ventricle CP (GSE3594) (Marques et al. 2011).

In order to identify the genes expressed by the BCSFB in hCPEpiC, a human mRNA microarray analysis using HumanHT-12 v4 Expression BeadChip array which included 19,355 probe set sequences for 14,413 coding transcripts was

performed by Cambridge Genomic Services. Under normal conditions, it was found that 32% (4,613) of genes analysed were expressed in hCPEpiC. To confirm the BCSFB-gene transcripts expressed by hCPEpiC, I compared them with the mouse CP transcripts identified by Marques as BCSFB-enriched, and then identified their biological functions using bioinformatic analysis. Of the positively associated hCPEpiC transcripts, 42% (1,982) were found to be in common with the mouse CP-enriched transcripts. Of the 59 most expressed genes from the mouse CP, 54% (32) were found to be in common with the positively associated hCPEpiC transcripts and are listed in Table 6.4 in Appendix Section 6.10, page 293.

Statistical significance of biological pathways associated with the BCSFB-enriched transcripts expressed by hCPEpiC was confirmed using KEGG/GO for biological processes including: positive regulation of biological process ($P \leq 0.01$), transport ($P \leq 0.01$), response to organic substance ($P \leq 0.05$) (visualised using ClueGo software) (Fig. 3.56). Other minor pathways shown include structure (protein localization, cellular component assembly) and signalling (cellular response to chemical stimulus, regulation of signal transduction, and response to nitrogen compound). The structure of the BCSFB is important for CSF secretion in terms of the organisation and localisation of the tight junctions. However, membrane organization was not found to be as significant as other pathways, consistent with the observations from immunocytochemistry that ZO-1 and Claudin-1 were detectable in the cytosol but not at the tight junctions between the hCPEpiC.

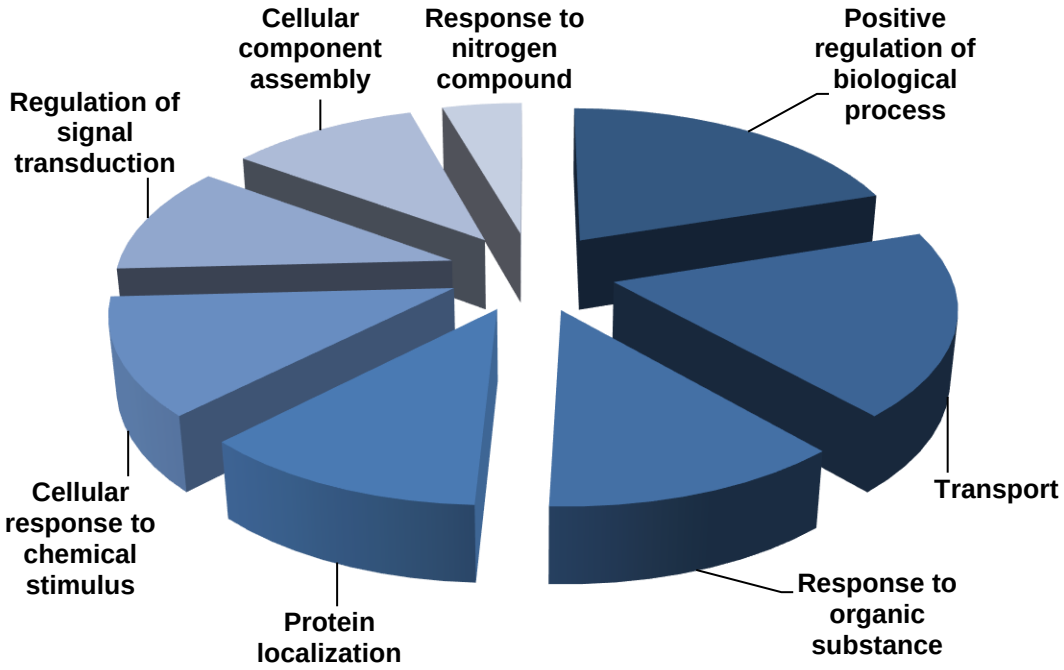

Figure 3.26: BCSFB-enriched transcripts expressed by hCPEpiC.
Transcriptome analysis in hCPEpiC was performed and ClueGo, a cytoscape plug-in was used to create a visualisation map using KEGG and GO molecular function terms (n=3).

In addition, expression of the characterised proteins, transporters/channels and cytokine receptors that was observed by immunocytochemistry and flow cytometry was confirmed (with the exception of aquaporin-1) by transcriptome analysis in hCPEpiC as shown in Table 3.2.

	Name	Symbol	Accession No.
Proteins	Prealbumin (TTR)	RBP1	NM_002899.2
	ZO-1	TJP1	NM_003257.3
	Claudin-1	CLDN1	NM_021101.3
Transporters and Channels	Na^+K^+ATPase	ATP1A1	NM_000701.6
	NKCC1	SLC12A2	NM_001046.2
	ENaC	SCNN1A	NM_001038.4
Cytokine Receptors	TNF-R1	TNFRSF1A	NM_001065.2
	IL6R	IL6R	NM_000565.2
	IL-17Rα	IL17RA	NM_014339.4
	CCR2	CCR2	NM_000647.4

Table 3.1: Choroid plexus epithelial proteins, transporters/channels and cytokine receptor genes expressed in hCPEpiC.

Identifying BCSFB-enriched genes expressed by hCPEpiC following mRNA regulation by cytokines in cultured hCPEpiC was also performed. Table 6.5 and 6.6 in the Appendix (page 298, 299) list the genes with, respectively, the greatest increase and greatest decrease in modulation following 24h hCPEpiC treatment with HC. Tables 6.7 and 6.8 (page 300, 301) show the same for TNF-α modulation and Tables 6.9 and 6.10 (page 305) for IL-6 modulation. Fifteen genes transcripts with the greatest modulated expression (although not statistically significant) between all three treatment groups are shown in Tables 3.3 and 3.4 and depicted by a Venn diagram in Fig. 3.57.

Greatest increase in expression between HC, TNF-α and IL-6			
Symbol	**Accession no.**	**LogFC**	**adj.P.Val**
TROVE2	NM_001042369.1	1.739270885	0.940691294
LOC650132	XM_939218.1	1.253837704	0.940691294
NCDN	NM_014284.2	1.22796179	0.940691294
UPLP	NM_001114403.1	1.145920732	0.940691294

Table 3.2: Genes with the greatest increase in expression between HC, TNF-α and IL-6 following transcriptome analysis on hCPEpiC.

Greatest decrease in expression between HC, TNF-α and IL-6			
Symbol	**Accession no.**	**LogFC**	**adj.P.Val**
LOC201229	XM_942296.1	-1.618517107	0.940691294
ZNF146	NM_001099639.1	-1.406134901	0.940691294
THRA	NM_003250.4	-1.31102174	0.940691294
TEAD4	NM_201443.1	-1.278201128	0.940691294
VPS37C	NM_017966.4	-1.277421609	0.940691294
ZC3H5	XM_940903.2	-1.260756522	0.940691294
INF2	NM_001031714.3	-1.249494292	0.940691294
FLAD1	NM_025207.3	-1.151772743	0.940691294
SPAG16	NM_001025436.1	-1.11450463	0.940691294
ALDH1B1	NM_000692.3	-1.078883914	0.940691294
CCM2	NM_001029835.1	-1.050637438	0.940691294

Table 3.3: Genes with the greatest decrease in expression between HC, TNF-α and IL-6 following transcriptome analysis on hCPEpiC.

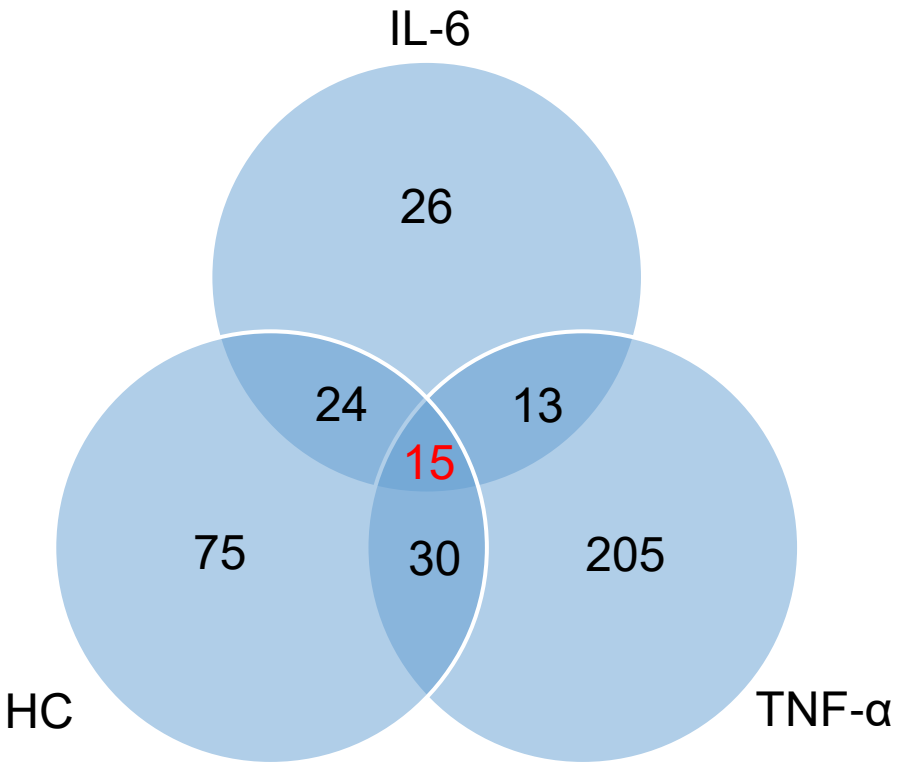

Figure 3.27: Venn diagram showing the numbers of genes up-regulated and down-regulated between each treatment group of HC, TNF-α and IL-6 following transcriptome analysis of hCPEpiC.

3.13 Validation of mRNA transcripts by RT-qPCR

The effect of 24h treatment incubation on the expression of genes on hCPEpiC; initially found to be up-regulated or down-regulated following transcriptome analysis, were not confirmed with real-time quantitative PCR (RT-qPCR) as shown in Fig. 3.58.

Four genes were selected for RT-qPCR analysis based on their upregulation/downregulation following transcriptome analysis, and further effects in possible cilia function, associated with increased CSF secretion. These included *TROVE2* (a TROVE module found in telomerase and Ro and Vault proteins) and neurochondrin (*NCDN*), a negative regulator of Ca/calmodulin-

dependent protein kinase II phosphorylation, which showed an up-regulation; and *SPAG16* (a sperm associated antigen) and cerebral cavernous malformation 2 (*CCM2*) a scaffold protein that functions in the stress-activated p38 Mitogen-activated protein kinase (MAPK) signalling cascade, which displayed a down-regulation in gene expression on hCPEpiC, respectively (Tables 3.3 and 3.4).

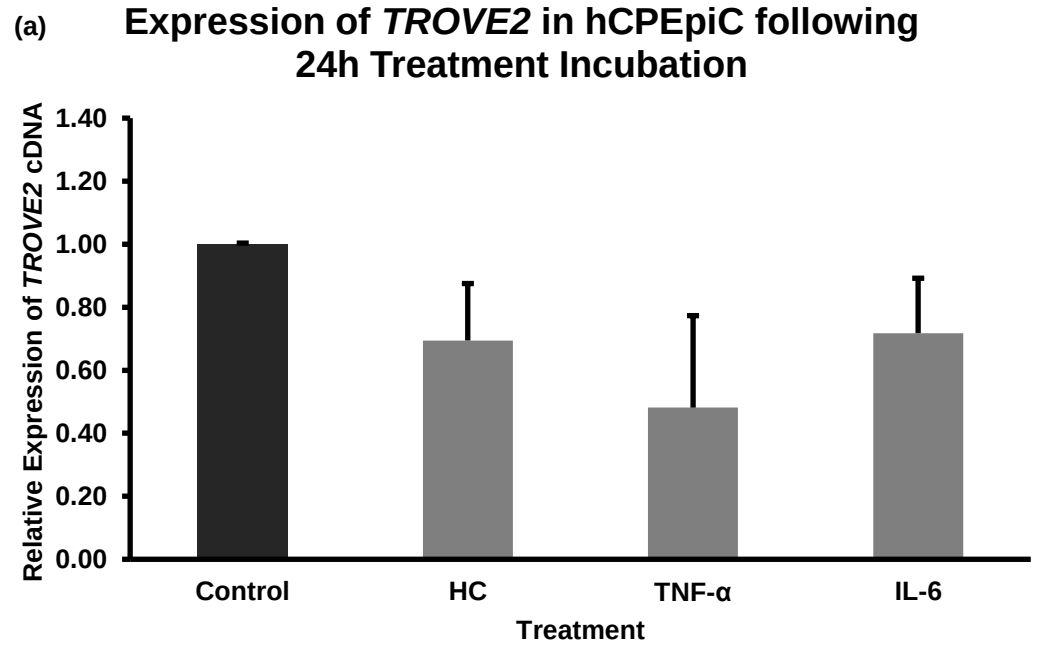

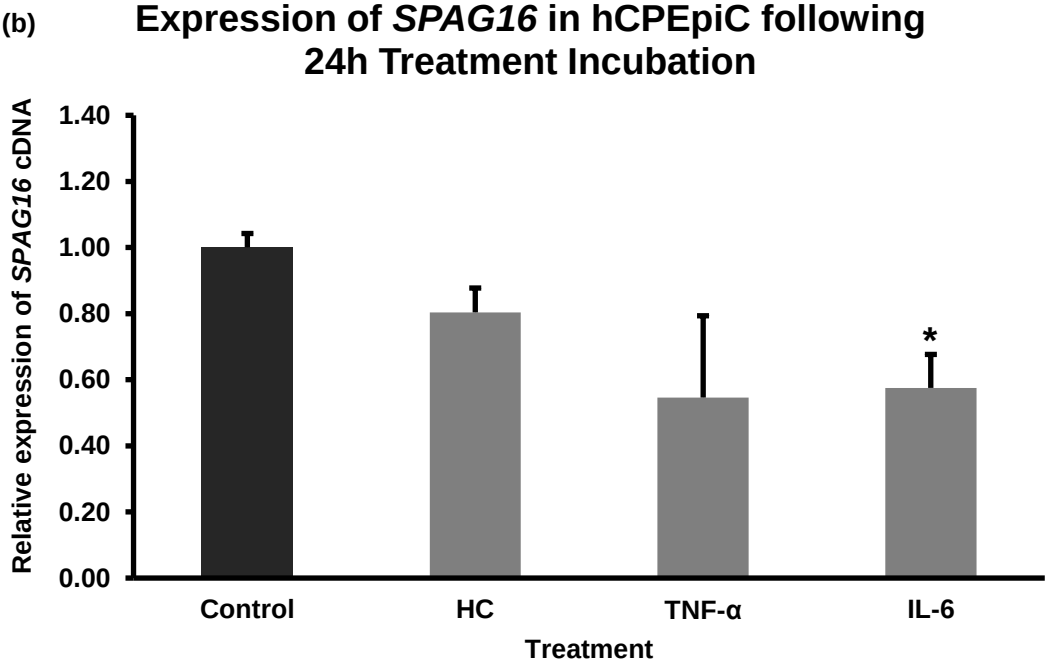

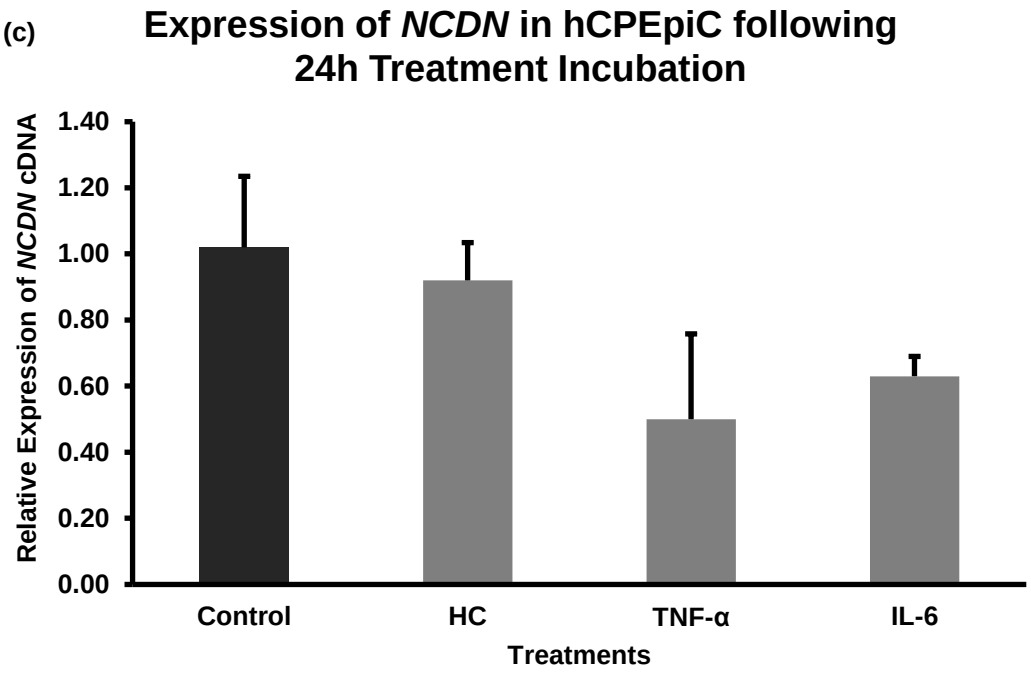

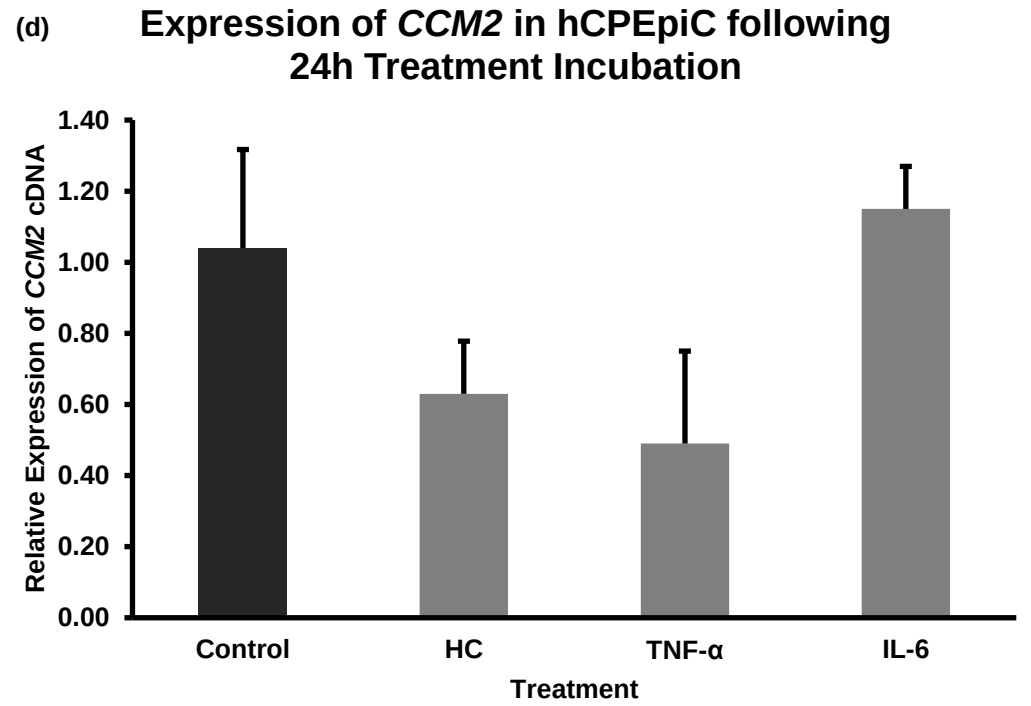

Figure 3.28: The effects of HC, TNF-α, and IL-6 on the mRNA levels of *TROVE2*, *SPAG16*, *NCDN*, and *CCM2* following 24h incubation in hCPEpiC.
Fully confluent hCPEpiC were incubated with HC (500 ng/ml), TNF-α (0.1 ng/ml) and IL-6 (0.1 ng/ml) for 24h and the mRNA levels of (a) *TROVE2*, (b) *SPAG16*, (c) *NCDN*, and (d) *CCM2* were calculated using RT-qPCR. Data represents mean ± SEM. n=3 experiments with duplicate samples. A one-way ANOVA was used to analyse the statistical significance. The significant results are shown following an unpaired t test with Welch-correction comparing comparative expression levels ($2^{-\Delta\Delta CT}$) values. *P=<0.05.

The increase in *TROVE2* expression following 24h incubation with HC and TNF-α may possibly highlight a role of the *TROVE2* gene in increasing the number of cilia in choroid plexus cells. Studies have shown *TROVE2* may play a role in cilia formation and/or maintenance following *TROVE2* knockdown in both murine 3T3 fibroblast cell line and intermedullary collecting duct (IMCD3) cells (Lai et al. 2011). Increasing cilia numbers may be a potential mechanism by which CSF secretion might be increased in patients with IIH.

However, the RT-qPCR results indicated no significant changes of gene expression with most treatments. Nevertheless, there was a downregulation of *SPAG16* following IL-6 treatment (0.58 ±0.10 relative cDNA expression) over controls (1.00 ±0.04 relative cDNA expression), which did also match the results found in the transcriptome data.

4 Discussion

Idiopathic intracranial hypertension (IIH) is a neurological disorder characterized by raised cerebrospinal fluid (CSF) and intracranial pressure (ICP) with the greatest rate of incidence affecting obese women between the ages of 15 and 45. During this study, female Wistar rats on a HF diet were shown to have the highest CSF secretion and lowest CSF drainage levels under control conditions. In addition, cytokines whose expression has been found to be elevated in the CSF of IIH patients have also been found to modulate both CSF secretion and CSF drainage, which therefore may also contribute to the raised ICP observed in IIH patients, as summarised in Table 4.1, 4.2.

CSF Secretion Rates				
	Male		Female	
	ND	HF	ND	HF
HC	↑	↑	↑↑	↑
TNF-α	↑	↑	↑↑	↑
IL-6	↓	n/s	n/s	n/s
CCL2	n/s	n/s	n/s	n/s
IL-17	n/s	n/s	n/s	n/s

Table 4.1: A summary of the differences observed in CSF secretion rates between male and female rats on either a normal (ND) or high-fat (HF) diet following treatment with either HC, TNF-α, IL-6, CCL2 or IL-17 against their corresponding untreated control animals of the same sex and diet.
Increase in CSF secretion rate (red arrow); decrease in CSF secretion rate (blue arrow); not significant (n/s). Significant increase in CSF secretion rate indicated by a single red arrow ($P \leq 0.05$); double red arrow ($P \leq 0.01$); decrease indicated by single blue arrow ($P \leq 0.05$), over corresponding controls.

Resistance to CSF Drainage				
	Male		Female	
	ND	HF	ND	HF
HC	n/s	n/s	↓ ↓	n/s
TNF-α	↓ ↓	n/s	↓ ↓ ↓	n/s
IL-6	n/s	↑	n/s	n/s
CCL2	n/s	↓ ↓	↑ ↑ ↑	↑ ↑ ↑
IL-17	n/s	n/s	n/s	↑ ↑

Table 4.2: A summary of the differences observed in resistance to CSF drainage between male and female rats on either a normal (ND) or high-fat (HF) diet following treatment with either HC, TNF-α, IL-6, CCL2 or IL-17.

Increase in resistance CSF drainage (red arrow); decrease in resistance CSF drainage (blue arrow); not significant (n/s). Significant increase in resistance to CSF drainage indicated by single red arrow ($P \leq 0.05$); double red arrow ($P \leq 0.01$); triple red arrow ($P \leq 0.001$); decrease indicated by double blue arrow ($P \leq 0.01$); triple blue arrow ($P \leq 0.001$) over corresponding controls.

Increased CSF secretion was observed in rats of both sexes and diets following TNF-α or glucocorticoid hydrocortisone (HC) treatment, however the greatest increase was seen with female rats raised on a HF diet (Table 4.1). In addition, female rats on a HF diet, treated with CCL2 or IL-17, displayed an increase in resistance to CSF drainage when compared to untreated controls (indicating lower levels of CSF drainage) (Table 4.2). Both CSF secretion and resistance to CSF drainage pathways, whether separately or in combination, may contribute to the raised ICP observed in IIH patients as described in Figure 4.1.

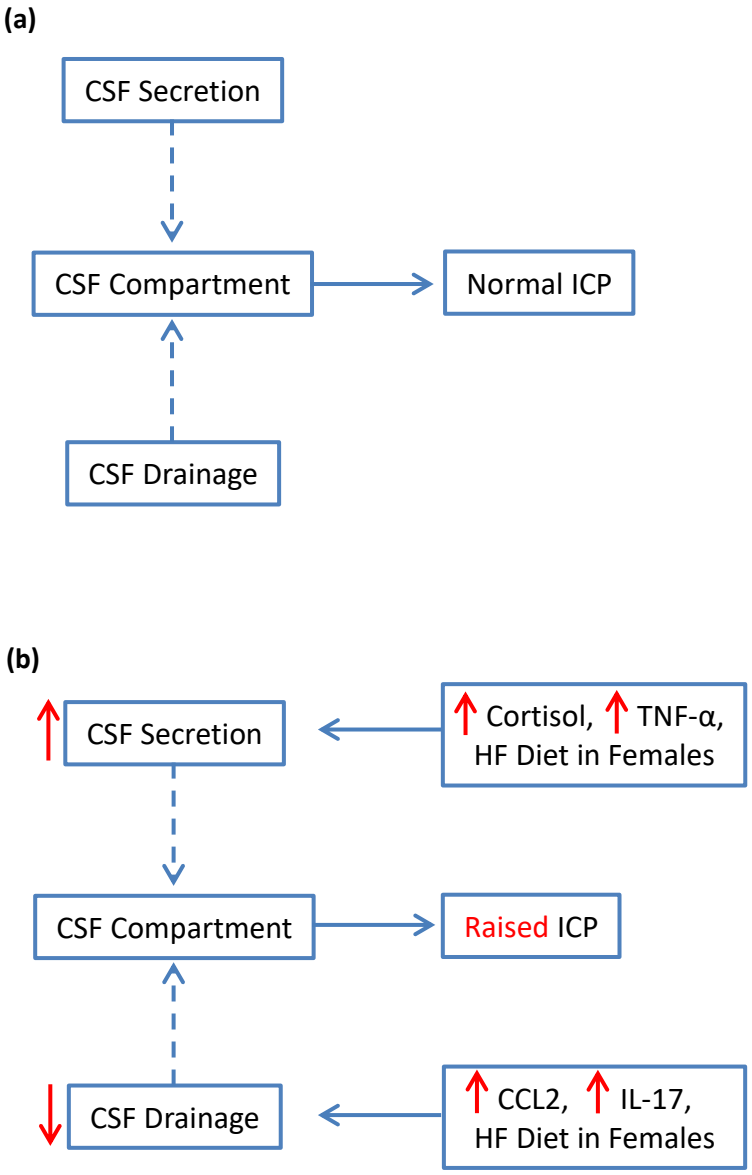

Figure 4.1: Possible mechanisms contributing to increased intracranial pressure in IIH. (a) In healthy individuals a balance between CSF secretion and drainage results in normal intracranial pressure. (b) In IIH, factors that increase CSF secretion and/or decrease CSF drainage may lead to increased intracranial pressure. Factors identified in this study are shown in (b). ICP, intracranial pressure.

4.1 Role of cytokines in CSF secretion

IIH is a result of raised ICP, possibly due to increased CSF secretion, decreased drainage, or a combination of both. During an initial investigation, TNF-α, a cytokine found to be elevated in the CSF of IIH patients, as well as HC were found to stimulate CSF secretion rates *in vivo*. In contrast, IL-6, which was also elevated in the CSF of IIH patients, caused a decrease in CSF secretion rates. There was no modulation of CSF secretion seen with leptin, IL-1β, CCL2 or IL-17 (cytokines also found to be elevated in the CSF of IIH patients) (see Introduction Section 1.10, Table 1.2). However, CCL2 and IL-17, cytokines which did not cause an increase in CSF secretion rates, were the only cytokines found to increase initial CSF volumes *in vivo* as discussed further in Section 4.2. Figure 4.2 shows a summary of the putative pathways induced by these cytokines mediating CSF secretion rates.

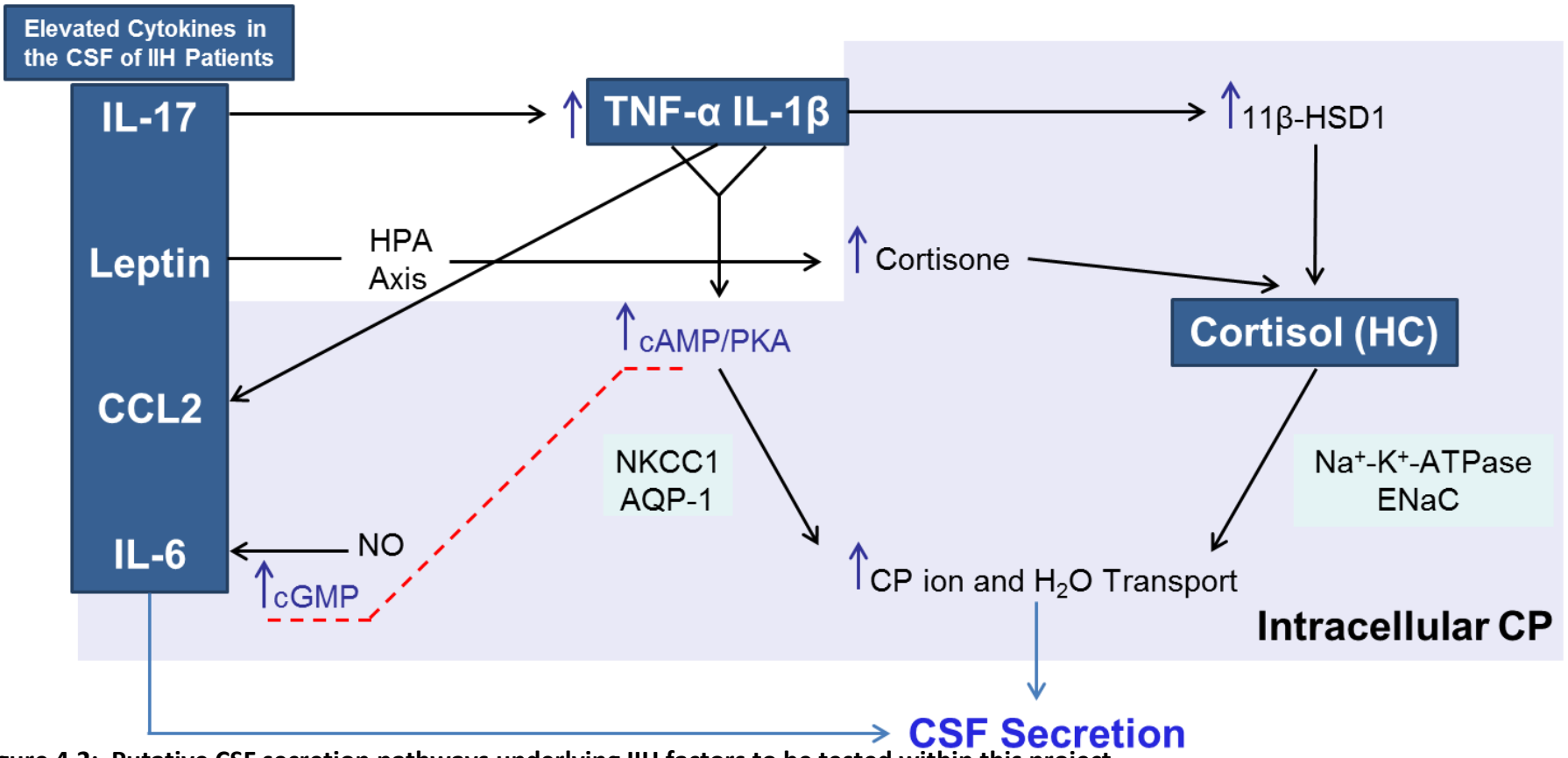

Figure 4.2: Putative CSF secretion pathways underlying IIH factors to be tested within this project.

IL-17 triggers the release TNF-α and IL-1β from macrophages and produces 11β-HSD1 enzyme, which activates the intracellular conversion of cortisone into cortisol. Cortisol binds to glucocorticoid receptors which activates serum glucocorticoid kinase (sgk-1) pathways, increasing Na^+ movement across the choroid plexus (CP) epithelium. Leptin activates the hypothalmo-pituitary-adrenal (HPA) axis. The adrenal cortex of the axis produces cortisone through stimulation of adrenocorticotropic hormone (ACTH). TNF-α and IL-1β activate protein kinase A (PKA) pathways and increase intracellular cAMP, which causes a conformational change in the NKCC1 transporter driving the movement of ions into the CSF. Nitric oxide (NO) stimulates an increase in IL-6 in peripheral blood mononuclear cells (PBMCs) which increases intracellular cGMP. cGMP reverses the movement of ions across epithelia which is the opposite to cAMP. This would indicate that IL-6 could decrease CSF secretion. TNF-α and IL-1β increase the expression of CCL2 which could also play a role in increasing CSF secretion. Dashed red arrows indicate opposite action of cAMP and cGMP on ion movement across the CP cells. Based on references cited in the Introduction.

For the *in vivo* ventriculo-cisternal perfusion experiments, it was important to determine that CSF secretion reached a steady-state before any CSF secretion rate readings were taken. Male rats that had been administered HC and TNF-α showed a lower C_{out} vs. C_{in} ratio than controls, indicating an increased CSF secretion rate, whereas rats administered IL-6 showed a greater C_{out} vs. C_{in} ratio and therefore a decrease in CSF secretion rates compared to controls. By contrast, leptin, CCL2 and IL-17 did not induce changes in C_{out} vs. C_{in} ratio compared to controls indicating no change in CSF secretion rates.

The increased CSF secretion rates associated with HC are consistent with the hypothesis that an increased activity of the 11β-HSD1 enzyme in choroid plexus epithelial cells leads to increased Na^+ transport through the ENaC channel (Sinclair et al. 2010). Indeed, HC increases the activity of the ENaC channel in retinal pigmented epithelium of New Zealand White Albino rabbits (Sinclair et al. 2010) and it is possible that a similar mechanism operates in choroid plexus epithelium. In this putative pathway, corticosterone would be converted to cortisol through NADP(H) activation of the 11β-HSD1 enzyme in choroid plexus epithelial cells. Cortisol would then bind to intracellular glucocorticoid receptors thereby activating serum glucocorticoid kinase 1 (SGK1) pathways to increase the movement of Na^+ across the cells via ENaC route, creating an osmotic gradient in order to drive water into the CSF.

The increased CSF secretion rate observed with HC is also supported by studies performed by Rauz and colleagues, who demonstrated 11β-HSD1-mediated synthesis of cortisol in the ocular ciliary epithelium in humans, the site of aqueous

humour drainage (Rauz et al. 2003) (Rauz et al. 2001). Immunohistochemical and RT-PCR studies showed the presence of 11β-HSD1 in human ocular tissues and a ciliary non-pigmented epithelial (NPE) cell-line. Intraocular pressure was measured in eight male volunteers before and after oral ingestion of carbenoxolone (CBX), a known inhibitor of 11β-HSD1. CBX-treated patients displayed the greatest decrease in intraocular pressure. The results by Rauz and colleagues suggest that the 11β-HSD1 isozyme may modulate steroid-regulated sodium transport across the NPE, thereby influencing intraocular pressure. It is thus possible that these are common mechanisms regulating fluid secretion by epithelia and this system may play a similar role in increasing ICP as regulated by CSF secretion by the choroid plexus.

In order to confirm the role of 11β-HSD1 on CSF secretion, studies should be performed *in vivo* to further establish the effects of the 11β-HSD1 enzyme on Na^+ movement. First, expression of 11β-HSD1 by choroid plexus epithelial cells could be investigated by immunohistochemistry and, second, *in vivo* knock-out of 11β-HSD1, whether general or tissue- and time-specific, could demonstrate a link between cortisol and CSF secretion rate. These experiments would allow comparison of the effects seen with HC during ventriculo-cisternal perfusion when the 11β-HSD1 enzyme is present or inhibited.

The 11β-HSD1 pathway, which may modulate CSF secretion rate, may also be induced by TNF-α. TNF-α up-regulates 11β-HSD1 enzyme through the secretion of phospholipase A2 (PLA2) in rat glomerular mesangial cells (Tomlinson et al. 2004). The joint perfusion of TNF-α and HC in the aCSF for example could be useful to

investigate whether an additive effect of these treatments could be seen on CSF secretion rates.

In addition, TNF-α may induce additional pathways to modulate CSF secretion rate, different to those induced by HC, by affecting different transporters/channels. Indeed, it has been shown that TNF-α increases swine airway submucosal gland secretion, through cyclic adenosine monophosphate (cAMP) and protein kinase A (PKA) elevation causing a conformational change on the NKCC1 transporter (Baniak et al. 2012) and increased activity of aquaporin 1 (AQP1) water channel. This could explain the increased CSF secretion effects seen with TNF-α in lean male rats.

The only other cytokine to cause a significant change in *in vivo* CSF secretion rates within our study was IL-6. The decreased CSF secretion rate observed with IL-6 treatment is consistent with reports by Siednienko and co-workers, of nitric oxide (NO) and cyclic guanosine monophosphate (cGMP) activation causing an increase in IL-6 expression, which reverses the movement of ions in the choroidal epithelium in human peripheral blood mononuclear cells (PBMCs), leading to a reduction in CSF secretion. The cGMP-dependent pathway is initiated when NO binds to the heme moiety of cytosolic guanylyl cyclase (GC) and stimulates its enzymatic activity (Siednienko et al. 2011). cGMP's role in increasing IL-6 expression in human PBMCs involving the GC/cGMP/protein kinase G (PKG) pathway (see Introduction Section 1.10.3) (Siednienko et al. 2011), highlights the possibility of a similar pathway of decreased CSF secretion across choroidal epithelium through protein kinase inhibition of Na^+-K^+-ATPase (Kolb et al. 1994).

As mentioned above, sodium transport across the choroid plexus epithelium, through the ENaC pathway, is essential for CSF secretion. However, IL-1β has been shown to significantly reduce sodium transport across rat alveolar epithelial type II (ATII) cell monolayers, by decreasing ENaC α-subunit mRNA levels (Roux et al. 2005). This may explain the absence of increased CSF secretion rates in our study following IL-1β treatment, which may be due to a similar mechanism as seen in the ATII cells. The reduced sodium transport and decreased α-ENaC expression is thought to be through p38 MAPK-dependent inhibition of α-ENaC promoter activity and an alteration in ENaC trafficking to the apical membrane of ATII cells (Roux et al. 2005). In addition, IL-1β was also found to reduce ENaC function in a dose- and time-dependent manner after 72h in human bronchial epithelial cells without reducing ENaC expression (Gray et al. 2004).

IL-1β has also been shown to antagonise the production of prostaglandin E2 (PGE2) which stimulates chloride transport in canine tracheal epithelium and in Calu-3 human bronchial epithelial cells (Clayton et al. 2005). The decrease in PGE2 production leads to a down regulation of EP_4 prostanoid receptors and subsequently to a reduction of PGE2 induced cAMP production (Clayton et al. 2005). As mentioned previously, cAMP elevation has been shown to increase AQP1 activity, leading to an increased movement of water across swine airway submucosal epithelium (Baniak et al. 2012). Therefore, the decreased cAMP activity by IL-1β in Calu-3 human bronchial epithelial cells may explain the reason for the lack of CSF secretion effect associated with this cytokine in our study.

Nevertheless further studies by Eisenhut and colleagues found IL-1β incubation caused an increase in airway surface liquid volume which altered ion transport, including an upregulation of Cl^- secretory currents, but did inhibit ENaC-mediated absorptive Na^+ currents (Eisenhut et al. 2006). Even though the results in the present study showed an absence of effect on CSF secretion by acute IL-1β administration to the CSF, whether possible effects of increased CSF secretion rates following IL-1β treatment under other conditions are observed through increased expression of NKCC1 transporters, leading to increased Cl^- movement across CP epithelia, as opposed to AQP1 and ENaC transporter expression, remain to be determined. Yet, all these studies and our results highlight the possibility that IL-1β may elicit responses on epithelial ion transport that are specific to the tissue under investigation.

As with all of the cytokines tested within this study, high levels of leptin have also been reported in the CSF of IIH patients (Ball et al. 2009). High leptin levels in the CSF would reduce satiety and consequently weight in IIH; yet, these patients remain obese, therefore a central leptin resistance in IIH has been suggested. It is not clear how dysregulation of leptin in IIH influences ICP balance (Markey et al. 2016). Studies have found acute dosing of leptin in animal models led to decreased Na^+-K^+-ATPase transporter activity in the kidney (Beltowski 2010). However, long-term administration of leptin within this same study by Beltowski, led to increased Na^+-K^+-ATPase activity in proximal tubule cells within the renal system. As the choroid plexus is very similar to the renal proximal tubules in terms of function and epithelial ultrastructure (Damkier et al. 2013), an increase in leptin could possibly increase Na^+-K^+-ATPase activity in epithelial choroid plexus cells

resulting in increased CSF secretion and hence raised ICP. However, these results were not seen following *in vivo* CSF secretion experiments within our study further supporting the notion of tissue-specific modulation of epithelial ion transport by inflammatory mediators and hormones.

Indeed, previous studies (van Dijk et al. 1997) (Zúñiga et al. 2010) may provide a rationale for the observed absence of effect in CSF secretion rates following leptin treatment in our study. Leptin could potentially affect CSF secretion rate via an indirect route through the release of corticosteroid hormones through hypothalamic-pituitary-adrenal (HPA) axis activation (van Dijk et al. 1997). In van Dijk's study, 3.5 µg of human leptin was infused directly into the third cerebral ventricle of lean male Long-Evans rats, 90 min prior to blood analysis, where leptin caused an increase in plasma corticosterone. However, the locations of leptin perfusion differ between van Dijk's and our study. In van Dijk's study, leptin was infused into the third ventricle of the rat brain, as opposed to the lateral ventricles in our study. This may mean that in our system leptin may not enter the systemic circulation in sufficient amounts to activate the HPA axis. Therefore, the lack of increased CSF secretion rates following leptin treatment in our study may be due to corticosterone not being converted into cortisol intracellularly, which would be needed to increase the movement of Na^+ across the cells via apical Na^+ channels, increasing this osmotic gradient and driving water into the CSF (Sinclair et al., 2010).

Leptin has also been shown to increase Na^+ efflux through Janus kinase (JAK) phosphorylation of signal transducers and activators of transcription STATS (see

Introduction Section 1.10.2), as seen in the glomerular epithelium of kidneys in anaesthetised rats (Jackson & Li 1997). The onset of adipogenesis is essential for the secretion of leptin (Ball et al. 2009). IL-17 is a known negative regulator of adipogenesis and glucose metabolism in mice, and results show that it delays the development of obesity (Zúñiga et al. 2010). This raises the possibility of reduced CSF secretion in IIH, caused by an IL-17-induced reduction in CSF leptin levels. However, even though the lack of effect in CSF secretion rates associated with leptin could be due to the increased levels of endogenous IL-17 following exogenous leptin administration *in vivo*, our results would not support this hypothesis as IL-17 did not modulate CSF secretion rate either.

There is no sufficient evidence to provide a rationale for the absence of effect of CCL2 on CSF secretion rates. It is however known that IL-1β, which also caused no change in CSF secretion rates in our study, increases the expression of CCL2 in rat choroid plexus monolayers, following IL-1β incubation (Paine et al. 1993) (Prodjosudjadi et al. 1995). As already mentioned, IL-1β also causes a decrease in expression of ENaC mRNA levels in rat ATII cells through p38 MAPK-dependent inhibition of α-ENaC promoter activity; however CCL2 also inhibits p38 MAPK phosphorylation in human breast cancer cells through the activation of its receptor, CCR2. Inhibition of p38 is also known to decrease AQP1 expression in mouse pulmonary microvascular endothelial cells (PMVECs) (Zhang et al. 2016). Therefore, a possible link may exist between IL-1β and CCL2 in decreasing ENaC expression, reducing sodium transport, decreasing AQP1 expression and hence decreasing water movement which would indicate that these two cytokines would cause a decrease in CSF secretion rates. This decrease was not seen within our

study as CCL2 and IL1β caused no change upon CSF secretion rates *in vivo*. Therefore, it may be possible that factors such as the upregulation of Cl^- secretory currents (Eisenhut et al. 2006), that may lead to an increase in CSF secretion rates, following IL-1β and therefore associated CCL2 treatment, may have acted as a compensatory mechanism to the initial decreases in sodium transport associated with IL-1β and CCL2 in previous studies.

Within this study, there are promising initial results associated with HC and TNF-α in increasing CSF secretion rates and IL-6 in decreasing CSF secretion rates in adult male Wistar rats. Further validation of these results could be carried out using specific neutralising antibodies against TNF-α and IL-6 stimulation in an animal model to test whether a reduction/increase, respectively, in CSF secretion is shown following cytokine/glucocorticoid inhibition.

4.1.1 Intraperitoneal administration of each treatment did not alter CSF secretion rates

There were no effects seen in CSF secretion rates following an intraperitoneal (i.p) injection of each treatment 90 minutes prior to perfusion with the same treatment within the aCSF. These results did not confirm our previous results with HC, TNF-α, and IL-6 when directly administered in aCSF. The lack of effect on CSF secretion was possibly due to the time frame of 90 minutes being too short for an effect to be seen, however this does not explain the lack of effect following perfusion of each treatment within the aCSF during this same experiment. A possible explanation could be the overload of treatment concentration causing a compensatory mechanism to take effect and reducing the amount of CSF secretion

that was established following the initial 90 minute pre-injection administration. In addition, the initial i.p. dose of each treatment may have been sufficient for the effect to take place and pass within the 90 minute window, so when further doses through direct aCSF administration occurred, they may have had a less profound effect on CSF secretion within the following 90 minutes.

The *in vivo* CSF secretion results following CCL2 and IL-17 treatment were interesting as they showed no effect upon CSF secretion, for both *in vivo* perfused aCSF and i.p injection in conjunction with perfused aCSF; but were the only two treatments to show a statistically significant increase in initial CSF volume within the rat brain. There is little evidence of as to the reasons of increased CSF volume or poor CSF clearance associated with IL-17 and CCL2. However, various studies have found that increased expression of CCL2 (Wang et al. 2016) and IL-17 (Hot et al. 2013) induce pro-thrombotic genes such as Tissue factor (TF), which encodes coagulation factor III, in mouse brains, which plays an essential role in impairing CSF drainage with microthrombi in the arachnoid villi in patients suffering from IIH (Kesler et al. 2006) (Glueck et al. 2005) (highlighted further in Section 4.1.2). Therefore, this may indicate a link between increased levels of CCL2 and IL-17 and increased resistance to CSF drainage creating a rise in ICP associated with IIH patients.

4.2 Model of obesity

Following on from the initial cytokine/mediator studies on lean male rats, it was important to test both mediator and diet effects on CSF secretion rates in rats fed

either normal or high-fat (HF) diet. This was essential due to the increasing incidence of IIH in obese individuals and several studies reporting weight gain in newly diagnosed IIH patients (Rowe & Sarkies 1999) (Radhakrishnan et al. 1993). Our model for obesity, as described further in this section, allowed us to compare the effects of diet intake on CSF secretion rates (Section 4.3) and resistance to CSF drainage (Section 4.6).

Following the completion of each diet over a 7 week period, average percentage weight gain, total cholesterol, and LDL/VLDL cholesterol levels over time were increased in the male and female HF diet groups compared to animals fed a standard diet, as expected. Percentage weight gain observed in HF diet groups in our study was comparable to the HF diet induced effects reported previously (Naderali et al. 2001) (Guerra et al. 2007). Guerra studied differences in weight gain between adult male rats fed a normal cholesterol chow diet or cholesterol-rich diet. The study found food intake to be 25% higher within the cholesterol-rich diet group (25.0g/day) compared to the normal cholesterol chow diet (19.8g/day) (Guerra et al. 2007). Within our study, however, a normal diet (20.5g/day) was consumed more than the HF diet (18.0g/day) by the male rats. In studies by Naderali, adult male and female rats fed either a standard pelleted laboratory chow or a highly palatable/high-energy diet, were studied for 16 and 12 weeks, respectively, compared to the 7 weeks within our study. Rats of either sex given the highly palatable diet gained progressively more weight than chow-fed controls, being significantly heavier after 4 weeks, and diet-induced weight gain was significantly greater in males than in females, differences also noticeable in our results. The final body weights of high-energy diet-fed rats were 32%

(males) and 9% (females) greater than those of their respective chowfed controls (Naderali et al. 2001). By contrast, in our study, final body weights did not differ between groups whereas percentage weight gain difference after 11 weeks in Naderali and colleagues' study was a more reliable parameter (161% males, 130% females) to differentiate between rats on a HF diet and those on a normal diet. Naderali and colleagues showed plasma cholesterol level increases on high-energy diet rats were comparable to those in the HF-diet rats within our study. However, this study reported an almost 100% greater total cholesterol plasma concentration in male rats in both controls and high-cholesterol fed diets compared to male rats in our study (Naderali et al. 2001). Nevertheless, LDL cholesterol plasma concentration in our model was similar to that reported in previous studies (Naderali et al. 2001) (Guerra et al. 2007), suggesting that LDL plasma levels may be a more reliable indicator of obesity induced physiological changes. The results from previous studies show that our model of obesity was comparable and allowed for appropriate comparisons to be made between the two diet groups.

4.3 Effects of diet on CSF secretion

A HF diet affected CSF secretion rates regardless of treatments and sex. When comparing controls it was evident that rats raised on a HF diet had significantly increased CSF secretion rates over rats fed a normal diet. This increase in CSF secretion rates was especially evident with the control groups of female rats on a HF diet having a greater CSF secretion rate over all other variables. The association between total cholesterol and LDL/VLDL cholesterol levels (but not HDL cholesterol levels) and increased CSF secretion rates was also observed. However, in terms of IIH, there are no studies in which the incidence of the condition has

been considered in relation to the variation in cholesterol levels, and this association may indeed just reflect the previous association between obesity and cholesterol levels (Naderali et al. 2001) (Guerra et al. 2007). In addition, there have been no studies that measured the effects of obesity or a HF diet on CSF secretion rates.

Increased cortisol levels resulting from HC administration were found to increase CSF secretion rates in animals on both diets. Cortisol plasma levels are found to be increased in humans on a HF diet (Venkatraman et al. 2001). In addition, high protein diets have been associated with elevated plasma cortisol levels in humans (Anderson et al. 1987). It is possible that, in our model, the HF diet led to elevated cortisol levels thereby contributing to higher CSF secretion rates.

Another factor contributing to increased CSF secretion rates in our model was TNF-α. Reports on the effect of HF diets on circulating TNF-α levels have been inconsistent. Bedoui et al. (2005), did not find a significant increase in circulating TNF-α plasma concentrations in obese rats. However, Cano et al. (2009) did observe increased TNF-a plasma levels in rats raised on a HF diet. In addition, Sharman & Volek (2004), found that switching to a low-fat diet decreases the plasma levels of TNF-α in overweight men. In spite of these apparently contradictory studies, there is growing evidence that TNF-α constitutes an adipokine secreted by adipose tissue. Obesity and HF diets have been shown to elevate the release of TNF-α by human adipose tissue (Fain 2006) and various studies have found TNF-α to be overexpressed in adipose tissue of rodents (Hotamisligil et al. 1995) (Hotamisligil et al. 1993) (Hamann et al. 1995) and

humans (Hotamisligil et al. 1995) (Kern et al. 1995) (Saghizadeh et al. 1996) (Hotamisligil et al. 1997) compared to other tissues.

In other studies, a HF diet in male Wistar rats caused increased cholesterol in the blood and elevated TNF-α levels in bone marrow mesenchymal stem cells (Cortez et al. 2013), as well as up-regulation in mouse liver (Mikula et al. 2014).

In addition, the soluble form TNF-α receptor, TNFR1, has also been found to be elevated in the serum of obese individuals. Studies by Ronnemaa and colleagues found serum TNFR1 levels were significantly greater in human obese individuals when compared to lean controls. The levels of the TNF-α receptor correlated positively with body mass index, percent body fat, and abdominal fat (Rönnemaa et al. 2000). Further studies demonstrated, under a HF diet, TNFR1 KO mice gain significantly less body mass in spite of increased caloric intake (Romanatto et al. 2009). Liang and colleagues fed Wistar rats a high-fat/high-sucrose diet for 16 weeks until obesity developed. In comparison with increased body weight and fat weight, enlarged adipocytes, and hypertriglyceridemia in the obese state, their subsequent 4 week treatment with TNFR1 blocking peptide-Fc fusion protein (TNFR1BP-Fc) resulted in significant weight loss characterised by decreased weight and adipocyte size and reduced plasma triglycerides (Liang et al. 2008). However, although TNFR1 has been shown to be expressed by choroid plexus epithelium within this study (see Section 4.7), no studies on the effect of a HF diet on TNFR1 have been published. Nevertheless, the results of these studies suggest a pivotal role for TNFR1-mediated TNF-α signalling in the pathogenesis of obesity, all of

which may contribute to the increased ICP pressure associated with obese IIH patients.

The markedly increased levels of cortisol and TNF-α in the HF diet groups of other studies (Venkatraman et al. 2001) (Cano et al. 2009) (Sharman & Volek 2004) may provide an explanation, at least partly, for the increase in CSF secretion rates in rats fed a HF diet within our study over rats raised on normal diets. Studies by Park have shown TNF-α to be associated with obesity, when comparing the levels in obese and non-obese adults free from inflammatory disease, and also to regulate 11β-HSD1 activity (Park et al. 2005), aspects which have already been highlighted in Section 4.2.2. Obesity-induced TNF-α may thus have a direct effect on CSF secretion rates, through increased activity of the 11β-HSD1 enzyme, much in the same way as HC, which is further supported by the observed increased CSF secretion rates, in rats on both diets, seen mainly with these two treatments. As 11B-HSD1 activity is up-regulated in obese human adipose tissue (Engeli et al. 2004), choroid plexus and arachnoid granulations (Sinclair, Walker, et al. 2010), specific inhibitors to reduce 11B-HSD1 activity could be developed as novel therapies for IIH. Inhibitors including curcumin have been shown to be a competitive inhibitor of human and rat 11β-HSD1 enzyme (Hu et al. 2013). This same study by Hu and co-workers found curcumin to reduce serum glucose, total cholesterol, triglyceride, and LDL cholesterol levels in HF diet induced obese rats. By contrast with HC and TNF-α, there was a decrease in CSF secretion rates following IL-6 treatment in male rats on a normal diet which was not observed in the HF diet rats. A HF diet may inhibit cGMP activation and IL-6 expression leading to a reduction in CSF secretion by reversing the movement of ions in the choroid

plexus epithelium (Siednienko et al. 2011), as initially shown in the initial study on male rats fed a normal diet. However, higher circulating concentrations of IL-6 have also been associated with obesity in humans (Vozarova et al. 2001) (Shoelson et al. 2007) (Rexrode et al. 2003), mice (Cortez et al. 2013) and rats (Cano et al. 2009). Studies by Stemmer et al. (2012) found a HF diet-induced obesity caused an increase in renal IL-6 expression in the rat kidney. IL-6 mRNA levels were also significantly higher in human peripheral fat tissue compared to that in leukocytes, vein and muscle tissues (Sonnenberg et al. 2008). Studies by Sindhu and colleagues showed higher IL-6, IL-6R and IL-6 mRNA expression in the adipose tissue of obese human subjects when compared with lean controls (Sindhu et al. 2015). The elevated IL-6 and IL-6R expression correlated positively with BMI and percentage body fat, results of which were confirmed in further studies by Wolford and colleagues. Results from these studies suggest that IL-6 may form part of the link between obesity and increasing CSF secretion rates over normal diet subjects. However, although IL-6 may be increased in HF/obesity, it does not seem to regulate CSF secretion when compared to HF diet controls (Wolford et al. 2003).

Finally, IL-17 and CCL2 showed no effect upon CSF secretion when compared with controls in either diet; however a HF diet in females showed increased effect on CSF secretion rates over normal diets, following treatment with both cytokines. Rodents raised on a HF diet have displayed elevated levels of CCL2 in rat plasma (Cano et al. 2009), rat kidneys (Sonnenberg et al. 2008) and mouse liver (Mikula et al. 2014). CCL2 mRNA has also been shown to be increased in obese mouse adipose tissue (Chen et al. 2005). This effect was also noticeable within plasma

after four weeks on a HF diet. In addition, CCL2 and its receptor, CCR2, is also increased in the adipose tissue of obese human subjects when compared to lean controls (Huber et al. 2008). Studies by Pandzic-Jaksic and colleagues also found the proportion of CCR2 was elevated in the serum of obese women when compared to lean controls and correlated with body weight, body mass index and fat mass (Pandzic Jaksic et al. 2013). IL-17 serum levels are known to be elevated in humans on a HF diet (Peluso et al. 2012) but there is no evidence of elevated levels of IL-17 receptor, IL17Rα, in plasma or adipose tissue of obese animals or human subjects. However, an IL-17 deficiency has been shown to enhance diet-induced obesity (Zúñiga et al. 2010). The same study also found that IL-17 delayed the development of obesity, acting as a negative regulator of adipogenesis and glucose metabolism by inhibiting preadipogenic transcription factors, adipokines and molecules involved with lipid and glucose metabolism. This observation emphasises the complex role of IL-17 in obesity although, in the context of CSF dynamics, it appears that IL-17 and CCL2 do not influence CSF secretion rate.

Further experiments using different diets within the present study attempted to differentiate the ultrastructure of male rat choroid plexus raised on either a normal or HF diet using electron microscopy (EM). A possible difference in cell ultrastructure which would help explain the changes in CSF secretion rates between the two diets would be defects in cilia function or formation. As described further in Section 4.8, defects in cilia have been related to hydrocephalus and neurological disorders that results in increased ICP (Badano et al. 2006) (Albee & Dutcher 2012) but also increases in cilia numbers are known to play an increased role in CSF secretion (Albee & Dutcher 2012). However, choroid

plexus ultrastructure and cilia numbers appeared to be similar in male rats raised on both normal and HF diets. However, as no quantitative analysis was performed due to the low number of tissues used it was not possible to categorically ascertain whether an increase in cilia numbers in the HF diet rats may have presented an added explanation of the increased CSF secretion associated within this group. Nevertheless, the EM images did show all of the characteristics associated with choroid plexus brain tissue including the cuboidal epithelial cells; tight junctions at the apical membranes; and microvilli and cilia on the surface of the epithelial cells, in the ventricular lumen, into which the CSF is secreted from the choroid plexus epithelium.

Therefore based on all of the results, the increased levels of cortisol and TNF-α in HF diet groups may provide part of an explanation for the increase in CSF secretion rates in rats fed a HF diet over rats raised on normal diets within this study. However this hypothesis does not explain the lack of increased CSF secretion associated with IL-6, IL-17 and CCL2 which suggests that other factors induced by a HF diet, rather than these cytokines, is the most important factor in increasing CSF secretion rates and ICP in obese IIH patients.

4.4 Effects of sex on CSF secretion

As IIH is found to mainly affect the female population, it was therefore important to test not only diet, but also sex effects on CSF secretion rates, as a combination of a HF diet and female sex hormones could be an important factor in elevated ICP associated with IIH patients.

In this study, there were strong associations observed between increased weight gain and CSF secretion rates in female Wistar rats. When comparing controls it was evident that female Wistar rats had a significantly increased CSF secretion rate over male rats but only in the HF diet group. These results may highlight the increasing prevalence of IIH occurring in the obese female population with a female to male IIH incidence ratio of 8:1, as reported by Dhungana et al. (2009).

Both pregnancy and exogenous oestrogens are thought to promote symptoms of IIH (Bagga et al. 2005). Endocrinological dysfunction within females of child-bearing age have been postulated as causes of increased ICP in female IIH patients (Farb et al. 2003). Increased amounts of adipose tissue, also associated with obesity, acts as an endocrine organ, releasing hormones such as leptin, and produces increased levels of oestrogen via the conversion of androstenedione. This can lead to physiologically abnormal amounts of these hormones in a person's body which may contribute to the development of IIH (Farb et al. 2003) (Higgins et al. 2004). Studies by Binder and colleagues found that the concentration of oestrogen in the CSF from young obese women with IIH was much greater than that found in normal subjects (Binder et al. 2004).

As with the initial studies in males, HC and TNF-α were the only treatments found to increase CSF secretion rates, but this time in both sexes over controls. Therefore, these two treatments may be a factor in elevated ICP, associated with IIH patients, regardless of sex. Female rats have a more intense corticosterone response to stress effect, which is partially mediated by oestrogen as the stress response was partially normalised by ovariectomy (Young 1996) In other studies,

orally administered oestrogen has been shown to increase cortisol plasma levels in men (Marks et al. 1961). Increase in cortisol plasma levels in female rats could offer a potential mechanism by which an increase in CSF secretion is associated with female rats over males.

TNF-α is also elevated in healthy control subjects of human females over males (Pfeiffer et al. 1997). Women generate high serum levels of anterior pituitary hormone prolactin, in response to stressful stimuli (Zhu et al. 1997). Prolactin is known to stimulate the immune system, enhancing proliferation and function of lymphocytes and macrophages; cells from which cytokines are secreted. Studies by Zhu have shown TNF-α plasma level increases following subcutaneous injection of prolactin in male mice (Zhu et al. 1997). This process in females could also be a cause of the elevated CSF secretion rates associated with TNF-α in female lean and obese rats.

IL-6 treatment in male rats decreased CSF secretion rates, as with the initial studies in Section 4.2.2. However, this effect was not observed in the female rats. These results may suggest that female sex hormones could possibly inhibit the actions of cGMP activation upon IL-6 expression, following NO stimulation, in reversing the movement of ions in the choroid plexus epithelium, leading to a reduction in CSF secretion (Siednienko et al. 2011), as initially shown with the male Wistar rats and initial screening results. NO levels are elevated in the urine of healthy premenopausal women (Forte et al. 1998). However, the levels of NO are decreased in HF diet associated hyperglycaemia when compared with normal diets (Giugliano et al. 1997). This may provide a rationale as to the lack of reduced

CSF secretion rates associated with IL-6 in HF diet female rats, as initially seen in normal diet male subjects. However, studies by Pakmon and colleagues found increases in basal cGMP in female rabbits over male controls following long-term 17-β-estradiol treatment (Palmon et al. 1998). This increase was mainly localised within the cerebellum. Whether increases in basal cGMP is noticeable in the choroid plexus epithelial cells following the same treatment is unknown. Nevertheless, other studies have described the addition of 17-β-estradiol in murine bone marrow-derived stromal cell lines, human bone-derived cells, and osteoblast cell lines from mice and rats exerted a dose-dependent inhibition of IL-6 as well as decreasing IL-6 mRNA levels. Testosterone and progesterone also inhibited IL-6, but their effective concentrations were two orders of magnitude higher than 17-β-estradiol (Girasole et al. 1992) (Jilka et al. 1992).

Human oestrogen receptor (hER) has also been implicated in impairing the induction of IL-6 in HeLa cells (derived from a human cervix carcinoma) by preventing protein binding to the NF-kappaB site of the IL-6 promoter (Galien & Garcia 1997) (Rays et al. 1994). Based on current evidence it is unknown whether female sex hormones such as oestrogen actively inhibit the IL-6 synthesis in choroid plexus epithelial cells, as they do HeLa cells for example. Therefore, the effects of decreased CSF secretion rates associated with IL-6 treatment in male rats may be due to lower levels of oestrogen in circulation. In addition, this may explain the abolished decreases in CSF secretion in IL-6 treated female rats due to the natural increased levels of oestrogen in females and subsequent inhibition of IL-6 promoter regions. Further experiments in measuring plasma sex hormone

levels, as well as determining the inhibitory effects of estrogen on IL-6 in choroid plexus epithelial cells would be beneficial.

However, there are no studies on the direct role of IL-17 and CCL2 on sex hormone levels and effects on CSF secretion but it is possible that increased resistance to CSF drainage may be due to increased expression of thrombotic genes by IL-17 and CCL2 and exogenous oestrogens in the arachnoid villi in female IIH patients, highlighted further in Section 4.6.3 (Glueck et al. 2005).

A study by Klein assessed the hormone profile of female IIH patients (Klein et al. 2013). There were no differences in the levels of estradiol, follicular-stimulating hormone, luteinizing hormone, or prolactin, however the study did show raised levels of testosterone and androstenedione, in young onset (<25 years of age) female patients with IIH.

Park and colleagues have reported an occurrence of IIH secondary to testosterone therapy in a transgender patient (Park et al. 2014). A 22-year-old male with a normal body mass used intramuscular injections of testosterone propionate (250mg) to maintain his male status. Based on the diagnosis of bilateral optic disc swelling, increased CSF pressure, normal estradiol plasma sex hormone levels; a diagnosis of IIH secondary to raised free testosterone was made. Following the substitution of testosterone propionate with a longer-acting testosterone undecanoate (1000 mg), to stabilise the raised free testosterone level; optic disc swelling, CSF pressure and testosterone levels were reduced after 3 months. The exact mechanism of how raised testosterone causes IH is not known, but it is not

thought to be due to raised oestrogen levels from peripheral aromatisation of testosterone stimulating CSF production and increasing ICP, due to the fact that in this report the oestrogen level was normal. Nevertheless, this study by Park and colleagues is the first to demonstrate a direct association with raised levels of free testosterone and IH.

It is not categorically clear how sex hormones could alter ICP, but interestingly, studies in rabbits have demonstrated that oestrogen and progesterone are able to reduce CSF secretion by the choroid plexus, on their own and in combination (Lindvall-Axelsson et al. 1989). Isolated choroid plexuses from rabbits were used to determine uptake and accumulation of 10^{-5} M radiolabelled choline following pre-treatment of the animals with 17-β-estradiol, alone or in combination with progesterone. The combined treatment reduced the choline uptake by 35% and also lowered the activity of Na^{+}-K^{+}-ATPase by 31% (Lindvall-Axelssson et al. 1989). These results do not correlate with our findings, which may suggest that the effects of female sex hormones and increased CSF secretion rates, with female rats in our study, may not be due to their effect on Na^{+}-K^{+}-ATPase but by increasing the expression of other choroid plexus transporters such as NKCC1, ENaC or AQP1, or due to increased plasma testosterone levels.

4.5 Summary (CSF secretion rate)

A HF diet seems to be the most important factor in increasing CSF secretion rates, as was evident in all HF diets over normal diets regardless of treatment used. TNF-α treated female Wistar rats on a HF diet showed the highest CSF secretion rate

of all the treatment groups. The role of obesity and gender on CSF secretion is highlighted further in Figure 4.3.

Studies by Newborg were the first to document diet as a treatment for IIH in humans. Weight loss occurred in 38% of IIH patients following a low calorie and low sodium diet, and resulted with improvement in IIH symptoms and papilledema (Newborg 1974). Other studies found a weight loss of just 6% in obese women resulted in improved papilledema symptoms associated with IIH patients in 74% of cases (Kupersmith et al. 1998) and re-evaluation after three months, following maintenance of a low energy diet with no evidence in weight gain, showed that reduced ICP and papilledema were maintained (Sinclair, Burdon, et al. 2010). This may suggest a collective treatment against TNF-α elevation, possibly through inhibition of 11B-HSD1 activity, and a low-fat diet could be the main course of therapy for reducing raised ICP associated with obese female IIH patients.

In addition, the elevated levels of sex hormones (namely oestrogen) in the CSF of IIH patients when compared with healthy controls have been shown (Donaldson & Horak 1982) and documented to promote symptoms of IIH (Bagga et al. 2005). However there are contradicting arguments in other studies (Lindvall-Axelssson et al. 1989). There has been evidence of increased oestrogen and prolactin hormone levels giving rise to cortisol and TNF-α, respectively, in females. This may help explain the role of these sex hormones in increasing CSF secretion and subsequent ICP in female IIH patients. Elevated levels of oestrogen have also been associated with IL-6 inhibition which may explain the lack of reduced CSF secretion associated with this cytokine in female rats.

Case reports have also shown a link with the use of oral contraceptive pills (Walsh et al. 1965), as well as polycystic ovarian disease (Glueck et al. 2003) (highlighted further in Section 4.1.3), a condition which is associated with imbalance of the sex hormones. However, surprisingly, testosterone levels have also been shown to be raised in females (Klein et al. 2013) and transgender patients (Park et al. 2014) with IIH. The exact mechanism of how raised testosterone levels may lead to IIH in females is not known and would also not explain the slightly less elevated CSF secretion rates seen with the male rats as well as the greater incidence of IIH occurring in females. What is known is androgen receptor (AR) mRNA and protein are expressed in male and female rat CP epithelial cells (Alves et al. 2009), therefore highlighting, a possible mechanism of increased NKCC1, ENaC or AQP1 CP epithelial cell transporters expression be due to increased oestrogen or testosterone levels.

As mentioned in Introduction Sections 1.4.3, 1.4.7 and 1.7, treating elevated CSF secretion in IIH patients may be achieved through either serotonin to inhibit Na^+-K^+-ATPase pathway through the activation and phosphorylation of PKC (Fisone et al. 1995); antisense TTF-1 oligodeoxynucleotide to reduce AQP1 mRNA and protein expression in the choroid plexus (Kim et al. 2007); or acetazolamide and topiramate treatment to decrease intracellular HCO_3^- levels in the choroid plexus epithelium (Dhungana et al. 2009). However, based on the results within this study, reducing weight loss and inhibiting the actions of reproductive hormones as well as HC and TNF-α may result in decreased CSF formation and ICP in IIH patients.

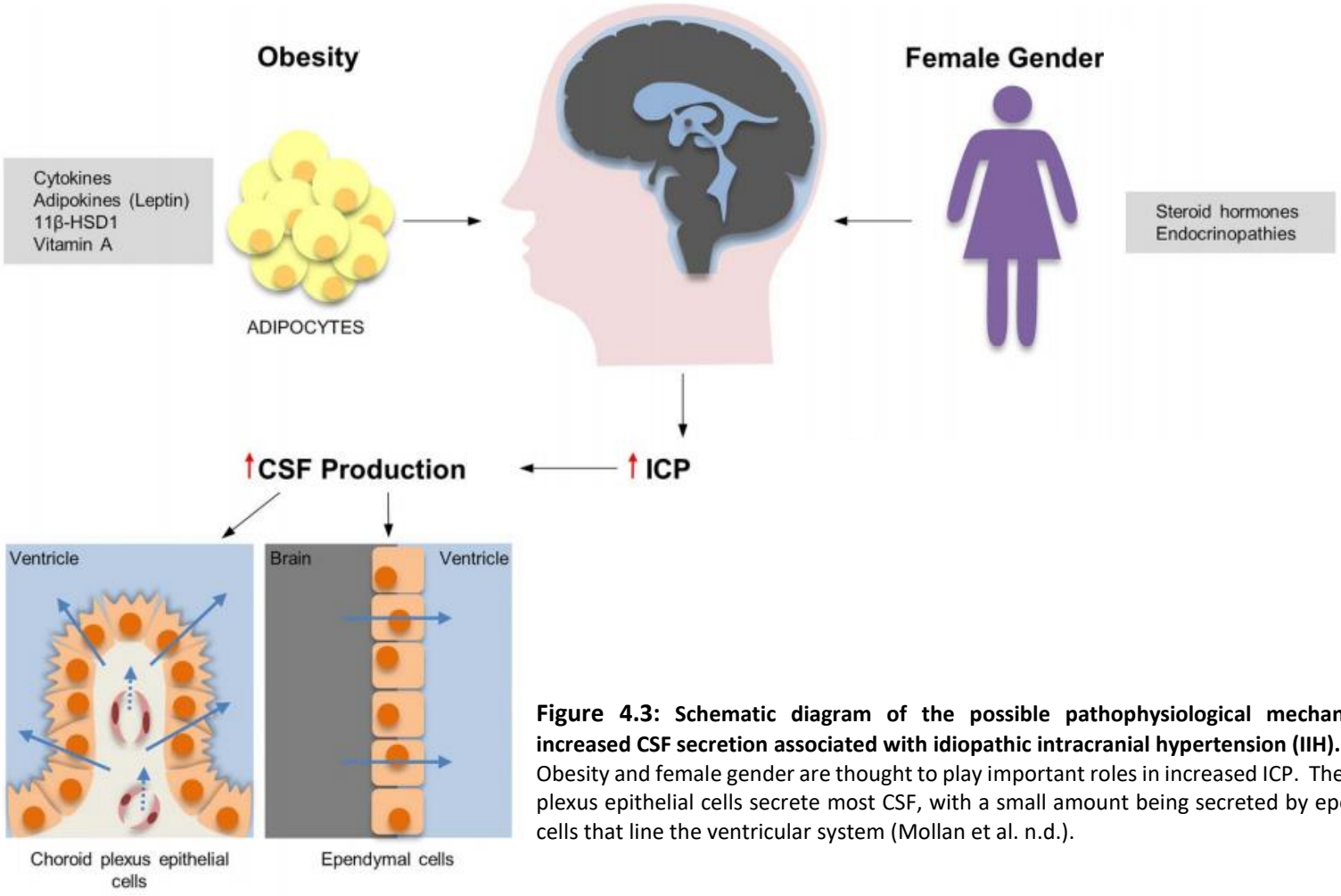

Figure 4.3: Schematic diagram of the possible pathophysiological mechanisms in increased CSF secretion associated with idiopathic intracranial hypertension (IIH).
Obesity and female gender are thought to play important roles in increased ICP. The choroid plexus epithelial cells secrete most CSF, with a small amount being secreted by ependymal cells that line the ventricular system (Mollan et al. n.d.).

4.6 Resistance to CSF drainage pathways

Reduced CSF drainage may also contribute to increased ICP. Drainage of the CSF from the subarachnoid space (SAS) through arachnoid granulations into the superior sagittal sinus was the initial perceived pathway regarding CSF absorption (Kida et al. 1988). In recent history, evidence of CSF drainage involving the nasal lymphatics has been shown in humans (Johnston et al. 2004) and mice (Louveau et al. 2015). An additional glymphatic pathway, involving the exchange of fluid between the CSF in the SAS and the interstitial fluid (ISF) in the brain parenchyma, described another route of fluid clearance through paravenous drainage pathways (Iliff et al. 2012). Therefore, three routes are involved in CSF drainage from the brain, all of which are highlighted in Figure 4.5.

4.6.1 Role of cytokines in resistance to CSF drainage

As with CSF secretion rate; initial screening resistance to CSF drainage results were obtained from normal diet male rats. CCL2, IL-17 and IL-6 cause a significantly increased resistance to CSF drainage, and HC treatment a significantly decreased resistance to CSF drainage when compared to controls. This could indicate a link between increased levels of CCL2 and IL-17 and increased resistance to CSF drainage creating an increase in pressure associated in patients with IIH. HC effects on resistance to CSF drainage may be the result of a possible compensatory mechanism whereby an initial increase in CSF secretion is counteracted by increased CSF drainage. The same observation, with regards to a compensatory mechanism, could be made of IL-6 which decreases CSF secretion whilst increasing resistance to CSF drainage. Further details regarding the effects of cytokines in

combination with differences in diet and sex are described in Sections 4.6.2 and 4.6.3, respectively.

Strahle stated that hydrocephalus, following intraventricular haemorrhage, is a result of the blockage of the arachnoid villi by microthrombi and lymphatics by blood cells or fibrosis (thickening of tissue following injury) causing CSF outflow obstruction (Strahle et al. 2012). Pro-inflammatory cytokines have been shown to mediate thrombosis in mice (Yoshida et al. 2009). As the pathophysiology of hydrocephalus appears to be strongly related to IIH, a similar mechanism of increased resistance to CSF efflux at the arachnoid villi and lymphatics may be the cause of elevated ICP associated with IIH patients.

AQP4 water channels are involved in CSF absorption through the glymphatic pathway and are localised in the basolateral membrane of the ependymal cells (Venero et al. 1999) (Zelenina 2010). Studies have shown that AQP4 plays an integral role in parenchymal CSF absorption, dependent on osmotic gradients (Bloch et al. 2006). Tourdias and colleagues found an up-regulation of periventricular AQP4 in hydrocephalic rats that was strongly correlated with CSF volume (Tourdias et al. 2009). However, there have been no studies on AQP4 expression at the arachnoid villi or cervical lymph nodes, the other two main sites of CSF drainage. Therefore, further studies may be performed to ascertain if AQP4 is expressed at these CSF drainage sites, and more importantly at decreased levels following CCL2 and IL-17 treatment, which may explain the reasons for the increased resistance to CSF drainage associated with these cytokines within this study.

4.6.2 Effects of diet on resistance to CSF drainage

As with the control CSF secretion rates, female rats raised on a HF diet showed a significant increase in resistance to CSF drainage over female normal diet rats and male rats on both diets. These results again implicate a HF diet in not only increasing CSF secretion rates but also resistance to CSF drainage more so than treatments and sex alone. This is also further suggested by the associations found between increased percentage weight gain; total cholesterol and LDL/VLDL cholesterol levels, and resistance to CSF drainage in female rats.

However, no association was found between increased percentage weight gain and resistance to CSF drainage in male rats. It is important to note however that when comparing the male rats in normal and HF diets it is evident that there is a lack of significance between the two groups and the pattern of results does not match the initial observations, perhaps as a consequence of the differences in the experimental set up used for experiments on the male and female rats, i.e different types of cannula were attached to the syringe that perfused the aCSF into the one lateral ventricle of the rat brain. Specifically for the experiments with the male rats, a plastic cannula was used whereas a metal cannula was used for experiments with the females as well as the initial screening experiments on lean male rats as described in Section 4.6.1. Over time, the plastic cannula may have expanded, therefore decreasing the pressure readings due to the increase in volume. This would not be seen with a metal cannula. The resistance to CSF drainage measurements in females were similar to those made in the initial screening experiments. Consequently, only the differences in resistance to CSF drainage between diets in female rats will be discussed here.

A study by Orefice found reduced CSF absorption in obese women suffering IIH. Isotope methods evaluated CSF circulation and absorption, and cisternographic findings showed an increased arachnoid resistance to CSF efflux might be present (Orefice et al. 1992). The impact a HF diet in females has on increasing resistance to CSF drainage in our study is supported by these findings by Orefice and co-workers. It therefore appears that a HF diet, regardless of cytokine treatment, has the biggest impact on resistance to CSF drainage *in vivo*, possibly through increased arachnoid resistance to CSF outflow.

The effects of a deficiency of vitamin A in diets has also been shown to increase ICP through increased resistance to CSF drainage (Mollan et al. n.d.). Following vitamin A deficiency in female rabbits, Millen and colleagues showed morphological changes of the arachnoid villi leading to increased ICP. The thickening of the dura mater around the arachnoid granulations following mucopolysaccharide infiltration lead to a decrease in CSF absorption (Millen & Woollam 1956). Other studies have reported in Holstein-Friesian calves with toxic levels of vitamin A (hypervitaminotic A) to have a thinner and smaller arachnoid villi morphology when compared to controls (Gorgacz et al. 1975). This would imply a healthy diet is important for normal function of CSF clearance from the brain.

A HF diet alone has significant effects in increasing resistance to CSF drainage. A HF diet female group not only increases CSF secretion rates, but the initial effect of HC and TNF-α in decreasing resistance to CSF drainage, is abolished in HF animals. When taking into account TNF-α treatment, between both diets, there is

a significant increase in resistance to CSF drainage in HF female rats over both normal diet female rats. Again, the reason possibly being the elevated plasma TNF-α levels in human HF diet subjects (Fain 2006) as well as increased pro-thrombotic effects leading to an inflammation of the arachnoid villi in mice following treatment with TNF-α (Edwards et al. 2013).

However, in rat models of traumatic brain injury (TBI), there is a sustained elevation of aquaporin-4 (AQP4) levels due to transcriptional up-regulation caused by neuroinflammation and the release of inflammatory cytokines such as TNF-α into the CSF (Stover et al. 2000). Studies have shown that AQP4 plays an integral role in parenchymal CSF absorption through the glymphatic pathway, which is dependent on osmotic gradients (Bloch et al. 2006). An increase in the expression of AQP4, due to the release of TNF-α, may explain the decreased resistance to CSF drainage associated with TNF-α in rats raised on a normal diet. Whether this mechanism is altered in rats fed a HF diet remains a matter for further investigation.

There was no effect in resistance to CSF drainage with the female rats raised on either a HF or normal diet following IL-6 treatment. Previous studies have reported increased levels of IL-6 in HF diets (Fain 2006) (Giugliano et al. 1997); possibly overriding the NO pathway of IL-6 expression associated with healthy individuals. However, the mechanism behind decreased CSF drainage in HF diet females, associated with IL-6 treatment, is unknown and would need to be investigated further.

In female rats fed the HF diet, IL-17 and CCL2 treatments caused an increase in resistance to CSF drainage, in a similar fashion to the effect observed in lean male rats during the initial studies (see Section 4.6.1). By contrast, only CCL2, but not IL-17, increased resistance to CSF drainage in the normal diet female rats. The fact that CCL2 significantly increases resistance to CSF drainage in both normal and HF diet female rats, would imply that sex, diet and treatment do not correlate with the resistance to CSF drainage results associated with CCL2.

Further studies describe increases in the levels of CCL2 in the CSF of cryptococcal meningitis infected rats has been associated with altered CSF drainage pathways. A study by Fries found a greater polysaccharide accumulation in the CSF and brains of cryptococcus neoformans mucoid (MC) variant-infected rats (Fries et al. 2005). Cryptococcal antigen from CSF is thought to be the best test for diagnosis of cryptococcal meningitis in humans (Antinori et al. 2005). The finding that MC variant-infected rats accumulated more polysaccharide in the CSF and brain tissues mimics the findings in humans, in whom elevated ICP is associated with high cryptococcal antigen titers in the CSF (Graybill et al. 2000). The accumulation of MC variant glucorunoxylomannan (GXM) was associated with elevated levels of CCL2 in CSF (Fries et al. 2001). GXM appears to promote polysaccharide clumping in the CSF, which may contribute to the obstruction of the natural passage of CSF across the arachnoid villi and may be involved in the response to CCL2 observed in our study.

As mentioned previously in Section 4.4, CCL2 and its receptor, CCR2, are elevated in adipose tissue (Huber et al. 2008) and plasma (Pandzic Jaksic et al. 2013) of

obese human subjects when compared to lean controls. It is also known that IL-17 serum levels, are elevated in obese women (Sumarac-Dumanovic et al. 2009) (Peluso et al. 2012). However there is no evidence of increased levels of IL17R in obesity. Obesity is a pro-thrombotic state and it is known that IIH patients who are obese have a higher prevalence of circulating pro-thrombotic factors than non-obese IIH patients (Redzic 2013a) (Csuka et al. 1999). As already mentioned a key factor in impaired CSF drainage are microthrombi in the arachnoid villi in female patients suffering from IIH (Kesler et al. 2006) (Glueck et al. 2005). As already mentioned in Section 4.6.1, pro-inflammatory cytokines have been shown to mediate thrombosis in mice (Yoshida et al. 2009). IL-17 in particular induces pro-thrombotic genes such as TF in human umbilical vein endothelial cells (Hot et al. 2013). TF gene is the primary initiator of the extrinsic coagulation cascade, and plays an essential role in contributing to thrombosis in humans (Mackman 2012) (Mackman 2008). Exposure of perivascular TF associated with increased vascular permeability could be one of the mechanisms that triggers microvascular thrombosis in the ischemic tissue in organs expressing high levels of TF, such as the brain. Whether elevated levels of TF cause microvascular thrombosis in the arachnoid villi is unknown. However, Wang et al (2016) performed an ELISA cytokine array analysis in brain tissue of low-TF mice and revealed decreased expression of CCL2 compared with the brains of WT mice (Wang et al. 2016). This would indicate that higher levels of TF within the brain, leading to thrombosis, would correlate with increased levels of CCL2 and IL-17. If TF is found to be present at elevated levels within the arachnoid granulations, facilitating the formation of microthrombi leading to inflammation of the arachnoid villi; then this pathway may explain the role of increased levels of CCL2 and IL-17, in female rats

raised on a HF diet, and increased resistance to CSF drainage leading to raised ICP associated with IIH patients, as highlighted in Figure 4.3 (Edwards et al. 2013).

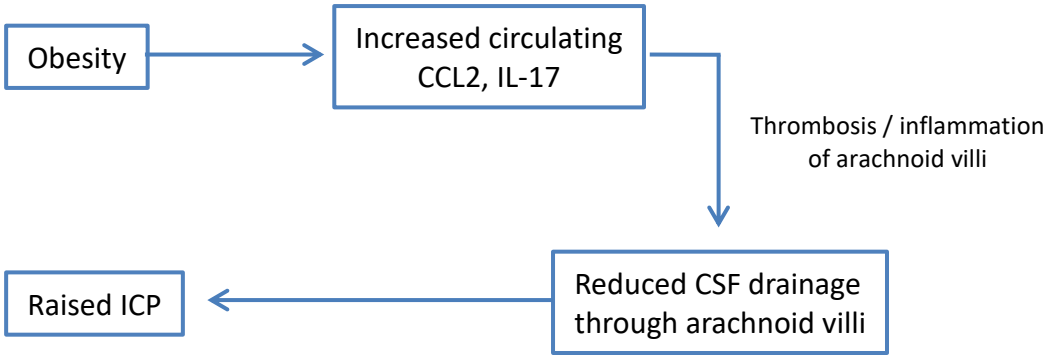

Figure 4.4: Flow diagram showing the possible mechanism through which obesity and its associated pro-inflammatory and pro-thrombotic profile contribute to increased resistance to CSF drainage and subsequent raised intracranial pressure (ICP) in IIH patents. Adapted from (Edwards et al. 2013).

Therefore, a HF diet may lead to increased resistance to CSF drainage, as it may also result in increasing CSF secretion rates associated with HF diet female rats over their normal diet counterparts. Without any other treatment the increased resistance to CSF drainage associated with a HF diet in females may be due to an increased pro-thrombotic state leading to an inflammation of the arachnoid villi and subsequent raised ICP. However, activity of this pathway may be further increased with the addition of increased levels of circulating pro-inflammatory cytokines such as CCL2 and IL-17.

4.6.3 Effects of sex on resistance to CSF drainage

IIH is predominantly seen in obese females of childbearing age; therefore, it is possible that female steroid hormones have a pathogenic role in altering CSF drainage pathways. However, a distinctive hormonal profile has not yet been described in IIH (Markey et al. 2016).

Following HC and TNF-α treatment a decrease in resistance to CSF drainage over controls is reported within our study. This decrease is evident with HC and TNF-α treated female rats raised on a normal diet when compared with controls. As already mentioned in Section 4.2.1 there is evidence of elevated plasma TNF-α levels in females (Zhu et al. 1997). Thus, it is possible that increased levels of HC and TNF-α may not only increase CSF secretion rates but also decrease resistance to CSF drainage in females, possibly through a compensatory mechanism taking effect.

IL-6 did cause a significant increase in resistance to CSF drainage in the male rats (raised on a normal diet in our previous results) as opposed to females. IL-6 serum levels were statistically higher in males relative to females following traumatic injury (Sperry et al. 2008). It is possible that the higher levels of IL-6 found in males, as opposed to females, following injury leading to a cranial inflammation may be responsible for the increase in resistance to CSF drainage. However there is no evidence of sex differences and IL-6 levels in IIH patients.

CCL2 and IL-17 treatment caused an increase in resistance to CSF drainage in female rats. However, premenopausal women have been shown to have lower

levels of CCL2 than men (Jilma & Jilma-Stohlawetz 2002). This therefore would not explain the reason for the increase in resistance to CSF drainage associated with females.

Nevertheless, studies by Glueck and colleagues, described further in Section 4.6.2 and Figure 4.3, highlight thrombosis, possibly associated with increased levels of CCL2 and IL-17 contributing to increased thrombotic gene expression, and further association with increased resistance to CSF drainage through inflammation of the arachnoid villi in female IIH patients, is often aggravated by thrombophilic exogenous oestrogens (Glueck et al. 2005). Glueck and colleagues found that of 65 women with IIH, 38% were homozygous for the thrombophilic C677T methylenetetrahydrofolate reductase (MTHFR) mutation, compared with 14% of controls, highlighting the pathway involved. The risk factor of pro-thrombotic effects may be a cause of the increased resistance to CSF drainage and consequent raised ICP associated with female IIH patients.

Further studies have revealed that the thrombophilia and hypofibrinolysis are not only exacerbated by thrombophilic exogenous oestrogens but also pregnancy, or the paradoxical hyperoestrogenemia of polycystic ovarian disease (PCOS) in females (Glueck et al. 2005). In addition, it has also been speculated that PCOS can promote IIH and this same study Glueck and colleagues found that between 39% and 57% of IIH patients also suffer from PCOS. PCOS is also known to be characterised by androgen dysregulation (O'Reilly et al. 2014). Hyperandrogenism, or androgen excess, is one of the primary symptoms of PCOS, and as previously mentioned in Section 4.5 AR mRNA and protein have been

expressed in male and female rat CP epithelial cells (Alves et al. 2009). It may therefore be possible that these receptors are also expressed on the arachnoid villi, however that is unconfirmed. Characterising inflammation of the arachnoid villi, hyperandrogenism and PCOS, in female IIH patients may highlight a possible role of androgens resistance to CSF drainage and subsequent IIH aetiology.

4.6.4 Summary (resistance to CSF drainage)

As with CSF secretion rates, a HF diet was the most important factor in increasing resistance to CSF drainage in all HF diet treatments over normal diets, excluding CCL2. CCL2 caused increased resistance in the both female groups and the initial results in lean male rats. Therefore overall, a combination of CCL2 and IL-17 in female rats raised on a HF diet had the biggest impact on resistance to CSF drainage *in vivo*, possibly through this increased arachnoid resistance to CSF outflow. Obesity is an inflammatory condition where increased circulating or CSF cytokines may result in fibrotic changes or lead to a hypercoagulable state causing blockage of the arachnoid villi and, therefore reducing drainage of CSF (Markey et al. 2016). This pathway is also often aggravated by thrombophilic exogenous oestrogens. In addition, further studies on the associations between CCL2 and IL-17 on inflammation of the arachnoid villi, hyperandrogenism and PCOS, may highlight a possible role of cause of increased resistance to CSF drainage and elevated ICP in obese female IIH patients.

Decreases in resistance to CSF drainage were seen in the female rats fed a normal diet following HC and TNF-α treatment, which was abolished in the HF diet female group. Studies have shown an increase in the expression of AQP4 in the

glymphatic pathway, due to the release of TNF-α, during parenchymal CSF absorption (Bloch et al. 2006). This may explain the decrease in resistance to CSF drainage associated with TNF-α in rats raised on a normal diet due to the increased flow. Whether this mechanism is altered in rats fed a HF diet remains to be determined.

Overall, pro-inflammatory cytokines, especially CCL2, could be used as diagnostic markers and may serve as targets for therapeutic intervention. This being if they are found to alter CSF drainage pathways; cause elevated ICP through increased resistance to CSF drainage; and therefore contribute to IIH. Developing an inhibitory treatment against CCL2 elevation in patients with IIH could be advantageous in reducing this resistance of CSF drainage, possibly around the arachnoid granulations, and therefore lowering ICP.

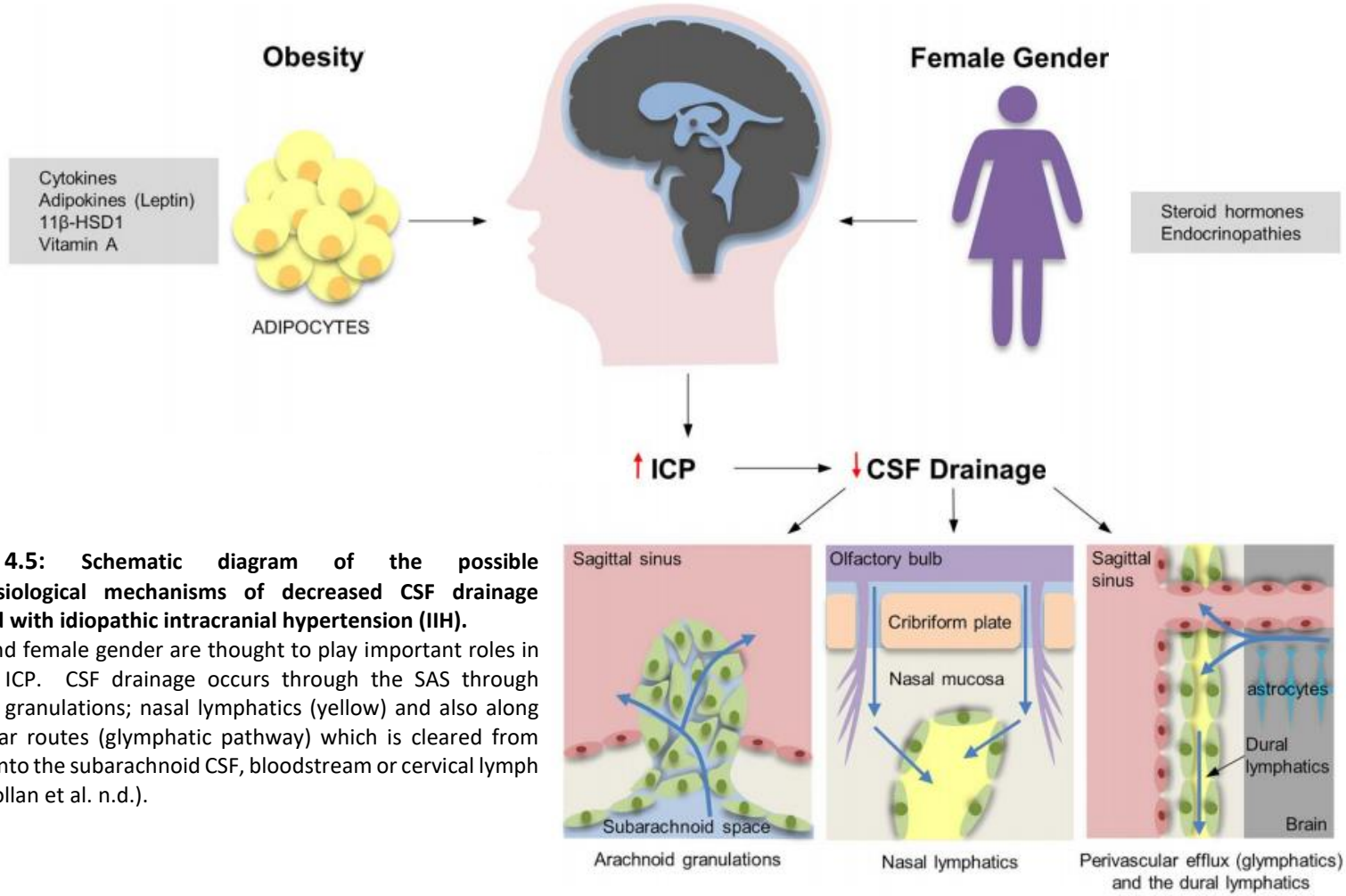

Figure 4.5: Schematic diagram of the possible pathophysiological mechanisms of decreased CSF drainage associated with idiopathic intracranial hypertension (IIH).
Obesity and female gender are thought to play important roles in increased ICP. CSF drainage occurs through the SAS through arachnoid granulations; nasal lymphatics (yellow) and also along perivascular routes (glymphatic pathway) which is cleared from the brain into the subarachnoid CSF, bloodstream or cervical lymph nodes (Mollan et al. n.d.).

4.7 In vitro expression of transporters/channels involved in CSF secretion by choroid plexus epithelium

Characterisation of hCPEpiC protein transtyretin (TTR); and ZO-1 and Claudin-1 tight junctional proteins by immunocytochemistry showed that TTR protein was distributed uniformly at the cell surface of hCPEpiC. However, ZO-1 and Claudin-1 were not found to be expressed at the apical tight junction sites associated with choroid plexus epithelial cells. Reviews by (Redzic 2013) also confirmed this to be true of the primary hCPEpiC. Immunocytochemistry and flow cytometry analysis showed Na^+-K^+-ATPase, NKCC1, AQP1 and ENaC transporters/channels, and CCR2, IL17α, TNFR1 and IL-6R receptors were also expressed on hCPEpiC. These data suggested that, although the hCPEpiC cells may not be a suitable BCSFB *in vitro* model to study CSF secretion assays because of the absence of tight junctions, they constitute a good model to study the increase/decrease in expression of transporters/channels involved in CSF secretion across the choroid plexus epithelium.

4.7.1 Treatments do not modulate transporter/channel expression on hCPEpiC

The flow cytometry analysis of transporter/channel expression on hCPEpiC following a 24h incubation with either HC, TNF-α, IL-6 results show evidence that the three main cytokines that were found to either increase or decrease CSF secretion rates in both male and female rats *in vivo,* as well as IL-17 which was initially found to increase the resistance to CSF drainage, have no effect on the expression of transporters and channels *in vitro*, that are involved in the movement of ions into the CSF. The reasons for the lack of increase in transporter

expression could be due to the *in vitro* time-frame of 24h for the incubation of the cytokines onto the hCPEpiC being too short for an effect to occur. However, the time-frame may also have been too long as, *in vivo*, the rats were exposed to the cytokines for a 90 min period and an effect in both CSF secretion rates and resistance to CSF drainage had occurred. A 24h exposure, *in vitro*, may have been too long, made the expression transient, and resulted in the increased expression of transporters occurring at a shorter incubation time.

The pathways used by these cytokines in affecting the CSF secretion/drainage rates may not occur through increased transporter expression but through a different molecular pathway. However in previous studies, TNF-α, a cytokine that increased *in vivo* CSF secretion, has been shown to decrease the activity of Na^+-K^+-ATPase channels in Sprague–Dawley rat liver hepatocellular carcinoma (HepG2) cells (Kreydiyyeh et al. 2007), but had no impact on α_1 and β_1 Na^+-K^+-ATPase mRNA expression in alveolar epithelial cells in the same species (Dagenais et al. 2004). The original decrease in Na^+-K^+-ATPase activity is through PGE2 production which in turn reduces the activity and protein expression of the Na^+-K^+-ATPase by activating prostaglandin EP2 receptors (Kreydiyyeh et al. 2007). Further studies found TNF-α to downregulate AQP1 protein expression in mouse retinal pigmented epithelial cells (Motulsky et al. 2010) and primary rat lung microvessel endothelial cells (Xie et al. 2005). Dagenais and co-workers did however find TNF-α to decrease the expression of α-, β-, and γ-subunits of ENaC mRNA after 24h treatment and reduced the amount of α-ENaC protein by 50% in alveolar epithelial cells from male Sprague-Dawley rats (Dagenais et al. 2004). However the decrease in ENaC protein and mRNA expression associated with TNF-α was reversed

following dexamethasone treatment in human colon (Bergann et al. 2009) and alveolar epithelial cells (Dagenais et al. 2006). In addition, studies by Topper and colleagues describe TNF-α to significantly upregulate the mRNA and protein expression of one of the two major isoforms of NKCC1 cotransporter, bumetanide-sensitive cotransporter BSC2, in human umbilical vein endothelial cells (Topper et al. 1997). Based on these previous studies, increases in CSF secretion, associated with TNF-α, may be through increased NKCC1 transporter expression and not ENaC, AQP1 or Na^+-K^+- ATPase channels. However, no *in vitro* modulation effects were seen with any of the transporters/channels analysed following TNF-α incubation on hCPEpiC within our study. Neverthless, TNF-α has been shown to stimulate the single K^+ channel activity in the rat thick ascending limb through activation of tyrosine phosphatase. In addition, the same study reported that IL-1β suppressed the activity and gene expression of the K^+ channel in cultured human proximal tubule cells (Nakamura et al. 2012). Whether *in vivo* increases in CSF secretion rate are associated with TNF-α through single K^+ channel stimulation as opposed to increased NKCC1 transporter expression (also involved in K^+ transport) is undetermined, therefore a case for further research on the TNF-α stimulation of single K^+ channels causing increased CSF secretion rates may be beneficial.

HC was the only other mediator found to increase *in vivo* CSF secretion, but also showed no effect on hCPEpiC transporter/channel expression *in vitro*. In terms of transporter/channel expression following cortisol treatment in previous studies, Janer and colleagues (2011) obtained blood, saliva, and cells from the nasal epithelium of 69 human infants in order to measure correlations between cortisol

concentration and ENaC expression. The results showed expression of α-ENaC correlated with plasma and salivary cortisol concentrations and therefore supported a role in humans for endogenous glucocorticoids in the regulation of airway epithelial cell ion transport (Janer et al. 2011). Further studies by Jesse and colleagues describe an increase in cortisol coinciding with elevated α-ENaC mRNA expression, but not AQP1 mRNA in ovine lungs (Jesse et al. 2009). However, cortisol infusion was also found to significantly increase AQP1 mRNA levels in sheep foetal lungs (Liu et al. 2003) and rat peritoneum (Stoenoiu et al. 2003).

Studies by Ding and co-workers revealed aldosterone to regulate NKCC1 protein expression in human colorectal adenocarcinoma (HT-29) cell lines (Ding et al. 2014). Aldosterone is a corticosteroid hormone, similar to HC, which stimulates absorption of sodium by the kidneys and so regulates water and salt balance. In addition, aldosterone was found to increase water permeability through the choroid plexus following determination of drainage of tritiated water injected into the lateral ventricle in anaesthetised dogs (Perekhval'skaia et al. 1987). Further studies by Killerich and colleagues found cortisol to increase NKCC1 and Na^+-K^+-ATPase mRNA levels in gill cells of tilapia fish (Kiilerich et al. 2011). If taking into account the results on transporter/channel expression following cortisol treatment in previous studies, this would suggest that increases in CSF secretion associated with HC could be due to increased expression of Na^+-K^+-ATPase, NKCC1, AQP1 and ENaC, however these results were not seen with the hCPEpiC within our study. Therefore further studies testing the effects of cortisol on transporter/channel expression in a time and dose dependent manner may

present a more accurate insight into the effects of HC on possible increases in *in vitro* CSF secretion, as was seen with our *in vivo* studies.

IL-6 was the only cytokine to show a decrease in CSF secretion rates both in the initial studies and with male rats raised on a normal diet. IL-6 has been shown to decrease Na^+-K^+-ATPase activity in rat hepatocytes (Green et al. 1994) but increased NKCC1 protein expression in mouse dorsal root ganglion nerve cells and α-ENaC protein and mRNA expression in cortical collecting duct cells of the mouse kidney (Li et al. 2010). Based on previous studies, the decreases in CSF secretion associated with IL-6, following *in vivo* studies on male rats raised on a normal diet within our study may be due to decreases in Na^+-K^+-ATPase activity. However, this effect was not seen in any transporter expression within the hCPEpiC. Therefore as mentioned previously in Section 4.1, further experimental studies on the effects of cGMP increases (Siednienko et al. 2011) in the choroid plexus may provide a theory as to the possible cause of decreased CSF secretion associated with IL-6.

4.8 Blood cerebrospinal fluid barrier (BCSFB) enriched transcripts in hCPEpiC following 24h incubation with treatment

Following a human microarray analysis on hCPEpiC we found that 32% of genes analysed were expressed in hCPEpiC. These genes were compared with mouse CP transcripts. Of the 32% positively associated hCPEpiC transcripts, 42% were found to be in common with the mouse CP-enriched transcripts. Of the 59 most highly expressed genes from the mouse CP, 54% were found to be in common with the positively associated hCPEpiC transcripts and these 32 genes are listed in Table 6.4 in Appendix Section 6.10, page 293. In addition, expression of the characterised

proteins, transporters/channels and cytokine receptors that was observed by immunocytochemistry and flow cytometry was confirmed (with the exception of AQP1) by transcriptome analysis in hCPEpiC. These results confirmed that the hCPEpiC genes were somewhat similar to that of the choroid plexus transcriptome expressed in the mouse, as well as highlighting the gene expression of choroid plexus markers, transporters/channels and cytokine receptors originally confirmed following immunocytochemistry and flow cytometry analysis. Further analysis of the effect of 24h treatment incubation on gene expression in hCPEpiC was performed.

Following a 24h incubation with HC, TNF-α or IL-6, on gene expression in hCPEpiC; 15 genes were found to be up-regulated or down-regulated by all three treatments following transcriptome analysis, although none of them statistically significant. Of these, four genes were selected for further real-time quantitative PCR (RT-qPCR) analysis, including *TROVE2* and *NCDN*, which showed an up-regulation, and *SPAG16* and *CCM2* which displayed a down-regulation in gene expression on hCPEpiC, respectively, with all of the three treatments. In addition, two of these genes, *TROVE2* and *SPAG16*, are involved in cilia function and maintenance (Lai et al. 2011) (Zhang et al. 2006).

Defects in cilia have been related to various human diseases including hydrocephalus and neurological disorders that results in increased ICP (Badano et al. 2006). It is known that motile cilia in choroid plexus epithelial cells are involved in direct CSF movement and increases in cilia numbers plays a role in CSF secretion (Albee & Dutcher 2012). These studies found cilia can be motile on the CP

epithelium as on the epithelial surface of respiratory tract, the oviduct, and the fourth ventricle of the brain, where each cell has multiple cilia (Albee & Dutcher 2012). Cilia growth is regulated by intraflagellar transport (IFT). IFT is the bidirectional transport of multi-subunit protein complexes, called IFT particles, along axonemal microtubules beneath the ciliary membrane (Hao & Scholey 2009). IFT is essential for the formation of cilia and is required to build all cilia located within a membrane projection from the cell surface. Mutations in IFT subunits have been shown to disrupt cilia formation and function (Eggenschwiler & Anderson 2007).

Sjögren's syndrome antigen A2 (*SSA2*) (also known as *TROVE2* or *RO60*) is a component of the Ro ribonucleoprotein (Millard et al. 2002) with a von Willebrand factor A (VWA) domain and a so-called TROVE module (found in Telomerase and Ro and Vault proteins) (Bateman & Kickhoefer 2003). Studies by (Lai et al. 2011) have suggested *TROVE2* may play a role in cilia formation and/or maintenance. Changes in cilia structure and function were measured by proteomics analysis and a decrease in total cilia numbers and numbers of long cilia (≥1.5 µm in length) on *SSA2* knockdown was observed in both the murine 3T3 fibroblast cell line and in intermedullary collecting duct (IMCD3) cells when compared to controls (Lai et al. 2011).

Studies have also shown *SPAG16* to play a role in cilia function in mice (Zhang et al. 2006). *SPAG16* encodes Spag16L protein which is found in all murine cells with motile cilia. *SPAG16L mRNA* is expressed in testis, brain, lung, and oviduct, but

not in heart tissue, which does not contain cells with motile cilia (Nagarkatti-Gude et al. 2011), and has been shown to regulate ciliary motility.

The increase in expression of *TROVE2* as seen with the transcriptome analysis of the hCPEpiC following 24h incubation with HC and TNF-α may possibly reflect a role of the *TROVE2* gene in increasing the number of cilia in choroid plexus epithelial cells, possibly leading to an increase in CSF secretion associated with patients with IIH. However, the RT-qPCR results showed no significant changes of gene expression with most treatments. Nevertheless, the down-regulation of *SPAG16* following IL-6 treatment did match the results found in the transcriptome data. Studies by (Nagarkatti-Gude et al. 2011) have shown mice containing a mutation deleting the *SPAG16L* transcript to cause a defect in spermatogenesis, but could also cause decreased ciliary motility. This decrease in ciliary motility and the down-regulation of SPAG16 after treatment with IL-6 may reflect the expression of this gene leading to a decrease in CSF secretion, due to a defect in ciliary function, associated with the CSF secretion results with IL-6 within our study.

4.9 *In vitro* summary

Even though all transporters/channels and cytokine receptors were found to be expressed in hCPEpiC, there was no change in the expression of each of the four transporters, Na^+-K^+-ATPase, NKCC1, AQP1 and ENaC, following a 24h incubation with either HC, TNF-α, IL-6 or IL-17. The lack of transporter/channel modulation changes may be due to a time- or dose-dependent manner or that CSF secretion/drainage rates may not occur through increased transporter expression

but through a different molecular pathway such as increased single K^+ channel activity associated with an increased stimulation by TNF-α (Nakamura et al. 2012). In addition, although the genes encoding the four transporters and cytokine receptors CCR2, IL17α, TNFR1 and IL-6R were found to be expressed, their expression was not increased significantly in a transcriptome analysis of the hCPEpiC following a 24h incubation with either HC, TNF-α or IL-6. Following transcriptome analysis, expression of two genes, TROVE2 and NCDN was increased by cytokines whereas SPAG16 and CCM2 expression decreased (although none of these changes were statistically significant). However, the cytokine-induced expression patterns of all four genes was not confirmed following a RT-qPCR analysis apart from the down-regulation of SPAG16 following IL-6 treatment. As indicated above, SPAG16 has been shown to increase ciliary motility (Zhang et al. 2006), which is associated with increased CSF movement, and may highlight a possible cause of the decrease in CSF secretion associated with IL-6.

4.10 Future work

In addition to earlier suggestions, measuring the levels of sex hormones (oestrogen, progesterone and testosterone) in the serum of female rats raised on both a normal and HF diet, and in conjunction, performing a sex hormone *in vivo* experiment between HF female rats and ovariectomised HF females would determine the sex hormone effects on CSF secretion and resistance to CSF drainage as opposed to diet alone.

In addition, measuring the cytokine plasma levels in all Wistar rats to ascertain the amount of each treatment present within the blood circulation during the time of the experiment would be valuable as added evidence when comparing the CSF secretion rates and resistance to CSF drainage values in all experiments. Further validation of these results could be carried out using specific neutralising antibodies against TNF-α and IL-6 stimulation in an animal model to test whether a decrease/increase, respectively, in CSF secretion is shown following cytokine/glucocorticoid inhibition.

In addition, further studies should be performed *in vivo* to establish the effects of the 11β-HSD1 enzyme on Na^+ movement and CSF secretion. First by investigating the expression of 11β-HSD1 by choroid plexus epithelial cells using immunohistochemistry and then by *in vivo* knock-out of 11β-HSD1. Performing tests, whether general or tissue- and time-specific, could demonstrate a link between cortisol and CSF secretion rate and allow for comparison of the effects seen with hydrocortisone during ventriculo-cisternal perfusion when the 11β-HSD1 enzyme is present or inhibited.

As studies have shown that AQP4 to play an integral role in parenchymal CSF absorption through the glymphatic pathway, which is dependent on osmotic gradients (Bloch et al. 2006); an increase in the expression of AQP4, due to the release of TNF-α, and whether this mechanism is altered in rats fed a HF diet may be beneficial in explaining the decreased resistance to CSF drainage associated with TNF-α in rats raised on a normal diet.

Reference

1. Abbott, N.J., 2004. Evidence for bulk flow of brain interstitial fluid: significance for physiology and pathology. *Neurochemistry International*, 45(4), pp.545–552.
2. Abbott, N.J. et al., 2010. Structure and function of the blood–brain barrier. *Neurobiology of Disease*, 37(1), pp.13–25.
3. Akira, S., Taga, T. & Kishimoto, T., 1993. Interleukin-6 in biology and medicine. *Advances in immunology*, 54, pp.1–78.
4. Albee, A.J. & Dutcher, S.K., 2012. Cilia and human disease. In *eLS*. Chichester, UK: John Wiley & Sons, Ltd.
5. Allt, G. & Lawrenson, J.G., 2001. Pericytes: cell biology and pathology. *Cells, tissues, organs*, 169(1), pp.1–11.
6. Alves, C.H. et al., 2009. Androgen receptor is expressed in murine choroid plexus and downregulated by 5α-Dihydrotestosterone in male and female mice. *Journal of molecular neuroscience*, 38(1), pp.41–49.
7. Anderson, K.E. et al., 1987. Diet-hormone interactions: protein/carbohydrate ratio alters reciprocally the plasma levels of testosterone and cortisol and their respective binding globulins in man. *Life sciences*, 40(18), pp.1761–8.
8. Antinori, S. et al., 2005. The role of cryptococcal antigen assay in diagnosis and monitoring of cryptococcal meningitis. *Journal of clinical microbiology*, 43(11), pp.5828–9.
9. Azizi, G., Khannazer, N. & Mirshafiey, A., 2014. The potential role of chemokines in alzheimer's disease pathogenesis. *American journal of Alzheimer's disease and other dementias*, 29(5), pp. 415-424.
10. Badano, J.L. et al., 2006. The ciliopathies: an emerging class of human genetic disorders. *Annual review of genomics and human genetics*, 7, pp.125–148.
11. Bagga, R. et al., 2005. Choice of therapy and mode of delivery in idiopathic intracranial hypertension during pregnancy. *Medscape general medicine*, 7(4), p.42.
12. Balabanov, R. & Dore-Duffy, P., 1998. Role of the CNS microvascular pericyte in the blood-brain barrier. *Journal of neuroscience research*, 53(6), pp.637–44.
13. Ball, a K. et al., 2009. Elevated cerebrospinal fluid (CSF) leptin in idiopathic intracranial hypertension (IIH): evidence for hypothalamic leptin resistance? *Clinical endocrinology*, 70(6), pp.863–9.
14. Ballabh, P., Braun, A. & Nedergaard, M., 2004. The blood–brain barrier: an overview: Structure, regulation, and clinical implications. *Neurobiology of disease*, 16(1), pp.1–13.
15. Baniak, N. et al., 2012. The cytokines interleukin-1β and tumor necrosis factor-α stimulate CFTR-mediated fluid secretion by swine airway submucosal glands. *American journal of physiology. Lung cellular and molecular physiology*, 303(4), pp.L327–33.
16. Banks, W.A., 2008. The blood-brain barrier as a cause of obesity. *Current pharmaceutical design*, 14(16), pp.1606–14.
17. Bateman, A. & Kickhoefer, V., 2003. The TROVE module: a common element in Telomerase, Ro and Vault ribonucleoproteins. *BMC bioinformatics*, 4, p.49.
18. Bateman, G.A., 2008. Arterial inflow and venous outflow in idiopathic intracranial hypertension associated with venous outflow stenoses. *Journal of clinical neuroscience : official journal of the Neurosurgical Society of Australasia*, 15(4), pp.402–8.

19. Baumgartner, R.N. et al., 1999. Serum leptin in elderly people: associations with sex hormones, insulin, and adipose tissue volumes. *Obesity research*, 7(2), pp.141–9.
20. Bedoui, S. et al., 2005. Unaltered TNF-α production by macrophages and monocytes in diet-induced obesity in the rat. *Journal of Inflammation*, 2(1), p.2.
21. Beltowski, J., 2010. Leptin and the regulation of renal sodium handling and renal Na+- transporting ATPases: Role in the pathogenesis of arterial hypertension. *Current cardiology reviews*, 6(1), pp.31–40.
22. Bergann, T. et al., 2009. Glucocorticoids and tumor necrosis factor-α synergize to induce absorption by the epithelial sodium channel in the colon. *Gastroenterology*, 136(3), pp.933–942.e2.
23. Binder, D.K. et al., 2004. Idiopathic intracranial hypertension. *Neurosurgery*, 54(3), pp.538–51; discussion 551–2.
24. Bloch, O. et al., 2006. Accelerated progression of kaolin-induced hydrocephalus in aquaporin-4-deficient mice. *Journal of cerebral blood flow and metabolism : official journal of the International Society of Cerebral Blood Flow and Metabolism*, 26(12), pp.1527–37.
25. Bloomfield, G.L. et al., 1997. A proposed relationship between increased intra-abdominal, intrathoracic, and intracranial pressure. *Critical care medicine*, 25(March 1997), pp.496–503.
26. Boehm, U. et al., 1997. Cellular responses to interferon-gamma. *Annual review of immunology*, 15, pp.749–95.
27. Brinker, T. et al., 2014. A new look at cerebrospinal fluid circulation. *Fluids and barriers of the CNS*, 11(1), p.10.
28. Brown, P.D. et al., 2004. Molecular Mechanisms of Cerebrospinal Fluid Production. *Neuroscience*, 129(4), pp.957–70.
29. Buyukbese, M.A. et al., 2004. Leptin levels in obese women with and without type 2 diabetes mellitus. *Mediators of inflammation*, 13(5-6), pp.321–5.
30. Cano, P. et al., 2009. Effect of a high-fat diet on 24-hour pattern of circulating adipocytokines in rats. *Obesity (Silver Spring, Md.)*, 17(10), pp.1866–71.
31. Caro, J.F. et al., 1996. Decreased cerebrospinal-fluid/serum leptin ratio in obesity: a possible mechanism for leptin resistance. *Lancet (London, England)*, 348(9021), pp.159–61.
32. Çelebisoy, N. et al., 2007. Treatment of idiopathic intracranial hypertension: Topiramate vs acetazolamide, an open-label study. *Acta Neurologica Scandinavica*, 116(5), pp.322–327.
33. Chapman, K., Holmes, M. & Seckl, J., 2013. 11B-hydroxysteroid dehydrogenases: Intracellular gate-keepers of tissue glucocorticoid action. *Physiological reviews*, 93(3), pp.1139–206.
34. Chen, A. et al., 2005. Diet induction of monocyte chemoattractant protein-1 and its impact on obesity. *Obesity research*, 13(8), pp.1311–20.
35. Clayton, A. et al., 2005. Interleukin-1β differentially regulates β_2 adrenoreceptor and prostaglandin E_2 -mediated cAMP accumulation and chloride efflux from calu-3 bronchial epithelial cells. *Journal of biological chemistry*, 280(25), pp.23451–23463.
36. Conn, P.M. et al., 1986. Synthesis and use of diacylglycerols as activators of protein kinase C in neuroendocrine tissue. *Methods in enzymology*, 124, pp.57–63.
37. Considine, R. V et al., 1996. Serum immunoreactive-leptin concentrations in normal-weight and obese humans. *The New England journal of medicine*, 334(5), pp.292–295.

38. Cora, M.C., Kooistra, L. & Travlos, G., 2015. Vaginal cytology of the laboratory rat and mouse: Review and criteria for the staging of the estrous cycle using stained vaginal smears. *Toxicologic pathology*, 43(6), pp.776–793.
39. Cortez, M. et al., 2013. A high-fat diet increases IL-1, IL-6, and TNF-α production by increasing NF-κB and attenuating PPAR-γ expression in bone marrow mesenchymal stem cells. *Inflammation*, 36(2), pp.379–86.
40. Craig, J.J., Mulholland, D. a. & Gibson, J.M., 2001. Idiopathic intracranial hypertension; incidence, presenting features and outcome in Northern Ireland (1991-1995). *Ulster Medical Journal*, 70(1), pp.31–35.
41. Crum, J., Alvarez, F. & Alvarez-Leefmans, F., 2012. The Apical NKCC1 Cotransporter Debate. *The FASEB Journal*. Available at: http://corescholar.libraries.wright.edu/ncbp/615.
42. Cserr, H.F. & Knopf, P.M., 1992. Cervical lymphatics, the blood-brain barrier and the immunoreactivity of the brain: a new view. *Immunology today*, 13(1990), pp.507–512.
43. Csuka, E. et al., 1999. IL-10 levels in cerebrospinal fluid and serum of patients with severe traumatic brain injury: relationship to IL-6, TNF-alpha, TGF-beta1 and blood-brain barrier function. *Journal of neuroimmunology*, 101(2), pp.211–21.
44. Dagenais, A. et al., 2006. Dexamethasone inhibits the action of TNF on ENaC expression and activity. *American journal of physiology. Lung cellular and molecular physiology*, 291(6), pp.L1220–31.
45. Dagenais, A. et al., 2004. Downregulation of ENaC activity and expression by TNF-α in alveolar epithelial cells. *American journal of physiology - Lung Cellular and Molecular Physiology*, 286(2), pp.301-311.
46. Damkier, H.H., Aalkjaer, C. & Praetorius, J., 2010. Na+-dependent HCO3- import by the slc4a10 gene product involves Cl- export. *The Journal of biological chemistry*, 285(35), pp.26998–7007.
47. Damkier, H.H., Brown, P.D. & Praetorius, J., 2013. Cerebrospinal fluid secretion by the choroid plexus. *Physiological reviews*, 93(4), pp.1847–92.
48. Daneman, R., 2012. The blood-brain barrier in health and disease. *Annals of Neurology*, 72(5), pp.648–672.
49. Davson, H., 1967. Chemical composition and secretory nature of the fluids. In *Physiology of the cerebrospinal Fluid*. London: J & A Churchill, pp. 33–54.
50. Davson, H. et al., 1987. *Physiology and pathophysiology of the cerebrospinal fluid*, Edinburgh: Churchill Livingstone.
51. Deaton, M.A., Glorioso, J.E. & Mclean, D.B., 1999. Congenital Adrenal Hyperplasia: Not Really a Zebra. *American family physician,* 59(5), pp.1190-1196.
52. Deng, Q.S. & Johanson, C.E., 1992. Cyclic AMP alteration of chloride transport into the choroid plexus-cerebrospinal fluid system. *Neuroscience letters*, 143(1-2), pp.146–50.
53. Dhungana, S., Sharrack, B. & Woodroofe, N., 2009. Cytokines and chemokines in idiopathic intracranial hypertension. *Headache*, 49, pp.282–285.
54. Van Dijk, G. et al., 1997. Central leptin stimulates corticosterone secretion at the onset of the dark phase. *Diabetes*, 46(11), pp.1911–4.
55. Dinarello, C.A., 2000. Proinflammatory cytokines. *Chest*, 118(2), pp.503–508.
56. Ding, B. et al., 2014. Direct control of Na+-K+-2Cl--cotransport protein (NKCC1) expression with aldosterone. *AJP: Cell physiology*, 306(1), pp.C66–C75.
57. Donaldson, J.O. & Horak, E., 1982. Cerebrospinal fluid oestrone in pseudotumour cerebri. *Journal of neurology, neurosurgery, and psychiatry*, 45(8), pp.734–6.
58. Du, P., Kibbe, W.A. & Lin, S.M., 2008. lumi: a pipeline for processing Illumina microarray. *Bioinformatics (Oxford, England)*, 24(13), pp.1547–8.

59. Durcan, F.J., Corbett, J.J. & Wall, M., 1988. The incidence of pseudotumor cerebri. Population studies in Iowa and Louisiana. *Archives of neurology*, 45(8), pp.875–877.
60. Edwards, L.J. et al., 2013a. Increased levels of interleukins 2 and 17 in the cerebrospinal fluid of patients with idiopathic intracranial hypertension. *American journal of clinical and experimental immunology*, 2(3), pp.234–44.
61. Edwards, L.J. et al., 2013b. Increased levels of interleukins 2 and 17 in the cerebrospinal fluid of patients with idiopathic intracranial hypertension. *American journal of clinical and experimental immunology*, 2(3), pp.234–44.
62. Eggenschwiler, J.T. & Anderson, K. V, 2007. Cilia and developmental signaling. *Annual review of cell and developmental biology*, 23, pp.345–73.
63. Eisenhut, M. et al., 2006. Changes in ion transport in inflammatory disease. *Journal of inflammation*, 3(1), p.5.
64. Ellis, D.Z., Nathanson, J. a & Sweadner, K.J., 2000. Carbachol inhibits Na(+)-K(+)-ATPase activity in choroid plexus via stimulation of the NO/cGMP pathway. *American journal of physiology. Cell physiology*, 279(6), pp.C1685–C1693.
65. Engeli, S. et al., 2004. Regulation of *11β-HSD* genes in human adipose tissue: Influence of central obesity and weight loss. *Obesity research*, 12(1), pp.9–17.
66. Escher, G. et al., 1997. Tumor necrosis factor alpha and interleukin 1beta enhance the cortisone/cortisol shuttle. *J Exp Med*, 186(2), pp.189–198.
67. Van Everbroeck, B. et al., The role of cytokines, astrocytes, microglia and apoptosis in Creutzfeldt-Jakob disease. *Neurobiology of aging*, 23(1), pp.59–64.
68. Fain, J.N., 2006. Release of interleukins and other inflammatory cytokines by human adipose tissue is enhanced in obesity and primarily due to the nonfat cells. *Vitamins and hormones*, 74, pp.443–77.
69. Farb, R.I. et al., 2003. Idiopathic intracranial hypertension: the prevalence and morphology of sinovenous stenosis. *Neurology*, 60(9), pp.1418–24.
70. Fisone, G. et al., 1995. Na+,K(+)-ATPase in the choroid plexus. Regulation by serotonin/protein kinase C pathway. *J Biol Chem*, 270(6), pp.2427–2430.
71. Flier, J.S., 2004. Obesity Wars: Molecular Progress Confronts an Expanding Epidemic. *Cell*, 116(2), pp.337–350.
72. Forte, P. et al., 1998. Evidence for a difference in nitric oxide biosynthesis between healthy women and men. *Hypertension*, 32(4), pp.730–4.
73. Friedman, D.I. & Jacobson, D.M., 2002. Diagnostic criteria for idiopathic intracranial hypertension. *Neurology*, 59(10), pp.1492–1495.
74. Fries, B.C. et al., 2005. Phenotypic switching of Cryptococcus neoformans can produce variants that elicit increased intracranial pressure in a rat model of cryptococcal meningoencephalitis. *Infection and immunity*, 73(3), pp.1779–87.
75. Fries, B.C. et al., 2001. Phenotypic switching of Cryptococcus neoformans occurs in vivo and influences the outcome of infection. *The Journal of clinical investigation*, 108(11), pp.1639–48.
76. Galien, R. & Garcia, T., 1997. Estrogen receptor impairs interleukin-6 expression by preventing protein binding on the NF-κB site. *Nucleic Acids Research*, 25(12), pp.2424–2429.
77. Galvin, J. a. & Van Stavern, G.P., 2004. Clinical characterization of idiopathic intracranial hypertension at the Detroit Medical Center. *Journal of the Neurological Sciences*, 223, pp.157–160.
78. Gerhardt, C.C. et al., 2001. Chemokines control fat accumulation and leptin secretion by cultured human adipocytes. *Molecular and cellular endocrinology*, 175(1-2), pp.81–92.

79. Girasole, G. et al., 1992. 17 beta-estradiol inhibits interleukin-6 production by bone marrow-derived stromal cells and osteoblasts in vitro: a potential mechanism for the antiosteoporotic effect of estrogens. *Journal of clinical investigation*, 89(3), pp.883–891.
80. Giugliano, D. et al., 1997. Vascular effects of acute hyperglycemia in humans are reversed by L-arginine. Evidence for reduced availability of nitric oxide during hyperglycemia. *Circulation*, 95(7), pp.1783–90.
81. Giuseffi, V. et al., 1991. Symptoms and disease associations in idiopathic intracranial hypertension (pseudotumor cerebri): a case-control study. *Neurology*, 41(2 (Pt 1)), pp.239–44.
82. Glueck, C.J., Aregawi, D., et al., 2005. Idiopathic intracranial hypertension, polycystic-ovary syndrome, and thrombophilia. *The Journal of laboratory and clinical medicine*, 145(2), pp.72–82.
83. Glueck, C.J. et al., 2003. Idiopathic intracranial hypertension: associations with coagulation disorders and polycystic-ovary syndrome. *Journal of Laboratory and Clinical Medicine*, 142(1), pp.35–45.
84. Glueck, C.J., Goldenberg, N., et al., 2005. Idiopathic intracranial hypertension: associations with thrombophilia and hypofibrinolysis in men. *Clinical and applied thrombosis/hemostasis : official journal of the International Academy of Clinical and Applied Thrombosis/Hemostasis*, 11(4), pp.441–448.
85. Gomez-Sanchez, E.P. et al., 2003. Regulation of 11 beta-hydroxysteroid dehydrogenase enzymes in the rat kidney by estradiol. *American journal of physiology. Endocrinology and metabolism*, 285(2), pp.E272–E279.
86. Goodwin, J., 2003. Recent developments in idiopathic intracranial hypertension (IIH). *Seminars in ophthalmology*, 18(4), pp.181–9.
87. Gorgacz, E.J. et al., 1975. Morphologic alterations associated with decreased cerebrospinal fluid pressure in chronic bovine hypervitaminosis A. *American journal of veterinary research*, 36(2), pp.171–80.
88. Gray, T. et al., 2004. Regulation of MUC5AC mucin secretion and airway surface liquid metabolism by IL-1beta in human bronchial epithelia. *American journal of physiology. Lung cellular and molecular physiology*, 286(2), pp.L320–30.
89. Graybill, J.R. et al., 2000. Diagnosis and management of increased intracranial pressure in patients with AIDS and cryptococcal meningitis. The NIAID Mycoses Study Group and AIDS Cooperative Treatment Groups. *Clinical infectious diseases : an official publication of the Infectious Diseases Society of America*, 30(1), pp.47–54.
90. Green, R.M. et al., 1994. Interleukin-6 inhibits hepatocyte taurocholate uptake and sodium-potassium-adenosinetriphosphatase activity. *The American journal of physiology*, 267(6 Pt 1), pp.G1094–100.
91. Griffin, G.K. et al., 2012. IL-17 and TNF-α sustain neutrophil recruitment during inflammation through synergistic effects on endothelial activation. *Journal of immunology (Baltimore, Md. : 1950)*, 188(12), pp.6287–99.
92. Guerra, R.L. et al., 2007. Effects of 2 or 5 consecutive exercise days on adipocyte area and lipid parameters in Wistar rats. *Lipids in Health and Disease*, 6(1), p.16.
93. Hamann, A. et al., 1995. Characterization of insulin resistance and NIDDM in transgenic mice with reduced brown fat. *Diabetes*, 44(11), pp.1266–73.
94. Hao, L. & Scholey, J.M., 2009. Intraflagellar transport at a glance. *Journal of cell science*, 122(Pt 7), pp.889–92.

95. Haselbach, M. et al., 2001. Porcine Choroid plexus epithelial cells in culture: regulation of barrier properties and transport processes. *Microscopy research and technique*, 52(1), pp.137–152.
96. Hayakata, T. et al., 2004. Changes in CSF S100B and cytokine concentrations in early-phase severe traumatic brain injury. *Shock (Augusta, Ga.)*, 22(2), pp.102–107.
97. Hershko, D.D. et al., 2002. Multiple transcription factors regulating the IL-6 gene are activated by cAMP in cultured Caco-2 cells. *American journal of physiology - regulatory, integrative and comparative physiology*, 283(5), pp.R1140–R1148.
98. Hertz, L. et al., 2013. Astrocytic and neuronal accumulation of elevated extracellular K+ with a 2/3 K+/Na+ flux ratio—consequences for energy metabolism, osmolarity and higher brain function. *Frontiers in computational neuroscience*, 7, p.114.
99. Higgins, J.N.P. et al., 2004. MR venography in idiopathic intracranial hypertension: unappreciated and misunderstood. *Journal of neurology, neurosurgery, and psychiatry*, 75(4), pp.621–5.
100. Hladky, S.B. & Barrand, M.A., 2016. Fluid and ion transfer across the blood–brain and blood–cerebrospinal fluid barriers; a comparative account of mechanisms and roles. *Fluids and Barriers of the CNS*, 13(1), p.19.
101. Hot, A. et al., 2013. Simvastatin inhibits the pro-inflammatory and pro-thrombotic effects of IL-17 and TNF-α on endothelial cells. *Annals of the rheumatic diseases*, 72(5), pp.754–760.
102. Hotamisligil, G.S. et al., 1997. Differential regulation of the p80 tumor necrosis factor receptor in human obesity and insulin resistance. *Diabetes*, 46(3), pp.451–5.
103. Hotamisligil, G.S. et al., 1995. Increased adipose tissue expression of tumor necrosis factor-alpha in human obesity and insulin resistance. *The Journal of clinical investigation*, 95(5), pp.2409–15.
104. Hotamisligil, G.S., Shargill, N.S. & Spiegelman, B.M., 1993. Adipose expression of tumor necrosis factor-alpha: direct role in obesity-linked insulin resistance. *Science (New York, N.Y.)*, 259(5091), pp.87–91.
105. Hu, G.-X. et al., 2013. Curcumin as a potent and selective Inhibitor of 11β-hydroxysteroid dehydrogenase 1: Improving lipid profiles in high-fat-diet-treated rats C. Verma, ed. *PLoS ONE*, 8(3), p.e49976.
106. Huber, J. et al., 2008. CC chemokine and CC chemokine receptor Profiles in visceral and subcutaneous adipose tissue are altered in human obesity. *The journal of clinical endocrinology & metabolism*, 93(8), pp.3215–3221.
107. Iliff, J.J. et al., 2012. A paravascular pathway facilitates CSF flow through the brain parenchyma and the clearance of interstitial solutes, including amyloid β. *Science translational medicine*, 4(147), p.147ra111.
108. Jackson, E.K. & Li, P., 1997. Human leptin has natriuretic activity in the rat. *Am J Physiol*, 272(3 Pt 2), pp.F333–8.
109. Janer, C. et al., 2011. Airway expression of the epithelial sodium shannel alpha-subunit correlates with cortisol in term newborns. *Pediatrics*, 128(2), pp.e414–e421.
110. Jesse, N.M. et al., 2009. Expression of ENaC subunits, chloride channels, and aquaporins in ovine fetal lung: ontogeny of expression and effects of altered fetal cortisol concentrations. *AJP: Regulatory, integrative and comparative physiology*, 297(2), pp.R453–R461.
111. Jilka, R.L. et al., 1992. Increased osteoclast development after estrogen loss: mediation by interleukin-6. *Science (New York, N.Y.)*, 257(5066), pp.88–91.

112. Jilma, B. & Jilma-Stohlawetz, P., 2002. F emale gender, menstrual cycle and estradiol affect plasma levels of monocyte chemotactic protein-1 (MCP-1) in humans. *Cardiovascular research*, 55, p. 416.
113. Johanson, C.E. et al., 2008. Multiplicity of cerebrospinal fluid functions: New challenges in health and disease. *Cerebrospinal fluid research*, 5, p.10.
114. Johnston, M. & Papaiconomou, C., 2002. Cerebrospinal Fluid Transport: a Lymphatic Perspective. *Physiology*, 17(6). Available at: http://physiologyonline.physiology.org/content/17/6/227.
115. Johnston, M. et al., 2004. Evidence of connections between cerebrospinal fluid and nasal lymphatic vessels in humans, non-human primates and other mammalian species. *Cerebrospinal fluid research*, 1(1), p.2.
116. Jones, H.C., Deane, R. & Bucknall, R.M., 1987. Developmental changes in cerebrospinal fluid pressure and resistance to absorption in rats. *Brain research*, 430(1), pp.23–30.
117. Jovanovic, D. V et al., 1998. IL-17 stimulates the production and expression of proinflammatory cytokines, IL-β and TNF-α, by human macrophages. *The journal of immunology* , 160 (7), pp.3513–3521.
118. Kandel, E.R., Schwartz, J.H. & Jessel, T.M., 2000. Principles of neural science. New York: McGraw-Hill. Vol. 4. pp. 1227-1246.
119. Keep, R.F., Xiang, J. & Betz, A.L., 1994. Potassium cotransport at the rat choroid plexus. *The American journal of physiology*, 267(6 Pt 1), pp.C1616–22.
120. Kern, P.A. et al., 1995. The expression of tumor necrosis factor in human adipose tissue. Regulation by obesity, weight loss, and relationship to lipoprotein lipase. *The journal of clinical investigation*, 95(5), pp.2111–9.
121. Kesler, a & Gadoth, N., 2001. Epidemiology of idiopathic intracranial hypertension in Israel. *Journal of neuro-ophthalmology : the official journal of the North American neuro-ophthalmology society*, 21(1), pp.12–14.
122. Kesler, A. et al., 2006. Increased red blood cell aggregation in patients with idiopathic intracranial hypertension. A hitherto unexplored pathophysiological pathway. *Thrombosis and haemostasis*, 96(4), pp.483–7.
123. Kida, S. et al., 1988. A light and electron microscopic and immunohistochemical study of human arachnoid villi. *Journal of neurosurgery*, 69(3), pp.429–35.
124. Kida, S., Pantazis, a & Weller, R.O., 1993. CSF drains directly from the subarachnoid space into nasal lymphatics in the rat. Anatomy, histology and immunological significance. *Neuropathology and applied neurobiology*, 19(6), pp.480–488.
125. Kiilerich, P. et al., 2011. Differential effects of cortisol and 11-deoxycorticosterone on ion transport protein mRNA levels in gills of two euryhaline teleosts, Mozambique tilapia (Oreochromis mossambicus) and striped bass (Morone saxatilis). *The Journal of endocrinology*, 209(1), pp.115–26.
126. Kim, J.G. et al., 2007. Thyroid transcription factor-1 facilitates cerebrospinal fluid formation by regulating aquaporin-1 synthesis in the brain. *The Journal of biological chemistry*, 282(20), pp.14923–31.
127. Klein, A. et al., 2013. Hyperandrogenism is associated with earlier age of onset of idiopathic intracranial hypertension in women. *Current eye research*, 38(9), pp.972–976.
128. Klok, M.D., Jakobsdottir, S. & Drent, M.L., 2007. The role of leptin and ghrelin in the regulation of food intake and body weight in humans: A review. *Obesity reviews*, 8(1), pp.21–34.

129. Kolb, J.P. et al., 1994. Interleukin-4 stimulates cGMP production by IFN-gamma-activated human monocytes. Involvement of the nitric oxide synthase pathway. *The Journal of biological chemistry*, 269(13), pp.9811–6.
130. Kotera, T. & Brown, P.D., 1994. Evidence for two types of potassium current in rat choroid plexus epithelial cells. *Pflügers Archiv : European journal of physiology*, 427(3-4), pp.317–24.
131. Kreydiyyeh, S.I. et al., 2007. TNF-α modulates hepatic Na+-K+ ATPase activity via PGE2 and EP2 receptors. *Prostaglandins & Other Lipid Mediators*, 83(4), pp.295–303.
132. Kupersmith, M.J. et al., 1998. Effects of weight loss on the course of idiopathic intracranial hypertension in women. *Neurology*, 50(4), pp.1094–8.
133. Lai, C.K. et al., 2011. Functional characterization of putative cilia genes by high-content analysis. *Molecular biology of the cell*, 22(7), pp.1104–1119.
134. Laman, J.D. & Weller, R.O., 2013. Drainage of Cells and Soluble Antigen from the CNS to regional lymph nodes. *Journal of neuroimmune pharmacology*, 8(4), pp.840–856.
135. Leonard, M. et al., 1999. Role of MAP kinase pathways in mediating IL-6 production in human primary mesangial and proximal tubular cells. *Kidney international*, 56(4), pp.1366–1377.
136. Lepercq, J. et al., 2001. Prenatal leptin production: evidence that fetal adipose tissue produces leptin. *The Journal of clinical endocrinology and metabolism*, 86(6), pp.2409–13.
137. Li, K. et al., 2010. Interleukin-6 stimulates epithelial sodium channels in mouse cortical collecting duct cells. *American journal of physiology. Regulatory, integrative and comparative physiology*, 299(2), pp.R590–5.
138. Li, S. et al., 2012. IL-17 and IL-22 in cerebrospinal fluid and plasma are elevated in Guillain-Barré syndrome. *Mediators of inflammation*, 2012, p.260473.
139. Liang, H. et al., 2008. Blockade of tumor necrosis factor (TNF) receptor type 1-mediated TNF-α signaling protected wistar rats from diet-induced obesity and insulin resistance. *Endocrinology*, 149(6), pp.2943–2951.
140. Lindvall-Axelsson, M. & Owman, C., 1989. Changes in transport functions of isolated rabbit choroid plexus under the influence of oestrogen and progesterone. *Acta physiologica scandinavica*, 136(1), pp.107–111.
141. Liu, G.T., Glaser, J.S. & Schatz, N.J., 1994. High-dose methylprednisolone and acetazolamide for visual loss in pseudotumor cerebri. *American journal of ophthalmology*, 118(1), pp.88–96.
142. Liu, H. et al., 2003. Aquaporin gene expression and regulation in the ovine fetal lung. *The Journal of physiology*, 551(Pt 2), pp.503–14.
143. Lobato-Álvarez, J.A. et al., 2016. The apical localization of Na(+), K(+)-ATPase in cultured human retinal pigment epithelial cells depends on expression of the β2 subunit. *Frontiers in physiology*, 7, p.450.
144. Lombardi, A. et al., 2009. Molecular mechanisms underlying the pro-inflammatory synergistic effect of tumor necrosis factor alpha and interferon gamma in human microvascular endothelium. *European journal of cell biology*, 88(12), pp.731–42.
145. Losada, a et al., 2000. Down-regulation of thyroid transcription factor-1 gene expression in fetal lung hypoplasia is restored by glucocorticoids. *Endocrinology*, 141(6), pp.2166–73.
146. Louveau, A. et al., 2015. Structural and functional features of central nervous system lymphatic vessels. *Nature*, 523(7560), pp.337–341.

147. Lucki, N.C. & Sewer, M.B., 2008. Multiple roles for sphingolipids in steroid hormone biosynthesis. *Sub-cellular biochemistry*, 49, pp.387–412.
148. Lyon, C.J., Law, R.E. & Hsueh, W. a., 2003. Minireview: Adiposity, inflammation, and atherogenesis. *Endocrinology*, 144(6), pp.2195–2200.
149. Mackenzie, P.J. & Cioffi, G.A., 2008. Vascular anatomy of the optic nerve head. *Canadian journal of ophthalmology. Journal canadien d'ophtalmologie*, 43(3), pp.308–12.
150. Mackman, N., 2012. New insights into the mechanisms of venous thrombosis. *Journal of clinical investigation*, 122(7), pp.2331–2336.
151. Mackman, N., 2008. Triggers, targets and treatments for thrombosis. *Nature*, 451(7181), pp.914–918.
152. Markey, K.A. et al., 2016. Idiopathic intracranial hypertension, hormones, and 11β-hydroxysteroid dehydrogenases. *Journal of pain research*, 9, pp.223–32.
153. Marks, L.J., Friedman, G.R. & Duncan, F.J., 1961. Effect of estrogen administration on hydrocortisone metabolism in man. *The Journal of laboratory and clinical medicine*, 57, pp.47–53.
154. Masuzawa, T. & Sato, F., 1983. The enzyme histochemistry of the choroid plexus. *Brain : a journal of neurology*, 106 (Pt 1), pp.55–99.
155. McCoy, M.K. & Tansey, M.G., 2008. TNF signaling inhibition in the CNS: implications for normal brain function and neurodegenerative disease. *Journal of neuroinflammation*, 5, p.45.
156. Mikula, M. et al., 2014. Obesity increases histone H3 lysine 9 and 18 acetylation at Tnfa and Ccl2 genes in mouse liver. *International journal of molecular medicine*, 34(6), pp.1647–54.
157. Millard, T.P. et al., 2002. Human Ro60 (SSA2) genomic organization and sequence alterations, examined in cutaneous lupus erythematosus. *The British journal of dermatology*, 146(2), pp.210–5.
158. Millen, J.W. & Woollam, D.H.M., 1956. The effect of the duration of vitamin-A deficiency in female rabbits upon the incidence of hydrocephalus in their young. *Journal of neurology, neurosurgery and psychiatry*, 19.
159. Mitchell, K. et al., 2009. Monocyte chemoattractant protein-1 in the choroid plexus: a potential link between vascular pro-inflammatory mediators and the CNS during peripheral tissue inflammation. *Neuroscience*, 158(2), pp.885–95.
160. Mollan, S.P. et al., Evolving evidence in adult idiopathic intracranial hypertension: pathophysiology and management. *Journal of neurology, neurosurgery and psychiatry,* 10.
161. Morrison, C.D., 2009. Leptin signaling in brain: A link between nutrition and cognition? *Biochimica et biophysica acta (BBA) - molecular basis of disease*, 1792(5), pp.401–408.
162. Morrison, J.L. et al., 2012. Antenatal steroids and the IUGR fetus: Are exposure and physiological effects on the lung and cardiovascular system the same as in normally grown fetuses? *Journal of pregnancy*, 2012, pp.1–15.
163. Motulsky, E. et al., 2010. Aquaporin expression in blood-retinal barrier cells during experimental autoimmune uveitis. *Molecular vision*, 16, pp.602–10.
164. Murphy, P.M. et al., 2000. International union of pharmacology. XXII. Nomenclature for chemokine receptors. *Pharmacological reviews*, 52(1), pp.145–76.
165. Naderali, E.K. et al., 2001. Dietary obesity in the rat induces endothelial dysfunction without causing insulin resistance: a possible role for triacylglycerols. *Clinical science*, 101, pp.499–506.

166. Nagarkatti-Gude, D.R. et al., 2011. Spag16, an axonemal central apparatus gene, encodes a male germ cell nuclear speckle protein that regulates SPAG16 mRNA expression. *PloS one*, 6(5), p.e20625.
167. Nakamura, K., Komagiri, Y. & Kubokawa, M., 2012. Effects of cytokines on potassium channels in renal tubular epithelia. *Clinical and experimental nephrology*, 16(1), pp.55–60.
168. Neville, B.G. & Wilson, J., 1970. Benign intracranial hypertension following corticosteroid withdrawal in childhood. *British medical journal*, 3(5722), pp.554–6.
169. Newborg, B., 1974. Pseudotumor cerebri treated by rice reduction diet. *Archives of internal medicine*, 133(5), pp.802–7.
170. O'Reilly, M.W. et al., 2014. Hyperandrogenemia predicts metabolic phenotype in polycystic ovary syndrome: The utility of serum androstenedione. *The journal of clinical endocrinology & metabolism*, 99(3), pp.1027–1036.
171. Odermatt, A. et al., 1999. The N-terminal anchor sequences of 11??-hydroxysteroid dehydrogenases determine their orientation in the endoplasmic reticulum membrane. *Journal of biological chemistry*, 274, pp.28762–28770.
172. Orefice, G. et al., 1992. Radioisotopic cisternography in benign intracranial hypertension of young obese women. A seven-case study and pathogenetic suggestions. *Acta neurologica*, 14(1), pp.39–50.
173. Oshio, K. et al., 2005. Reduced cerebrospinal fluid production and intracranial pressure in mice lacking choroid plexus water channel aquaporin-1. *The FASEB journal : official publication of the federation of American societies for experimental biology*, 19(1), pp.76–78.
174. Paine, R. et al., 1993. MCP-1 expression by rat type II alveolar epithelial cells in primary culture. *Journal of immunology (Baltimore, Md. : 1950)*, 150(10), pp.4561–70.
175. Palmon, S.C. et al., 1998. Estrogen increases cGMP in selected brain regions and in cerebral microvessels. *Journal of cerebral blood flow & metabolism*, pp.1248–1252.
176. Pandzic Jaksic, V. et al., 2013. Association of monocyte CCR2 expression with obesity and insulin resistance in postmenopausal women. *Clinical and investigative medicine. Medecine clinique et experimentale*, 36(1), pp.E24–31.
177. Park, H.S., Park, J.Y. & Yu, R., 2005. Relationship of obesity and visceral adiposity with serum concentrations of CRP, TNF-alpha and IL-6. *Diabetes research and clinical practice*, 69(1), pp.29–35.
178. Park, S. et al., 2014. Secondary intracranial hypertension from testosterone therapy in a transgender patient. *Seminars in ophthalmology*, 29(3), pp.156–158.
179. Parker, M.D. et al., 2008. Characterization of Human SLC4A10 as an Electroneutral Na/HCO3 Cotransporter (NBCn2) with Cl- Self-exchange Activity. *Journal of Biological Chemistry*, 283(19), pp.12777–12788.
180. Pazos, A., Hoyer, D. & Palacios, J.M., 1984. The binding of serotonergic ligands to the porcine choroid plexus: Characterization of a new type of serotonin recognition site. *European journal of pharmacology*, 106(3), pp.539–546.
181. Pearce, J.M.S., 2009. From pseudotumour cerebri to idiopathic intracranial hypertension. *Practical neurology*, 9(6), pp.353–6.
182. Peluso, I. et al., 2012. High fat meal increase of IL-17 is prevented by ingestion of fruit juice drink in healthy overweight subjects. *Current pharmaceutical design*, 18(1), pp.85–90.
183. Perekhval'skaia, T. V et al., 1987. [Effect of vasopressin, aldosterone and angiotensin on the permeability of the choroid plexus to water]. *Fiziologicheskii*

zhurnal SSSR imeni I. M. Sechenova, 73(3), pp.424–9.
184. Pfeiffer, A. et al., 1997. Circulating tumor necrosis factor alpha is elevated in male but not in female patients with type II diabetes mellitus. *Hormone and metabolic research*, 29(3), pp.111–4.
185. Pietropaoli, A.P., 2004. Gender differences in the sepsis syndrome: Clinical evidence and potential mechanisms. In *principles of gender-specific medicine*. pp. 360–373.
186. Pott Godoy, M.C. et al., 2008. Central and systemic IL-1 exacerbates neurodegeneration and motor symptoms in a model of Parkinson's disease. *Brain: A journal of neurology*, 131(Pt 7), pp.1880–94.
187. Prodjosudjadi, W. et al., 1995. Production and cytokine-mediated regulation of monocyte chemoattractant protein-1 by human proximal tubular epithelial cells. *Kidney Int*, 48(5), pp.1477–1486.
188. Radhakrishnan, K. et al., 1993. Epidemiology of idiopathic intracranial hypertension: a prospective and case-control study. *Journal of the neurological sciences*, 116(1), pp.18–28.
189. Ramesh, G. et al., 2013. Cytokines and chemokines at the crossroads of neuroinflammation, neurodegeneration, and neuropathic pain. *Mediators of inflammation*, 2013, pp.1–20.
190. Ransohoff, R.M., 2002. The chemokine system in neuroinflammation: An update. *The journal of infectious diseases*, 186(s2), pp.S152–S156.
191. Raoof, N. et al., 2011. The incidence and prevalence of idiopathic intracranial hypertension in Sheffield, UK. *European journal of neurology*, 18, pp.1266–1268.
192. Rash, J.E. et al., 1998. Direct immunogold labeling of aquaporin-4 in square arrays of astrocyte and ependymocyte plasma membranes in rat brain and spinal cord. *Proceedings of the national academy of sciences of the United States of America*, 95(20), pp.11981–6.
193. Raubenheimer, P.J. et al., 2006. The role of corticosterone in human hypothalamic– pituitary–adrenal axis feedback. *Clinical Endocrinology*, 65, pp.22–26.
194. Rauz, S. et al., 2003. Expression and distribution of the serum and glucocorticoid regulated kinase and the epithelial sodium channel subunits in the human cornea. *Experimental eye research*, 77(1), pp.101–108.
195. Rauz, S. et al., 2001. Expression and putative role of 11 beta-hydroxysteroid dehydrogenase isozymes within the human eye. *Investigative ophthalmology & visual science*, 42(9), pp.2037–42.
196. Rays, A., Prefontaine, K.E. & Ray, P., 1994. Down-modulation of interleukin-6 gene expression by l7p-estradiol in the absence of high affinity DNA binding by the estrogen receptor. The journal of bilogical chemistry, 269(17), pp.12940–12946.
197. Redzic, Z.B., 2013a. Studies on the human choroid plexus in vitro. *Fluids and barriers of the CNS*, 10(1), p.10.
198. Redzic, Z.B., 2013b. Studies on the human choroid plexus in vitro. *Fluids and barriers of the CNS*, 10(1), p.10.
199. Redzic, Z.B. et al., 2005. The choroid plexus-cerebrospinal fluid system: From development to aging. *Current topics in developmental biology*, 71, pp.1-52.
200. ReihaniKermani, H. et al., 2008. Cerebrospinal fluid concentration of interleukin-6 and interleukin-10 in idiopathic intracranial hypertension. *The journal of medical sciences(Faisalabad)*, 8(2), pp.205-208.
201. Rexrode, K.M. et al., 2003. Relationship of total and abdominal adiposity with CRP and IL-6 in women. *Annals of epidemiology*, 13(10), pp.674–82.

202. Reynolds, E.S., 1963. The use of lead citrate at high pH as an electron-opaque stain in electron microscopy. *The Journal of cell biology*, 17(1), pp.208–12.
203. Ritchie, M.E. et al., 2015. limma powers differential expression analyses for RNA-sequencing and microarray studies. *Nucleic acids research*, 43(7), p.e47.
204. Rizzolo, L.J., 1998. Polarization of the Na+, K+-ATPase in epithelia derived from the neuroepithelium. *International review of cytology*, 185, pp.195–235.
205. Romanatto, T. et al., 2009. Deletion of tumor necrosis factor-alpha receptor 1 (TNFR1) protects against diet-induced obesity by means of increased thermogenesis. *The journal of biological chemistry,* 284(52), pp. 36213-36222.
206. Rönnemaa, T., Pulkki, K. & Kaprio, J., 2000. Serum soluble tumor necrosis factor-α receptor 2 is elevated in bbesity but is not related to insulin sensitivity: A study in identical twins discordant for obesity. *The journal of clinical endocrinology & metabolism*, 85(8), pp.2728–2732.
207. Rosenberg, M.L. et al., 1993. Cerebrospinal fluid diversion procedures in pseudotumor cerebri. *Neurology*, 43(6), pp.1071–1072.
208. Roux, J. et al., 2005. Interleukin-1beta decreases expression of the epithelial sodium channel alpha-subunit in alveolar epithelial cells via a p38 MAPK-dependent signaling pathway. *The Journal of biological chemistry*, 280(19), pp.18579–89.
209. Rowe, F.J. & Sarkies, N.J., 1998. Assessment of visual function in idiopathic intracranial hypertension: A prospective study. *Eye*, 12(1), pp.111–118.
210. Rowe, F.J. & Sarkies, N.J., 1999. The relationship between obesity and idiopathic intracranial hypertension. *International journal of obesity and related metabolic disorders : journal of the international association for the study of obesity*, 23(1), pp.54–9.
211. Ruhl, C.E. & Everhart, J.E., 2001. Leptin concentrations in the United States: relations with demographic and anthropometric measures. *The American journal of clinical nutrition*, 74(3), pp.295–301.
212. Russell, J.M., 2000. Sodium-potassium-chloride cotransport. *Physiol Rev*, 80(1), pp.211–276.
213. Saghizadeh, M. et al., 1996. The expression of TNF alpha by human muscle. Relationship to insulin resistance. *The Journal of clinical investigation*, 97(4), pp.1111–6.
214. Saito, Y. & Wright, E.M., 1983. Bicarbonate transport across the frog choroid plexus and its control by cyclic nucleotides. *The Journal of physiology*, 336, pp.635–48.
215. Saito, Y. & Wright, E.M., 1984. Regulation of bicarbonate transport across the brush border membrane of the bull-frog choroid plexus. *The Journal of physiology*, 350, pp.327–42.
216. Das Sarma, J. et al., 2009. Functional interleukin-17 receptor A is expressed in central nervous system glia and upregulated in experimental autoimmune encephalomyelitis. *Journal of neuroinflammation*, 6, p.14. A
217. Schwartz, M.W. et al., 1996. Identification of targets of leptin action in rat hypothalamus. *The Journal of clinical investigation*, 98(5), pp.1101–6.
218. Sharman, M.J. & Volek, J.S., 2004. Weight loss leads to reductions in inflammatory biomarkers after a very-low-carbohydrate diet and a low-fat diet in overweight men. *Clinical science (London, England : 1979)*, 107(4), pp.365–9.
219. Shoelson, S.E., Herrero, L. & Naaz, A., 2007. Obesity, inflammation, and insulin resistance. *Gastroenterology*, 132(6), pp.2169–80.

220. Siednienko, J. et al., 2011. Nitric oxide affects IL-6 expression in human peripheral blood mononuclear cells involving cGMP-dependent modulation of NF-κB activity. *Cytokine*, 54, pp.282–8.
221. Simons, P.J. et al., 2005. Cytokine-mediated modulation of leptin and adiponectin secretion during in vitro adipogenesis: evidence that tumor necrosis factor-alpha- and interleukin-1beta-treated human preadipocytes are potent leptin producers. *Cytokine*, 32(2), pp.94–103.
222. Sinclair, A.J., Walker, E.A., et al., 2010. Cerebrospinal fluid corticosteroid levels and cortisol metabolism in patients with idiopathic intracranial hypertension: a link between 11beta-HSD1 and intracranial pressure regulation? *The Journal of clinical endocrinology and metabolism*, 95(12), pp.5348–5356.
223. Sinclair, A.J. et al., 2007. Corticosteroids, 11B-hydroxysteroid dehydrogenase isozymes and the rabbit choroid plexus. *Journal of neuroendocrinology*, 19(8), pp.614–620.
224. Sinclair, A.J. et al., 2008. Exploring the pathogenesis of IIH: An inflammatory perspective. *Journal of neuroimmunology*, 201–202, pp.212–220.
225. Sinclair, A.J., Burdon, M.A., et al., 2010. Low energy diet and intracranial pressure in women with idiopathic intracranial hypertension: prospective cohort study. *BMJ (Clinical research ed.)*, 341(8), p.c2701.
226. Sindhu, S. et al., 2015. Obesity Is a positive modulator of IL-6R and IL-6 expression in the subcutaneous adipose tissue: Significance for metabolic inflammation. *PloS one*, 10(7), p.e0133494.
227. Singhal, A. et al., 2002. Association between cerebrospinal fluid interleukin-6 concentrations and outcome after severe human traumatic brain injury. *Journal of neurotrauma*, 19(8), pp.929–937.
228. Sobhani, I. et al., 2000. Leptin secretion and leptin receptor in the human stomach. *Gut*, 47(2), pp.178–83.
229. Söderberg, S. et al., 2001. A strong association between biologically active testosterone and leptin in non-obese men and women is lost with increasing (central) adiposity. *International journal of obesity and related metabolic disorders : journal of the international association for the study of obesity*, 25(1), pp.98–105.
230. Sonnenberg, S. et al., 2008. Level of ex vivo interleukin 6 expression in human peripheral fat compared with other tissues. *European journal of vascular and endovascular surgery*, 35(3), pp.314–319.
231. Speake, T. et al., 2001. Mechanisms of CSF secretion by the choroid plexus. *Microscopy research and technique*, 52(1), pp.49–59.
232. Sperry, J.L. et al., 2008. Male gender is associated with excessive IL-6 expression following severe injury. *The Journal of trauma*, 64(3), pp.572–8; discussion 578–9.
233. Steardo, L. & Nathanson, J. a, 1987. Brain barrier tissues: end organs for atriopeptins. *Science (New York, N.Y.)*, 235(4787), pp.470–3.
234. Stemmer, K. et al., 2012. High-fat-diet-induced obesity causes an inflammatory and tumor-promoting microenvironment in the rat kidney. *Disease models & mechanisms*, 5(5), pp.627–35.
235. Stoenoiu, M.S. et al., 2003. Corticosteroids induce expression of aquaporin-1 and increase transcellular water transport in rat peritoneum. *Journal of the american society of nephrology : JASN*, 14(3), pp.555–65.
236. Stover, J.F. et al., 2000. Temporal profile of cerebrospinal fluid glutamate, interleukin-6, and tumor necrosis factor-alpha in relation to brain edema and

contusion following controlled cortical impact injury in rats. *Neuroscience letters*, 288(1), pp.25–8.
237. Straczkowski, M. et al., 2002. Plasma interleukin-8 concentrations are increased in obese subjects and related to fat mass and tumor necrosis factor-alpha system. *The Journal of clinical endocrinology and metabolism*, 87(10), pp.4602–6.
238. Strahle, J. et al., 2012. Mechanisms of hydrocephalus after neonatal and adult intraventricular hemorrhage. *Translational stroke research*, 3(Suppl 1), pp.25–38.
239. Strazielle, N. & Ghersi-Egea, J.-F., 2000. Choroid plexus in the central nervous system: Biology and physiopathology. *Journal of neuropathology & experimental neurology*, 59(7), pp.561–574.
240. Sugerman, H.J. et al., 1997. Increased intra-abdominal pressure and cardiac filling pressures in obesity associated pseudotumor cerebri. *Neurology*, 49, pp.507–511.
241. Sumarac-Dumanovic, M. et al., 2009. Increased activity of interleukin-23/interleukin-17 proinflammatory axis in obese women. *International journal of obesity*, 33(1), pp.151–6.
242. Szentistványi, I. et al., 1984. Drainage of interstitial fluid from different regions of rat brain. *The American journal of physiology*, 246(6 Pt 2), pp.F835–F844.
243. Szmydynger-Chodobska, J. et al., 2012. Posttraumatic invasion of monocytes across the blood–cerebrospinal fluid barrier. *Journal of cerebral blood flow & metabolism*, 32(1), pp.93–104.
244. Tabassi, A., Salmasi, A.H. & Jalali, M., 2005. Serum and CSF vitamin A concentrations in idiopathic intracranial hypertension. *Neurology*, 64(11), pp.1893–6.
245. Tartaglia, L. a et al., 1995. Identification and expression cloning of a leptin receptor, OB-R. *Cell*, 83(7), pp.1263–1271.
246. Thomas, S. a et al., 2001. Leptin transport at the blood--cerebrospinal fluid barrier using the perfused sheep choroid plexus model. *Brain research*, 895(1-2), pp.283–90.
247. Tirapelli, L.F., Tamega, O.J. & Martinez, F.E., 1998. Ultrastructural changes of the choroid plexus of the lateral ventricles of rats (rattus norvegicus) submitted to experimental alcohol withdrawal. *Revista chilena de anatomía*, 16(2).
248. Tomlinson, J.W. et al., 2004. 11β-Hydroxysteroid dehydrogenase type 1: A tissue-specific regulator of glucocorticoid response. *Endocrine reviews*, 25, pp.831–866.
249. Topper, J.N. et al., 1997. Expression of the bumetanide-sensitive Na-K-Cl cotransporter BSC2 is differentially regulated by fluid mechanical and inflammatory cytokine stimuli in vascular endothelium. *Journal of Clinical Investigation*, 99(12), pp.2941–2949.
250. Tourdias, T. et al., 2009. Aquaporin 4 correlates with apparent diffusion coefficient and hydrocephalus severity in the rat brain: a combined MRI-histological study. *NeuroImage*, 47(2), pp.659–66.
251. Tuttolomondo, A. et al., 2008. Inflammatory cytokines in acute ischemic stroke. *Current pharmaceutical design*, 14(33), pp.3574–89.
252. Valls-Solé, J., 2004. The central nervous system. Structure and function, 3rd edition. *Clinical neurophysiology*, 115(10), pp.2424–2425.
253. Venero, J.L. et al., 1999. Detailed localization of aquaporin-4 messenger RNA in the CNS: preferential expression in periventricular organs. *Neuroscience*, 94(1), pp.239–50.
254. Venkatraman, J.T., Feng, X. & Pendergast, D., 2001. Effects of dietary fat and endurance exercise on plasma cortisol, prostaglandin E2, interferon-gamma and

lipid peroxides in runners. *Journal of the American college of nutrition*, 20(5), pp.529–36.
255. Vogh, B.P., Godman, D.R. & Maren, T.H., 1987. Effect of AlCl3 and other acids on cerebrospinal fluid production: a correction. *The Journal of pharmacology and experimental therapeutics*, 243(1), pp.35–9.
256. Vozarova, B. et al., 2001. Circulating interleukin-6 in relation to adiposity, insulin action, and insulin secretion. *Obesity research*, 9(7), pp.414–7.
257. Wall, M. & George, D., 1991. Idiopathic intracranial hypertension. A prospective study of 50 patients. *Brain : a journal of neurology*, 114(Pt 1), pp.155–80.
258. Walsh, F.B. et al., 1965. Oral contraceptives and neuro-ophthalmologic interest. *Archives of ophthalmology*, 74(5), pp.628–640.
259. Wang, S. et al., 2016. Protective and detrimental effects of neuroectodermal cell–derived tissue factor in mouse models of stroke. *JCI Insight*, 1(11), pp.399–415.
260. Weisberg, S.P. et al., 2003. Obesity is associated with macrophage accumulation in adipose tissue. *The Journal of clinical investigation*, 112(12), pp.1796–808.
261. Weller, R.O. et al., 2009. Lymphatic drainage of the brain and the pathophysiology of neurological disease. *Acta neuropathologica*, 117(1), pp.1–14.
262. Wilkinson, M., Morash, B. & Ur, E., 2000. The brain is a source of leptin. *Frontiers of hormone research*, 26, pp.106–25.
263. Wolford, J.K. et al., 2003. Variants in the interleukin 6 receptor gene are associated with obesity in Pima Indians. *Molecular genetics and metabolism*, 80(3), pp.338–43.
264. Wolinski, P. et al., 2013. Chemokines and neurodegeneration in the early stage of experimental ischemic stroke. *Mediators of inflammation*, 2013(8).
265. Wosik, K. et al., 2007. Death receptor expression and function at the human blood brain barrier. *Journal of the neurological sciences*, 259(1-2), pp.53–60.
266. Wu, Q. et al., 1998. Functional demonstration of Na+-K+-2Cl- cotransporter activity in isolated, polarized choroid plexus cells. *The American journal of physiology*, 275(6 Pt 1), pp.C1565–72.
267. Xie, Y. et al., 2005. [Experimental study on the expression and function of aquaporin-1 and aquaporin-5 in rats with acute lung injury induced by lipopolysaccharide]. *Zhonghua jie he he hu xi za zhi = Zhonghua jiehe he huxi zazhi = Chinese journal of tuberculosis and respiratory diseases*, 28(6), pp.385–9.
268. Yoshida, H., Russell, J. & Granger, D.N., 2009. Pro-inflammatory cytokines mediate the extra-intestinal thrombus formation associated with inflammatory bowel disease (IBD). *The FASEB Journal*, 23(1), pp.593.2–593.2.
269. Young, E.A., 1996. Sex differences in response to exogenous corticosterone: a rat model of hypercortisolemia. *Molecular psychiatry*, 1(4), pp.313–9.
270. Yudkin, J.S. et al., 2000. Inflammation, obesity, stress and coronary heart disease: is interleukin-6 the link? *Atherosclerosis*, 148(2), pp.209–214. Zdanov, A. & Wlodawer, A., 2008. A new look at cytokine signaling. *Cell*, 132, pp.179–181.
271. Zelenina, M., 2010. Regulation of brain aquaporins. *Neurochemistry international*, 57(4), pp.468–88.
272. Zhang, Y. et al., 2016. The effects of aquaporin-1 in pulmonary edema induced by fat embolism syndrome. *International journal of molecular sciences*, 17(7), p.1183.
273. Zhang, Z. et al., 2006. Deficiency of SPAG16L causes male infertility associated with impaired sperm motility. *Biology of reproduction*, 74, pp.751–759.
274. Zhu, X.H. et al., 1997. Effects of prolactin and metoclopramide on macrophage cytokine gene expression in late sepsis. *Cytokine*, 9(6), pp.437–46.

275. Zlokovic, B. V et al., 1993. Differential expression of Na,K-ATPase alpha and beta subunit isoforms at the blood-brain barrier and the choroid plexus. *The Journal of biological chemistry*, 268(11), pp.8019–25.
276. Zúñiga, L. a et al., 2010. IL-17 regulates adipogenesis, glucose homeostasis, and obesity. *Journal of immunology (Baltimore, Md. : 1950)*, 185, pp.6947–6959.

6 Appendix

6.1 Materials

Chemical or Solution	Supplier	Catalogue #
Sodium Chloride (NaCl)	Sigma-Aldrich, Dorset, UK	S7653
Potassium Chloride (KCl)	Sigma-Aldrich, Dorset, UK	P4504
Calcium Chloride ($CaCl_2$)	BDH Laboratory Supplies, Dorset, UK	26224
Magnesium Chloride ($MgCl_2$)	Sigma-Aldrich, Dorset, UK	M-8266
Sodium Bicarbonate ($NaHCO_3$)	BDH Laboratory Supplies, Dorset, UK	10247
HEPES	Sigma-Aldrich, Dorset, UK	H-7006
Disodium Phosphate (Na_2HPO_4)	Sigma-Aldrich, Dorset, UK	S7907
Glucose	Sigma-Aldrich, Dorset, UK	G8270
Blue Dextran	Sigma-Aldrich, Dorset, UK	D5751
Hydrocortisone	Sigma-Aldrich, Dorset, UK	H0135
Leptin	Sigma-Aldrich, Dorset, UK	L4146
CCL2	Cambridge Bioscience, Cambridge, UK	00220-0-100
IL-6	Life Technologies, Paisley, UK	10398-H08H-5
IL-17	Miltenyi Biotech Ltd, Woking, UK	130-093-959
TNF-α	Sigma-Aldrich, Dorset, UK	H8916
IL-1 β	Miltenyi Biotech Ltd, Woking, UK	130-093-897
Domitor (Medetonidine Hydrochloride)	Red Kite Veterinary Consultants, Centaur services, Castle Cary, UK	
Vetalar (Ketamine)	Red Kite Veterinary Consultants Centaur Services, Castle Cary, UK	
Hand Chuck Drill	Farnell Element, Leeds, UK	146443
PBS Phosphate Buffered Saline	Sigma-Aldrich, Dorset, UK	P4417
p-formaldehyde	Sigma-Aldrich, Dorset, UK	P6148
Glutaraldehyde	Agar Scientific, Essex, UK	R1311
Osmium tetroxide	Agar Scientific, Essex, UK	R1017
Araldite	Agar Scientific, Essex, UK	R1040
Agar 100 resin (Epon)	Agar Scientific, Essex, UK	R1043
dodecenyl succinic anhydride (DDSA)	Agar Scientific, Essex, UK	R1051

2,4,6-tris diemthylaminomethyl phenol (DMP-30)	Agar Scientific, Essex, UK	AGR1065
Human Choroid Plexus Epithelial Cells (hCPEpiC)	Caltag Medsystems, Milton Keynes, UK	SC-1310
hCPEpiC Complete Medium	Caltag Medsystems, Milton Keynes, UK	SC4101
Chloroform Solution	Sigma-Aldrich, Dorset, UK	C2432
Anti-Prealbumin (TTR) Sheep Polyclonal IgG Primary Ab	Abcam, Cambridge, UK	ab9015
ZO-1 Rabbit Polyclonal IgG Primary Ab	Life Technologies, Paisley, UK	61-7300
Claudin-1 Rabbit Polyclonal IgG Primary Ab	Thermo Fisher Scientific, Hemel Hempstead, UK	51-9000
Na^+K^+ATPase Rabbit Polyclonal IgG Primary Ab	Abcam, Cambridge, UK	ab58475
NKCC1 Rabbit Polyclonal IgG Primary Ab	Abcam, Cambridge, UK	ab58475
Aquaporin-1 Rabbit Polyclonal IgG Primary Ab	Abcam, Cambridge, UK	ab15080
ENaC Rabbit Polyclonal IgG Primary Ab	Abcam, Cambridge, UK	ab65710
CCR2 Rabbit Polyclonal IgG Primary Ab	Abcam, Cambridge, UK	ab21667
IL-17Rα Rabbit Polyclonal IgG Primary Ab	St John's Laboratory	STJ93683
TNF-R1 Rabbit Polyclonal IgG Primary Ab	Abcam, Cambridge, UK	ab19139
IL6R Rabbit Polyclonal IgG Primary Ab	Abcam, Cambridge, UK	ab85105
FITC Conjugated Donkey Anti-Sheep IgG Secondary Ab	Abcam, Cambridge, UK	ab9015
Alexa 488 Goat Anti-rabbit IgG Secondary Ab	Life Technologies, Paisley, UK	A11008
BSA Albumin from Bovine Serum	Sigma-Aldrich, Dorset, UK	A9085
DAPI-fluoromount-G™ 4',6-diamidino-2-phenylindole	Southern Biotech, Birmingham, USA	C9791
DMSO Dimethyl Sulfoxide	Sigma-Aldrich, Dorset, UK	D2438
HBSS Hank's Balanced Salt Solution with Sodium Bicarbonate, Calcium and Magnesium Free, No Phenol Red	Sigma-Aldrich, Dorset, UK	H8264
HBSS Hank's Balanced Salt Solution with Sodium Bicarbonate, Calcium and	Sigma-Aldrich, Dorset, UK	H6648

Magnesium, No Phenol Red		
Trypsin-EDTA Solution	Sigma-Aldrich, Dorset, UK	T5941
Tween-20 Polyoxyethylenesorbitan Monolaureate	Sigma-Aldrich, Dorset, UK	P7949

Table 6.1: Complete list of all experimental chemicals, solutions, and reagents used in this project including suppliers and catalogue numbers.

Treatment	CSF IIH (ng/ml)	CSF Normal (ng/ml)	Plasma IIH (ng/ml)	Plasma Normal (ng/ml)
Hydrocortisone* (Sinclair et al., 2010)	**3.4**	**3.6** (Holub et al., 2007)	**85.37**	**72.5** (Oppert et al., 2000)
Leptin (Dhungana et al., 2009)	**0.72**	**0.63**	**135.8**	**64.8**
CCL2 (Dhungana et al., 2009)	**0.99**	**0.71**	**0.28**	**0.25**
IL-6 (Orshal, J.M., 2004)	**0.000024** (Reihani-Kermani et al., 2008)	**0.000018** (Reihani-Kermani et al., 2008)	**0.25**** (Singhal et al, 2002)	**0.002** (Brambilla et al., 2001)
IL-17 (Edwards, L., 2010)	**0.024***** (Li et al., 2012)	**0.018** (Li et al., 2012)	**0.017***** (Li et al., 2012)	**0.013** (Li et al., 2012)
TNF-α (Straczkowski et al., 2002)	**0.03**** (Hayakata et al., 2004)	**0.004** (Lopez-Cortez et al., 2000)	**0.002** (Ball et al., 2009)	**1.6** (Nakai et al., 2000)
IL-1β (Dhungana et al., 2009)	**0.02**** (Hayakata et al., 2004)	**0.001** (Lopez-Cortez et al., 2000)	**0.02** (Dhungana et al., 2009)	**0.006** (Brambilla et al., 2001)

Table 6.2: Levels of treatments in the CSF and blood plasma of IIH patients compared to concentrations in the CSF and blood plasma of normal healthy individuals. *in tension type headache patients controls; **in ICP following Traumatic Brain Injury (TBI); ***in Guillan-Barre Syndrome (GBS); (–) indicates no change between IIH patients and healthy individuals.

6.2 Description of ventriculo-cisternal perfusion calculations

Blank Reading (ABS)	35

Avg C_{in} ABS	Tube	Time (min)	C_{out} ABS	C_{out} ABS -blank	i-o/o	Total Perfusion flow rate (µl/min)	CSF secretion rate (µl/min)	Time (min)	Total CSF secreted (µl)	Steady state 0
392	1	0-9.9	210	175	1.083	40	43.31	5	216.57	0.480
396	2	10-19.9	302	267	0.365	40	14.61	10	146.07	0.733
401	3	20-29.9	339	304	0.199	20	3.98	10	39.80	0.834
409	4	30-39.9	349	314	0.161	20	3.22	10	32.17	0.861
Avg = 399.5	5	40-49.9	340	305	0.195	20	**3.90**	10	39.02	0.837
-blank = 364.5	6	50-59.9	371	336	0.085	20	**1.70**	10	16.96	0.922
	7	60-69.9	375	340	0.072	20	**1.44**	10	14.41	0.933
	8	70-79.9	360	325	0.122	20	**2.43**	10	24.31	0.892
	9	80-89.9	362	327	0.115	20	**2.29**	10	22.94	0.897
	10	90-92 +tube	360	325	0.122	20	**2.43**	6.9	16.77	0.892

Table 6.3: Example of a spreadsheet document used to calculate CSF secretion rate (red), initial CSF volume (blue) and sample steady states (green) for an individual ventriculo-cisternal perfusion experiment. Average initial CSF absorbances (C_{in}) (grey). Sample used to explain calculations in equations 6.1, 6.2 and 6.3 (orange).

Secretion rate (µl/min) 2.49
Secretion in 90 min (µl) 223.85

Total secreted (µl) 569.02
Initial CSF volume - 90 min new secretion (µl) 345.16

Example calculations for CSF secretion rate (equation 6.1), initial CSF volume (equation 6.2) and sample steady state (equation 6.3), shown below, were used from sample tube 5 (Time: 4-50 min) as highlighted in orange in Table 6.3.

Equation 6.1:

$$\textbf{CSF Secretion Rate } (\mu\text{l min}^{-1}) = \frac{C_{in} - C_{out}}{C_{out}} \times \textbf{Perfusion Rate } (\mu\text{l min}^{-1})$$

$$\textbf{CSF Secretion Rate } (\mu\text{l min}^{-1}) = \frac{364.5 \text{ Abs} - 305 \text{ Abs}}{305 \text{ Abs}} \times 20 \ (\mu\text{l min}^{-1})$$

$$= 3.9 \ \mu\text{l min}^{-1}$$

Equation 6.2:

$$\textbf{Initial CSF Volume } (\mu\text{l}) =$$

$$\textbf{Total volume secreted during whole experiment}(\mu\text{l})^{*} -$$

$$(\textbf{Average CSF Secretion Rate} \times \textbf{90 min}(\mu\text{l/90 min}))$$

$$\textbf{Initial CSF Volume } (\mu\text{l}) = 569.02 \ \mu\text{l} - (2.49 \ \mu\text{l min}^{-1} \times 90 \text{ min})$$

$$= 345.16 \ \mu\text{l}$$

Equation 6.3:

$$\textbf{aCSF Sample Steady State} = \frac{C_{out}(\text{Abs})}{C_{in}(\text{Abs})}$$

$$\textbf{aCSF Sample Steady State} = \frac{305 \text{ Abs}}{364.5 \text{ Abs}}$$

$$= 0.837 \text{ Abs}$$

6.3 *In vivo* steady state values of treatments in perfused aCSF

Steady state values following treatment with each mediator during the initial CSF secretion experiments on normal diet male Wistar rats are shown in Figures 6.1-6.7.

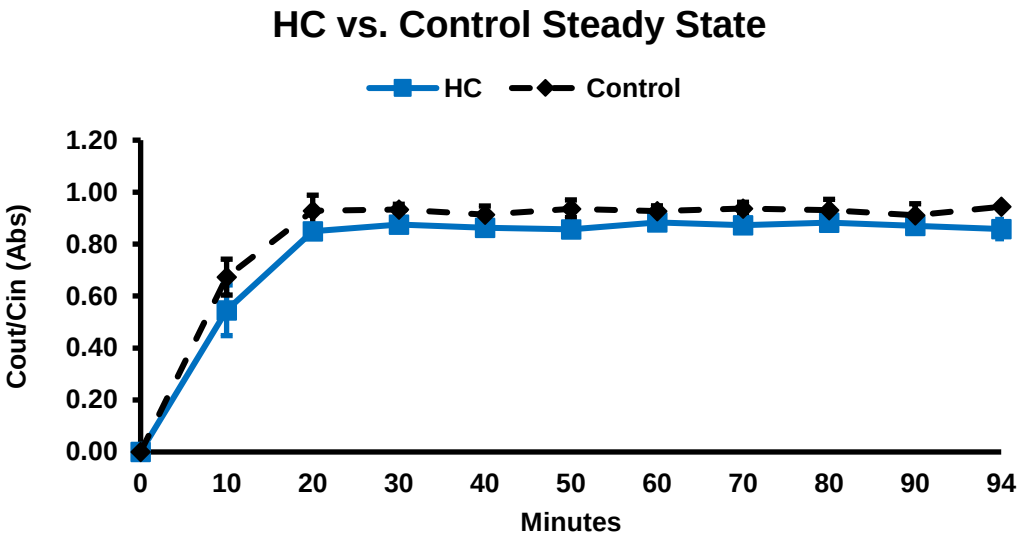

Figure 6.1: The mean hydrocortisone (aCSF 0.5 µg/ml, n=4) steady state values of the perfused aCSF ventriculo-cisternal perfusion experiments compared to control (n=5).

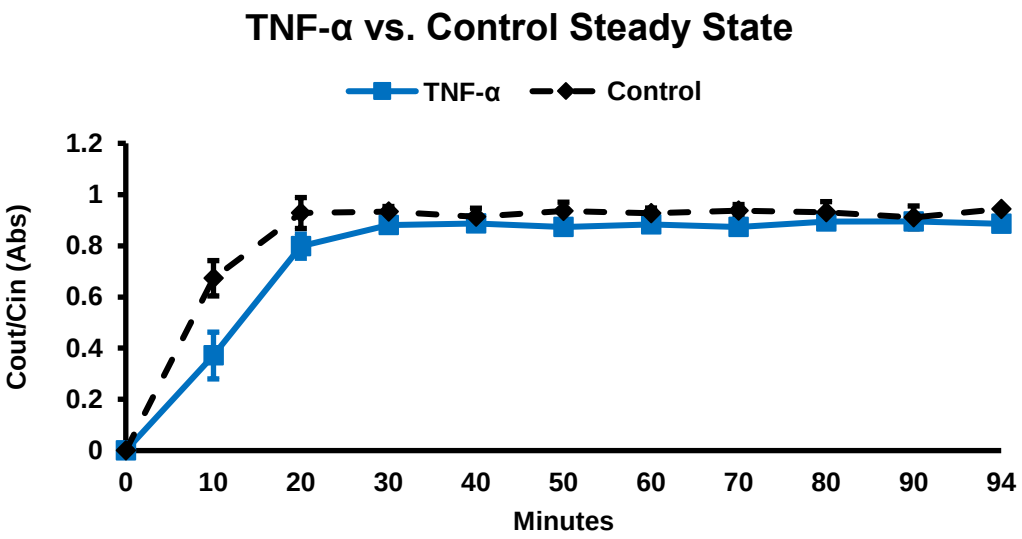

Figure 6.2: The mean TNF-α (aCSF 0.0001 µg/ml, n=3) steady state values of the perfused aCSF ventriculo-cisternal perfusion experiments compared to control (n=5).

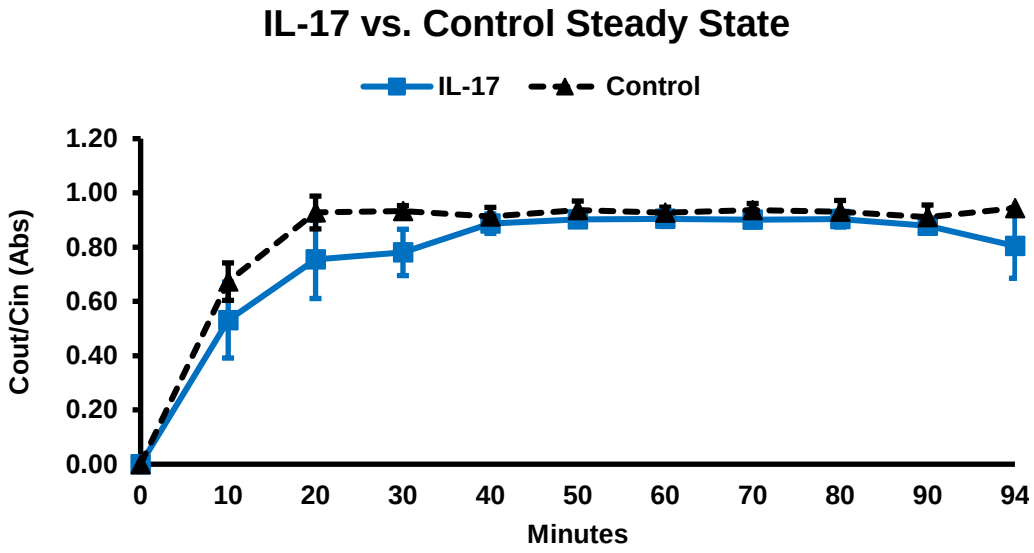

Figure 6.3: The mean IL-17 (aCSF 0.0001 µg/ml, n=3) steady state values of the perfused aCSF ventriculo-cisternal perfusion experiments compared to control (n=5).

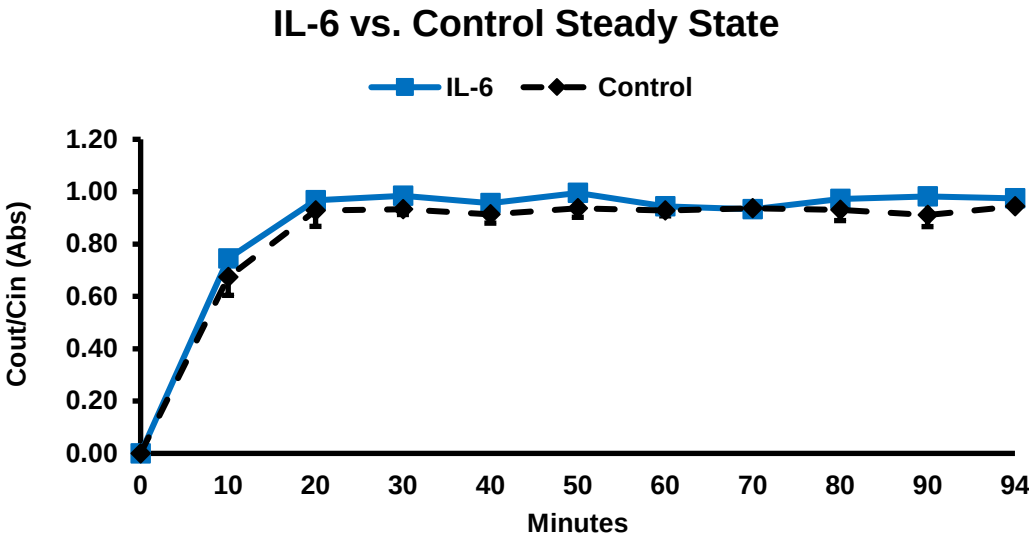

Figure 6.4: The mean IL-6 (aCSF 0.0001 µg/ml, n=3) steady state values of the perfused aCSF ventriculo-cisternal perfusion experiments compared to control (n=5).

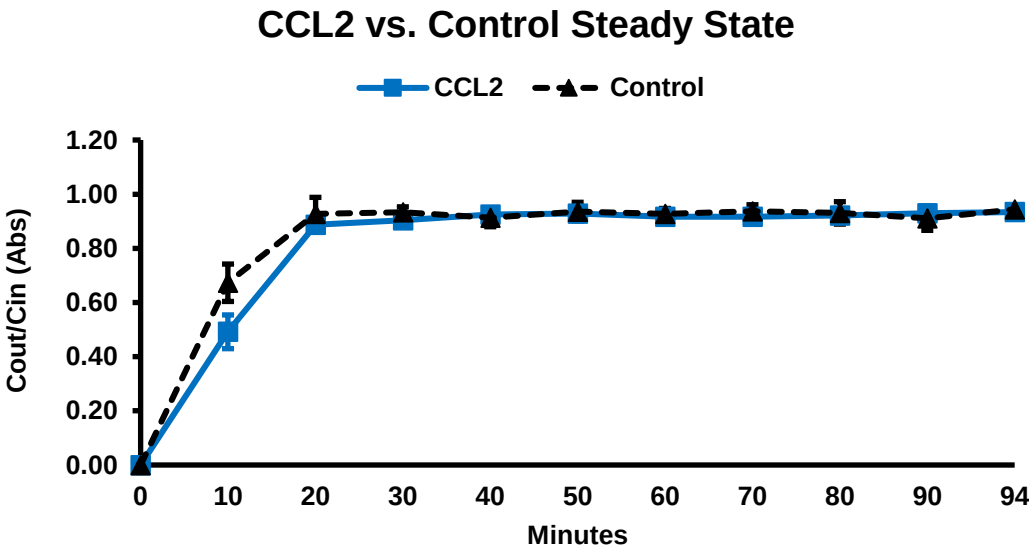

Figure 6.5: The mean CCL2 (aCSF 0.05 µg/ml, n=4) steady state values of the perfused aCSF ventriculo-cisternal perfusion experiments compared to control (n=5).

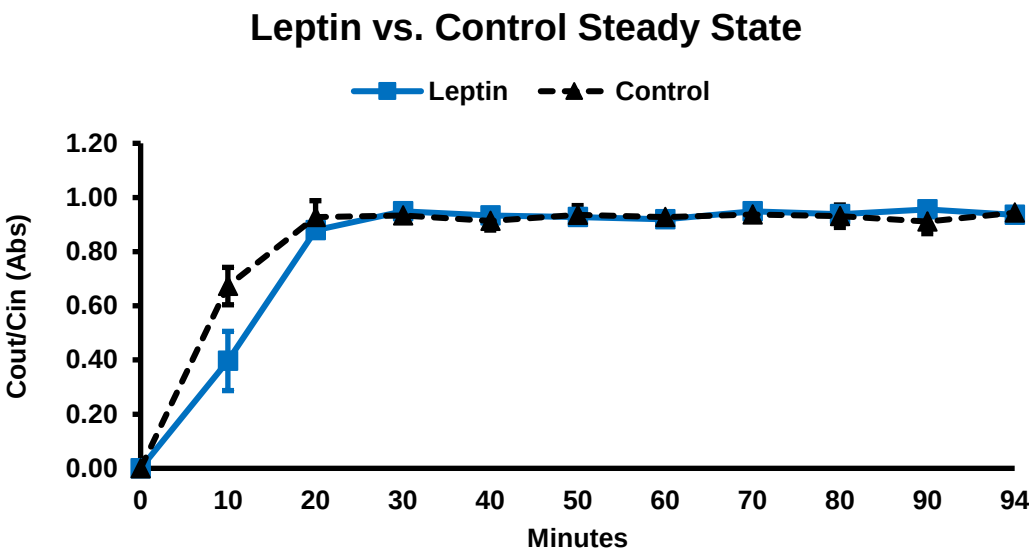

Figure 6.6: The mean Leptin (aCSF 0.1 µg/ml, n=4) steady state values of the perfused aCSF ventriculo-cisternal perfusion experiments compared to control (n=5).

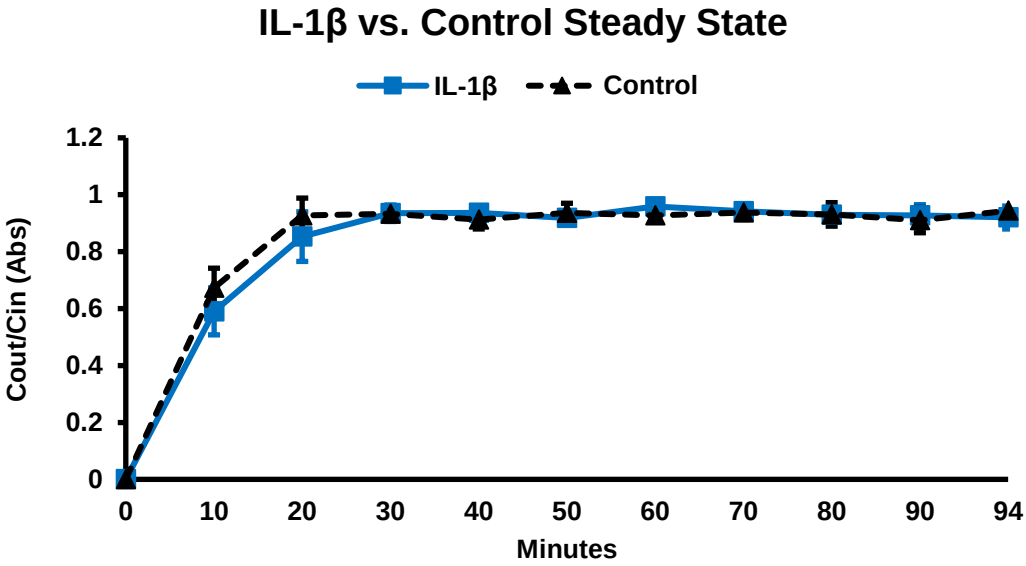

Figure 6.7: The mean IL-1β (aCSF 0.0001 µg/ml, n=3) steady state values of the perfused aCSF ventriculo-cisternal perfusion experiments compared to control (n=5).

6.4 *In vivo* steady state values of treatments in perfused aCSF following i.p injection of treatment

Steady state values following treatment with each mediator in perfused aCSF and following i.p injection of each treatment during the initial CSF secretion experiments on normal diet male Wistar rats are shown in Figures 6.8-6.14.

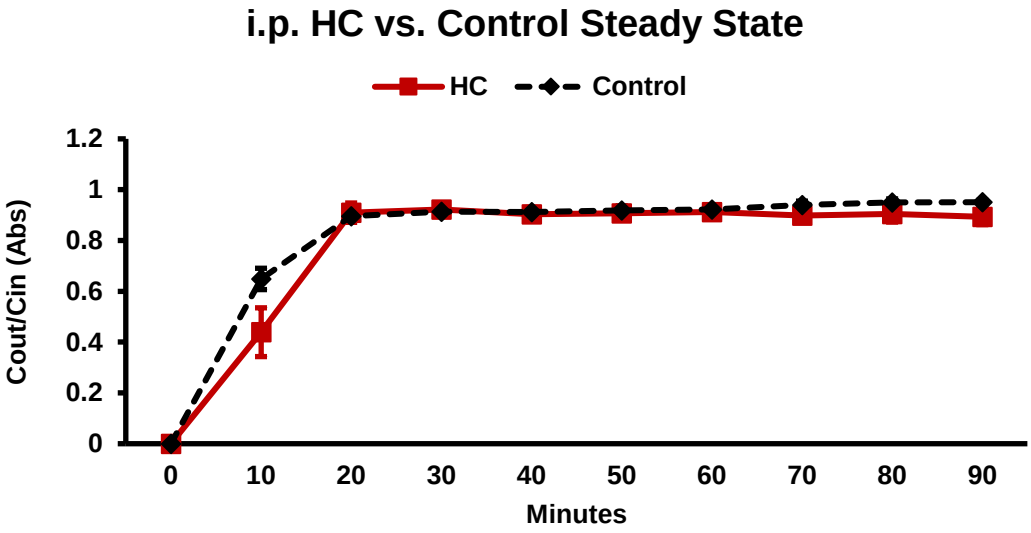

Figure 6.8: The mean hydrocortisone (aCSF 0.5 µg/ml, i.p. 100 µg/ml, n=3) steady state values of the i.p. ventriculo-cisternal perfusion experiments compared to control (n=4).

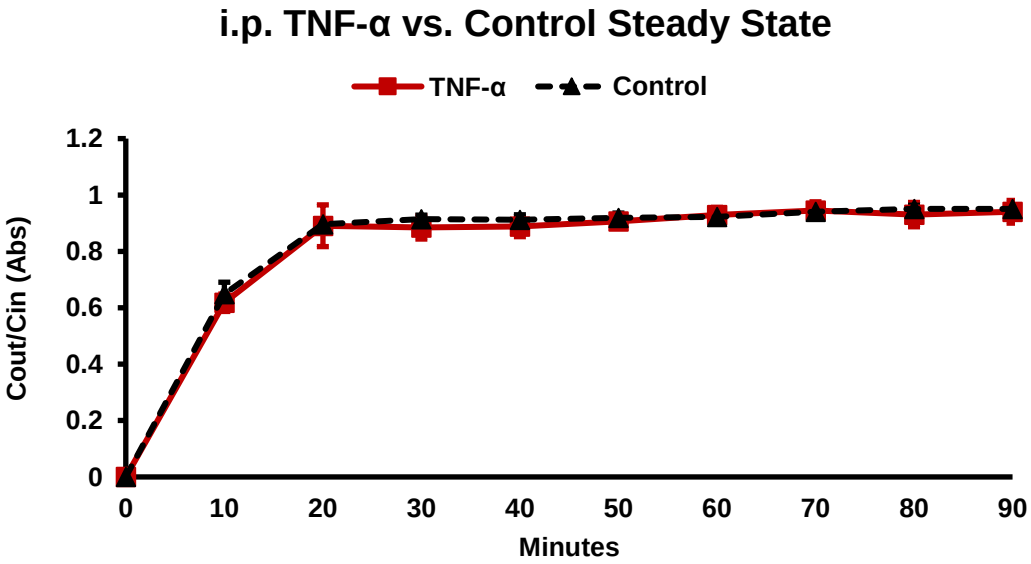

Figure 6.9: The mean TNF-α (aCSF 0.0001 µg/ml, i.p. 0.025 µg/ml, n=3) steady state values of the i.p. ventriculo-cisternal perfusion experiments compared to control (n=4).

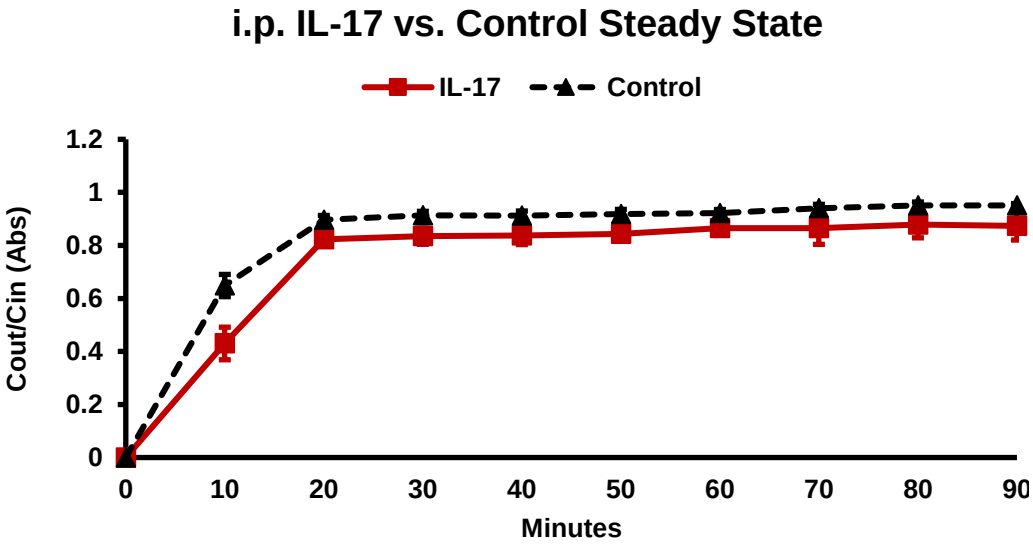

Figure 6.10: The mean IL-17 (aCSF 0.0001 µg/ml, i.p. 0.025 µg/ml, n=3) steady state values of the i.p. ventriculo-cisternal perfusion experiments compared to control (n=4).

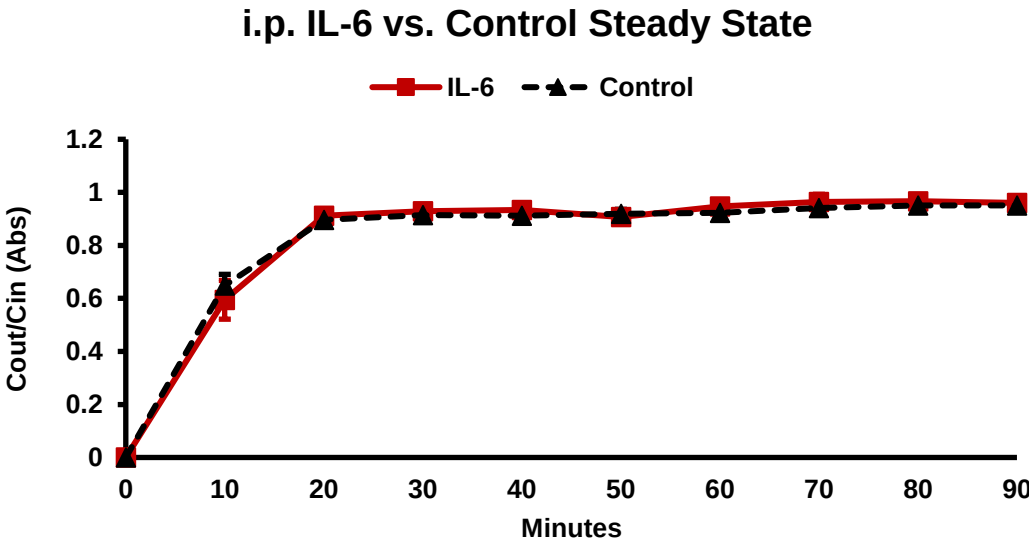

Figure 6.11: The mean IL-6 (aCSF 0.0001 µg/ml, i.p. 0.025 µg/ml, n=3) steady state values of the i.p. ventriculo-cisternal perfusion experiments compared to control (n=4).

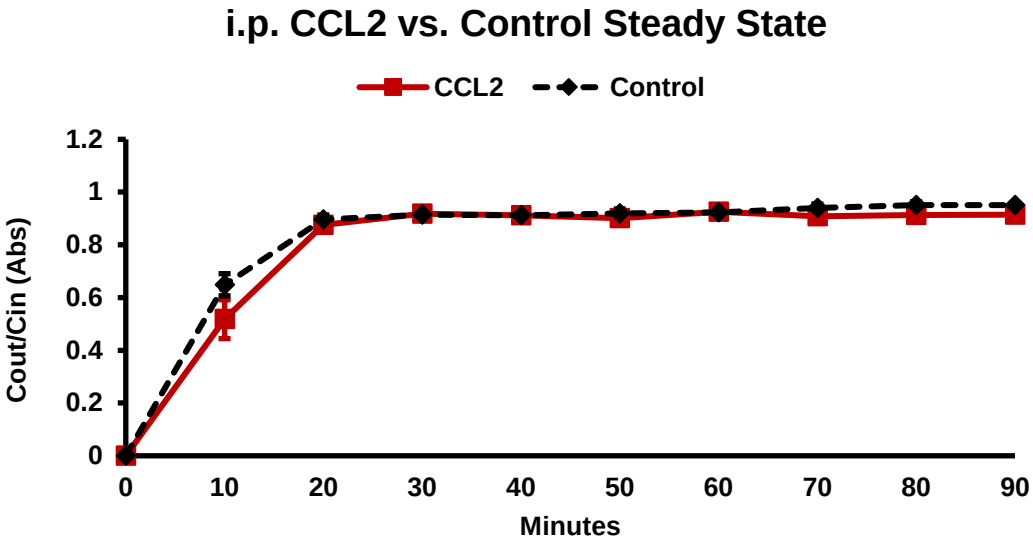

Figure 6.12: The mean CCL2 (aCSF 0.05 µg/ml, i.p. 10 µg/ml, n=4) steady state values of the i.p. ventriculo-cisternal perfusion experiments compared to control (n=4).

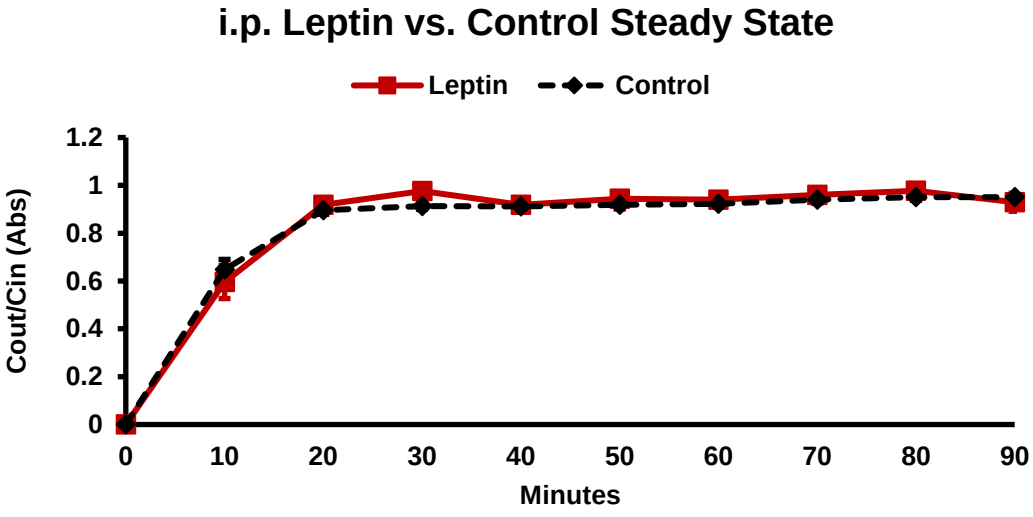

Figure 6.13: The mean Leptin (aCSF 0.1 µg/ml, i.p. 25 µg/ml, n=3) steady state values of the i.p. ventriculo-cisternal perfusion experiments compared to control (n=4).

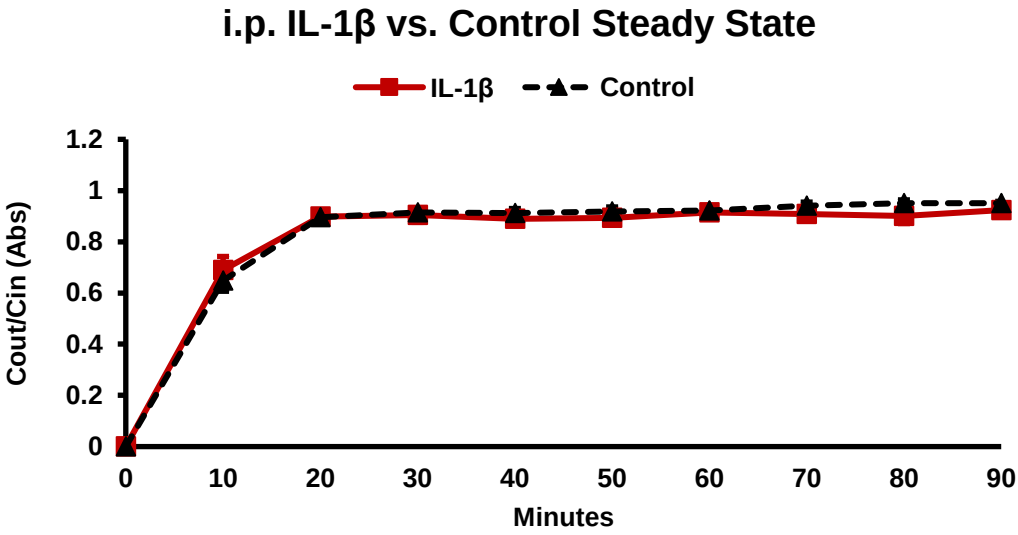

Figure 6.14: The mean IL-1β (aCSF 0.0001 µg/ml, i.p. 0.025 µg/ml, n=3) steady state values of the i.p. ventriculo-cisternal perfusion experiments compared to control (n=4).

6.5 *In vivo* steady state values of treatments in perfused aCSF on male Wistar rats fed on a normal pellet diet

Steady state values following treatment with each mediator during the next CSF secretion experiments on normal diet male Wistar rats are shown in Figures 6.15-6.19.

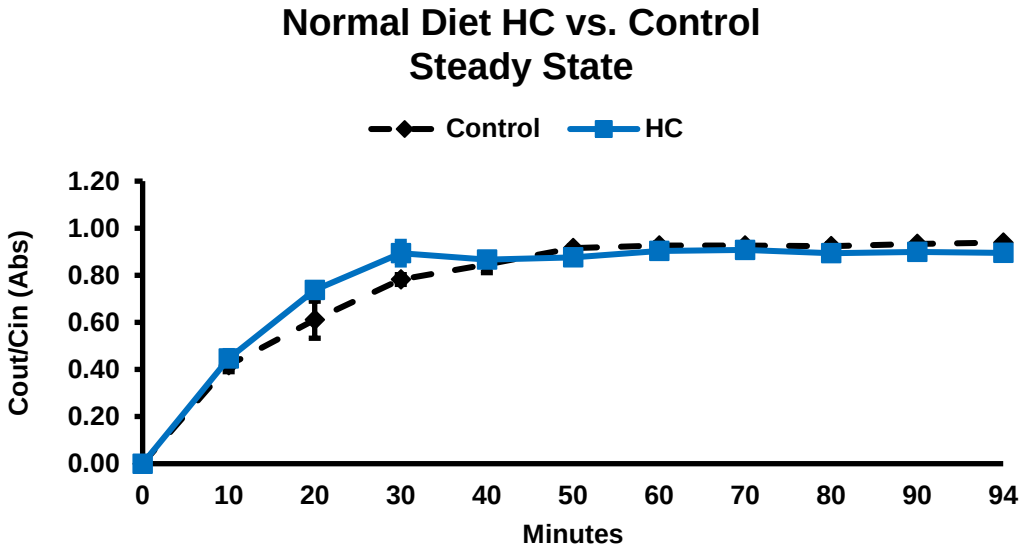

Figure 6.15: The mean normal diet hydrocortisone (aCSF 0.5 µg/ml, n=3) against control (n=3) steady state values of the ventriculo-cisternal perfusion experiments.

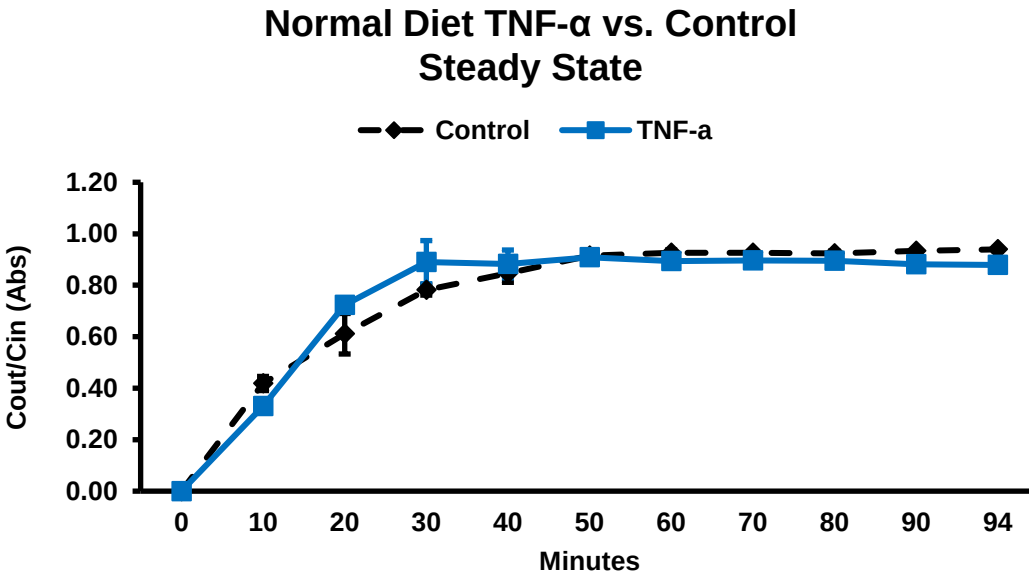

Figure 6.16: The mean normal diet TNF-α (aCSF 0.0001 µg/ml, n=3) against control (n=3) steady state values of the ventriculo-cisternal perfusion experiments

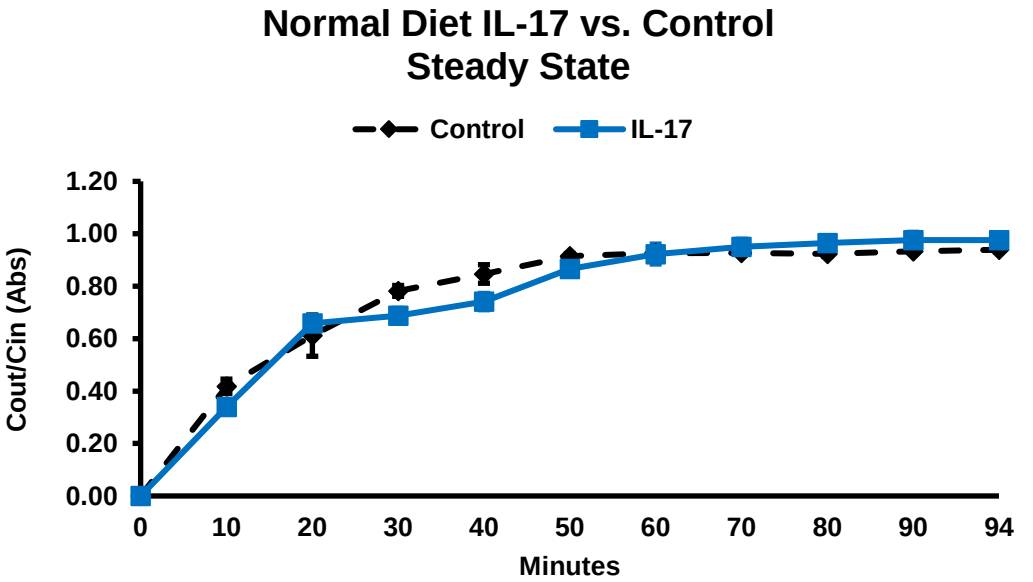

Figure 6.17: The mean normal diet IL-17 (aCSF 0.0001 µg/ml, n=3) against control (n=3) steady state values of the ventriculo-cisternal perfusion experiments.

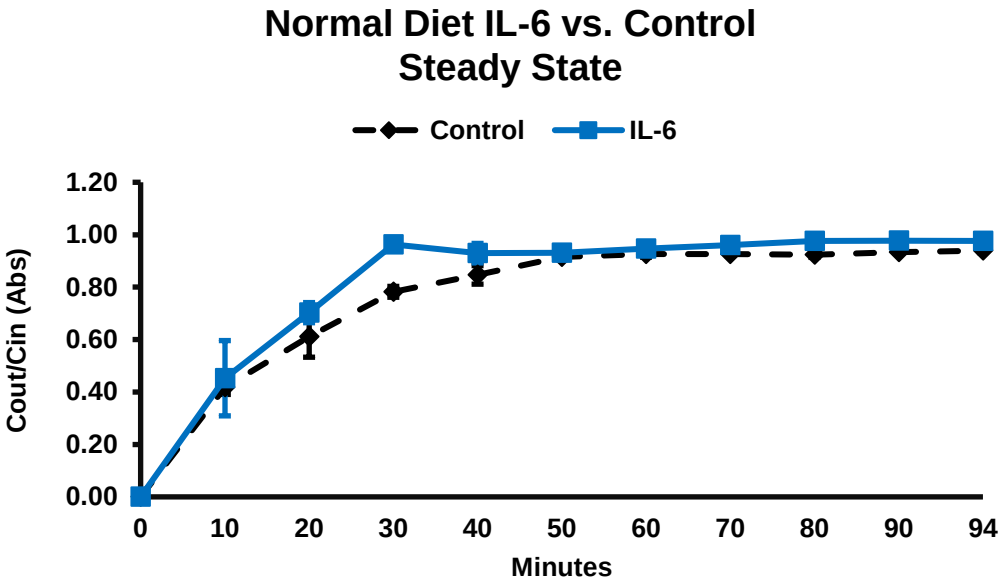

Figure 6.18: The mean normal diet IL-6 (aCSF 0.0001 µg/ml, n=3) against control (n=3) steady state values of the ventriculo-cisternal perfusion experiments.

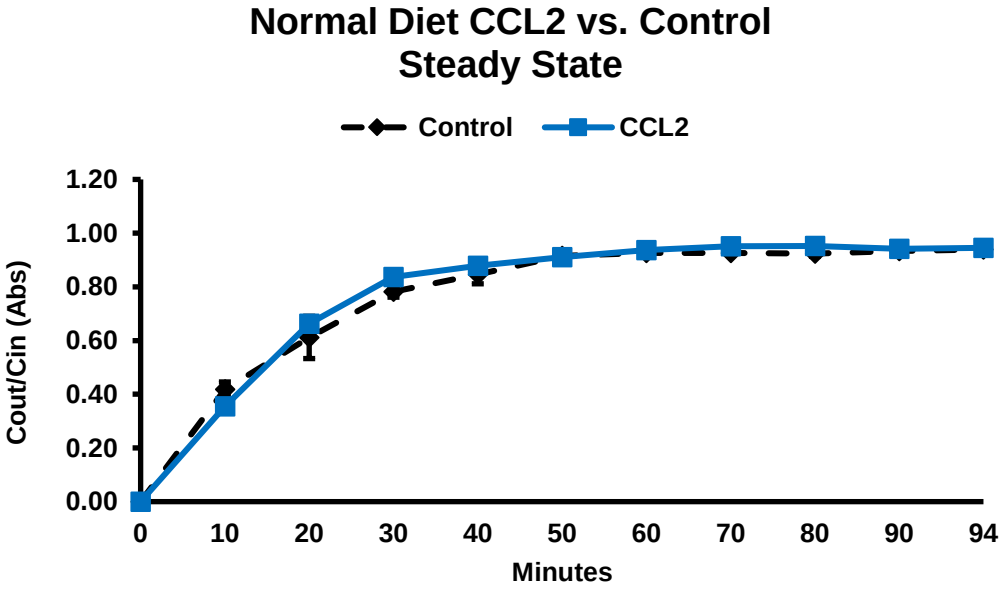

Figure 6.19: The mean normal diet CCL2 (aCSF 0.05 µg/ml, n=3) against control (n=3) steady state values of the ventriculo-cisternal perfusion experiments.

6.6 *In vivo* steady state values of treatments in perfused aCSF on male Wistar rats fed on a high fat diet

Steady state values following treatment with each mediator during the next CSF secretion experiments on male Wistar rats fed a HF diet are shown in Figures 6.20-6.24.

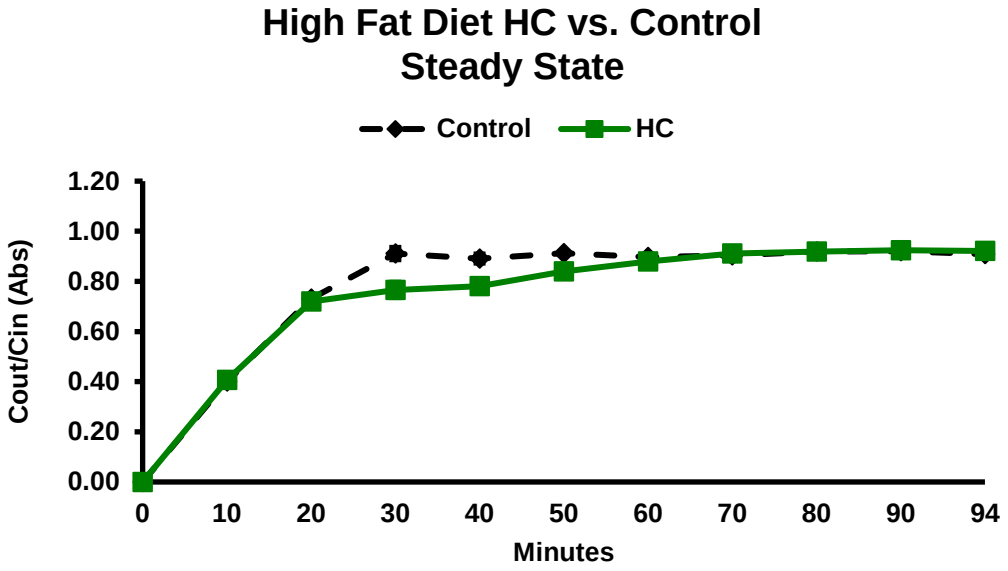

Figure 6.20: The mean high fat diet hydrocortisone (aCSF 0.5 µg/ml, n=4) against control (n=4) steady state values of the ventriculo-cisternal perfusion experiments.

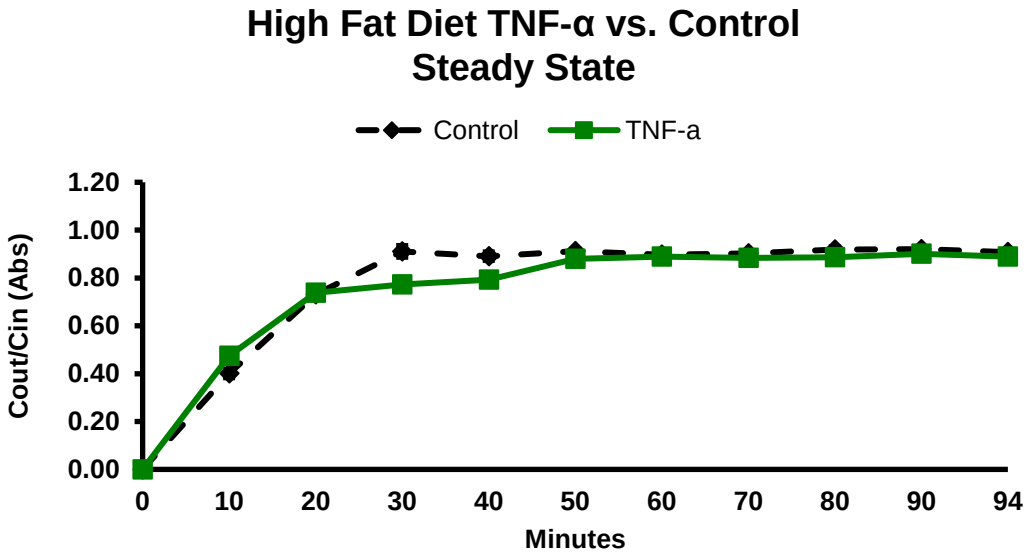

Figure 6.21: The mean high fat diet TNF-α (aCSF 0.0001 µg/ml, n=3) against control (n=4) steady state values of the ventriculo-cisternal perfusion experiments.

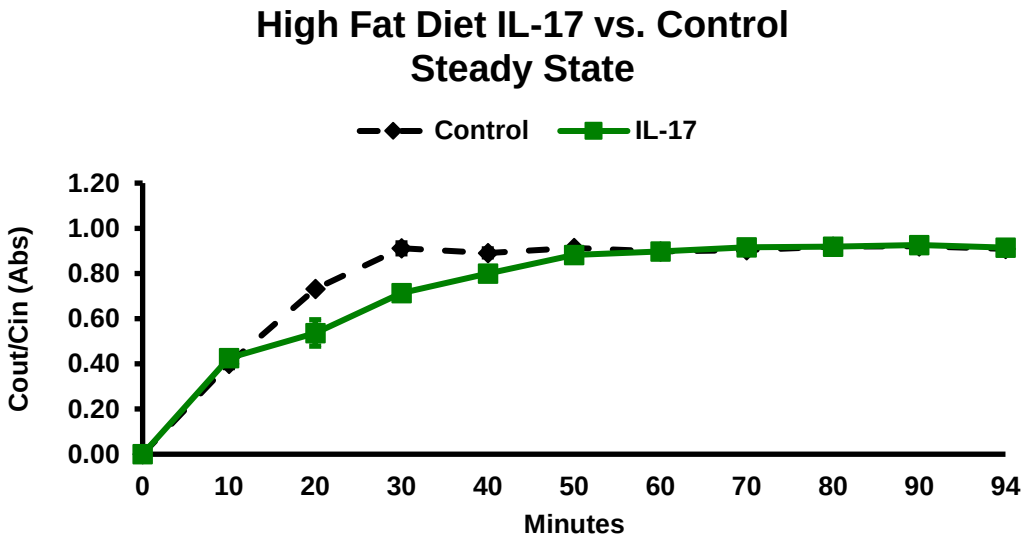

Figure 6.22: The mean high fat diet IL-17 (aCSF 0.0001 µg/ml, n=4) against control (n=4) steady state values of the ventriculo-cisternal perfusion experiments.

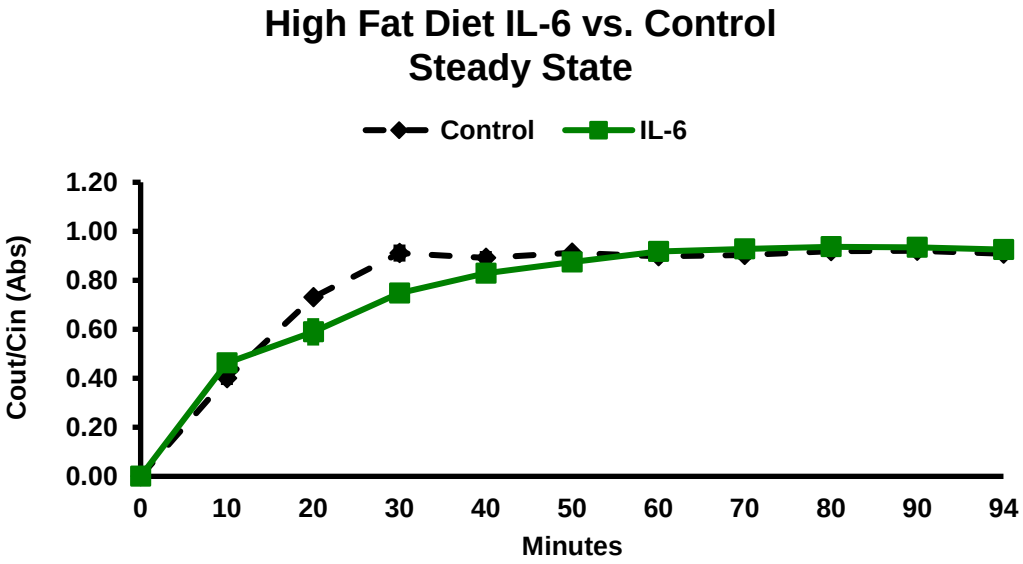

Figure 6.23: The mean high fat diet IL-6 (aCSF 0.0001 µg/ml, n=4) against control (n=4) steady state values of the ventriculo-cisternal perfusion experiments.

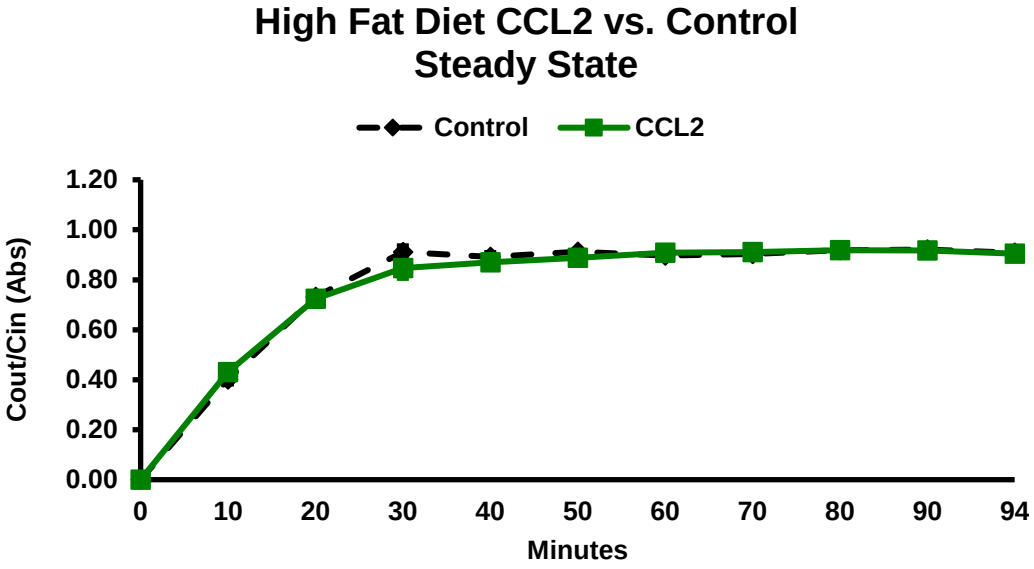

Figure 6.24: The mean high fat diet CCL2 (aCSF 0.05 µg/ml, n=4) against control (n=4) steady state values of the ventriculo-cisternal perfusion experiments.

6.7 *In vivo* steady state values of treatments in perfused aCSF on female Wistar rats fed on a normal pellet diet

Steady state values following treatment with each mediator during the next CSF secretion experiments on female Wistar rats fed a normal diet are shown in Figures 6.25-6.29.

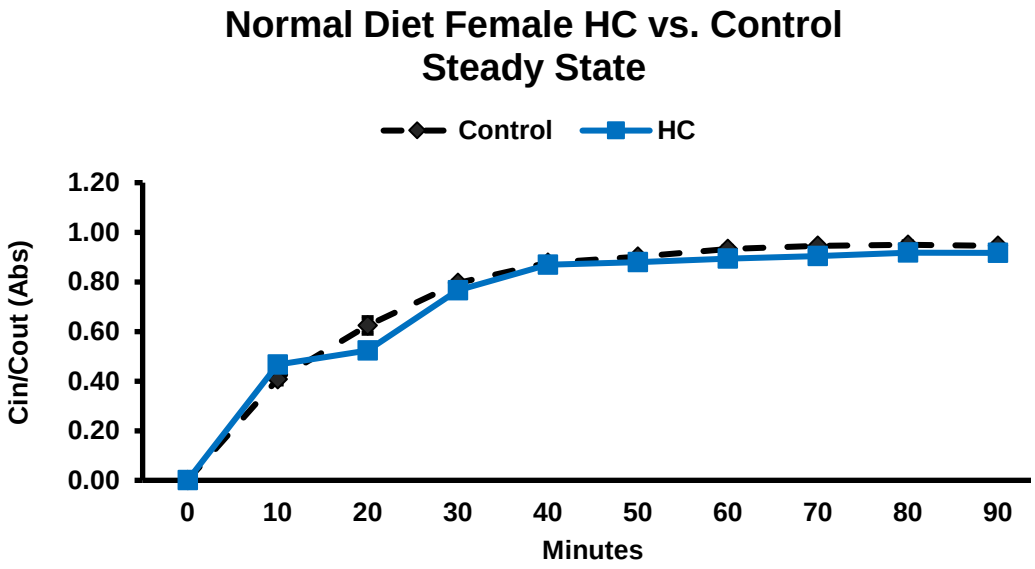

Figure 6.25: The mean normal diet hydrocortisone (aCSF 0.5 µg/ml, n=3) against control (n=3) steady state values of the ventriculo-cisternal perfusion experiments.

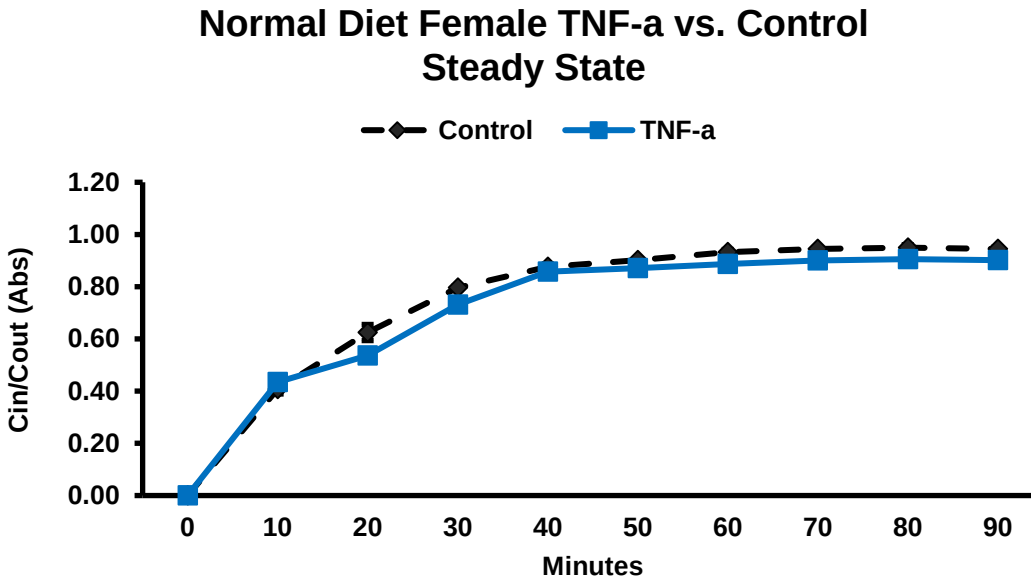

Figure 6.26: The mean normal diet TNF-α (aCSF 0.0001 µg/ml, n=3) against control (n=3) steady state values of the ventriculo-cisternal perfusion experiments.

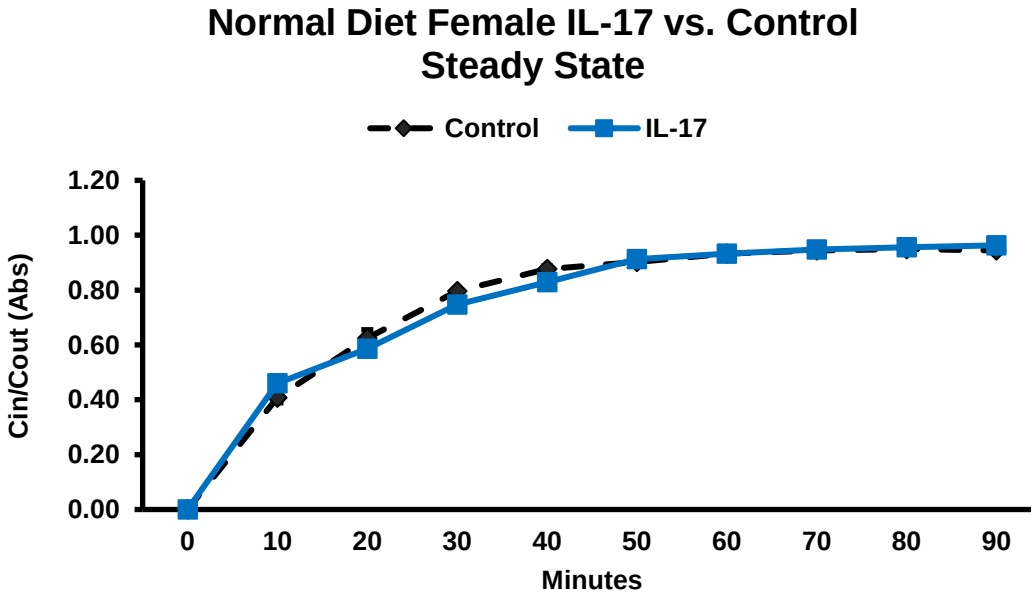

Figure 6.27: The mean normal diet IL-17 (aCSF 0.0001 µg/ml, n=3) against control (n=3) steady state values of the ventriculo-cisternal perfusion experiments.

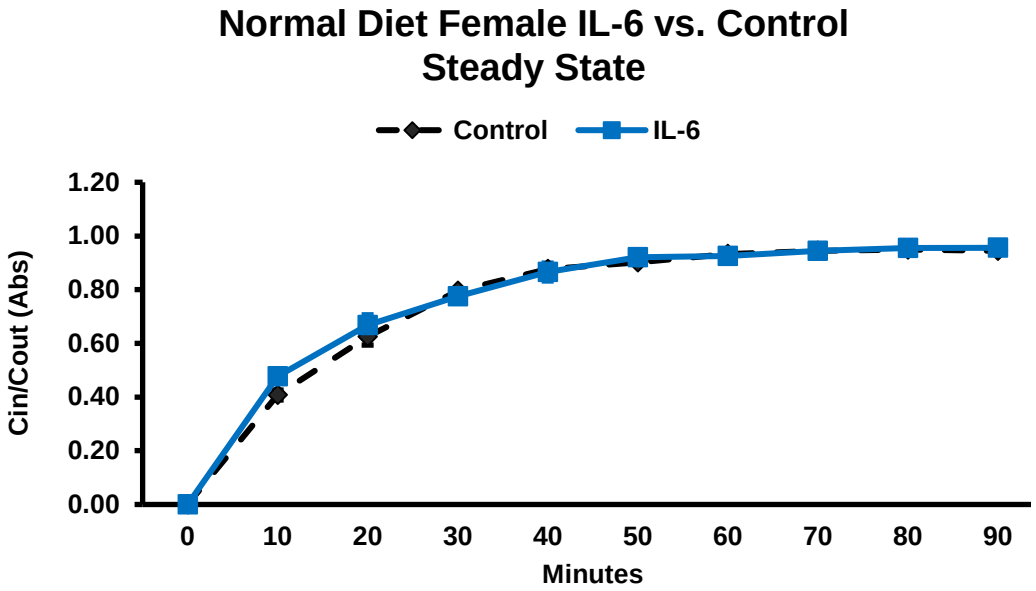

Figure 6.28: The mean normal diet IL-6 (aCSF 0.0001 µg/ml, n=3) against control (n=3) steady state values of the ventriculo-cisternal perfusion experiments.

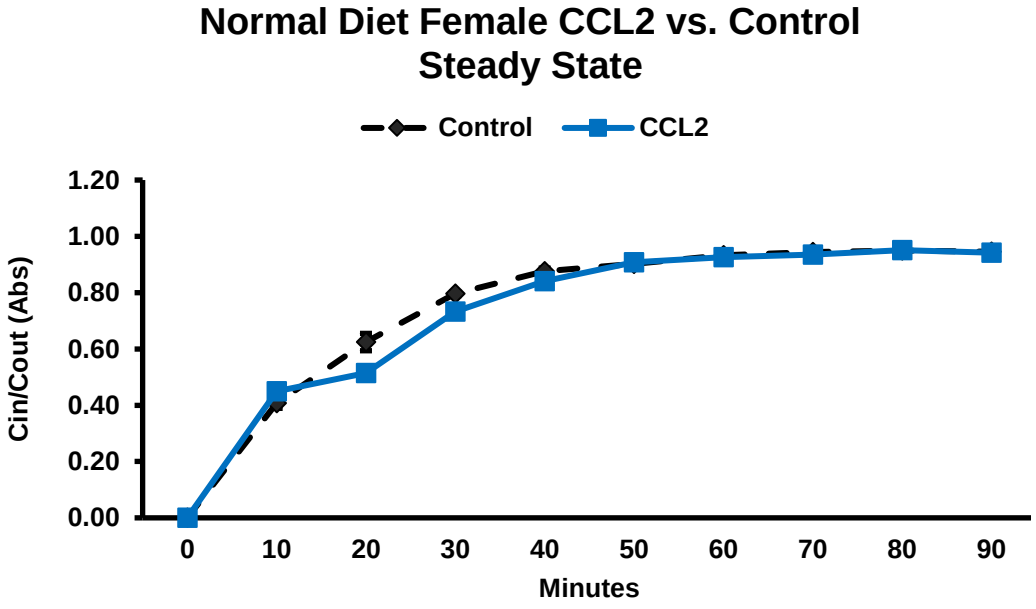

Figure 6.29: The mean normal diet CCL2 (aCSF 0.05 µg/ml, n=3) against control (n=3) steady state values of the ventriculo-cisternal perfusion experiments.

6.8 *In vivo* steady state values of treatments in perfused aCSF on female Wistar rats fed on a high fat diet

Steady state values following treatment with each mediator during the next CSF secretion experiments on female Wistar rats fed a HF diet are shown in Figures 6.30-6.34.

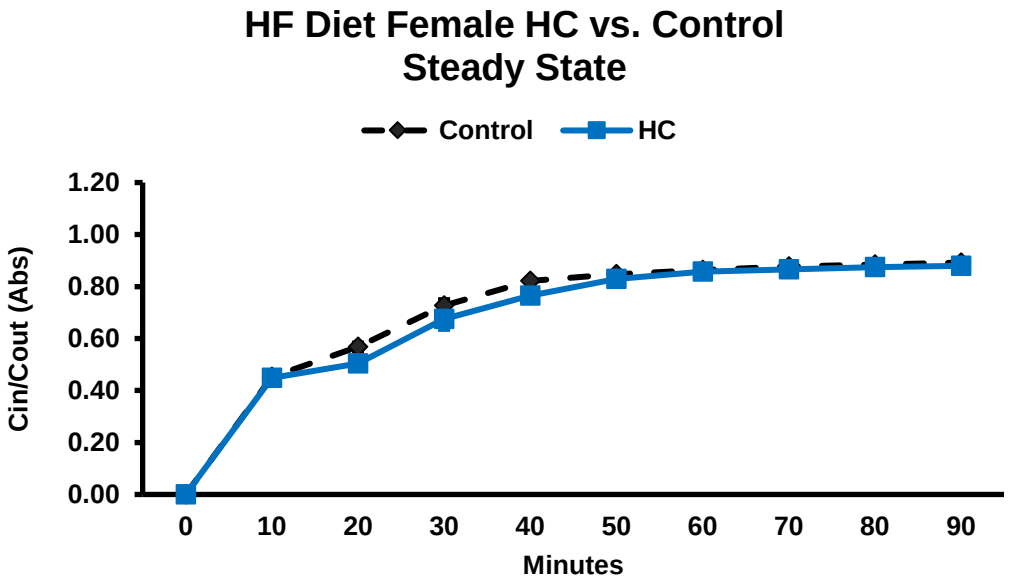

Figure 6.30: The mean female HF diet hydrocortisone (aCSF 0.5 µg/ml, n=3) against control (n=3) steady state values of the ventriculo-cisternal perfusion experiments.

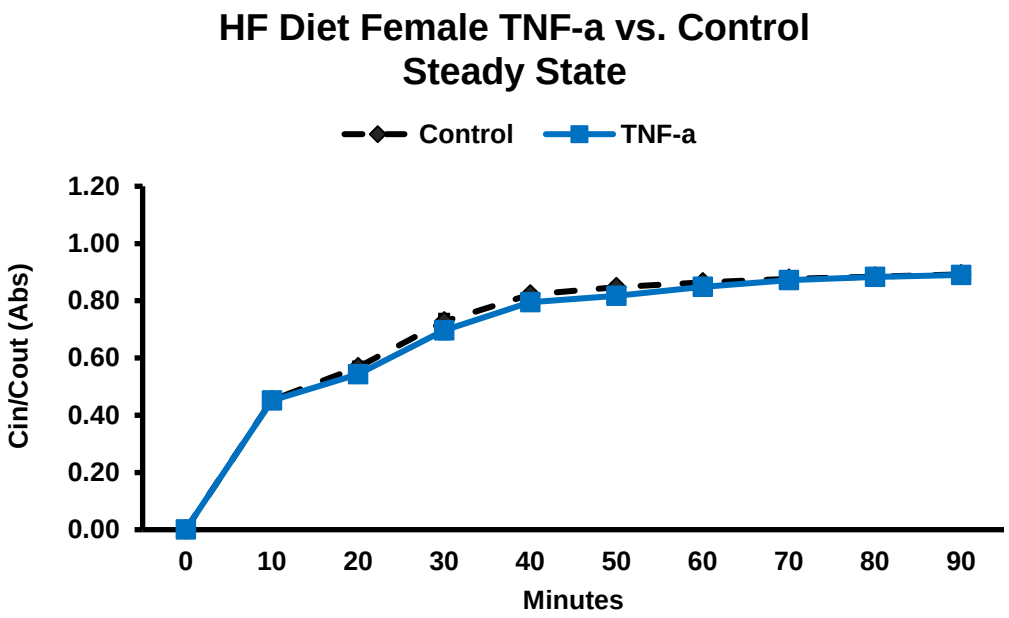

Figure 6.31: The mean female HF diet TNF-α (aCSF 0.0001 µg/ml, n=3) against control (n=3) steady state values of the ventriculo-cisternal perfusion experiments.

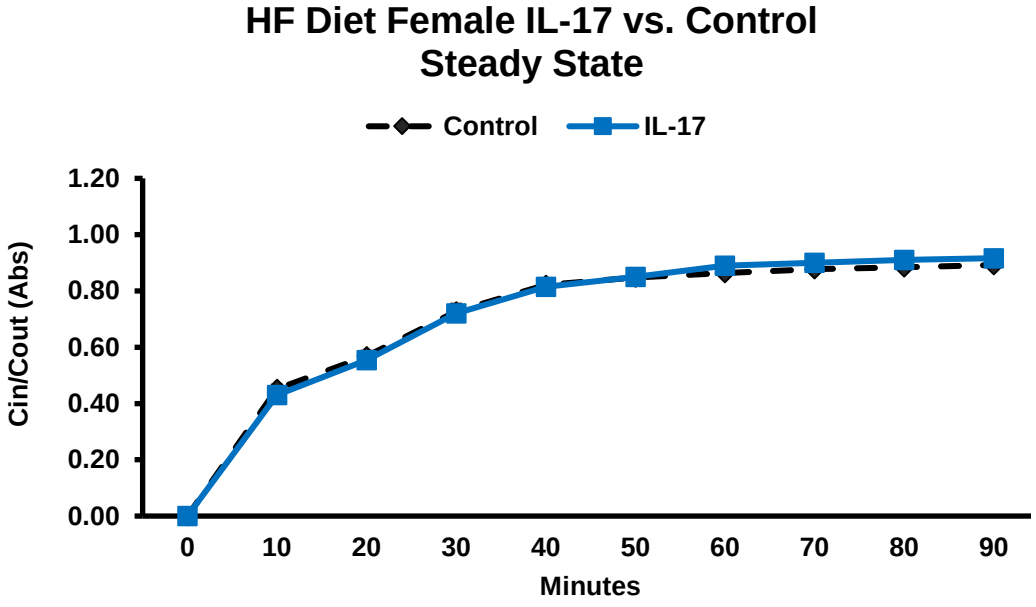

Figure 6.32: The mean female HF diet IL-17 (aCSF 0.0001 µg/ml, n=3) against control (n=3) steady state values of the ventriculo-cisternal perfusion experiments.

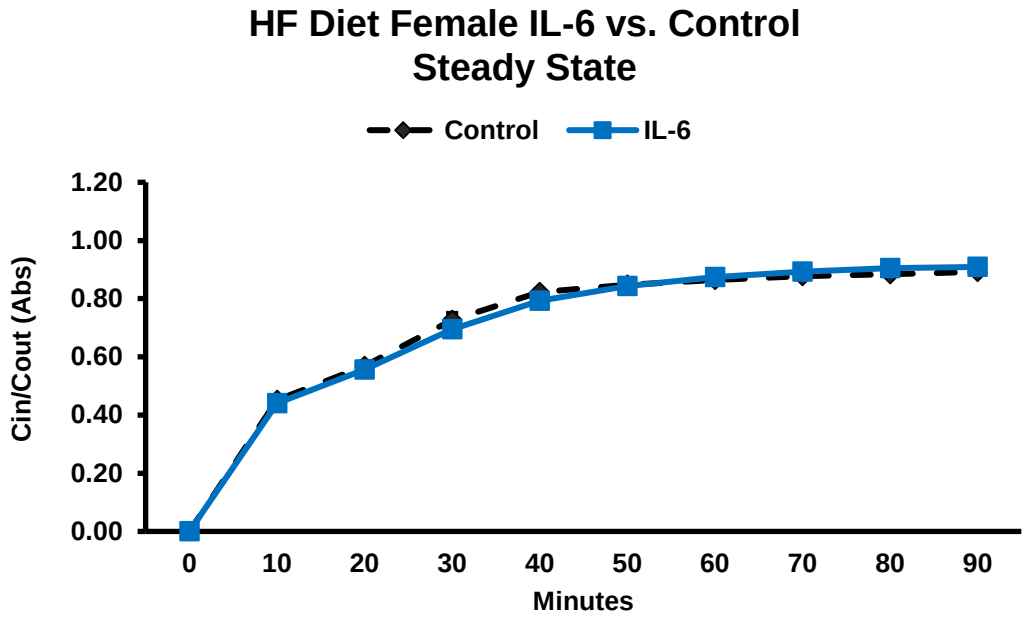

Figure 6.33: The mean female HF diet IL-6 (aCSF 0.0001 µg/ml, n=3) against control (n=3) steady state values of the ventriculo-cisternal perfusion experiments.

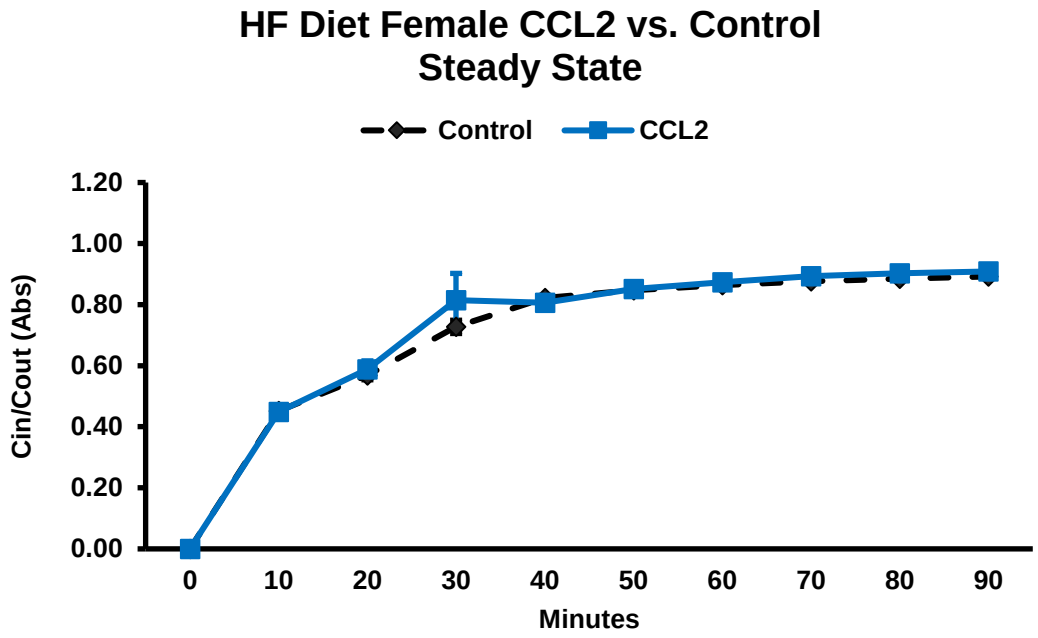

Figure 6.34: The mean female HF diet CCL2 (aCSF 0.05 µg/ml, n=4) against control (n=3) steady state values of the ventriculo-cisternal perfusion experiments.

6.9 Comparison of normal and HF diet male Wistar rats on resistance to CSF drainage following mediator treatment

Male Wistar rat resistance to CSF drainage comparisons between each mediator in both normal and HF diets are shown in Figures 6.35-6.40.

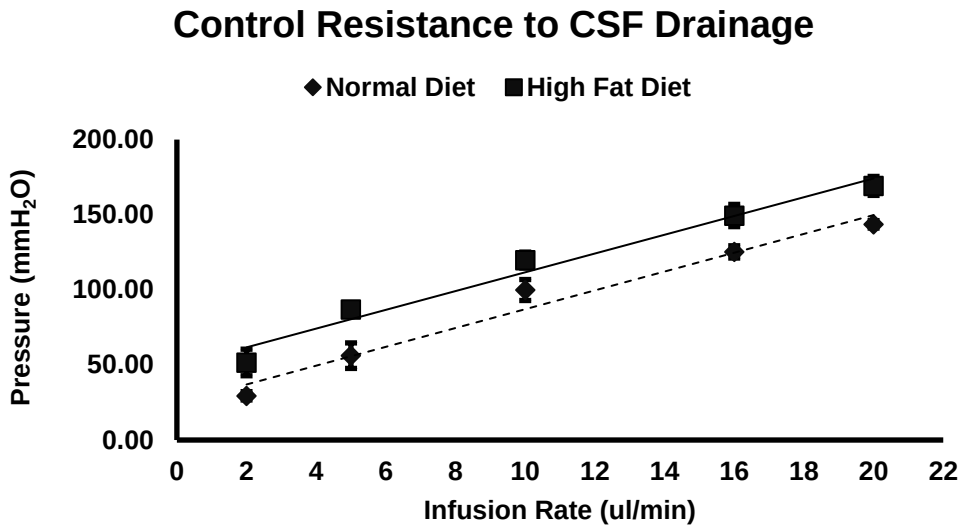

Figure 6.35: Line graph to show the control variable rate infusion pressures (mm H_2O·min/µl) of male Wistar rats raised on a normal diet (dashed line) and high fat diet (solid line).

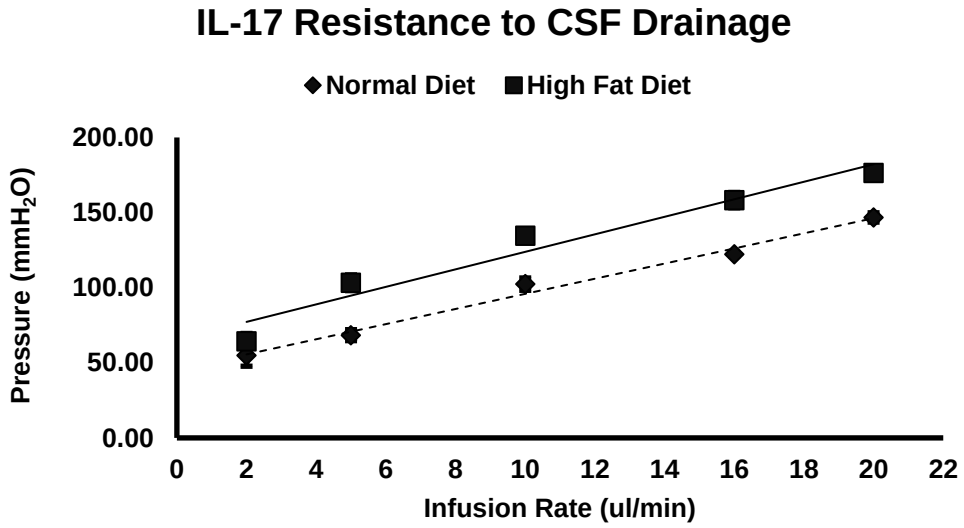

Figure 6.36: Line graph to show the IL-17 variable rate infusion pressures (mm H_2O·min/µl) of male Wistar rats raised on a normal diet (dashed line) and high fat diet (solid line).

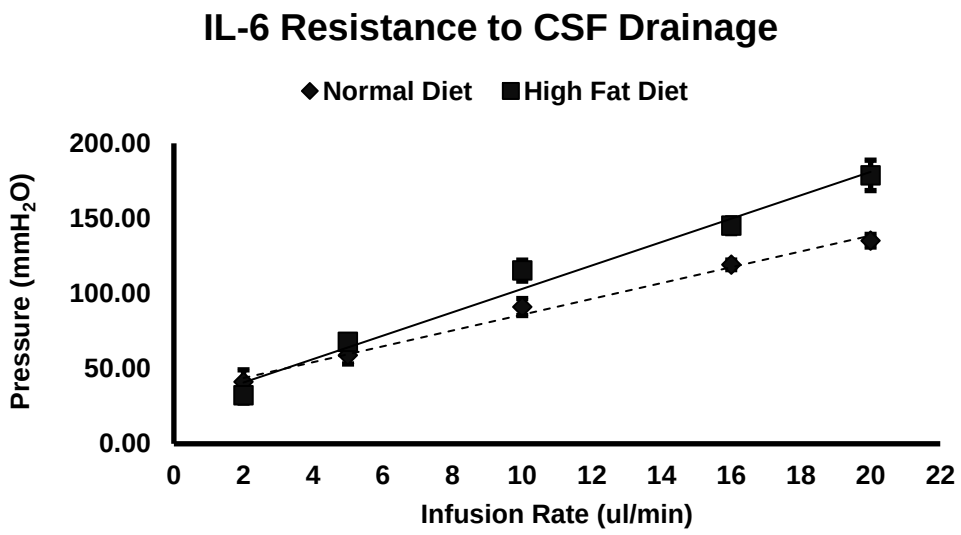

Figure 6.37: Line graph to show the IL-6 variable rate infusion pressures (mm H_2O·min/µl) of male Wistar rats raised on a normal diet (dashed line) and high fat diet (solid line).

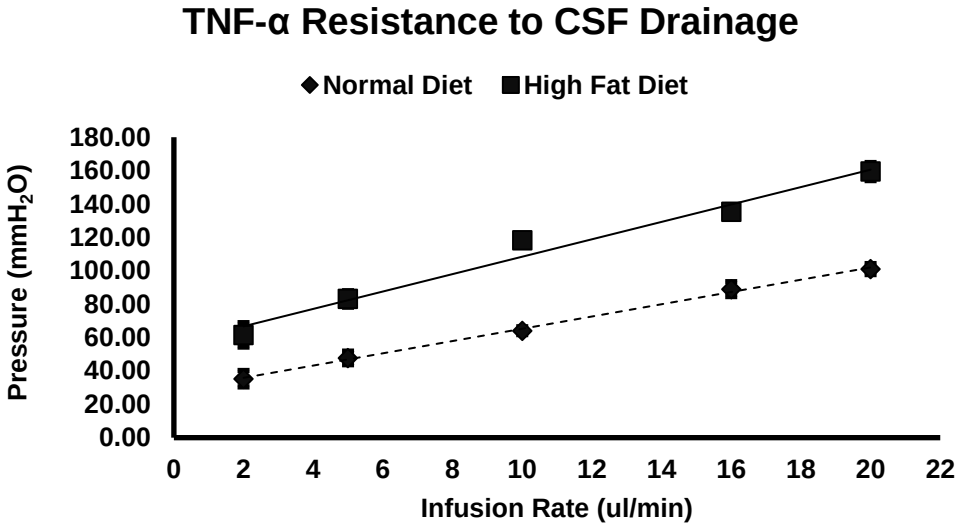

Figure 6.38: Line graph to show the TNF-α variable rate infusion pressures (mm H_2O·min/µl) of male Wistar rats raised on a normal diet (dashed line) and high fat diet (solid line).

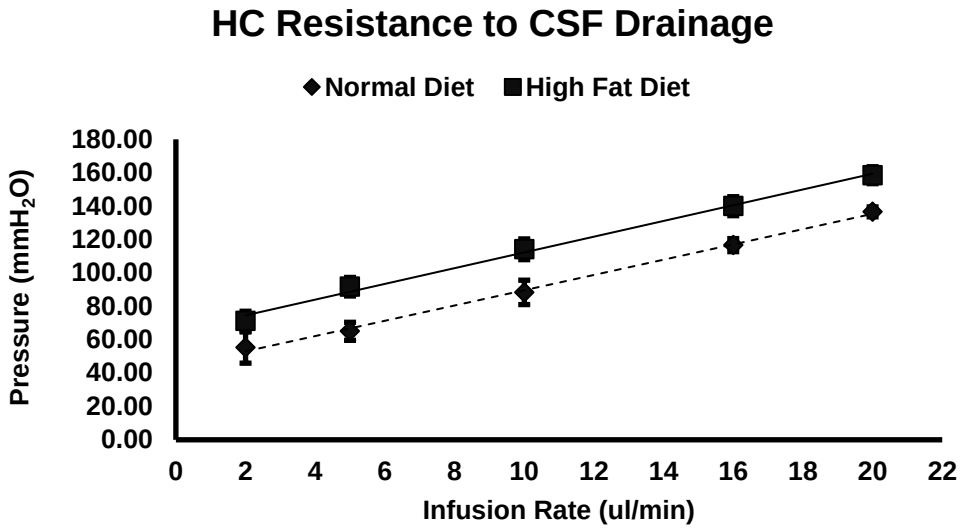

Figure 6.39: Line graph to show the HC variable rate infusion pressures (mm H_2O·min/µl) of male Wistar rats raised on a normal diet (dashed line) and high fat diet (solid line).

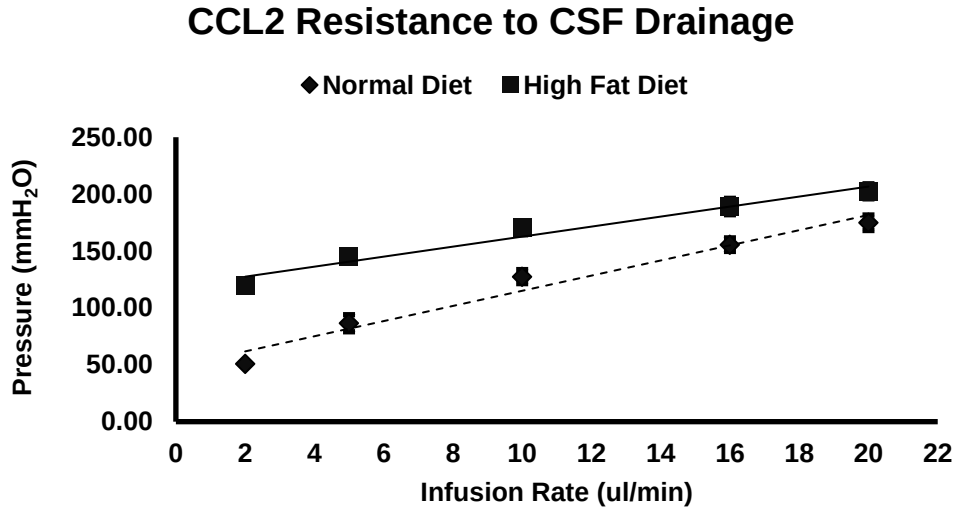

Figure 6.40: Line graph to show the CCL2 variable rate infusion pressures (mm H_2O·min/µl) of male Wistar rats raised on a normal diet (dashed line) and high fat diet (solid line).

6.10 hCPEpiC gene transcripts most in common with mouse CP transcriptome.

ACCESSION	SYMBOL	DEFINITION	logFC
NM_213720.1	Chchd10	coiled-coil-helix-coiled-coil-helix domain containing 10	0.6513637
NM_001042576.1	Rbp1	retinol binding protein 1. cellular	0.3445119
NM_002032.2	Fth1	ferritin heavy chain 1	0.2898001
NM_001001787.1	Atp1b1	ATPase. Na+/K+ transporting, beta 1 polypeptide	0.282886
NM_003374.1	Vdac1	voltage-dependent anion channel 1	0.1554399
NM_001033930.1	Uba52	ubiquitin A-52 residue ribosomal protein fusion product 1	0.0899128
NM_001035267.1	Rpl41	ribosomal protein L41	0.0893397
NM_004544.2	Ndufa1	NADH dehydrogenase (ubiquinone) 1 alpha subcomplex. 1	0.0837867
NM_001686.3	Atp5b	ATP synthase, H+ transporting mitochondrial F1 complex. beta subunit	0.0427921
NM_007209.3	Rpl35	ribosomal protein L35	0.0088475
NM_000099.2	Cst3	cystatin C	-0.012587
NM_004356.3	Cd81	Cd81 antigen	-0.019841
NM_001642.1	Aplp2	amyloid beta (A4) precursor-like protein 2	-0.022418
NM_001867.2	Cox7c	cytochrome c oxidase. subunit VIIc	-0.028557
NM_001040034.1	Cd63	Cd63 antigen	-0.065696
NM_000701.6	Atp1a1	ATPase, Na+/K+ transporting. alpha 1 polypeptide	-0.096175
NM_000999.2	Rpl3	ribosomal protein L3	-0.11448
NM_001032.3	Rps29	ribosomal protein S29	-0.130226
NM_002489.2	Ndufa4	NADH dehydrogenase (ubiquinone) 1 alpha subcomplex, 4	-0.134598
NM_001023.2	Rps20	ribosomal protein S20	-0.149265
NM_001861.2	Cox4i1	cytochrome c oxidase subunit IV isoform 1	-0.237825
NM_015161.1	Arl6ip1	ADP-ribosylation factor-like 6 interacting protein 1	-0.249884
NM_018955.2	Ubb	ubiquitin B	-0.260371

NM_002954.3	Rps27a	ribosomal protein S27a	-0.262877
NM_001003785.1	Atp5h	ATP synthase. H+ transporting, mitochondrial F0 complex. subunit d	-0.272161
NM_001003714.1	Atp5j2	ATP synthase, H+ transporting. mitochondrial F0 complex, subunit f. isoform 2	-0.349432
NM_213725.1	Rplp1	ribosomal protein. large, P1	-0.480786
NM_006004.2	Uqcrh	ubiquinol-cytochrome c reductase hinge protein	-0.499744
NM_004074.2	Cox8a	cytochrome c oxidase, subunit VIIIa	-0.601493
NM_004373.2	Cox6a1	cytochrome c oxidase. subunit VI a, polypeptide 1	-0.654124
NM_001025070.1	Rps14	ribosomal protein S14	-0.68929
NM_020548.4	Dbi	diazepam binding inhibitor	-0.878132

Table 6.4: 32 genes from the positively associated hCPEpiC transcripts are found to be in common with the 59 most expressed genes in the mouse CP.

6.11: Increases/decreases in gene modulation following cytokine treatments

Highest increase in modulation following 24h HC treatment				
ACCESSION	**SYMBOL**	**LogFC**	**adj.P.Val**	**Regulation**
NM_006606.2	RBBP9	1.978712321	0.940691294	+
NM_001042369.1	TROVE2	1.739270885	0.940691294	+
NM_023010.2	UPF3B	1.676106453	0.940691294	+
NM_001710.4	CFB	1.674518271	0.940691294	+
NM_006556.3	PMVK	1.611790572	0.940691294	+
NM_003335.2	UBA7	1.489689258	0.940691294	+
NM_022744.1	C16orf58	1.426152843	0.940691294	+
NM_003459.4	SLC30A3	1.417037158	0.940691294	+
NR_002977.1	SNORA45	1.400264969	0.940691294	+
NM_001077628.1	APH1A	1.352402797	0.940691294	+
NM_001005373.1	LRSAM1	1.352038988	0.940691294	+
XM_944302.1	EXOSC1	1.34093607	0.940691294	+
NM_019067.4	GNL3L	1.323718913	0.940691294	+
NM_006493.1	CLN5	1.315609789	0.940691294	+
NM_005382.1	NEFM	1.291550639	0.940691294	+
NM_004126.3	GNG11	1.291230137	0.940691294	+
NM_004707.2	ATG12	1.286095607	0.940691294	+
NR_002918.1	SNORA48	1.279619497	0.940691294	+
NM_032448.1	FAM120B	1.264297392	0.940691294	+
XM_939218.1	LOC650132	1.253837704	0.940691294	+
NM_152330.2	FRMD6	1.243695841	0.940691294	+
NM_014284.2	NCDN	1.22796179	0.940691294	+
NM_032970.2	SEC22C	1.226124554	0.940691294	+
NR_000028.1	SNORD83B	1.221898687	0.940691294	+
NM_016050.2	MRPL11	1.219555513	0.940691294	+
NM_032778.4	MINA	1.209983835	0.940691294	+
NM_013398.1	ZNF224	1.209426594	0.940691294	+
NM_004738.3	VAPB	1.201505542	0.940691294	+
NM_005346.3	HSPA1B	1.200324944	0.940691294	+
NM_014165.1	C6orf66	1.190904184	0.940691294	+
NM_001013.3	RPS9	1.186941114	0.940691294	+
NM_001039619.1	PRMT5	1.169161804	0.940691294	+
NM_052897.3	MBD6	1.151192683	0.940691294	+
NM_001013.3	RPS9	1.14890683	0.940691294	+
NM_001085471.1	FOXN3	1.148522972	0.940691294	+
NM_001114403.1	UPLP	1.145920732	0.940691294	+
NM_006861.4	RAB35	1.14444147	0.940691294	+
XM_942536.1	LOC651143	1.142885422	0.940691294	+
NM_002958.3	RYK	1.142675107	0.940691294	+
AK124143		1.138776649	0.940691294	+
NM_001011516.1	PDLIM5	1.134515908	0.940691294	+
XM_001713657.1	LOC100130707	1.134389375	0.940691294	+
NM_002575.1	SERPINB2	1.130243511	0.940691294	+
NM_021961.4	TEAD1	1.125966975	0.940691294	+
NM_138389.1	FAM114A1	1.121464216	0.940691294	+
NM_013342.2	TFPT	1.118858275	0.940691294	+
NR_002319.1	PIPSL	1.117418663	0.940691294	+
XM_001713608.1	LOC100133836	1.105457629	0.940691294	+
NM_012094.3	PRDX5	1.103757919	0.940691294	+
XR_017973.1	C12orf47	1.102997314	0.940691294	+
NR_003265.3	SDHAP2	1.097570946	0.940691294	+
NM_000368.3	TSC1	1.094600559	0.940691294	+
XM_939987.1	LOC650898	1.092937042	0.940691294	+
NM_001251.1	CD68	1.088143794	0.940691294	+
NM_005008.2	NHP2L1	1.076722124	0.940691294	+
NR_003051.2	RMRP	1.073074774	0.940691294	+
NM_006666.1	RUVBL2	1.069029782	0.940691294	+
NR_000037.1	TRQ1	1.068888083	0.940691294	+
NM_019592.5	RNF20	1.064470047	0.940691294	+
NM_017757.2	ZNF407	1.063876374	0.940691294	+
NM_002504.3	NFX1	1.060653156	0.940691294	+
NM_020310.2	MNT	1.059614249	0.940691294	+
NM_153717.2	EVC	1.058788171	0.940691294	+
NM_003545.3	HIST1H4E	1.05830021	0.940691294	+
NM_032316.3	NICN1	1.058259462	0.940691294	+
NM_012318.1	LETM1	1.054121663	0.940691294	+
NM_001238.1	CCNE1	1.048874604	0.940691294	+

NM_030800.1	C15orf44	1.048420936	0.940691294	+
NM_003290.1	TPM4	1.047938789	0.940691294	+
NM_014138.3	FAM156A	1.029219145	0.940691294	+
NM_003776.2	MRPL40	1.026678727	0.940691294	+
NM_001347.2	DGKQ	1.020054018	0.940691294	+
NM_031263.1	HNRPK	1.019525442	0.940691294	+
NM_013283.3	MAT2B	1.019133506	0.940691294	+
NM_003164.3	STX5	1.014411166	0.940691294	+
NM_004707.2	ATG12	1.012182551	0.940691294	+
NM_080652.2	TMEM41A	1.009371812	0.940691294	+
NM_001008408.3	RBM33	1.007583907	0.940691294	+
NM_001827.1	CKS2	1.004033381	0.940691294	+
NM_000320.1	QDPR	1.003494559	0.940691294	+
NR_002963.1	SNORA24	1.001002333	0.940691294	+
NM_016535.3	ZNF581	1.000197545	0.940691294	+

Table 6.5: Genes with greatest increase in modulation following 24h hCPEpiC treatment with HC.

Highest decrease in modulation following 24h HC treatment				
ACCESSION	**SYMBOL**	**LogFC**	**adj.P.Val**	**Regulation**
XM_942296.1	LOC201229	-1.618517107	0.940691294	-
NM_138284.1	IL17D	-1.609309399	0.940691294	-
NM_001039571.1	KREMEN1	-1.491588586	0.940691294	-
XM_001129663.1	ZNF703	-1.417541925	0.940691294	-
NM_001099639.1	ZNF146	-1.406134901	0.940691294	-
NM_017503.2	SURF2	-1.388190377	0.940691294	-
NM_032861.2	SERAC1	-1.357068977	0.940691294	-
NM_004715.3	CTDP1	-1.341601661	0.940691294	-
NM_203382.1	AMACR	-1.322454647	0.940691294	-
XR_042006.1	LOC728975	-1.313239254	0.940691294	-
NM_003250.4	THRA	-1.31102174	0.940691294	-
NM_201443.1	TEAD4	-1.278201128	0.940691294	-
NM_017966.4	VPS37C	-1.277421609	0.940691294	-
NM_003216.2	TEF	-1.274313964	0.940691294	-
XM_940903.2	ZC3H5	-1.260756522	0.940691294	-
XM_001126243.1	LOC727958	-1.251062228	0.940691294	-
NM_001031714.3	INF2	-1.249494292	0.940691294	-
NM_001157.2	ANXA11	-1.242250167	0.940691294	-
NM_173566.2	C22orf30	-1.241122611	0.940691294	-
NM_004517.2	ILK	-1.240379926	0.940691294	-
NM_024330.1	SLC27A3	-1.23662906	0.940691294	-
NM_007254.2	PNKP	-1.23452579	0.940691294	-
NM_032592.3	ACCS	-1.222008813	0.940691294	-
NM_002237.3	KCNG1	-1.216149819	0.940691294	-
NM_199293.2	TH	-1.211489511	0.940691294	-
NM_000360.3	TH	-1.20541426	0.940691294	-
XM_933784.1	LOC646631	-1.184121994	0.940691294	-
NM_004715.3	CTDP1	-1.160082862	0.940691294	-
XM_939186.2	GPSM1	-1.155588438	0.940691294	-
NM_025207.3	FLAD1	-1.151772743	0.940691294	-
NM_138927.1	SON	-1.143403342	0.940691294	-
NM_148956.1	NSUN5	-1.142243507	0.940691294	-
NM_018239.2	LRRC20	-1.137412518	0.940691294	-
NM_019624.2	ABCB9	-1.137269311	0.940691294	-
AI860517		-1.134058207	0.940691294	-
NM_017715.2	ZNF3	-1.128384459	0.940691294	-
NM_001078172.1	FAM127B	-1.122008075	0.940691294	-
NM_001025436.1	SPAG16	-1.11450463	0.940691294	-
NM_001099400.1	SGCE	-1.111213794	0.940691294	-
NM_001032364.1	GGT1	-1.102647995	0.940691294	-
NM_018044.2	NSUN5	-1.098842777	0.940691294	-
NR_002215.1	C21orf41	-1.087666362	0.940691294	-
NM_000692.3	ALDH1B1	-1.078883914	0.940691294	-
NM_004512.3	IL11RA	-1.065073652	0.940691294	-
NM_001038618.1	NARF	-1.062693824	0.940691294	-
NM_001752.2	CAT	-1.061646196	0.940691294	-
NM_144683.3	DHRS13	-1.056604187	0.940691294	-
XM_001722466.1	LOC100129186	-1.053279619	0.940691294	-

NM_001029835.1	CCM2	-1.050637438	0.940691294	-
NM_021806.1	FAM3A	-1.04884977	0.940691294	-
NM_016256.2	NAGPA	-1.048299451	0.940691294	-
NM_021807.3	EXOC4	-1.045912012	0.940691294	-
NM_019030.2	DHX29	-1.028578702	0.940691294	-
NM_015100.2	POGZ	-1.021067942	0.940691294	-
NM_001009814.1	KIAA0564	-1.020809998	0.940691294	-
NM_024640.3	YRDC	-1.01710884	0.940691294	-
XM_001715452.1	LOC100132369	-1.014499755	0.940691294	-
NM_033138.2	CALD1	-1.014440485	0.940691294	-
NM_022087.2	GALNT11	-1.009187525	0.940691294	-
NM_017956.2	TRMT12	-1.007277034	0.940691294	-
NM_138431.1	MFSD3	-1.004837965	0.940691294	-
NM_016498.3	MTP18	-1.00423326	0.940691294	-

Table 6.6: Genes with greatest decrease in modulation following 24h hCPEpiC treatment with HC.

Highest increase in modulation following 24h TNF-α treatment				
ACCESSION	**SYMBOL**	**LogFC**	**adj.P.Val**	**Regulation**
NM_001042369.1	TROVE2	2.204761434	0.584900067	+
NM_144635.3	FAM131A	2.04970528	0.955775508	+
NM_016535.3	ZNF581	2.02994054	0.65265835	+
AI557007		1.875315457	0.584900067	+
XR_017973.1	C12orf47	1.859400528	0.955775508	+
NM_007279.2	U2AF2	1.827013324	0.955775508	+
NM_005706.2	TSSC4	1.789284489	0.955775508	+
NM_173079.1	RUNDC1	1.683385271	0.871195616	+
NM_016066.3	GLRX2	1.659278071	0.946981573	+
NM_033281.5	MRPS36	1.634566599	0.955775508	+
NM_001238.1	CCNE1	1.573358027	0.955775508	+
NM_006736.5	DNAJB2	1.541237581	0.955775508	+
NM_032316.3	NICN1	1.534197083	0.955775508	+
NM_145687.2	MAP4K4	1.510886851	0.584900067	+
NM_005333.2	HCCS	1.462571812	0.955775508	+
NM_023010.2	UPF3B	1.461098972	0.955775508	+
NM_000320.1	QDPR	1.426906217	0.955775508	+
NM_001157.2	ANXA11	1.423898631	0.955775508	+
NM_001114403.1	UPLP	1.421373792	0.955775508	+
NM_001303.2	COX10	1.403055654	0.955775508	+
NM_175920.3	LNPEP	1.400220772	0.955775508	+
NM_207291.1	USF2	1.390563918	0.955775508	+
NM_001014380.1	KATNAL1	1.383954878	0.65265835	+
NM_020177.2	FEM1C	1.373371213	0.955775508	+
NM_018146.2	RNMTL1	1.357115642	0.65265835	+
NM_018198.2	DNAJC11	1.347638848	0.955775508	+
NM_004050.2	BCL2L2	1.329841433	0.955775508	+
NM_018352.2	C4orf43	1.322405278	0.955775508	+
NM_001080393.1	GXYLT2	1.309798569	0.955775508	+
NM_001031727.2	MRI1	1.307426974	0.871195616	+
NM_030809.1	CSRNP2	1.288176273	0.955775508	+
NM_003580.2	NSMAF	1.273828468	0.955775508	+
NM_005720.2	ARPC1B	1.270152623	0.955775508	+
NM_181472.1	CMTM7	1.26737169	0.584900067	+
NM_014284.2	NCDN	1.253227095	0.955775508	+
NM_025204.2	TRABD	1.251175444	0.955775508	+
NM_145800.2	Sep-06	1.241807627	0.955775508	+
NM_030808.3	NDEL1	1.240594171	0.955775508	+
NM_182984.3	TRMT2A	1.239146451	0.955775508	+
NM_153033.1	KCTD7	1.227258019	0.955775508	+
NM_017518.5	UCHL5IP	1.221904641	0.955775508	+
NM_015878.4	AZIN1	1.215417578	0.584900067	+
NM_014652.2	IPO13	1.207054219	0.955775508	+
NM_018171.3	APPL2	1.206634958	0.955775508	+
NM_005585.3	SMAD6	1.201777641	0.955775508	+
NM_014614.1	PSME4	1.192380801	0.955775508	+
NM_015609.2	C1orf144	1.189985096	0.955775508	+
NM_021915.2	ZNF69	1.185718518	0.955775508	+
NM_001011546.1	DSTN	1.184967928	0.955775508	+

NM_180989.4	GPR180	1.183839231	0.955775508	+
XM_939218.1	LOC650132	1.176997481	0.955775508	+
NR_004390.1	SNORA57	1.164318207	0.955775508	+
NM_013362.1	ZNF225	1.163129491	0.955775508	+
NM_012317.2	LDOC1	1.148813225	0.955775508	+
NM_000271.3	NPC1	1.142125013	0.955775508	+
NM_006493.1	CLN5	1.139582053	0.955775508	+
BU632198		1.13914528	0.907353371	+
NM_032525.1	TUBB6	1.138677948	0.955775508	+
NM_202001.1	ERCC1	1.136728865	0.955775508	+
NM_138440.2	VASN	1.136090711	0.955775508	+
NM_032548.2	ABTB1	1.135439312	0.955775508	+
XM_933028.2	FLJ20444	1.126787156	0.955775508	+
NM_144568.1	TMEM55B	1.119574771	0.955775508	+
NM_032305.1	POLR3GL	1.119067289	0.955775508	+
NM_002710.1	PPP1CC	1.103192119	0.955775508	+
NM_133377.2	RAD1	1.098912443	0.955775508	+
NM_020806.4	GPHN	1.097277393	0.955775508	+
XM_942150.1	LOC652615	1.095062024	0.955775508	+
NR_002210.1	COX6BP1	1.090689917	0.955775508	+
NM_001042539.1	MAZ	1.087243991	0.955775508	+
NM_014328.2	RUSC1	1.083808859	0.955775508	+
NM_001120.3	MFSD10	1.083537373	0.955775508	+
NM_182909.2	FILIP1L	1.082327587	0.955775508	+
NM_145792.1	MGST1	1.079996859	0.955775508	+
NM_178526.1	SLC25A42	1.079781771	0.955775508	+
NM_182801.1	EGFLAM	1.074804927	0.955775508	+
NM_015028.1	TNIK	1.072978314	0.955775508	+
XM_001133393.1	KCMF1	1.072967471	0.955775508	+
NM_024589.1	ROGDI	1.070492575	0.955775508	+
NM_001560.2	IL13RA1	1.07048166	0.955775508	+
NM_014504.1	RABGEF1	1.066525068	0.955775508	+
AA057856		1.066181521	0.955775508	+
NM_004236.1	COPS2	1.060858632	0.955775508	+
NM_015164.1	PLEKHM2	1.057661916	0.955775508	+
NM_013338.3	ALG5	1.057217059	0.955775508	+
NM_001080826.1	PRAGMIN	1.053944901	0.955775508	+
NM_152877.1	FAS	1.046892105	0.955775508	+
NM_030768.2	ILKAP	1.042138819	0.955775508	+
NM_015577.1	RAI14	1.037053674	0.955775508	+
NM_014389.1	PELP1	1.036084047	0.955775508	+
NM_020998.2	MST1	1.035544309	0.955775508	+
NM_012265.1	RHBDD3	1.034888895	0.955775508	+
NM_014463.1	LSM3	1.023983145	0.955775508	+
NM_016287.3	HP1BP3	1.020964099	0.955775508	+
NM_018054.4	ARHGAP17	1.020419382	0.955775508	+
NM_201453.2	CBWD3	1.016820146	0.955775508	+
NM_033294.2	CASP1	1.016117009	0.955775508	+
XR_018376.1	LOC648509	1.011791476	0.955775508	+
NM_181509.1	MAP1LC3A	1.010846221	0.955775508	+
NM_004723.2	ARHGEF2	1.008412713	0.955775508	+
NM_144729.1	DUSP10	1.00770475	0.955775508	+
NM_004270.3	CRSP9	1.000847525	0.955775508	+

Table 6.7: Genes with greatest increase in modulation following 24h hCPEpiC treatment with TNF-α.

Highest decrease in modulation following 24h TNF-α treatment				
ACCESSION	**SYMBOL**	**LogFC**	**adj.P.Val**	**Regulation**
NM_001037633.1	SIL1	-2.232905346	0.65265835	-
DN997246		-2.026239611	0.955775508	-
NM_180981.1	MRPL52	-1.814332862	0.565923504	-
NM_001031714.3	INF2	-1.730860063	0.955775508	-
XM_942296.1	LOC201229	-1.689671655	0.955775508	-
NM_001025436.1	SPAG16	-1.676684851	0.955775508	-
NM_032038.1	SPNS1	-1.666612656	0.955775508	-
NM_003760.3	EIF4G3	-1.63167934	0.955775508	-
NM_001567.2	INPPL1	-1.627556281	0.955775508	-
NM_181716.2	CENPV	-1.596925097	0.584900067	-

NM_000692.3	ALDH1B1	-1.594512578	0.955775508	-
NM_001029835.1	CCM2	-1.572768338	0.955775508	-
NM_022455.3	NSD1	-1.56673598	0.955775508	-
NM_001099639.1	ZNF146	-1.553415179	0.955775508	-
AL157484		-1.553407098	0.955775508	-
NM_019015.1	CHPF2	-1.532407176	0.955775508	-
NM_002569.2	FURIN	-1.499854715	0.955775508	-
NM_003250.4	THRA	-1.495391659	0.955775508	-
NM_018235.1	CNDP2	-1.483419637	0.955775508	-
NM_138927.1	SON	-1.480605249	0.955775508	-
NM_002818.2	PSME2	-1.452319802	0.955775508	-
NM_015326.2	SRGAP2	-1.442133412	0.584900067	-
NM_017702.2	DEF8	-1.430488242	0.65265835	-
NM_173701.1	WARS	-1.421049203	0.584900067	-
NM_148956.1	NSUN5	-1.419577656	0.955775508	-
NM_130851.1	BMP4	-1.413331418	0.955775508	-
NM_016406.1	UFC1	-1.403097544	0.955775508	-
NM_005587.1	MEF2A	-1.40249886	0.955775508	-
NM_003869.4	CES2	-1.399882509	0.955775508	-
NR_003038.1	SNHG5	-1.396362397	0.793442166	-
NM_002899.2	RBP1	-1.390078674	0.955775508	-
XM_945932.1	LOC654135	-1.384282331	0.955775508	-
NM_013379.2	DPP7	-1.378649284	0.955775508	-
NM_017615.1	NSMCE4A	-1.35191496	0.955775508	-
NM_001240.2	CCNT1	-1.345221127	0.955775508	-
NM_001038618.1	NARF	-1.342172356	0.955775508	-
NM_001009570.1	CCT7	-1.328095908	0.955775508	-
NM_033138.2	CALD1	-1.326814255	0.955775508	-
XM_937735.1	LOC648668	-1.322768423	0.955775508	-
NM_001032364.1	GGT1	-1.32230675	0.955775508	-
NM_025207.3	FLAD1	-1.319712874	0.955775508	-
NM_017503.2	SURF2	-1.315281287	0.955775508	-
NM_032861.2	SERAC1	-1.312624319	0.955775508	-
NM_019030.2	DHX29	-1.309457318	0.584900067	-
NM_178863.2	KCTD13	-1.30922989	0.955775508	-
NM_020699.1	GATAD2B	-1.300906255	0.955775508	-
XM_001126243.1	LOC727958	-1.288813634	0.955775508	-
NM_000679.3	ADRA1B	-1.288767932	0.955775508	-
NM_000404.1	GLB1	-1.285247762	0.955775508	-
NM_145871.1	GSTZ1	-1.279029515	0.955775508	-
NM_019624.2	ABCB9	-1.261849802	0.955775508	-
XM_940903.2	ZC3H5	-1.259713359	0.955775508	-
NM_024824.3	ZC3H14	-1.251096582	0.955775508	-
NM_014680.2	KIAA0100	-1.245958371	0.955775508	-
NM_017926.2	C14orf118	-1.244136203	0.955775508	-
NM_198595.2	AFAP1	-1.243801393	0.955775508	-
XR_017355.2	LOC644877	-1.238929092	0.955775508	-
NM_201443.1	TEAD4	-1.236500532	0.955775508	-
NM_004168.1	SDHA	-1.224599943	0.955775508	-
NM_013250.1	ZNF215	-1.224269513	0.946981573	-
XM_001129663.1	ZNF703	-1.215422219	0.955775508	-
NM_152260.1	RPUSD2	-1.215315058	0.955775508	-
NM_017966.4	VPS37C	-1.2138954	0.955775508	-
NR_003664.1	LOC389517	-1.212238991	0.955775508	-
XR_038849.1	LOC100128353	-1.209914802	0.955775508	-
NM_001032289.1	SLC35A2	-1.208796436	0.955775508	-
NM_017805.2	RASIP1	-1.202352706	0.955775508	-
NM_170753.1	PGBD3	-1.199815614	0.955775508	-
NM_058243.2	BRD4	-1.199284324	0.955775508	-
NM_001004698.1	OR2W5	-1.199229569	0.955775508	-
NM_001037163.1	C7orf70	-1.197453023	0.955775508	-
NM_002714.2	PPP1R10	-1.191740305	0.955775508	-
NM_024330.1	SLC27A3	-1.190992746	0.955775508	-
NM_018464.2	CISD1	-1.190547867	0.955775508	-
NM_018249.4	CDK5RAP2	-1.190529489	0.955775508	-
NM_182676.1	PLTP	-1.188995014	0.955775508	-
NM_031412.2	GABARAPL1	-1.187007298	0.955775508	-
NM_001042635.1	NGDN	-1.185477626	0.955775508	-
NM_014962.2	BTBD3	-1.1843863	0.955775508	-
NM_013293.3	TRA2A	-1.181643165	0.955775508	-
NM_207333.2	ZNF320	-1.179819315	0.955775508	-

NM_207012.2	AP3M1	-1.177860649	0.955775508	-
XM_001133202.1	KIAA0363	-1.177496779	0.584900067	-
NM_001033564.1	C6orf225	-1.176030525	0.955775508	-
NM_145754.2	KIFC2	-1.173667828	0.955775508	-
NM_144563.2	RPIA	-1.172920471	0.955775508	-
NM_006371.3	CRTAP	-1.171175661	0.955775508	-
NR_002745.1	SNORD48	-1.167910511	0.955775508	-
NM_078471.3	MYO18A	-1.167504691	0.955775508	-
NM_007010.2	DDX52	-1.165197298	0.955775508	-
NM_178422.4	PAQR7	-1.165111966	0.955775508	-
NM_015527.2	TBC1D10B	-1.16418613	0.955775508	-
NM_005791.1	MPHOSPH10	-1.163872605	0.955775508	-
NM_001040144.1	CHTF8	-1.161958164	0.955775508	-
NM_004346.3	CASP3	-1.160589426	0.955775508	-
XM_933784.1	LOC646631	-1.158493716	0.955775508	-
NM_013436.3	NCKAP1	-1.158107452	0.955775508	-
XM_944131.1	LOC650280	-1.155944075	0.955775508	-
NM_000360.3	TH	-1.152995496	0.955775508	-
NM_001281.2	TBCB	-1.147928629	0.955775508	-
NM_001042601.1	TTC14	-1.147219651	0.955775508	-
NM_000701.6	ATP1A1	-1.141902271	0.955775508	-
NM_004517.2	ILK	-1.124574924	0.955775508	-
NM_032656.2	DHX37	-1.124051188	0.955775508	-
NM_199293.2	TH	-1.123157787	0.955775508	-
NM_184041.1	ALDOA	-1.122494501	0.955775508	-
NR_003249.1	HNRPDL	-1.117349388	0.955775508	-
NM_178865.3	SERINC2	-1.11303988	0.955775508	-
NM_000820.1	GAS6	-1.111371575	0.955775508	-
NM_025250.2	TTYH3	-1.105438448	0.955775508	-
NM_001126.2	ADSS	-1.105334518	0.955775508	-
NM_015373.3	CBY1	-1.104477453	0.955775508	-
NM_001039571.1	KREMEN1	-1.103669465	0.955775508	-
NM_015172.3	BAT2D1	-1.10187173	0.955775508	-
NM_006425.4	SLU7	-1.100769594	0.955775508	-
NM_173680.3	ZNF775	-1.09957067	0.955775508	-
NM_013443.3	ST6GALNAC6	-1.09804386	0.955775508	-
NM_017804.3	DERPC	-1.097920002	0.955775508	-
NM_005197.2	CHES1	-1.089283797	0.955775508	-
NM_004423.3	DVL3	-1.089226271	0.955775508	-
NM_032982.2	CASP2	-1.080424851	0.955775508	-
AU151944		-1.078630198	0.955775508	-
AK055969		-1.076543838	0.955775508	-
NM_001017981.1	RNF215	-1.069858434	0.955775508	-
NM_003216.2	TEF	-1.068750545	0.955775508	-
NM_001006610.1	SIAH1	-1.062391759	0.955775508	-
NM_018998.2	FBXW5	-1.061121378	0.955775508	-
XM_001132505.1	LOC728689	-1.059648523	0.955775508	-
NM_025128.3	MUS81	-1.054050563	0.955775508	-
NR_002215.1	C21orf41	-1.05374944	0.955775508	-
NM_018445.4	SELS	-1.053428283	0.955775508	-
XM_001717676.1	LOC730153	-1.051044373	0.955775508	-
NM_001078172.1	FAM127B	-1.044727813	0.955775508	-
NM_022740.2	HIPK2	-1.044596978	0.955775508	-
NM_180699.1	SNRNP35	-1.040146188	0.955775508	-
NM_014161.2	MRPL18	-1.037781216	0.955775508	-
NM_024662.1	NAT10	-1.036065392	0.955775508	-
NM_144683.3	DHRS13	-1.034128136	0.955775508	-
XM_001128310.1	LOC728226	-1.029545585	0.955775508	-
NM_014164.4	FXYD5	-1.029361771	0.955775508	-
NM_001020825.1	NR3C1	-1.028664755	0.955775508	-
NM_001024662.1	RPL6	-1.028320831	0.955775508	-
NM_025267.2	AARSD1	-1.021403396	0.955775508	-
NM_001378.1	DYNC1I2	-1.021331343	0.955775508	-
NM_023019.1	DCTN1	-1.019651969	0.955775508	-
NM_001039199.1	TTPAL	-1.019072548	0.955775508	-
NM_015100.2	POGZ	-1.018828327	0.955775508	-
NM_022804.2	SNURF	-1.018593421	0.955775508	-
NM_007254.2	PNKP	-1.017012489	0.955775508	-
XM_001722279.1	RGPD8	-1.014760504	0.955775508	-
NM_014886.3	NSA2	-1.013397513	0.955775508	-
XM_001715880.1	LOC100129652	-1.011265093	0.955775508	-

XM_001126750.1	ABI2	-1.01062819	0.955775508	-
NM_016391.3	HSPC111	-1.010275012	0.955775508	-
NM_002943.2	RORA	-1.008902449	0.955775508	-
NM_001101663.1	NBPF11	-1.005899019	0.955775508	-
NM_016360.2	TACO1	-1.005665156	0.955775508	-
NM_152629.3	GLIS3	-1.005303869	0.955775508	-
NM_007284.3	TWF2	-1.004314896	0.955775508	-
NM_001194.2	HCN2	-1.00309696	0.955775508	-
XM_001133059.1	LOC728772	-1.000268625	0.955775508	-

Table 6.8: Genes with greatest decrease in modulation following 24h hCPEpiC treatment with TNF-α.

Highest increase in modulation following 24h IL-6 treatment				
ACCESSION	**SYMBOL**	**LogFC**	**adj.P.Val**	**Regulation**
NM_006494.1	ERF	1.644959702	0.745735326	+
NR_002963.1	SNORA24	1.519878405	0.745735326	+
NR_004391.1	RNY1	1.442790773	0.745735326	+
NM_001114403.1	UPLP	1.403447114	0.745735326	+
NM_001042369.1	TROVE2	1.377912697	0.724447077	+
NM_014284.2	NCDN	1.278417483	0.745735326	+
NM_001013.3	RPS9	1.272279845	0.782171874	+
NM_016066.3	GLRX2	1.271629817	0.745735326	+
NM_000368.3	TSC1	1.271089613	0.688986932	+
NR_003051.2	RMRP	1.204534867	0.782171874	+
NM_005346.3	HSPA1B	1.197962198	0.745735326	+
NM_006009.2	TUBA1A	1.182231439	0.745735326	+
NM_001013.3	RPS9	1.175001933	0.802381309	+
NM_138720.1	HIST1H2BD	1.149826756	0.746652514	+
NM_001251.1	CD68	1.148784811	0.782171874	+
NM_003544.2	HIST1H4B	1.14251194	0.724447077	+
NM_003508.2	FZD9	1.135912451	0.745735326	+
NM_012094.3	PRDX5	1.134130806	0.782171874	+
NR_002312.1	RPPH1	1.13299077	0.745735326	+
NM_001827.1	CKS2	1.121233978	0.74628452	+
NM_004707.2	ATG12	1.121141732	0.745735326	+
NM_052897.3	MBD6	1.093022492	0.724447077	+
NR_002918.1	SNORA48	1.088700759	0.745735326	+
XR_017149.2	LOC392437	1.085260599	0.688986932	+
NM_138777.2	MRRF	1.080581714	0.745735326	+
XM_930777.1	LOC642393	1.065612777	0.746652514	+
NM_001040084.1	ANXA8	1.065487474	0.688986932	+
NM_006556.3	PMVK	1.059544741	0.805909597	+
NM_181839.1	PKIA	1.057169715	0.750148358	+
NM_003543.3	HIST1H4H	1.055773503	0.805909597	+
XM_001724769.1	LOC100134253	1.042591689	0.80561574	+
NM_030800.1	C15orf44	1.041758059	0.746652514	+
NM_020529.1	NFKBIA	1.038851078	0.762761846	+
XM_208281.7	LOC285053	1.03679764	0.745735326	+
NR_000028.1	SNORD83B	1.034499682	0.745735326	+
NM_021961.4	TEAD1	1.026541222	0.745735326	+
NM_004126.3	GNG11	1.014484117	0.688986932	+
XM_939218.1	LOC650132	1.007027006	0.745735326	+
NM_001011546.1	DSTN	1.006419932	0.724447077	+
NM_006184.3	NUCB1	1.005040673	0.804801883	+
XM_001725751.1	LOC100130592	1.003501072	0.782171874	+
NM_004514.3	FOXK2	1.000123132	0.762761846	+

Table 6.9: Genes with greatest increase in modulation following 24h hCPEpiC treatment with IL-6.

Highest decrease in modulation following 24h IL-6 treatment				
ACCESSION	**SYMBOL**	**LogFC**	**adj.P.Val**	**Regulation**
NM_032592.3	ACCS	-1.498903817	0.782171874	-
XM_942296.1	LOC201229	-1.397877621	0.745735326	-
NM_025207.3	FLAD1	-1.304327059	0.745735326	-
NM_138284.1	IL17D	-1.302034933	0.745735326	-
NM_004715.3	CTDP1	-1.299026007	0.745735326	-
XM_940903.2	ZC3H5	-1.289370508	0.76625971	-
NM_201443.1	TEAD4	-1.286999502	0.745735326	-
NM_180699.1	SNRNP35	-1.273304295	0.782171874	-
NM_001031714.3	INF2	-1.246624878	0.782171874	-
NM_004715.3	CTDP1	-1.234824123	0.750148358	-
NM_203382.1	AMACR	-1.15107274	0.746652514	-
NM_001025436.1	SPAG16	-1.134640791	0.762761846	-
XR_017355.2	LOC644877	-1.123036423	0.745735326	-
NM_001029835.1	CCM2	-1.120814761	0.762761846	-
XR_038716.1	LOC100131735	-1.119789368	0.77001028	-
NM_017966.4	VPS37C	-1.108133912	0.745735326	-
NM_004563.2	PCK2	-1.101245628	0.746652514	-
NM_178863.2	KCTD13	-1.088565153	0.789542791	-

DN997246		-1.086900545	0.746652514	-
XM_001714755.1	LOC100133588	-1.086208634	0.746652514	-
NM_001099639.1	ZNF146	-1.083573899	0.745735326	-
NM_207333.2	ZNF320	-1.073710384	0.815261485	-
NM_001194.2	HCN2	-1.07244273	0.745735326	-
NM_013250.1	ZNF215	-1.066554183	0.688986932	-
NM_024640.3	YRDC	-1.04086374	0.745735326	-
NM_145754.2	KIFC2	-1.031147959	0.745735326	-
NM_032656.2	DHX37	-1.025124679	0.745735326	-
NM_170753.1	PGBD3	-1.023619826	0.77001028	-
NM_003250.4	THRA	-1.017799826	0.782171874	-
NM_001037163.1	C7orf70	-1.017307233	0.805909597	-
NM_152629.3	GLIS3	-1.015975221	0.745735326	-
NM_012407.2	PRKCABP	-1.014995577	0.688986932	-
NM_177967.2	UBAC2	-1.011365894	0.745735326	-
NM_198282.1	TMEM173	-1.007314766	0.805909597	-
NM_000692.3	ALDH1B1	-1.005458305	0.762761846	-
NM_138431.1	MFSD3	-1.000081631	0.782171874	-

Table 6.10: Genes with greatest decrease in modulation following 24h hCPEpiC treatment with IL-6.